Some Applications of Cavity Ionisation Theory to the Condensed State

by

FOOK KHEONG CHAN, M.Sc., D.I.C., A.Inst.P.

A thesis presented for the degree of Doctor of Philosophy in the University of London.

1968

Abstract

The development of cavity ionisation theory has been reviewed and an experimental examination of recent theory undertaken. The necessary physical measurements on the Co^{60} unit used for the experimental work were carried out.

A general theory of cavity ionisation has been used to calculate the variation of the response of dosimeters with the size of the dosimeter and with the atomic number of the surrounding medium. The results of the calculations have been compared with experimental measurements.

The linear dimensions of condensed state dosimeters between 10^{-3} cm to 10 cm have been considered; this range extends from cavity sizes small compared with the ranges of electrons generated by Co^{60} gamma rays, up to sizes large compared with the electron ranges. Experiments have been performed using the Fricke dosimeter and also using "Perspex" surrounded by media with atomic number ranging from 4 to 82. It was found that in all cases theory and experiment were in agreement. It is concluded that the general theory of cavity ionisation is valid, at least for photons of this energy.

The general theory of cavity ionisation was then applied to several problems in condensed state dosimetry, including the dosimeters $FeSO_4$, LiF, $Li_2B_4O_7$, $CaSO_4$ and CaF_2 in spherical containers of various dimensions. The magnitudes of the corrections to the response of these dosimeters due to the interface effects were calculated. The derivation of the absorbed dose in a medium from the dose absorbed in a detector embedded in it was considered. Special attention has been given to the absorbed dose in soft tissue inclusions in bone irradiated by low energy photons.

Contents

CHAPTER 1

REVIEW OF THEORIES AND EXPERIMENTS ON CAVITY IONISATION

I Introduction

The physical, chemical and biological effects of ionising radiation are produced by the energy deposited in the system of interest. For this reason, a fundamental concept in radiation dosimetry is absorbed dose. 'The absorbed dose of any ionising radiation is the energy imparted to the matter by ionising particles per unit mass of irradiated material at the place of interest' (ICRU, 1962). The same ICRU report defines the unit of absorbed dose: the rad, where 1 rad = 100 ergs per gram.

In order to measure the absorbed dose in a medium exposed to ionising radiation, it is necessary to introduce a radiation-sensitive device into that medium. In general this device will differ in its density and in the atomic number of its constituents from the medium. A physical discontinuity occurs between the medium and the device, which will therefore be referred to as a cavity. The ionisation chamber has been, and still is, one of the most widely used devices in radiation dosimetry and the theory relating its response to the absorbed dose in the irradiated medium surrounding the cavity was formulated several decades ago. There have been refinements of cavity ionisation theory but always applied to the interpretation of the response of an ionisation chamber. In recent years an increasing number of non-ionmetric dosimeters have come into use (e.g. chemical dosimeters, thermoluminescent dosimeters, photoluminescent dosimeters and conductivity dosimeters).

This thesis discusses the application of cavity ionisation theory to the condensed state. A recent theory of cavity ionisation is evaluated for a chemical dosimeter and for two solid state dosimeters over a large range of photon energy and dosimeter size. These calculations are compared with the experimental response of these dosimeters to 1.25MeV photons. The theory is also applied to the

calculation of the dose received by soft tissue elements in irradiated bone.

II Assumptions Occurring in Cavity Theories

The assumptions occurring in the theories to be discussed are stated here and will be referred to in the discussion of each theory.

1. The stopping power ratio for electrons may be treated as constant.
2. Electrons lose energy continuously (i.e., δ-ray production is neglected).
3. The cavity is small so that the electron spectrum set up in the chamber wall is not modified by its presence.
4. The generation of electrons by the absorption of photons in the cavity itself is negligible. To satisfy assumptions 3 and 4, the size of the cavity should be very much smaller than the range of electrons. In practice this can be a very severe limitation, since there are many low-energy electrons.
5. Photonuclear reactions and positron formation are disregarded.
6. There is uniform primary photon fluence produced in the region of the cavity.

III Bragg-Gray Theory

The first rigorous derivation of cavity ionisation theory was by Gray (1929) but since it was anticipated qualitatively by Bragg (1910, 1912), this has come to be called the Bragg-Gray theory. All of the six assumptions in Section II were made in this derivation.

Gray (1936) considered two small geometrically similar volumes. One composed part of the chamber wall and had a volume Vw. The other was a gas filled cavity of volume Va, the linear dimensions of Va being greater than Vw by a factor S. Suppose that Vw and Va are exposed to a uniform field of electrons. The number of electrons crossing the larger volume, Va, is greater than the number crossing the smaller volume Vw by a factor S^2; but the volume of Va exceeds Vw by a factor S^3. Hence the energy lost by the electrons in volume Va per unit

volume will be less than that in Vw by a factor 1/S. Hence if Ea and Ew are the energies lost by the electrons per unit volume in traversing the volumes Va and Vw respectively, then the Bragg-Gray relation is expressed as

$$Ew = S\,Ea \qquad 1.1$$

Ea is proportional to the energy giving rise to ionisation in the cavity and is given by WJ where W is the average energy expended in the gas per ion pair formed and J is the number of ion pairs formed in the cavity per unit volume. Hence

$$E_w = S\,W\,J \qquad 1.2.$$

Gray subsequently identified S as the ratio of the stopping power for electrons of the wall to that of the gas; i.e. $S = (dT/dx)_w/(dT/dx)_a$. Inherent in this derivation is the assumption that the energy lost by electrons in crossing each volume Va or Vw is equal to the energy deposited in that volume. This is obviously true if the energy lost by secondary electrons is absorbed 'on the spot', i.e. the continuous energy loss model stated in assumption 2 is adopted.

Reviewing the information available in 1936, Gray assumed his factor of proportionality S (i.e. the total stopping power ratio) as practically constant over a very wide range of electron energies, at least to within the limits of experimental error. Deviations of the stopping power ratio from constancy are discussed below.

IV Laurence Theory

Laurence (1937) also assumed the continuous loss model in his formulating theory but unlike the earliest form of Bragg-Gray theory, it took into account the dependence of the stopping power ratio in a medium on the electron velocity. Thus assumptions 2 to 6 were made in his theory.

He considered two small air-filled cavities, one surrounded by a solid wall and the other by a gaseous wall. The cavities are exposed to a uniform field of electrons. The number of electrons and their energy spectrum crossing a cavity vary with the atomic number of the

surrounding wall. He calculated the energy of an electron entering the cavity boundary. The amount of ionisation produced by the electron in traversing the cavity can be obtained from a knowledge of its specific ionisation in the gas knowing the electron energy at the cavity boundary. The specific ionisation, G(T), is the number of ion pairs formed in a gas per unit length, G(T) is related to the average energy expended in the cavity per ion pair formed, W, by the following expression

$$G(T) = (dT/dx)a/W \qquad 1.3$$

where W is assumed independent of the energy of the electron.

Finally, Laurence expressed the total ionisation as being

$$J = \text{CONSTANT} \int_0^{T_{max}} \lambda \int_0^{To} \{(dT/dx)a/(dT/dx)w \, dT \, dT_o \qquad 1.4$$

- λ is the rate of production in the wall/c.c., per γ-ray per cm^2 of electrons having initial energies between To and To + dT. (dT/dx)a and (dT/dx)w are the stopping powers for the gas and wall respectively. The second integral is the total stopping power ratio for the electron, which is treated as an energy dependent variable. It should be noted that not only (dT/dx)a is treated by the continuous energy loss model but also (dT/dx)w. This is because the electron distribution is derived from the reciprocal of the stopping power. Spencer and Fano (1954) have shown that this is only correct in the case of the continuous energy loss model.

V Spencer-Attix Theory

The theories in the previous sections so far have assumed that the electron loses energy continuously. The Spencer-Attix theory (1955) approached the ionisation in a cavity by taking into account discrete energy losses resulting in the secondary electrons (δ-rays) which carry this energy outside the ~~chamber wall~~ cavity. Thus assumptions 3 to 6 (Section II) are inherent in this theory.

In formulating the theory, Spencer and Attix chose an arbitrary energy limit, Δ, in which secondary electrons originating with energy less than Δ were regarded as dissipating their energy at their point of

origin. There were three points to be considered as a consequence of this assumption. Firstly, all electrons having energies greater than Δ did not dissipate their energies on the spot and these electrons were included in the fast electron spectrum $Iw(To,T)$. Secondly, because the electron spectrum included the fast electrons, the stopping power had to be limited to energy losses below Δ. Thirdly, the lower limit for the integration of the energy deposited in the cavity by the electron flux was Δ rather than zero, as electrons with energies less than Δ deposited their energy on the spot.

Spencer and Attix expressed the mass stopping power ratio for electrons of the gas to the wall, $f_w(To,\Delta)$, by the following equation. This is of course the reciprocal of the stopping power ratio in equation (1.2).

$$f_w(T_o,\Delta)=\frac{(Z/A)_a}{(Z/A)_w}\left\{1+\frac{1}{T_o}\left[\int_\Delta^{T_o} R_w(T_o,T)\left(\frac{B_a(T)}{B_w(T)}-1\right)dT + \Delta.R_w(T_o,\Delta)\left(\frac{B_a(\Delta)}{B_w(\Delta)}-1\right)\right]\right\} \qquad 1.5$$

where To is the initial energy of the electrons,
Z is the atomic number,
A is the atomic weight.

Ba(T) and Bw(T) are the stopping numbers of the electrons of energy T for the gas and wall respectively.
Rw(To,T) is the ratio of the total electron flux to the primary electron flux at an energy T when the initial energy of the electrons is To.
Δ is the energy of an electron which will span the cavity.

$fw(To,\Delta)$ in equation 1.5 is clearly a function of Δ which depends on the size of the cavity. $fw(To,\Delta)$ will therefore vary with the cavity size or the gas pressure. This size dependence factor distinguishes the Spencer and Attix theory from the theories of Bragg-Gray and Laurence which result in the ionisation per unit mass of gas being independent of the cavity size or the pressure.

VI Burch Theory

Burch (1955) presented a theory which rested on the same assumptions as Spencer and Attix. He also predicted that the ionisation per unit mass of gas would be dependent on the size of the cavity. However, the detailed attention he gave to the problem prevented him from obtaining a full numerical solution so that it is not possible to calculate the mass stopping power ratio. For this reason, no experimental tests have been applied to the theory.

VII Burlin's General Theory of Cavity Ionisation

VIIa Basic Problem

As this thesis is primarily concerned with the application of Burlin's theory (1966) to the condensed state, his theory will be reviewed in more detail than were the earlier theories. The basic problem with all the earlier theories is that they assume the modification of the electron energy spectrum in the chamber wall due to the presence of the gas in the cavity is negligible (assumptions 3 and 4). This necessitates the size of the gas cavity being small compared to the range of electrons passing through it. Experiments with gas filled ionisation chambers indicate that this condition is not fulfilled when the cavity size exceeds 1cm. diameter in the case of 1.25MeV photons. This would imply that the mean linear dimensions cannot exceed 10^{-3}cm. for condensed state dosimeters for 1MeV photons. Linear dimensions must be smaller for low energy photons and neutrons. Hence, these theories are of limited practical use in condensed state dosimetry; and, indeed,no theory will be useful unless it treats the effect of the cavity on the electron spectrum (i.e. it eliminates assumptions 3 and 4). Several experimental workers (e.g. Greening (1957), Attix et al (1958), Burlin (1961)) have found deviations from the Spencer-Attix theory in the variation of the ionisation with the cavity size and atomic number of the wall, which they attributed to the modification of the electron spectrum by the cavity. This also indicates the need for a theoretical treatment of this problem.

VIIb Modification of the shape of the Electron Spectrum by the Cavity Gas

The presence of the cavity gas modifies the electron spectrum in two ways:(1) the shape of the electron spectrum, (2) the energy in the electron spectrum. The first will be considered in this subsection.

When the size of the gas cavity is comparable to the electron range, a significant number of photon interactions occur in the cavity and an electron spectrum is set up in the gas which may differ from that set up in the wall material. The spectrum of electrons in the cavity may therefore be regarded as having two components: the wall spectrum and the gas spectrum. As no theoretical means existed for treating an electron spectrum in the region of an interface, Burlin introduced approximations, which were based on experimental findings, in order to render the problem soluble. His approach was to modify the Spencer-Attix theory so as to account for the influence of the cavity on the electron spectrum.

The electrons originating from the wall electron spectrum are attenuated as they cross the cavity gas. Burlin deduced from experimental data (e.g. Schmidt (1906), Hahn et al (1908) and Odeblad (1955)) that the attenuation was nearly exponential having an attenuation coefficient β.

Since both the 'wall spectrum' and the 'gas spectrum' are generated by the same incident photons, the maximum electron energy, Emax, will be the same for both. Burlin also noted that experimental data indicated that the maximum energy determines the effective mass absorption coefficient of a spectrum (e.g. Curie (1931), Gleason (1951), Katz et al (1952)). In fact, he used Loevinger's expression for the effective mass absorption coefficient for beta rays in air, ignoring a term concerned with forbidden spectra:

$$\beta = \frac{16}{(E_{max} - 0.036)^{1.40}} \quad cm^2/gm \text{ of air} \qquad 1.6$$

Hence, he argued that if g is the average path length of electrons crossing the cavity, the 'wall spectrum' on average would be reduced by

a factor:-

$$\frac{\int_0^g e^{-\beta x}\,dx}{\int_0^g dx} = \frac{1-e^{-\beta g}}{\beta g} = d \qquad 1.7$$

and that on average the gas spectrum would build up to a fraction (1-d) of its equilibrium value since

$$\frac{\int_0^g (1-e^{-\beta x})\,dx}{\int_0^g dx} = \frac{\beta g + e^{-\beta g} - 1}{\beta g} = 1-d \qquad 1.8$$

Applying these correction factors to the term in the Spencer-Attix formula (equation 1.5) representing the influence of the shape of the electron spectrum resulted in two terms:-

$$d\left[\int_\Delta^{T_0} R_w(T_0,T)\left(\frac{B_a(T)}{B_w(T)}-1\right)dT + \Delta\cdot R_w(T_0,\Delta)\left(\frac{B_a(\Delta)}{B_w(\Delta)}-1\right)\right]$$

$$+ (1-d)\left[\int_\Delta^{T_0} R_a(T_0,T)\left(\frac{B_a(T)}{B_a(T)}-1\right)dT + \Delta\cdot R_a(T_0,\Delta)\left(\frac{B_a(\Delta)}{B_a(\Delta)}-1\right)\right] \qquad 1.9$$

and in fact, the second term was zero because in a perfectly matched chamber (e.g. an air-wall chamber) the electronic stopping power is unity.

VIIc Modification of the Energy of the Electron Spectrum by the Cavity Gas

The presence of the gas in the cavity also modifies the total energy in the electron spectrum. As stated in subsection VIIb, the electronic stopping power ratio is unity in the case of electronic equilibrium existing in a cavity matched for atomic number with the surrounding medium. In general, this is not the case and the electrons generated per gm are different in the two materials. Therefore Burlin multiplied the electronic stopping power ratio which was treated as unity

by a ratio $a\mu'_{en}/w\mu'_{en}$ where $a\mu'_{en}$ and $w\mu'_{en}$ are the electronic energy absorption coefficients of the photons in the gas cavity and wall medium respectively, i.e. of the form $1 \times \frac{a\mu'_{en}}{w\mu'_{en}}$. The gas spectrum would then on average attain a fraction (1 - d) of its equilibrium value so that the contribution to the electronic stopping power ratio is

$$(1-d) \times 1 \times \frac{a\mu'_{en}}{w\mu'_{en}} \qquad 1.10$$

instead of (1 - d) x 1. The correction to the electronic stopping power ratio is therefore

$$(1-d) \times 1 \times \left(\frac{a\mu'_{en}}{w\mu'_{en}} - 1\right) = \qquad 1.11$$

$$(1-d)\left(\frac{\left(\frac{\mu_{en}}{\rho}\right)_a \left(\frac{Z}{A}\right)_w}{\left(\frac{\mu_{en}}{\rho}\right)_w \left(\frac{Z}{A}\right)_a} - 1\right) \qquad 1.12$$

where $\left(\frac{\mu_{en}}{\rho}\right)_a$ and $\left(\frac{\mu_{en}}{\rho}\right)_w$ are the mass energy absorption coefficients of the cavity material and the medium respectively.

VIId General Theory of Cavity Ionisation

The final expression for the mass stopping power ratio obtained by applying the above considerations to the Spencer-Attix theory is

$$f_w(T_0,\Delta) = \frac{\left(\frac{Z}{A}\right)_a}{\left(\frac{Z}{A}\right)_w}\left\{1 + \frac{d}{T_0}\left[\int_\Delta^{T_0} R_w(T_0,T)\left(\frac{B_a(T)}{B_w(T)} - 1\right)dT + \Delta . R_w(T_0,\Delta)\left(\frac{B_a(\Delta)}{B_w(\Delta)} - 1\right)\right] + (1-d)\left[\frac{\left(\frac{\mu_{en}}{\rho}\right)_a \left(\frac{Z}{A}\right)_w}{\left(\frac{\mu_{en}}{\rho}\right)_w \left(\frac{Z}{A}\right)_a} - 1\right]\right\} \qquad 1.13$$

Referring to equations (1.7) and (1.8) it is seen that when the average path length g of the electrons crossing the cavity approaches zero (i.e. for very small cavities compared with the electron range), the weighting factor d is unity. The expression for the general theory of cavity ionisation (i.e. equation 1.13) reduces to the Spencer-Attix expression (equation 1.5). When g approaches infinity (i.e. for cavities with dimensions very much greater than the range of the electrons) equation

1.13 reduces to the ratio of the mass energy absorption coefficients of the gas to the wall

$$f_w(T_0, \Delta) = \left(\frac{\mu_{en}}{\rho}\right)_a \Big/ \left(\frac{\mu_{en}}{\rho}\right)_w \qquad 1.14$$

This theoretical approach to cavity ionisation applies to all sizes of cavity and to any combination of atomic numbers for the medium and the cavity. Moreover, the cavity may be in the solid, liquid or gas phase and may be more or less dense than the medium. For these reasons, Burlin refers to it as a general theory [illegible] of cavity ionisation.

VIII Earlier Experiments in Cavity Ionisation Using a Gas Filled Medium

Most of the earlier experiments in cavity ionisation used gases as the sensitive volume. These will be reviewed in this section. The use of liquid or solid as the sensitive volume will be discussed in the chapters dealing with these dosimeters. Gas filled cavity experiments are discussed under the headings of the following parameters and are summarised in Table 1.1

(a) Variation of the gas pressure or the size of the cavity;
(b) Variation of the atomic number of the gas;
(c) Variation of the atomic number of the wall;
(d) Variation of the energy of the incident photons.

VIIIa Variation of the Pressure of the Gas or Size of the Cavity

The variation of the gas pressure and the cavity size are considered to be different aspects of the same effect. The variation of the ionisation per gram with pressure provides the most direct test of a theory of cavity ionisation in that neither auxillary constants (e.g. mass energy absorption coefficient) which would introduce additional uncertainty in the experimental results nor are any corrections are required (e.g. wall absorption and scattering). Varying the pressure in the cavity also provides a crucial test for cavity theories in that the theories of Gray and Laurence predict that the ionisation per gram of the gas is independent of cavity size, whereas the theories of Spencer and Attix, Burch, and Burlin predict that the ionisation per gram of the

gas varies with the cavity size.

The only experimental evidence to support the constancy predicted by the Bragg-Gray theory is due to Cormack and Johns (1954). Cormack (1967) has since expressed doubt concerning their experimental results. The Spencer-Attix theory is supported by experimental evidence of Greening (1957), Attix, De Le Vergne and Ritz (1958), Attix and Ritz (1958), Burlin (1961, 1966a, and 1966b), Engelke and Oetzmann (1967). Thus the majority of the experimental evidence reveals that the ionisation per gram depends on the gas pressure or size of cavity.

Burlin (1966b) has compared the calculations obtained by the Bragg-Gray, Spencer-Attix and his general theory with the experimental results obtained by varying the gas pressure in large chambers (10cm diameter) and has found that the best agreement with the experimental results was with the general theory.

For the following three subsections, only the Bragg-Gray and Spencer-Attix theories are compared with the experimental results as no other comparisons have appeared in the literature. However, it should be noted that for small cavity sizes the general theory is identical with Spencer-Attix theory.

VIIIb Variation of the Atomic Number of the Gas

Few experimenters have actually used different gases to test cavity theory. Clarkson (1941) employed different gases but his work may have been affected by ionisation by collision occurring in the region of his wire collecting electrode (Greening, 1954).

Burlin (1966a, b), employing hydrogen, air and argon as the gases in chambers of about 1cm diameter, found the Bragg-Gray and Spencer-Attix theories agreed well with the results for argon at 10 and 70cm Hg pressure. Both theories disagreed with the results for hydrogen at 10cm Hg pressure but this was attributed to slow electron transfer between the electrodes. With hydrogen at 70cm Hg pressure, the Spencer-Attix theory agreed better with the results than did the Bragg-Gray theory. Thus, these results showed that the variation of the ionisation with the atomic number of the gas agreed with the predictions of the

Spencer-Attix theory but there were some deviations from the predictions of the Bragg-Gray theory for high atomic number chambers filled with hydrogen.

VIIIc Variation of the Atomic Number of the Wall Material

Experiments performed in chambers of different materials require correction for the following factors:

(a) Absorption and scattering arising from the walls due to photons;
(b) Scattered radiation from the source;
(c) Fluorescent radiation from the wall;
(d) Difference in volumes of ionisation chambers;
(e) The presence of a low atomic number insulator forming part of the chamber;
(f) The purity of the wall material.

Differences in the results reported by various workers may well be due to differences in the way these corrections were undertaken, making this a rather unsatisfactory method of testing the basic theory. The published data in the original papers on these corrections is inadequate for useful comparison. For high energy, monoenergetic γ-ray sources, the uncertainty associated with these corrections is minimal, but even under these conditions, large differences have been reported as illustrated in Figure 1.1 for the case of Co^{60} γ-rays (1.25MeV).

At high energies, the majority of experimenters found reasonably good agreement with the theory of Spencer and Attix but not with that of Bragg and Gray (Greening, 1957, Attix, De La Vergne and Ritz, 1958, Burlin, 1966a, b), the most notable exception being Cormack and Johns (1954). At lower energies, where the above corrections become very large, the experimental results do not agree with either theory well. Thus, for example, Burlin (1966a) found at 0.41MeV (Au^{198} γ-rays) the experimental results obtained using high atomic number chambers (copper, tin and lead) do not agree with either theory. Nevertheless, even at lower energies, the overall experimental results correlate better with the Spencer-Attix than the Bragg-Gray theory.

VIIId Variation of the Energy of the Incident Radiation

Estulin (1953), using seven γ-emitting isotopes, obtained the ratio of the ionisation in a lead chamber to that in a carbon chamber. His results showed that with decreasing incident photon energy, the ratio was lower than the Spencer-Attix theory predicts.

In his experiment to study the ionisation per gram with the atomic number of the wall, Burlin (1966a) has used 0.41, 0.66 and 1.25MeV photon energies but did not comment specially on photon energy as a variable parameter.

IX The Object of the Present Work

The Bragg-Gray theory, Spencer-Attix theory and Burlin's general theory have been subjected to experimental tests using various gas-filled cavities as discussed above. The experiments extending to large sizes of gas cavities appear to fit in best with the general theory rather than the Bragg-Gray and Spencer-Attix theories. However, even these large gas cavities do not offer a very stringent test to the general theory, in that it claims to extend to any cavity size (i.e. up to cavity dimensions which are very much larger than the range of the electrons). To provide an adequate examination of this theory using 1.25MeV photons, gas filled ionisation chambers would have to be extended to 10^4cm diameter at 1 atmosphere pressure, or smaller chambers be used at 10^4 atmospheres. Neither alternative is practicable. However, the required range of size could be covered using condensed state devices as the sensitive volume (cavity) and this would provide a stringent test of Burlin's general theory of cavity ionisation. This work is undertaken in the present thesis.

The influence on the response of the container for condensed state dosimeters which must be encapsulated, and the deduction of the absorbed dose in a medium from the absorbed dose to a condensed state dosimeter imbedded in it, is of considerable practical importance. Therefore application of the general cavity theory to this problem has been considered for several systems, viz. the Fricke dosimeter, clear perspex,

thermoluminescent material (LiF). The generality of Burlin's theory is further explored by a theoretical consideration of the dosimetry problems associated with irradiated human bone.

Table 1

Summarising the parameters used experimentally in cavity ionisation

Author	Z wall	Z gas	Volume (c.c)	Pressure cm (Hg)	Energy (MeV)
Gray (1936)	6 - 82	Air	0.1 - 2.0	10.0 - 76.0	1.1 (RaB + C)
Clarkson (1941)	6 - 82	1 - 8	~0.098 - 6.25	1.0 - 152.0	0.025 - 0.063
Ibrahim and Wilson (1952)	6 - 29	Air	0.25 - 4.9	76.0	0.025 - 0.124
Estulin (1953)	6 - 82	Air	400	76.0	0.33(Cr^{51}) - 2.06(Na^{24})
Myers (1952)	6 - 82	Air	7.9 - 196	76.0	1.1(RaB + C) - 1.25(Co^{60})
Cormack and Johns (1954)	6 - 82	Air	0.3 - 3.0	76.0	1.25(Co^{60}) - 22(MAx)
Larson (1956)	13 - 29	Air	195?	0.2 - 76.0	0.008 - 0.034
Whyte (1957)	4 - 29	Air	128	7.0 - 76.0	1.25(Co^{60})
Greening (1957)	6 - 82	Air	1.0	4.0 - 76.0	0.41(Au^{198}) - 1.25(Co^{60})
Attix and Ritz (1957)	6 - 29	Air	62	6.4 - 70.0	1.25 Co^{60}
Attix et al (1958)	6 - 82	Air	0.8 - 19.7	76.0	0.038 - 1.25(Co^{60})
Burlin (1961)	6 - 82	1, 18, Air	1.24 - 740	10 - 90	1.25(Co^{60})
Burlin (1966b)	6 - 82	1, 18, Air	1.24 - 740	10 - 90	.41(Cs^{137}) - .66(Au^{198})
Engelke and Oetzemann (1967)	6, 13 polystyrene	Air	2.5	5 - 76	.41(Cs^{137}), 1.25(Co^{60}) 30 and 45 X-rays

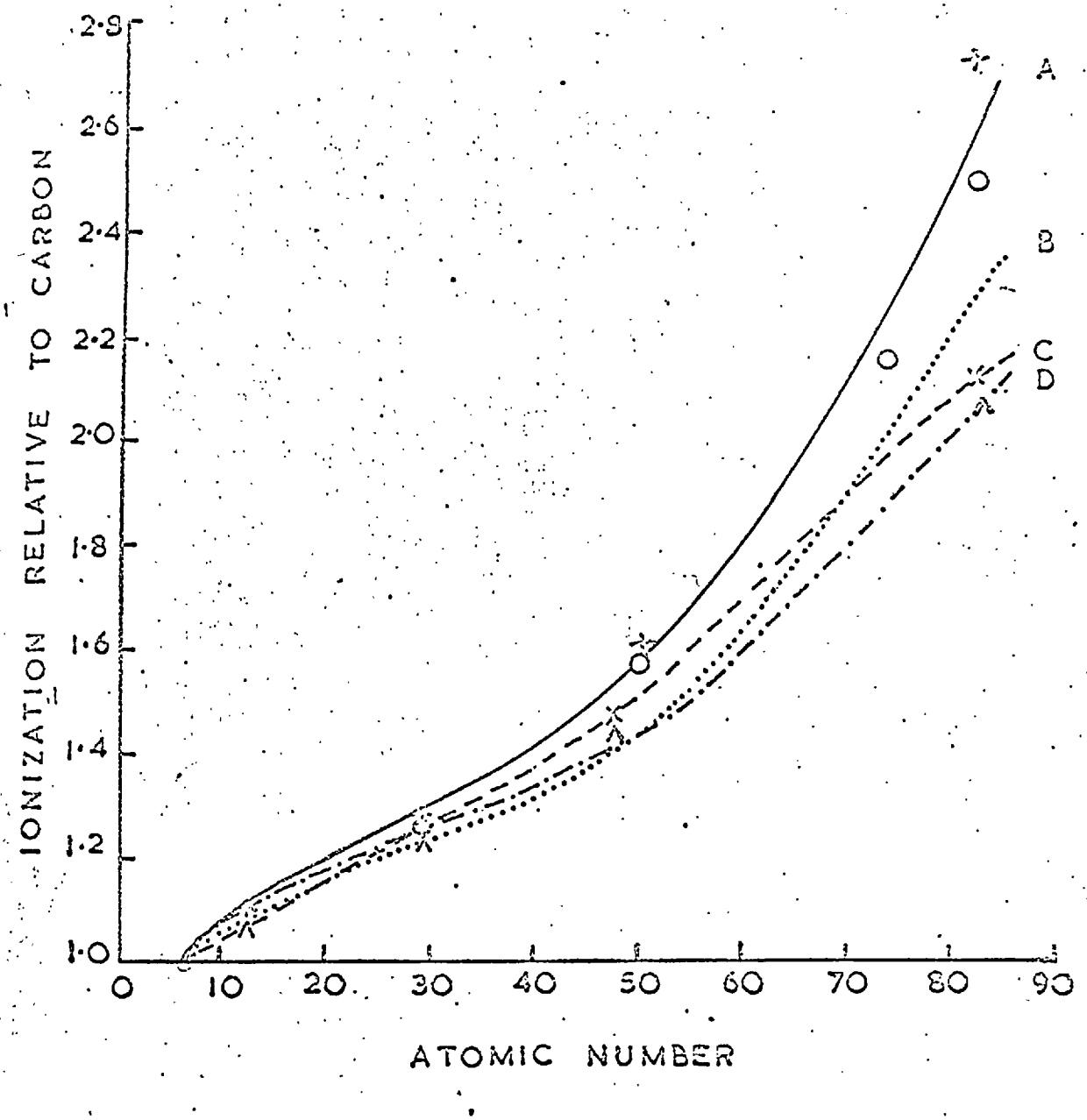

FIG. I.I. VARIATION OF IONIZATION WITH ATOMIC NUMBER FOR ^{60}Co RADIATION. + ATTIX & DE LA VERGNE, O GREENING, X CORMACK. & JOHNS, Δ MYERS. CURVE A, SPENCER – ATTIX THEORY. OTHER CURVES, BRAGG-GRAY THEORY ACCORDING TO SPENCER AND ATTIX, B, MYER, C, AND CORMACK AND JOHNS, D.

CHAPTER 2

PHYSICAL MEASUREMENTS ON THE IRRADIATION UNIT

I Description of the Irradiation Unit

This is a self-contained irradiation unit, made by Nuclear Chemical Plant Ltd. The source of gamma radiation is provided by twenty metallic Co^{60} rods singly encapsulated into stainless steel, forming a concentric ring about the irradiation chamber. The length and diameter of the Co^{60} rods measure 15.20cm and 0.95cm respectively. The total activity of these rods ~~were~~ was 3,079 curies on 1st August, 1966. Figure 2.1 shows a section through the unit.

The irradiation chamber is 15.25cm diameter and 19.0cm height and has a 12.70cm aperture. There are four connections through the upper part of the irradiation chamber and these are used for lead connections and a stirrer. The irradiation chamber is raised and lowered by a drive mechanism operated electrically.

II Protection Measurements for Co^{60} unit

IIa Measurement of Leakage Radiation from Co^{60} unit

The leakage radiation from the Co^{60} unit was measured using a 350c.c. ionisation chamber (E.I.L., model B37), connected to a battery operated electrometer (model 37C). The lowest exposure rate which could be read accurately on this dosimeter is 0.1 milli-roentgen per hour. Since the leakage radiation at certain positions outside the Co^{60} unit was less than this minimum value measured by the dosimeter, an EMI gamma probe type GP2 scintillation counter fitted to a portable contamination monitor was also used. One problem that arises using the scintillation counter is that it is energy dependent. Since the leakage radiation will include multiple scattered radiation, the energy of the leakage radiation will be less than the Co^{60} 1.25MeV gamma rays. The energy of the leakage radiation was assumed to be that of Cs^{137}, 0.66MeV gamma rays which corresponds approximately to the once-scattered photon radiation of the

Co^{60} gamma rays. To ascertain that this was a reasonable choice, the ionisation chamber and the scintillation counter were both used to measure the dose rate of a convenient magnitude of a few positions on the table top of the irradiation unit. The number of counts per second registered by the scintillation counter was converted into milli-roentgen per hour from a 'counts per second vs milli roentgen per hour' graph tabulated for Cs^{137}. The value in milli roentgen per hour obtained from the graph agreed well with the reading registered by the ionisation chamber.

The amount of leakage radiation at various positions on the irradiation unit depends on how far the vertical column is raised above the table top. For each measurement taken, the column was raised to a position that gave the maximum leakage radiation.

Figure 2.2 shows a cross-section of the table top of the irradiation unit and the positions of the measurements taken. The units are milli-roentgens per hour. Numbers in brackets represent the length in cm of the vertical column when it was raised. This length was measured from the top of the column to the top of the table. The lengths have only been placed by three points, as all other readings in Figure 2.2 were measured when the height of the vertical column was raised to 45.5cm.

Figures 2.3 and 2.4 show a cross section of the base and a plane 60cm from the base of the irradiation unit. The maximum leakage dose rates, (in milli-roentgen per hour) for the two planes were obtained with the vertical column totally raised with 89.5cm between the top of the column and the top of the table.

IIb Surface Contamination of Co^{60} Unit

The possibility of faults in the sealing of the Co^{60} rods was investigated by conducting 'wipe tests' over the unit. Two scintillation counters, one fitted with a beta ray window made of polycarbonate aluminised to a maximum thickness of 1.7 milligram per sq. cm, were used in conjunction with an EMI portable contaminator monitor to detect contamination on the cloth used for wiping. A count rate of 5c/sec above background could be detected with ease, corresponding to 10^{-10}

curie per sq. cm.

The inside surface of the irradiation chamber, the table top surface and the side surface of the Co^{60} unit were in turn wiped vigorously with clean pieces of cloth. The monitor was placed near the cloth and a negligible reading over the background was registered for both the counters. The experiment was repeated with some acetone in further pieces of clean cloth and again the monitor registered negligible readings. There was therefore no evidence of radioactive contamination arising from deficient source encapsulation.

III Analysis of the Radiation Field

The use of large Co^{60} sources requires considerable shielding and as a result, a certain proportion of the emitted gamma rays (1.17MeV and 1.33MeV) are scattered, giving photons of lower energy. In addition, electrons generated by photo-electric and Compton and pair production interactions are also present. Experiments were carried out (a) to study the amount of contamination of the photon field by electrons and (b) to obtain the photon spectrum.

IIIa Electron Contamination in the Photon Field

This was done using an electron detector, shown in Figure 2.5. It was a cylindrical perspex chamber having a clamping ring at one end which could be unscrewed to accommodate disc shaped absorbers. The absorber used was Mylar (aluminised polyethylene terephthalate sheet, 2.7×10^{-3}cm thick). The inner surfaces of the perspex were coated with alcohol aquadag, and a groove was machined to insulate the collector from the guard electrode. Similarly, a region of ungraphited perpsex insulates the guard from the H.T. electrode formed by the aluminised coating on the Mylar. The detector was fixed at the top of the irradiation chamber in the Co^{60} unit.

The ionisation current in air at atmospheric pressure was measured on a vibrating reed electrometer. The average of the ionisation current with positive and negative polarities was determined. Figure 2.6 shows

the ionisation current versus applied voltage. A voltage of 360 volts was used to obtain the saturation current. Figure 2.7 shows the variation of the ionisation current with thickness of absorber. The curve indicated a 'build down' of ionisation current. This suggested that the radiation field contained electrons or very low energy scattered photons besides the 1.25MeV (mean value) gamma rays. The amount of contamination was obtained from Figure 2.7 by taking the difference between the maximum and plateau ionisation currents and was 20 per cent.

To establish whether the contamination was due to electrons or very low energy scattered photons, the mass-energy absorption coefficient, $\frac{\mu_{en}}{\rho}$, of these ionising particles was found from the graph of ln I against absorber thickness, Figure 2.8., by drawing a tangent (TT) at the point A, where the filtration of the contaminant radiation is least, as this was the minimum thickness used. The value of $\frac{\mu_{en}}{\rho}$ was found to be 9.03cm^2/gm of mylar. If the ionising radiation were low energy scattered photons, this value of $\frac{\mu_{en}}{\rho}$ would correspond to a photon energy of 10keV. For an initial 1.25MeV photon to reach this value, it has to undergo many Compton interactions and the probability of doing so is negligible. Therefore, it is not conceivable that the contamination consists of low energy scattered photons.

In the case of electrons, the effective mass energy coefficient has been related to the maximum energy spectrum by the equation:

$$E_{max} = \left(\frac{17}{\frac{\mu_{en}}{\rho}}\right)^{\frac{1}{1.14}}$$

(Evans 1957). The average energy is approximately

$$E_{av} = \frac{1}{3} E_{max}. \quad \text{Thus } E_{av} = \frac{1}{3}\left(\frac{17}{\frac{\mu_{en}}{\rho}}\right)^{\frac{1}{1.14}}$$

Substituting 9.03cm^2/gm for $\frac{\mu_{en}}{\rho}$ gave an average electron energy of 581keV. The average energy of the Compton electrons associated with once scattered radiation from 1.25MeV photons is 589keV. The contaminant radiation was therefore electrons.

IIIb <u>The Photon Spectrum in the Irradiation Chamber</u>

Cylindrical ionisation chambers shown in Figure 2.9 were made of

graphite, aluminium, copper, tin and lead were used to study the photon spectrum. The walls of the chamber were of adequate thickness to provide full electron build-up. The wall thicknesses and nominal purity are given in Table 2.1. The central electrode had a thickness of 1.5mm. The volume of air enclosed in each chamber, 6.5cm^3, was constant.

A saturation curve was measured for the carbon and lead ionisation chambers, as given in Figure 2.10 and Figure 2.11 respectively. A saturation voltage of 600 volts was subsequently used. Measurements were carried out for each ionisation chamber with three different thicknesses of caps, 0.1mm., 0.3mm., and 0.5mm of the same material placed on top of the chambers. From these measurements correction factors for absorption and scattering in the chamber walls for the Co^{60} γ-rays (discussed in the next section) were calculated. The ionisation current for each chamber measured without caps and normalised to the carbon chamber wase obtained. These normalised values when corrected for absorption and scattering in the walls were used in analysing the Co^{60} spectrum.

Initially an attempt was made to represent the Co^{60} spectrum in the irradiation chamber by three photon energy components at 1.25, 0.66 and 0.41MeV. The 0.66 and 0.41MeV components closely represent the average energy of the once and twice scattered photons respectively. The contribution of these three components to the corrected and normalised ionisation current I for a particular chamber wall is

$$AK\left(\frac{\mu_{en}}{\rho}\right)_{1.25} f_w(T_\gamma)_{1.25} + BK\left(\frac{\mu_{en}}{\rho}\right)_{0.66} f_w(T_\gamma)_{0.66} + CK\left(\frac{\mu_{en}}{\rho}\right)_{0.41} f_w(T_\gamma)_{0.41} = I \qquad 2.1$$

where A, B and C are percentage intensities of 1.25, 0.66 and 0.41MeV photons respectively, $\left(\frac{\mu_{en}}{\rho}\right)_{1.25}$ is the mass energy absorption coefficient for the chamber wall at 1.25MeV, $f_w(T_\gamma)_{1.25}$ is the mass stopping power ratio of the chamber wall to air at 1.25MeV, and K is a constant.

Five equations similar to equation 2.1 for the five different walls were obtained. The numerical values obtained for A, B and C by solving

these equations were very inconsistent, one having a negative value.

The second attempt was to use an equation similar to equation 2.1 but with the values of the relative ionisation in the different chambers determined by small γ-ray sources which were nearly scatter free at these photon energies (Burlin 1961), i.e.

$$A.K(\bar{I})_{1.25} + BK(\bar{I})_{0.66} + CK(\bar{I})_{0.41} = \bar{I} \qquad 2.2$$

where $(\bar{I})_{1.25}$, $(\bar{I})_{0.66}$ and $(\bar{I})_{0.41}$ were Burlin's experimental values.

Negative values again appeared for one of the three components.

After these two unsuccessful attempts at trying to represent the photon spectrum using three energy components, it was decided to represent the photon spectrum using only two energy components i.e. the primary photons (A) and the whole of the scattered photon spectrum which was represented as a single energy component (B). This leads to the equation

$$AK\left(\frac{\mu_{en}}{\rho}\right)_{1.25} f_w(\bar{T}_\delta)_{1.25} + BK\left(\frac{\mu_{en}}{\rho}\right)_{0.41} f_w(\bar{T}_\delta)_{0.41} = \bar{I} \qquad 2.3$$

and

$$AK(\bar{I})_{1.25} + BK(\bar{I})_{0.41} = \bar{I} \qquad 2.4$$

The mean energy of the scattered photons was taken to be 0.41MeV. Table 2.2 gives the percentage of A and B for four combinations of material which were calculated using equations 2.3 and 2.4. The mean values of A obtained using equation 2.3 and 2.4 are 81.4 and 80.4 per cent respectively and for B, 18.6 and 19.6 per cent.

Costrell (1962) did an extensive series of measurements of the photon spectra emerging from teletherapy housings using a scintillation spectrometer. He obtained a very similar result for the ratio of primary to scattered radiation 85.4 per cent (1.0-1.33MeV) and 14.6 per cent (0-1.0MeV). The photon spectrum emerging from a small aperture should be very similar to that existing in the source housing close to the source. It was therefore decided to accept Costrell's results shown in Table 2.3 as a reasonable indication of the photon spectrum in the irradiation chamber.

IV Corrections for Absorption and Scattering of Photons in the Wall Material

Various theoretical corrections for absorption and scattering in the wall materials had been put forward (e.g. Mayneord and Roberts, 1939, Greening, 1957, Barnard, Axton and Marsh, 1959). The method of Barnard, Axton and Marsh was adopted here. They stated that after electronic equilibrium had been obtained, the change in the ionisation with increasing wall thickness could be accurately represented by an expression of the form

$$\exp\left\{-\left(\frac{\mu}{\rho}\right)X_e\right\}\left\{1+\sin\alpha X\right\}$$

where $\frac{\mu}{\rho}$ is the mass attenuation coefficient for the photons in the wall material, and X_e is the effective wall thickness of the chamber, allowance having been made for the curvature of the wall. X is the wall thickness of the chamber. $\exp\left\{-\left(\frac{\mu}{\rho}\right)X_e\right\}$ represents the decrease in the ionisation due to absorption of the primary photons, α being a scattering constant.

Thus the appropriate correction for absorption and scattering of photons in the wall material is

$$\frac{1}{\exp\left\{-\left(\frac{\mu}{\rho}\right)X_e\right\}\left\{1+\sin\alpha X\right\}}$$

Barnard, Axton and Marsh had calculated the percentage increase in the effective wall thickness of a cylindrical chamber. Their data are reproduced in Figure 2.12 and are used for determining the effective thickness (X_e) of the walls plus caps. The mass attenuation coefficient was weighted for Co^{60} gamma ray according to the percentage of the photon energy using Costrell's data in Table 2.3. Values of the mass attenuation coefficient obtained are shown in Table 2.4. The values of α were determined empirically by multiplying the primary photon attenuation curve $\left(\text{i.e. } \exp\left\{-\left(\frac{\mu}{\rho}\right)X_e\right\}\right)$ by the factor $(1 + \sin\alpha X)$, α being chosen so that the resulting curve closely fitted the experimental points. In general, a good fit was obtained by this technique as shown in Figures 2.13-2.17 where the points represent the experimental measurements and the lines the fitted curve. Table 2.5 gives the values of α obtained. The correction $\frac{1}{\exp\left\{-\left(\frac{\mu}{\rho}\right)X_e\right\}\left\{1+\sin\alpha X\right\}}$ was found for

the ionisation chambers with equilibrium wall thickness (Table 2.1) and are presented in Table 2.6 normalised on carbon.

In Chapter 5, a correction is made for absorption and scattering of photons in boxes containing perspex. These boxes have exactly the same equilibrium thickness as the ionisation chambers but their geometry is different. Nevertheless, it was assumed that the effective thickness of the wall, X_e, arising from the oblique incidence of the photons, was the same for these boxes, and therefore the corrections in Table 2.6 were applied to them.

V Measurements of Dose Rates Inside Co^{60} Irradiation Unit

Measurements of the absorbed dose rates at the centre of the irradiation unit were carried out using (a) ionisation chamber, (b) Fricke dosimeter, (c) perspex HX dosimeter. In the experiments, the dosimeters were supported by paper cylinders so that the centre of the dosimeter coincided with the centre of the irradiation chamber. All the measurements were corrected for decay of the Co^{60} source.

Va Measurement of the Absorbed Dose Rate Using an Ionisation Chamber

A cylindrical ionisation carbon chamber shown in Figure 2.9 was employed. Having determined the voltage, 360 volts, to give the plateau current from a I-V graph, the ionisation current in air at atmospheric pressure was measured with a vibrating reed electrometer for both polarising potentials. A small correction was made to the measured ionisation current for lack of saturation using an expression suggested by Greening (1954) which was based on Mie's theory (1904). Leakage current was measured before and after the experiment and was found to be negligible. The input resistor of the electrometer was calibrated by a capacity leak method and the voltage calibration was performed relative to a Weston standard cell. The average ionisation current thus obtained was 185×10^{-9} amps. The measured ionisation current was corrected for the attenuation of the photons in the wall by the method described in Section IV (viz., the method of Barnard et al). The correction factor for attenuation reduced the absorbed dose rate

throughout the volume of the ionisation chamber by 3.0 per cent. A correction was made for the non uniformity of the photon field in the region of the ionisation chamber but the average dose rate was in fact equal to the dose rate at the centre of the irradiation cell.

The value of the average energy expended per ion pair formed, W, recommended by the International Commission on Radiological Units and Measurements was adopted: $W = 33.73 eV$. The mass stopping power ratio of air to graphite, f, was calculated from Burlin's theory (see Chapter 3), using the photon spectrum given in Table 2.3. Suitable weighting was made for the photo-electric, Compton and pair-production processes and yielded a mass stopping power ratio of 0.998. These values were substituted in the Bragg-Gray equation

$$E_w = \frac{1}{f} \frac{WJ}{V\rho}$$

The maximum uncertainty in these parameters was estimated as

f: ± 1 per cent

W: ± 1 per cent

J= number of ion pairs formed (input resistor 1 per cent: potential drop 1 per cent): ± 2 per cent

V= volume of ionisation chamber: ± 1 per cent

ρ= density of air calculated to N.T.P.: ± 0.5 per cent.

Hence the absorbed dose rate in graphite at the centre of the irradiation cell was found to be 75.5 rads per second. The maximum error was 5.5 per cent and the most probable error 3 per cent.

Vb Measurement of the Absorbed Dose Rate Using a Fricke Dosimeter

The experimental procedure with the Fricke dosimeter is discussed in Chapter 3. The ferrous sulphate solution was placed in a cylindrical silica tube, closed at one end and was 10cm long and 0.6cm in diameter. An outer glass sheath enclosed the tube so as to ensure electronic equilibrium. The increase in optical density of ferrous sulphate solution due to the formation of ferric ions on irradiation was measured on a 'Uvispek' spectrophotometer at 305mμ. The irradiation

induced optical density averaged for four similar experiments was 0.157. The absorbed dose rate in ferrous sulphate is given by the equation (see Chapter 3)

$$\text{D rads per second} = \frac{N[\Delta(\text{O.D.})].100}{\Delta\epsilon.10^3 G(Fe^{3+}) f.\rho.\ell.t}$$

The maximum uncertainty in these parameters was estimated as

N = 6.023×10^{23} molecules per mole

Δ(O.D.) = increase in optical density: $\pm$ 1 per cent

$\Delta\epsilon$ = difference in molar extinction coefficients ($M^{-1}cm^{-1}$) of ferrous and ferric ions at 305mμ, $\Delta\epsilon$ = 2,197: $\pm$ 1 per cent.

G = the yield in Fe^{3+}. It increases slowly with photon energy between 0.1 to 16MeV (H. Fricke and E. J. Hart, 1966) and a value of 15.34 Fe^{3+} ions/100eV. was obtained by weighting according to the photon spectrum in the irradiation cell: $\pm$ 1 per cent.

f = 6.28×10^{13} eV/rad

ρ = density of ferrous sulphate , 1.024gm/c.c.: $\pm$ 0.1 per cent

ℓ = optical path length of cell used, 0.101cm: $\pm$ 1 per cent

t = time of irradiation, 542 seconds: $\pm$ 0.4 per cent.

Hence the absorbed dose rate in ferrous sulphate solution was 80 rads per second. This must be corrected for (1) effects of the silica wall which increase the response by 1.26 per cent (see Chapter 3), (2) the non uniformity of the photon field (section VI) which resulted in the average dose rate throughout the volume of the dosimeter being greater by 6.82 per cent than the dose rate at the centre of the irradiation cell, (3) the absorption of photons in the silica wall, which reduces the absorbed dose rate by 2.75 per cent (section IV). Thus the absorbed dose rate in ferrous sulphate solution was 76.0 rads per second. The maximum error was 4.5 per cent and the most probable error was 2.0 per cent.

Vc Measurement of Absorbed Dose Rate Using Perspex Dosimeter

Experimental details for using the perspex dosimeter are discussed in Chapter 4. The increase in optical density measured at 292mμ on a

'Uvispek' spectrophotometer, after four hours of irradiation of ten 0.1 × 1 × 4cm perspex pieces contained in a 1 × 1 × 4cm perspex box of sufficient thickness to establish electronic equilibrium, was found to be 0.32. Figure 2.18 shows the increase in optical density of the present batch of perspex with absorbed dose, measured four days after the irradiation by Co^{60} gamma rays. This data were obtained from the United Kingdom Panel on Gamma and Electron Irradiation. Since the optical density in this experiment was measured twenty four hours after irradiation, a correction was made for the fading which occurred four days after irradiation, 4.0 per cent (see Chapter 4). The dose rate was corrected for photon attenuation in the equilibrium wall (3.1 per cent) and for the non uniformity of the photon field 1.25 per cent. The absorbed dose rate in perspex was found to be 76.4 rads per second.

The maximum uncertainty in the parameters arising in this measurement was estimated as
Measured optical density: ± 1 per cent
Calibration data in Figure 2.18: ± 7 per cent.
The maximum error was 8 per cent and the most probable error 2.8 per cent.

Vd Exposure Rate from Ionisation Chamber, Fricke and Perspex Dosimeter Measurements

The absorbed dose rates obtained by the three methods were measured in different media (i.e. air, ferrous sulphate and perspex) and are therefore not directly comparable. The exposure rate at the centre of the irradiation cell may, however, be determined from each of these measurements. The relationship between the absorbed dose in a medium, D_m, in rad to the exposure ~~dose~~ X in roentgen is (ICRU 1964)

$$D_M = 0.869 \left[\frac{\left(\frac{\mu_{en}}{\rho}\right)_M}{\left(\frac{\mu_{en}}{\rho}\right)_{AIR}} \right] . X \qquad 2.5$$

The mass energy absorption coefficients appropriate to the photon spectrum in the irradiation cell are given in Table 2.7 and were used in this calculation. The values of the exposure rate found using equation

2.5 are given in Table 2.8. The three independent measurements of the exposure rate agree to within the limits of the experimental uncertainty. The grand mean was calculated as 81.0 roentgens per second and its precision index ± 1.2 roentgens per second (Worthing and Geffner, 1943). Thus, on 10th May, 1968, when the Co^{60} unit contained 2,447 curies of Co^{60} in the rods, the exposure rate at the centre of the irradiation cell was 81.0 ± 1.2 roentgens per second.

VI Dose Distribution in the Irradiation Chamber

VIa Calculation of the Dose Distribution

The dose rate in air, D_R, at a point, distant r cm from a point source emitting γ-rays is given (Hine and Brownell, 1956) by

$$D_R = \frac{\Gamma q}{r^2} \text{ rad per hour in air} \qquad 2.6$$

where Γ is the gamma ray dose rate constant. For Co^{60}, 1.25MeV gamma ray $\Gamma \triangleq$ (equals) 12.9 rad cm^2 per hour per millicurie (Rad. Dosimetry, 1968). q is the strength of the point source in millicuries at a distance 1cm away.

For a line source of length 'a' cm, the dose rate in air at a point is found by integrating over the length of the line,

$$D_R = \int_{x=0}^{x=a} \frac{\Gamma q}{a r^2}\, dx \text{ rad per hour}$$

$$= \frac{\Gamma q}{ah}\left[\tan^{-1}\left(\frac{b}{h}\right) + \tan^{-1}\left(\frac{a-b}{h}\right)\right] \qquad 2.7$$

h is the perpendicular distance from the point to the line source. b is part of the line source between one end and the foot of the perpendicular.

Figure 2.19 shows a horizontal cross section of the irradiation chamber; and the positions of the twenty equally spaced Co^{60} rods are denoted by A, B, C . . . , T. Seven concentric circles, each of increasing radius of 1cm are drawn. Take a point X such that it lies on the fourth circle and at a known height from the base of the Co^{60}

rods. The distance h in equation 2.7 is equivalent to the distance XA, XB, . . . , XT in Figure 2.19. These distances are expressed as

$$XA = \sqrt{\{R^2 + n_4^2 - 2Rn_4 \cos(0.3142i)\}}$$

where R is the distance from the centre of the chamber to the rods, R being constant. n_4 is the radius of the fourth circle (i.e. n_4 = 4cm). i is an integer depending on the angle subtended at the centre, i takes the value from i = 1, 2, 3, ...20.

Summing the contribution from the twenty sources obtained from equation 2.7, the dose rate at the point X was obtained. The exact strength of each rod was used in the calculations which were normalised at the centre of the irradiation chamber. The isodose curves are plotted and shown in Figure 2.20.

Since the rods have a diameter of 0.95cm and are encapsulated by a stainless steel sheath, self absorption (Evans and Evans, 1948) and wall absorption have to be accounted for if the absorbed dose is to be determined. However, these corrections will be identical for each source and will not affect the dose distribution.

Scattered radiation presents a more difficult problem. Accurate calculation of the scattered radiation in these 'broad beam' situations is rather complex and is treated by Fano et al (1959). A simplified way of estimating the scattered radiation is discussed in Section III. The energy of the scattered radiation is estimated as about 0.41MeV and the percentage contribution to the total observed dose rate by the scattered radiation is estimated as 19 per cent. Much of this scattered radiation will originate in the sources and the rest will either pass through the sources or originate close to them. It is therefore a close approximation to regard all the scattered radiation as having a point of origin within the sources, and to apply the same equation for calculating the dose distribution arising from both the primary and scattered photons.

VIb Measurement of the Dose Distribution

A perspex dosimeter is used to investigate the dose distribution.

The experimental technique of using perspex is described in Chapter 4, the size of the perspex used being 0.1 × 1 × 4cm. Seven of these pieces were placed in a perspex holder, standing vertically, having a wall thickness of 0.3cm to ensure electronic equilibrium. This was mounted on a base which permitted rotary and radial movement so that the holder could be placed at various positions in the irradiation chamber. Table 2.9 represents part of the experimental results. The experimental points and isodose curves, normalised at the centre of the irradiation chamber, are presented in Figure 2.21. The comparison between the calculation and measurement of the dose distribution is shown in Figure 2.22 and the agreement is considered good.

Table 2.1. Data for Wall Thicknesses and Purities of Cylindrical Ionisation Chambers

Material	Thicknesses mm	Percentage Purity
Carbon	2.5	99.90
Aluminium	1.7	99.85
Copper	1.0	99.85
Tin	1.1	99.90
Lead	0.8	99.90

Table 2.2. Scattered Incident Radiation Intensity as a Percentage of Total Incident Radiation Intensity for Co^{60} source

Combination of Materials	% obtained using calculated $\frac{\mu_{en}}{\rho}$ and fw(T_γ) values		% obtained using Burlin's experimental {(I)1.25 and (I)0.41} values	
	1.25 MeV	0.41 MeV	1.25 MeV	0.41 MeV
C, Al	93.1	6.9	68.4	31.57
C, Cu	74.9	25.1	87.1	12.9
C, Su	68.6	31.4	78.0	22.0
C, Pb	88.9	11.1	88.0	12.0
Mean	81.4	18.6	80.4	19.6

Table 2.3. Scattered Incident Radiation Intensity as a Percentage of Total Incident Radiation Intensity (Costrell 1962) for Co^{60} source

Energy (MeV)	1.25-1.0	1.0-0.8	0.8-0.6	0.6-0.4	0.4-0.2	0.2-0
Percentage	85.4	3.8	3.7	3.8	2.6	0.74

Table 2.4. Mass Attenuation Coefficients weighted according to Costrell's (1962) spectrum

Eo	Attenuation Coefficients of Materials (cm^2/gm)				
(MeV)	C	Al	Cu	Sn	Pb
0.1-1.25	.061	.0599	.0595	.0686	.1153

Table 2.5. Scattering constants, α, for use in the Equation of Barnard et al for Co^{60}. Units are arbitrary

Materials	Carbon	Aluminium	Copper	Tin	Lead
α	4.750	8.267	36.040	19.934	61.021

Table 2.6. Correction factors for absorption and scattering in chamber walls for Co^{60}

Materials	Carbon	Aluminium	Copper	Tin	Lead
Correction Factors	1.00	.9981	.9984	1.0301	1.0787

Table 2.7. Values of Mass Energy Absorption Coefficients, $\frac{\mu_{en}}{\rho}$ appropriate to the photon spectrum in the Irradiation Chamber

Material	Carbon	Air	Ferrous Sulphate	Silica	Perspex
$\frac{\mu_{en}}{\rho}$ (cm^2/gm)	0.0287	0.0271	0.0296	0.0265	0.0289

Table 2.8. Measurement of Absorbed and Exposure Dose Rates Using Various Dosimeters

Dosimeters	Absorbed Dose Rate (rad/sec)	Maximum Error (per cent)	Most Probable Error (per cent)	Exposure Rate (R/sec)
Ionisation chamber	75.5 in carbon	5.5	3.0	82.0
Ferrous Sulphate	76.0 in ferrous sulphate	4.5	2.0	80.0
Perspex	76.4 in perspex	8.0	2.8	82.4

Table 2.9. Dose Distribution in Co^{60} irradiation chamber

Position (m.m.)		O.D./m.m. at 292mμ	(O.D.)292 NOR.	(O.D./m.m. at 305mμ	(O.D.)305 NOR.	Av. NOR. O.D. i.e. ½(col.4 + col.6)
Vertical	Radial					
16	0	.1581	86.7	.1206	83.9	85.3
36	0	.1693	92.8	.1296	90.2	91.5
56	0	.1798	98.6	.1443	100.4	99.5
76	0	.1824	100.0	.1437	100.0	100.0
96	0	.1828	100.2	.1437	100.0	100.1
116	0	.1660	91.0	.1336	93.0	92.0
136	0	.1580	86.6	.1253	87.2	86.9
16	10	.1561	85.6	.1213	84.4	85.0
36	10	.1713	93.9	.1338	93.1	93.5
56	10	.1809	99.2	.1437	100.0	99.6
76	10	.1828	100.2	.1471	102.4	101.3
96	10	.1811	99.3	.1418	98.7	99.0
116	10	.1689	92.6	.1354	94.2	93.3
136	10	.1499	82.2	.1216	84.6	83.4
16	20	.1561	85.6	.1270	88.4	87.0
36	20	.1738	95.3	.1361	94.7	95.0
56	20	.1835	100.6	.1440	100.2	100.3
76	20	.1860	102.0	.1494	104.0	103.0
96	20	.1875	102.8	.1471	102.4	102.6
116	20	.1720	94.3	.1367	95.1	94.7
136	20	.1591	87.2	.1239	86.2	86.7

Table 2.9. contd. Dose Dostribution in Co^{60} irradiation chamber

Position (m.m)		O.D./m.m. at 292mμ	(O.D.)292 NOR.	(O.D./m.m. at 305mμ	(O.D.)305 NOR.	Av. NOR. O.D. i.e. $\frac{1}{2}$(col.4 + col.6)
Vertical	Radial					
16	30	.1642	90.0	.1299	90.4	90.2
36	30	.1749	95.9	.1415	98.5	97.2
56	30	.1917	105.1	.1507	104.9	105.0
76	30	.1937	106.2	.1543	107.4	106.8
96	30	.1926	105.6	.1509	105.0	105.3
116	30	.1751	96.0	.1411	98.2	97.1
136	30	.1603	87.9	.1280	89.1	88.5
16	40	.1700	93.2	.1319	91.8	92.5
36	40	.1882	103.2	.1497	104.2	103.7
56	40	.2019	110.7	.1588	110.5	110.6
76	40	.2043	112.0	.1625	113.1	112.6
96	40	.1985	108.8	.1609	112.0	110.4
116	40	.1893	103.8	.1493	103.9	103.9
136	40	.1658	90.9	.1315	91.5	91.2
16	50	.1773	97.2	.1390	96.7	97.0
36	50	.1988	109.0	.1581	110.0	109.5
56	50	.2167	118.8	.1719	119.6	119.2
76	50	.2216	121.5	.1759	122.4	122.0
96	50	.2189	120.0	.1729	120.3	120.2
116	50	.2033	110.9	.1609	112.0	111.5
136	50	.1751	96.0	.1395	97.1	96.6

Table 2.9. contd. Dose Distribution in Co^{60} irradiation chamber

Position (m.m)		O.D./m.m. at 292mμ	(O.D.)292 NOR.	(O.D./m.m. at 305mμ	(O.D.)305 NOR.	Av. NOR. O.D. i.e. $\frac{1}{2}$(col.4 + col.6)
Vertical	Radial					
16	60	.1924	105.5	.1512	105.2	105.4
36	60	.2187	119.9	.1733	120.6	120.3
56	60	.2307	126.5	.1811	126.0	126.3
76	60	.2318	127.1	.1847	128.5	127.8
96	60	.2311	126.7	.1818	126.5	126.6
116	60	.2218	121.6	.1768	123.0	122.3
136	60	.1977	108.4	.1552	108.0	108.2
16	70	.2026	111.1	.1638	114.0	112.6
36	70	.2304	126.3	.1831	127.4	126.8
56	70	.2389	131.0	.1898	132.1	131.6
76	70	.2455	134.6	.1953	135.9	135.3
96	70	.2397	131.4	.1880	130.8	130.6
116	70	.2316	127.0	.1841	128.1	127.6
136	70	.2225	122.0	.1727	120.1	121.6

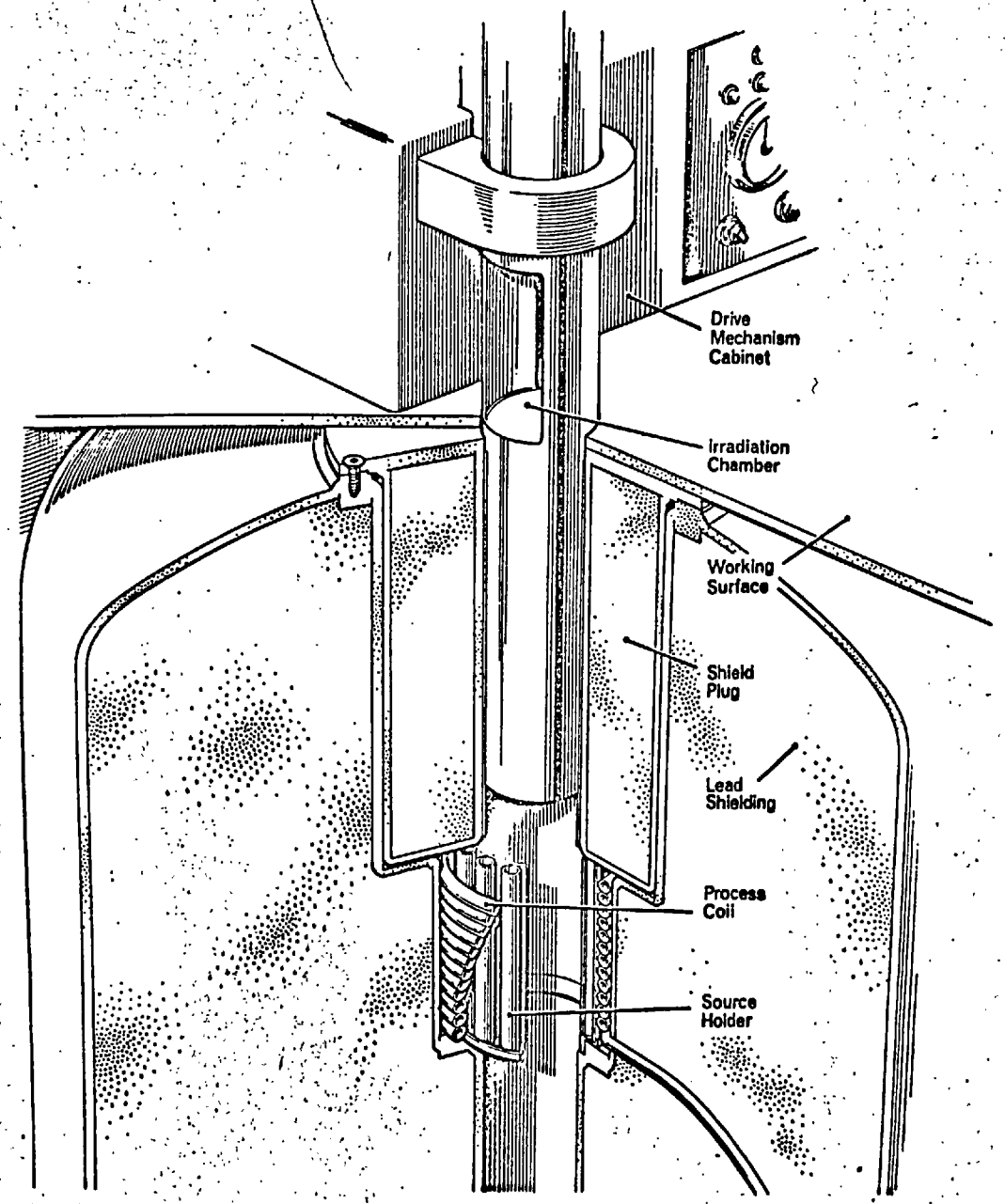

FIG. 2.1. SECTION THROUGH Co^{60} IRRADIATION UNIT.

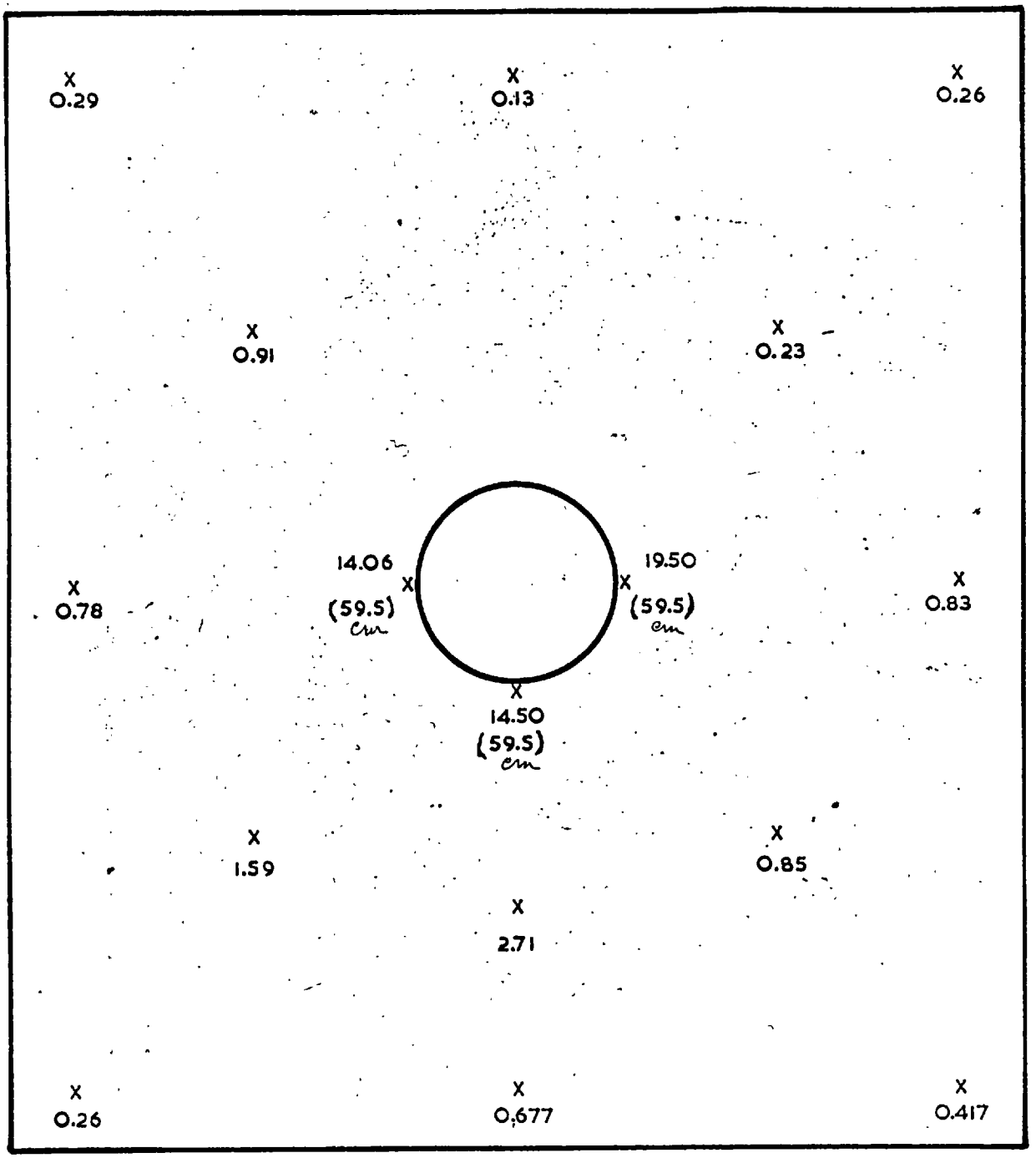

FIG. 2.2. MEASUREMENTS OF LEAKAGE RADIATION, MILLIROENTGEN/HOUR, ON TABLE TOP OF Co^{60} UNIT. TOTAL SOURCE STRENGTH 3,078 CURIES (1.8.1966). SCALE 1:6

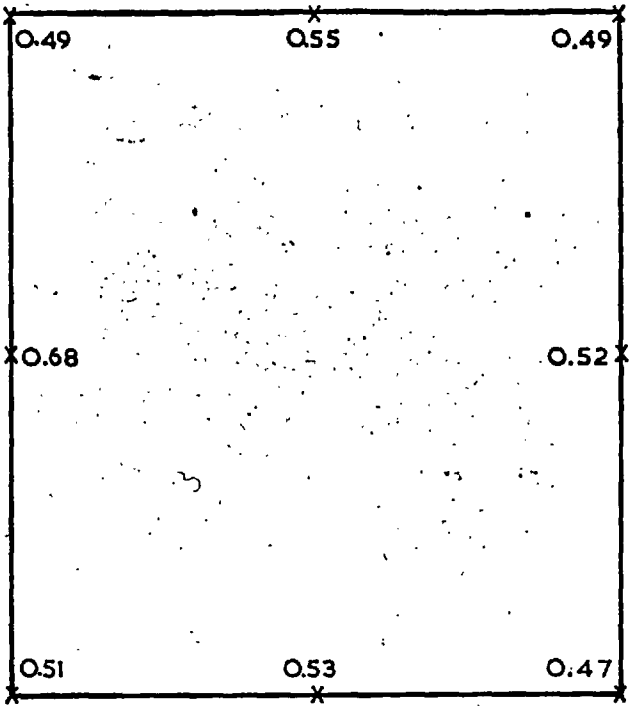

FIG. 2.3. MEASUREMENT OF LEAKAGE RADIATION, MILLIROENTGEN/HOUR, AT THE BASE OF Co^{60} IRRADIATION UNIT. TOTAL SOURCE STRENGTH 3,078 CURIES (1.8.1966). SCALE 1 : 12

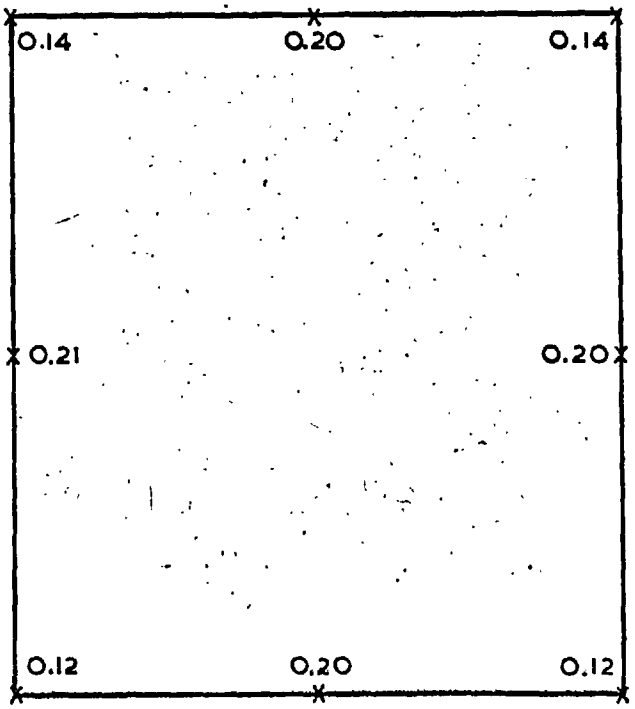

FIG. 2.4. MEASUREMENT OF LEAKAGE RADIATION, MILLIROENTGEN/HOUR, AT A DISTANCE 60cm FROM BASE OF Co^{60} IRRADIATION UNIT. TOTAL SOURCE STRENGTH 3,078 CURIES (1.8.1966). SCALE 1 : 12

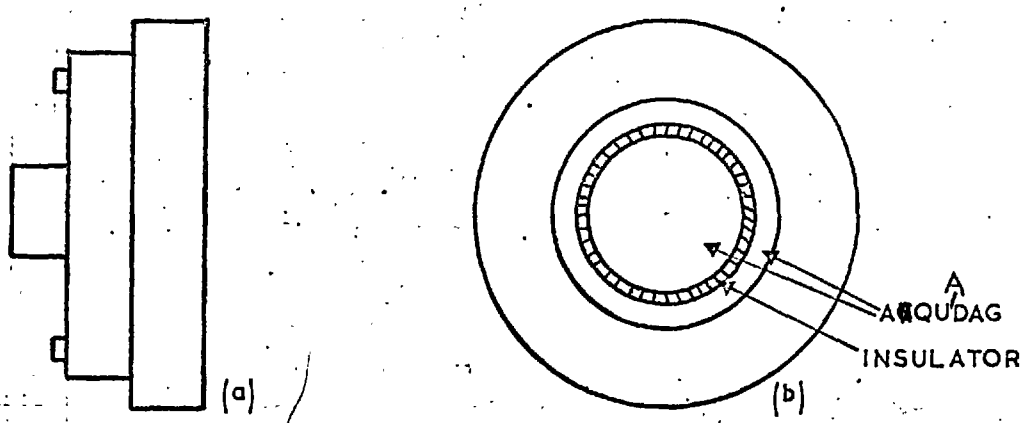

FIG. 2.5 (a) SIDE VIEW (b) FRONT VIEW OF ELECTRON DETECTOR. (FULL SCALE).

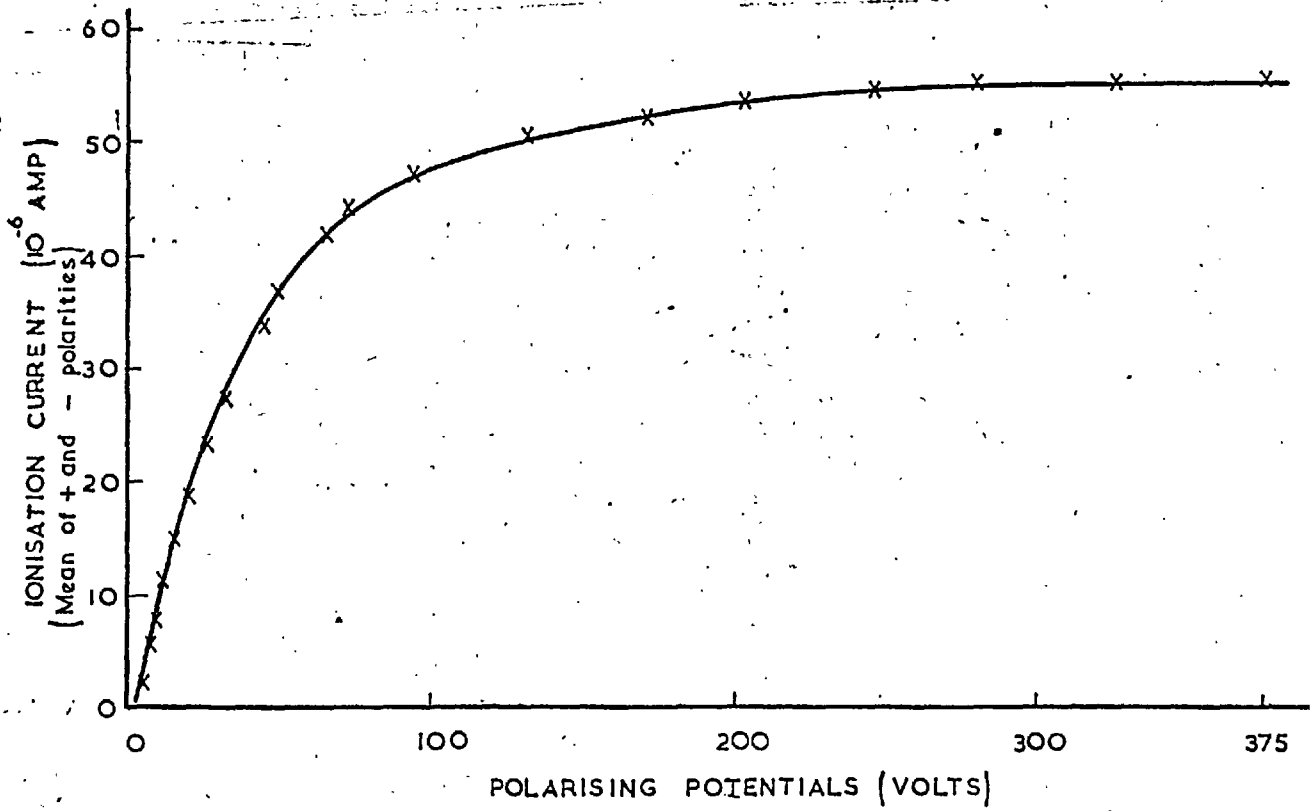

FIG. 2.6 SATURATION CURVE FOR ELECTRON DETECTOR.

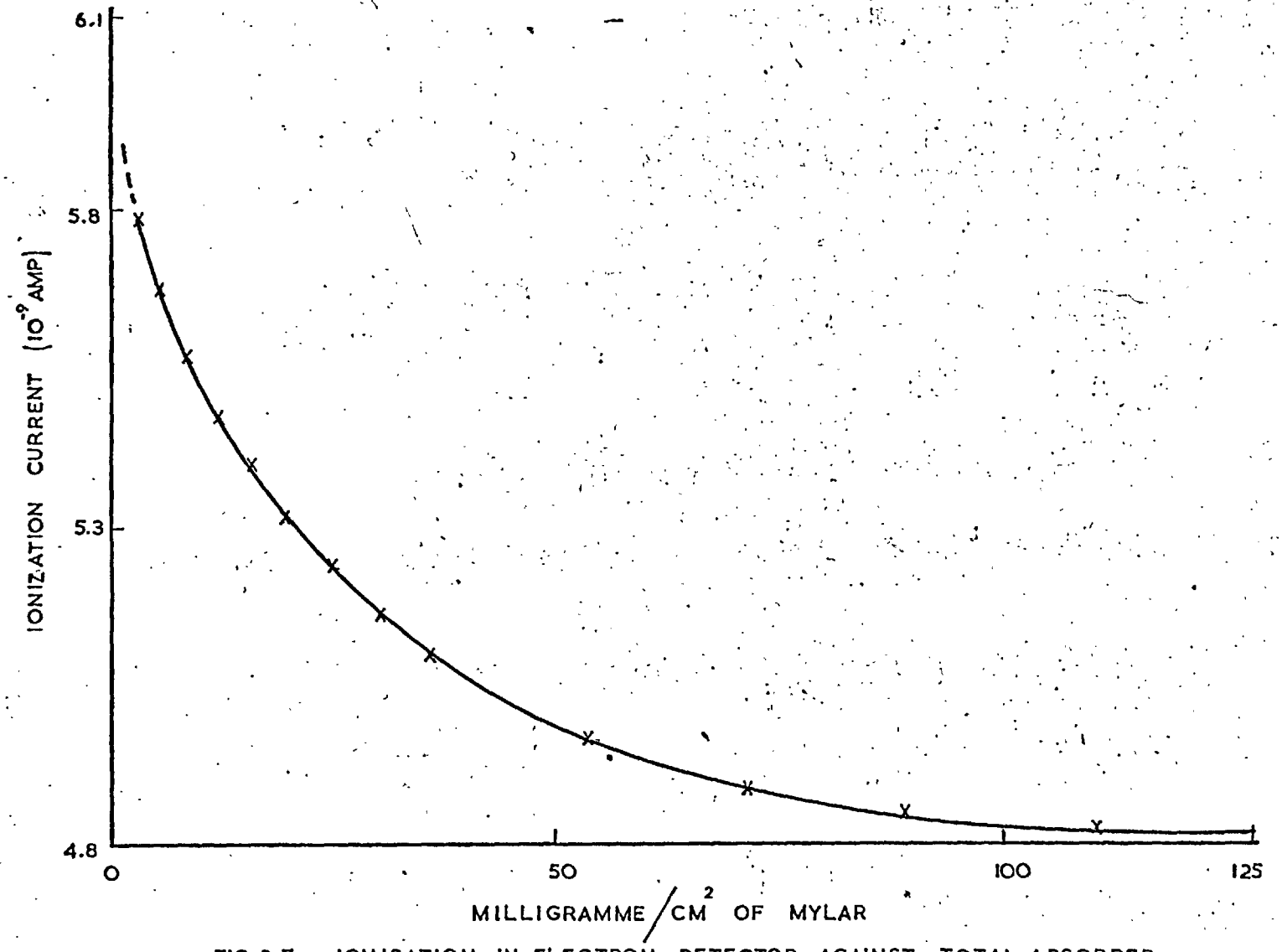

FIG 2.7. IONISATION IN ELECTRON DETECTOR AGAINST TOTAL ABSORBER THICKNESS.

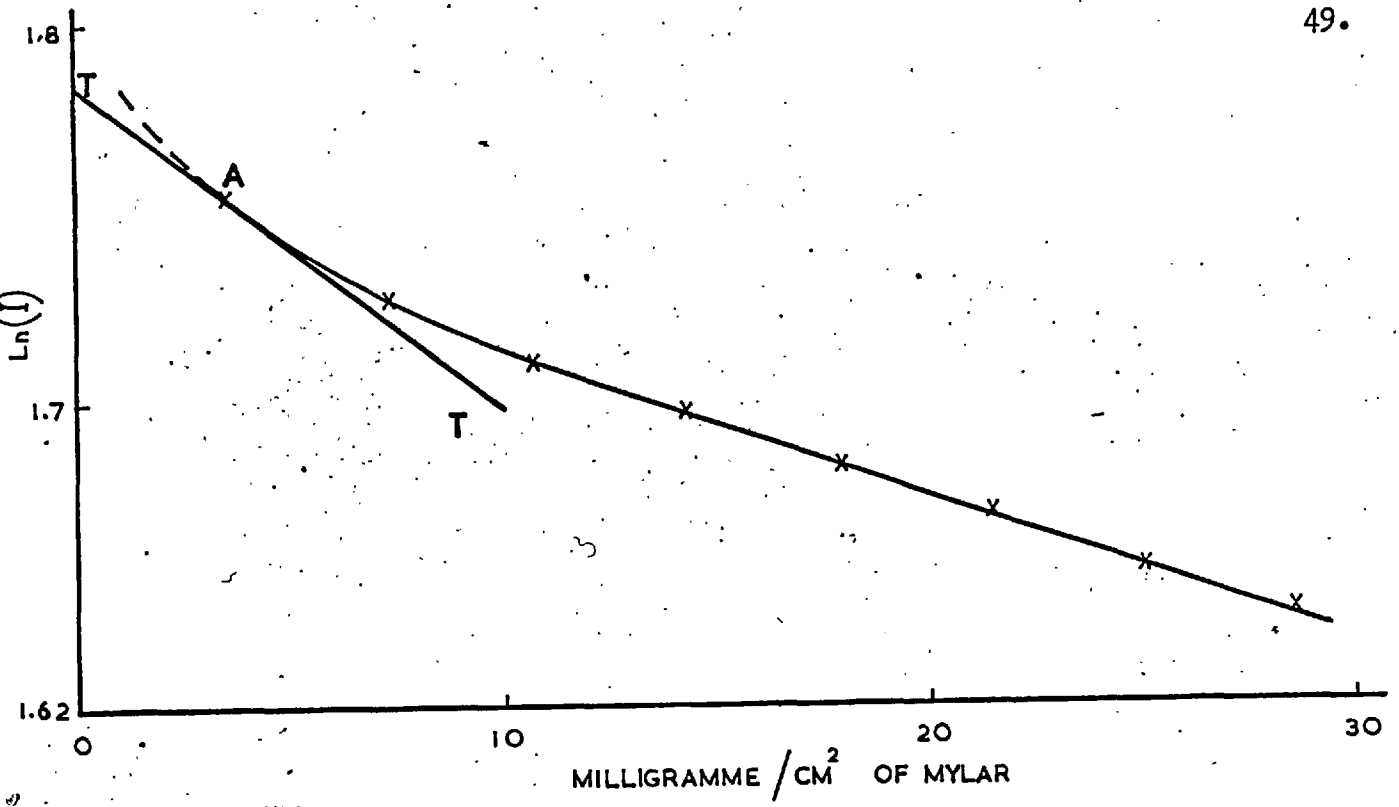

FIG 2.8. LOGARITHM OF THE IONIZATION IN ELECTRON DETECTOR AGAINST TOTAL ABSORBER THICKNESS.

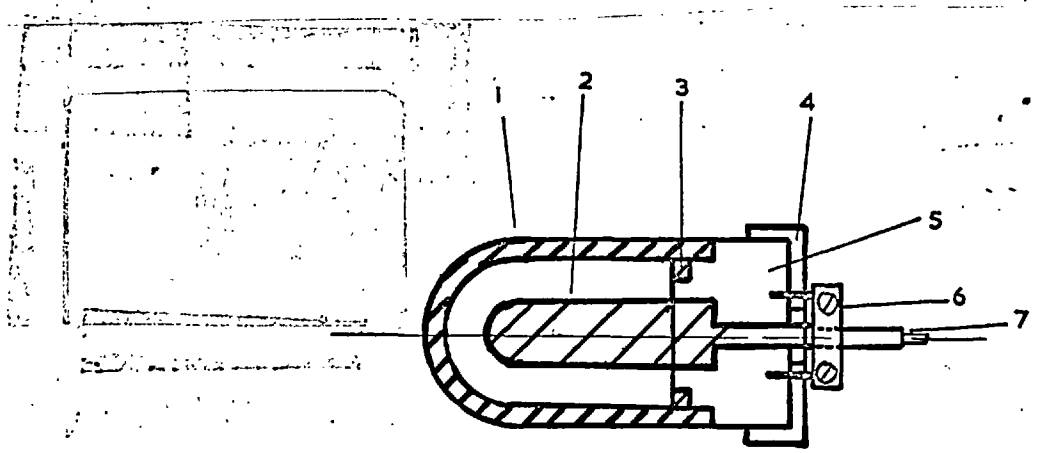

FIG. 2.9. SECTION THROUGH CYLINDRICAL IONIZATION CHAMBER. (TO SCALE)

KEY.

1. H.T.
2. COLLECTOR.
3. RING OF WALL MATERIAL.
4. EARTHING CAP.
5. INSULATOR.
6. CABLE CLAMP AND EARTHING POINT ASSEMBLY.
7. CO-AXIAL CABLE.

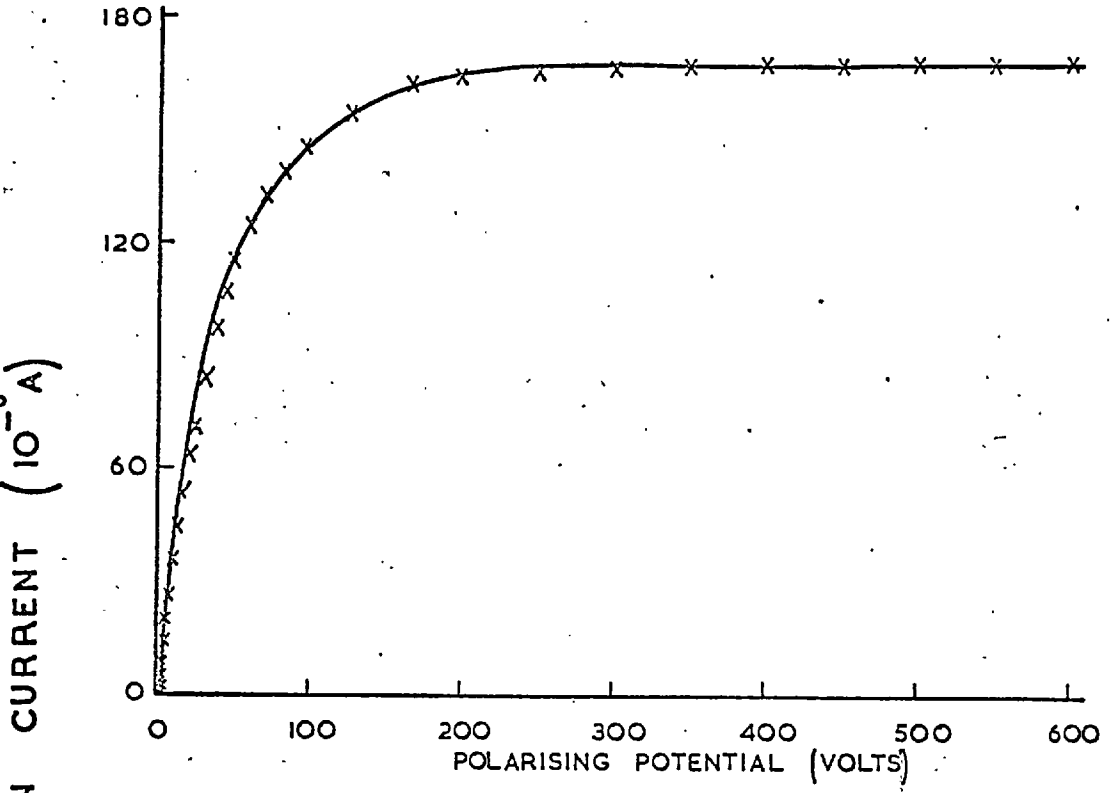

FIG. 2.10. SATURATION CURVE FOR AIR IN CYLINDRICAL IONIZATION CARBON CHAMBER.

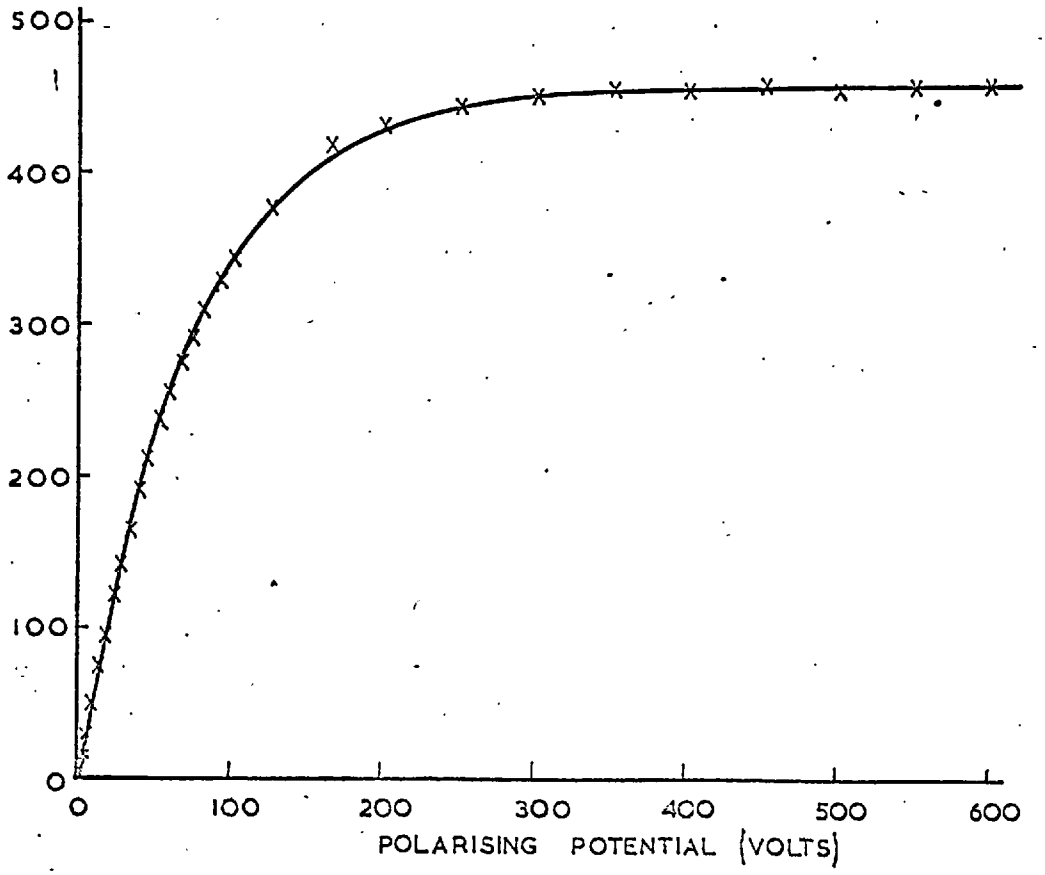

FIG. 2.11. SATURATION CURVE FOR AIR IN CYLINDRICAL IONISATION LEAD CHAMBER.

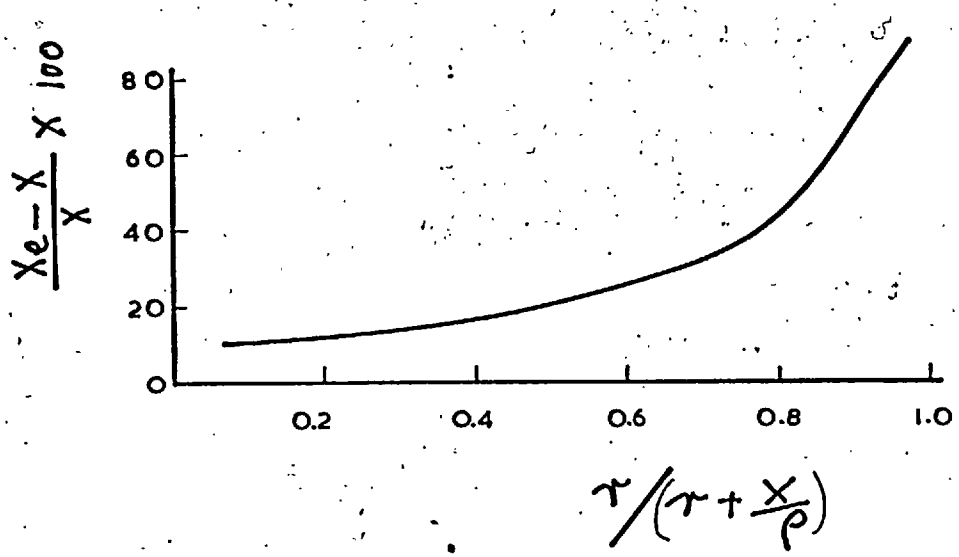

FIG. 2.12

FIG. 2.12. RELATING THE PERCENTAGE INCREASE IN THE EFFECTIVE WALL THICKNESS OF A CYLINDRICAL CHAMBER TO $\left(r/\left[r+\frac{X}{\rho}\right]\right)$.

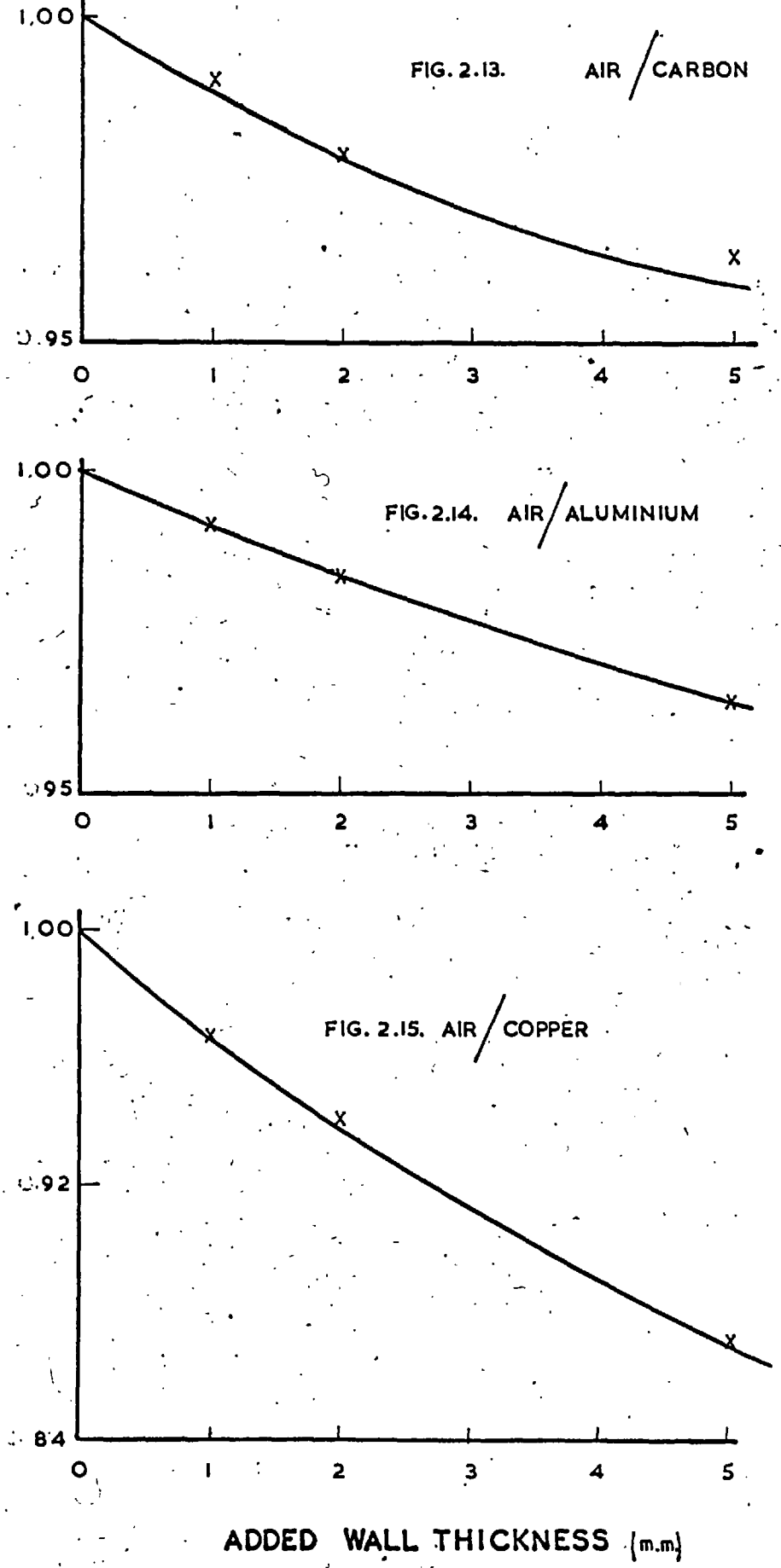

FIG. 2.13. AIR / CARBON

FIG. 2.14. AIR / ALUMINIUM

FIG. 2.15. AIR / COPPER

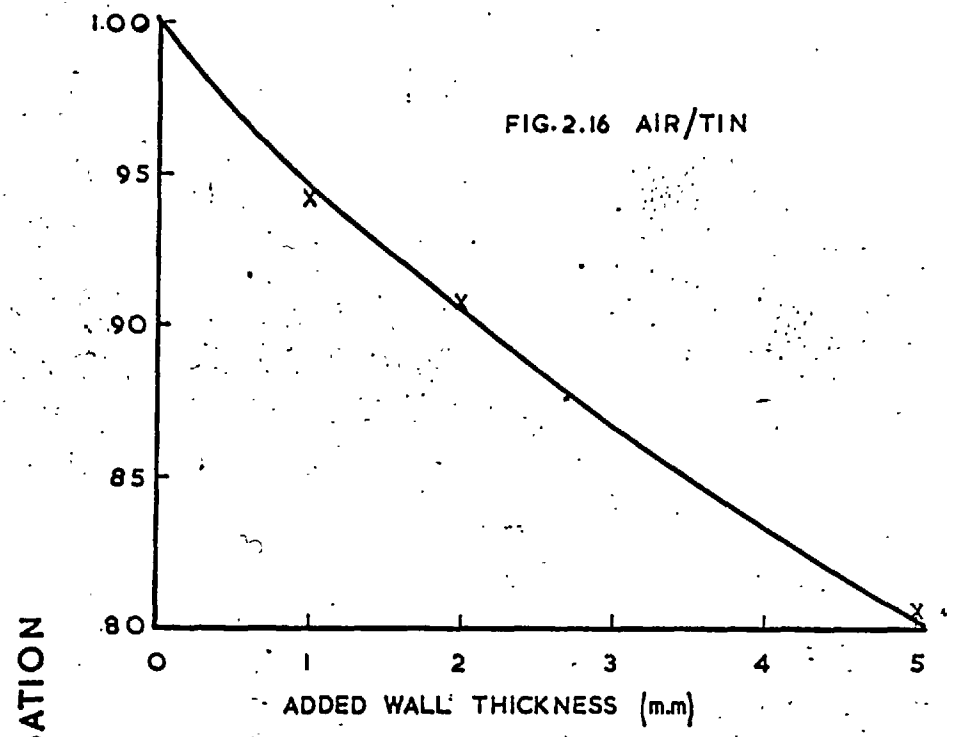

FIG. 2.16 AIR/TIN

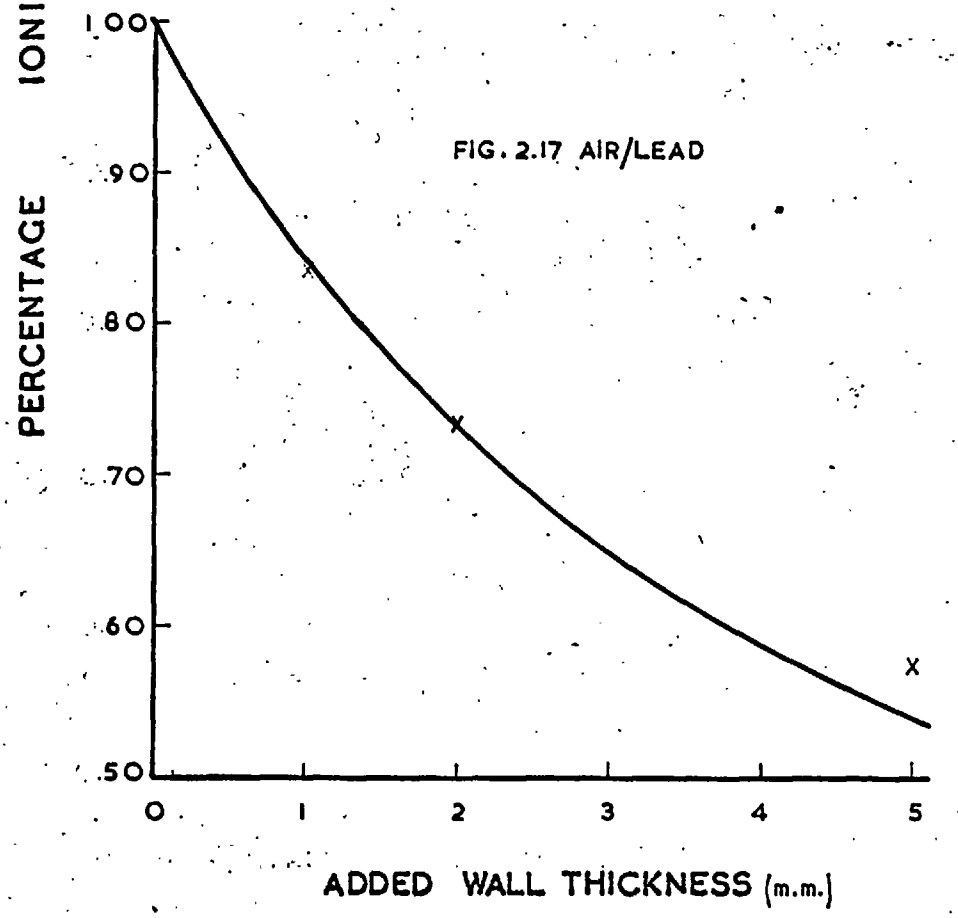

FIG. 2.17 AIR/LEAD

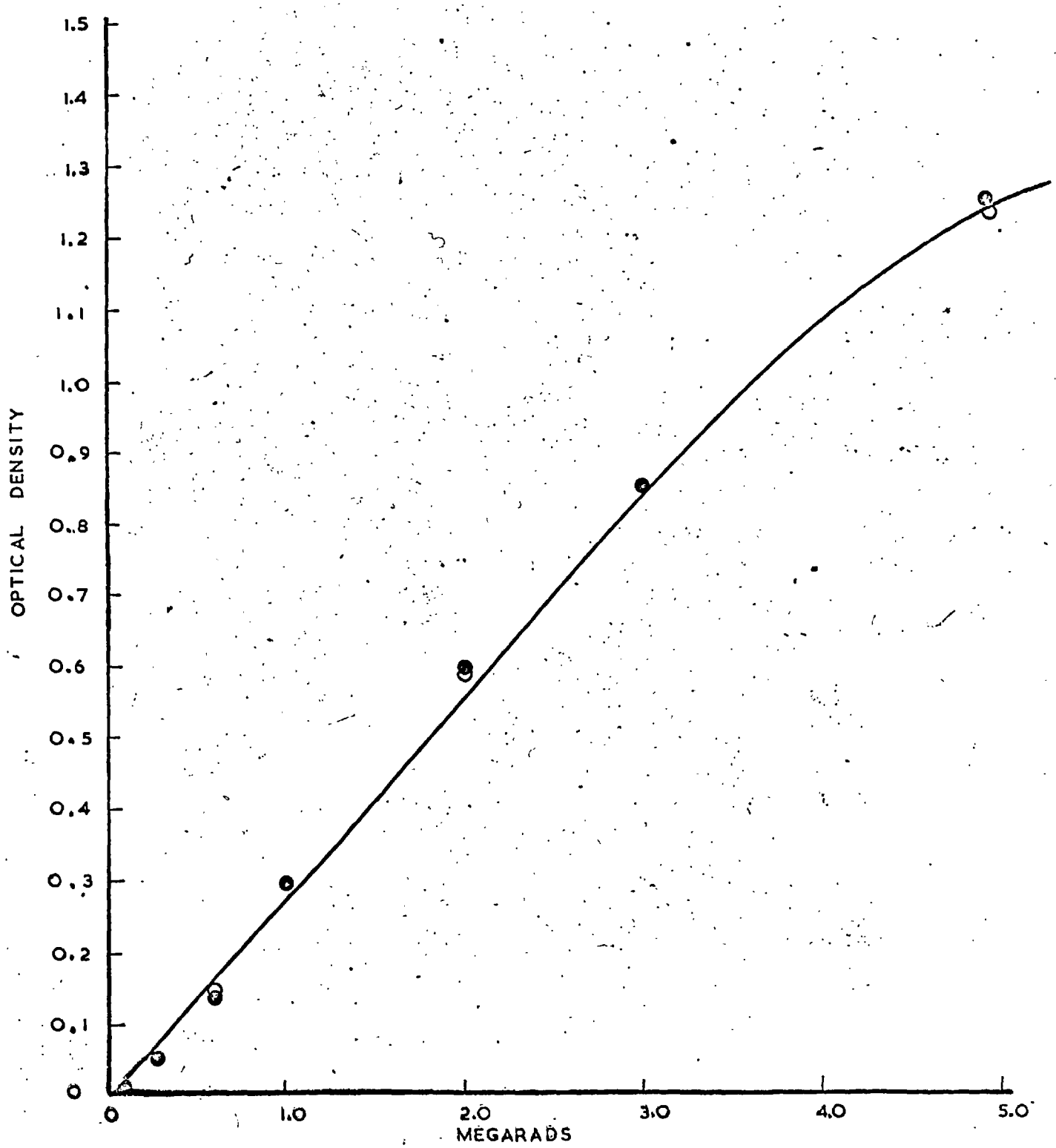

FIG. 2.18. OPTICAL DENSITY AT 292 mμ VERSUS ABSORBED DOSE FOR 0.1cm THICK PERSPEX PIECE. READ FOUR DAYS AFTER IRRADIATION. ○, ● TWO LABORATORIES Co^{60} IRRADIATION.

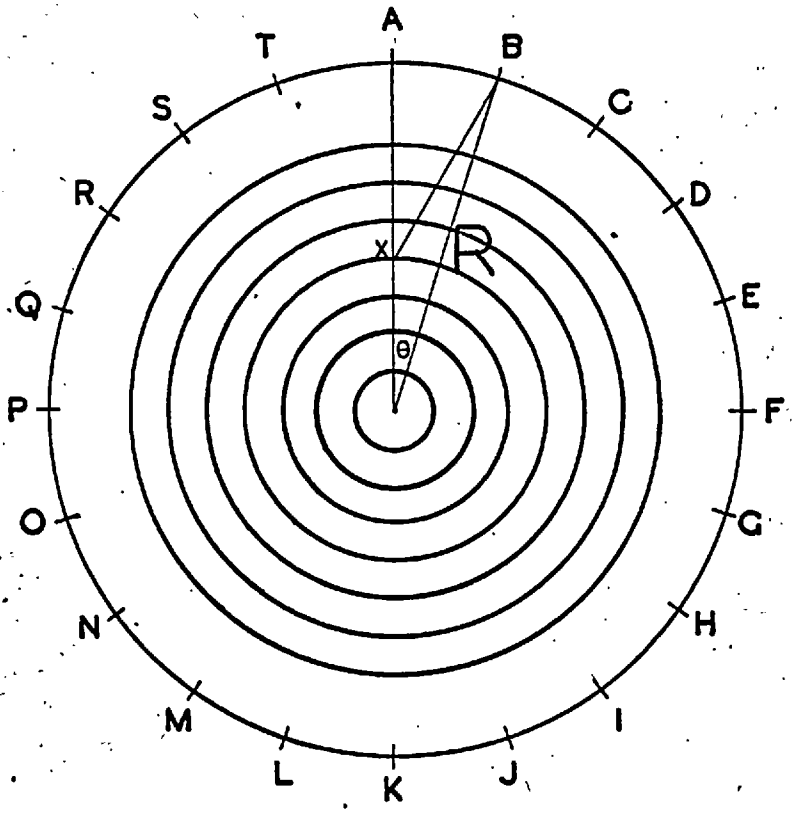

FIG. 2.19. DIAGRAMMATIC REPRESENTATION OF THE LOCATING OF THE POSITION OF A POINT 'X' IN THE IRRADIATION CHAMBER FROM THE Co^{60} RODS A,B,C ____T. TOTAL SOURCE STRENGTH 3,078 CURIES (1.8.1966).

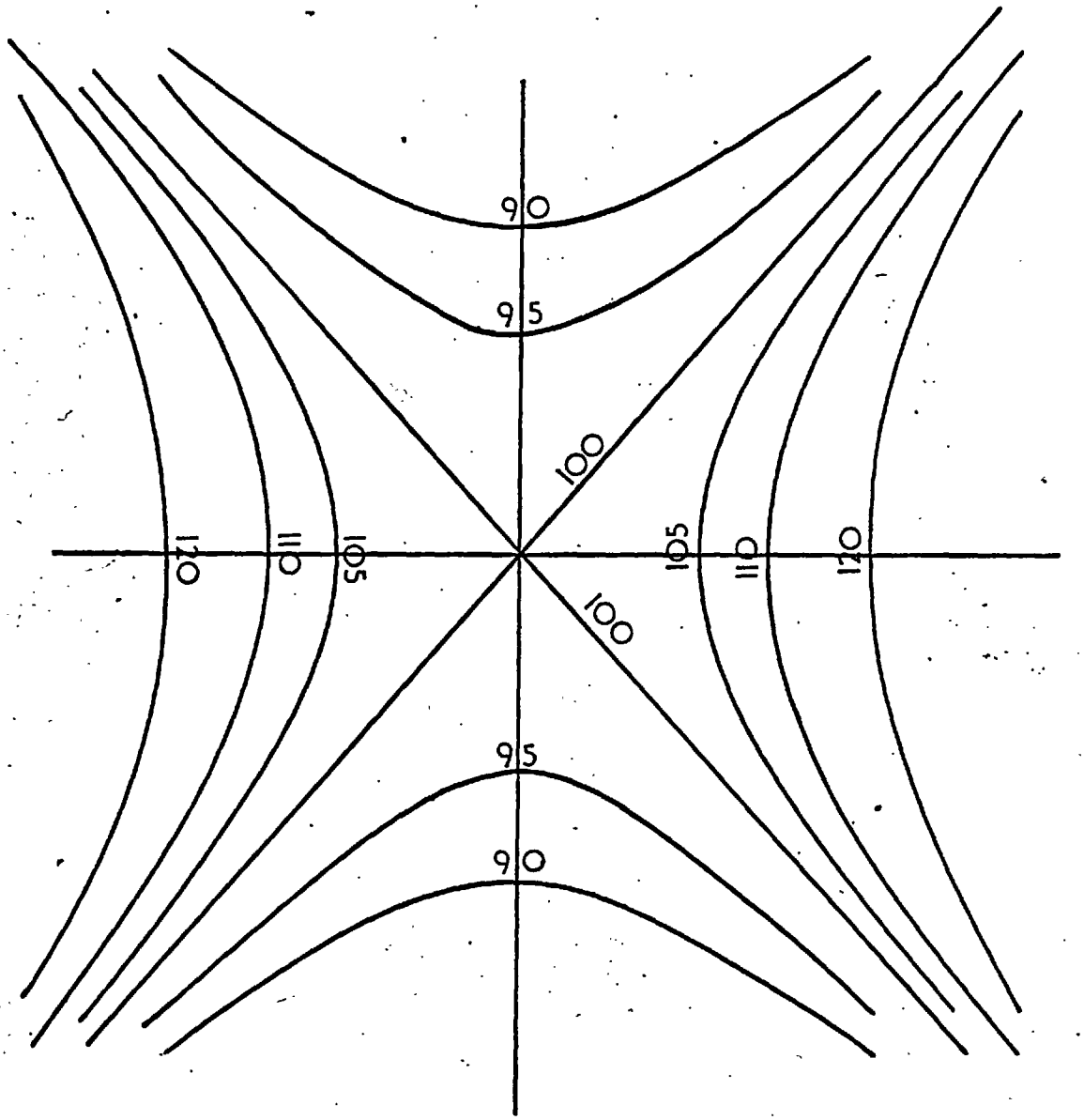

FIG. 2.20. CALCULATION OF DOSE DISTRIBUTION INSIDE Co^{60} IRRADIATION CHAMBER. THE ISODOSE CURVES ARE NORMALISED AT CENTRE OF IRRADIATION CHAMBER.

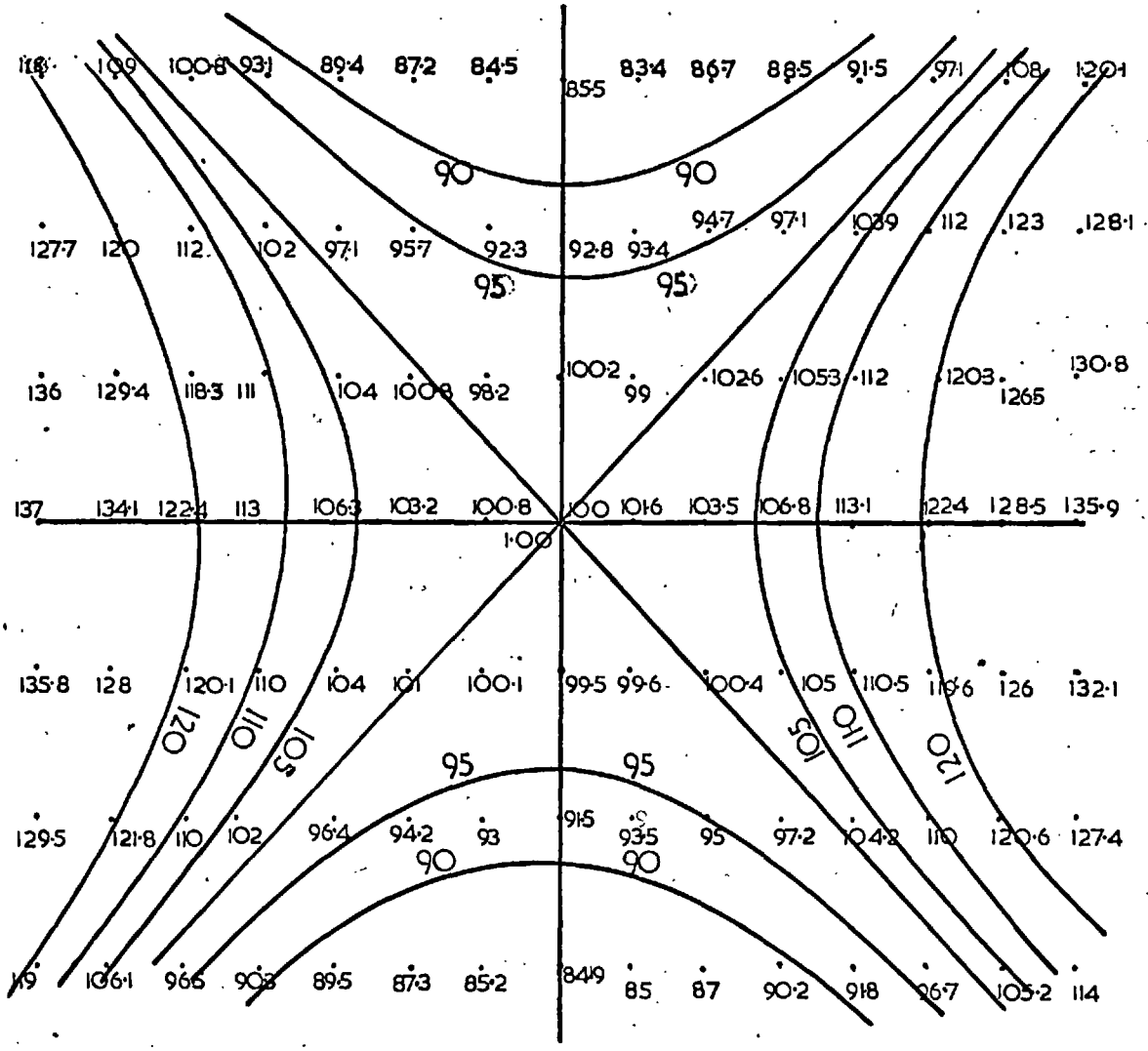

FIG. 2.21. MEASUREMENT OF DOSE DISTRIBUTION INSIDE Co^{60} IRRADIATION CHAMBER USING 0.1cm PERSPEX. THE EXPERIMENTAL POINTS AND ISODOSE CURVES ARE NORMALISED AT CENTRE OF IRRADIATION CHAMBER.

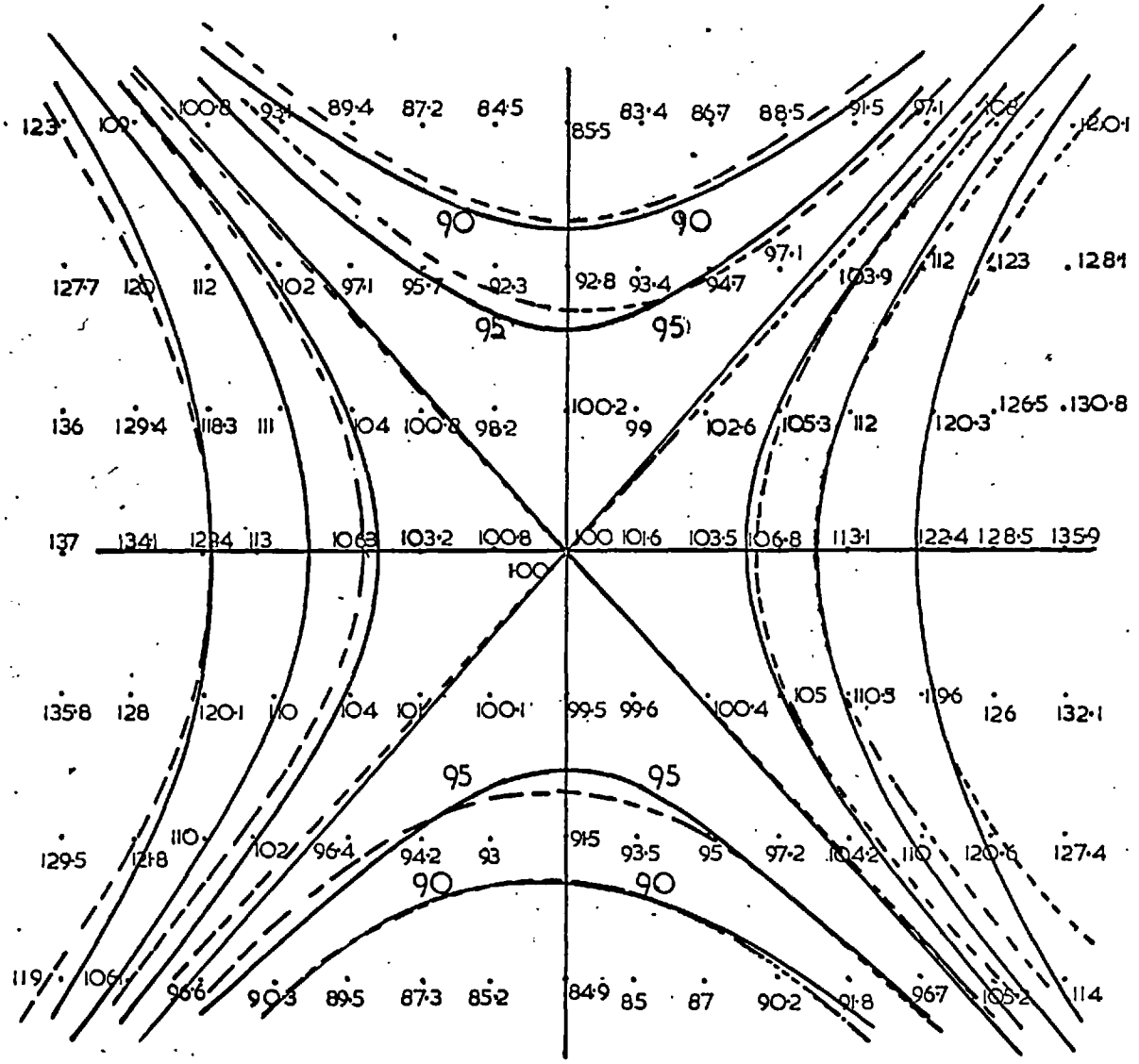

FIG. 2.22. COMPARISON OF THE ISODOSE CURVES OBTAINED BY CALCULATION (SOLID LINES) AND BY MEASUREMENTS (BROKEN LINES) INSIDE Co^{60} IRRADIATION CHAMBER.

CHAPTER 3

THE EXPERIMENTAL EXAMINATION OF GENERAL CAVITY THEORY APPLIED TO A LIQUID STATE DOSIMETER

I. Introduction

The use of liquid dosimeters, in particular the ferrous sulphate dosimeter, is now widely established. A great advantage of liquid dosimeters over gas or solid dosimeters is that the liquid can be prepared from reagents which are water or tissue equivalent in respect to density and atomic number. It therefore absorbs ionising radiation in a manner more similar to body tissues than those of gaseous or solid systems.

The aims of the experiments with a liquid dosimeter described in this chapter are, (1) to test Burlin's general theory of cavity ionisation when applied to a liquid state dosimeter, (2) to provide an experimental and theoretical treatment for the 'wall effects' (Weiss, (1952), Weiss et al (1955)) of the vessel which have been frequently commented on in the literature.

II Requirements for a Liquid Dosimeter

When a beam of ionising radiation passes through a liquid medium, chemical changes occur. If the chemical changes can be measured then the liquid system can be used for dosimetry. Ideally, any liquid used as a dosimeter would have the following properties.

(a) The response should be proportional to the absorbed dose irrespective of the nature of the incident radiation.

(b) The final product after irradiation should be stable and accurately measurable. The reproducibility of any measurement should be better than 1 per cent.

(c) The solution should be prepared easily, and should be stable, having a reasonable shelf life and not varying significantly with temperature and pressure.

There are at present no liquid systems that meet all the above requirements completely. The ferrous sulphate dosimeter was chosen

for these experiments because it fulfils most of the conditions stated above. In particular the repetition accuracy was stated to be better than 1 per cent, which was an essential requirement in this work where the differences in response with dosimeter size were only expected to be a few per cent.

III General Principles of the Ferrous Sulphate Dosimeter

IIIa Preparation of Ferrous Sulphate Solution

The standard ferrous sulphate dosimeter contains 1mM ferrous ammonium sulphate, 1m M sodium chloride (to counteract the effect of possible organic impurities) and usually 0.8N sulphuric acid. It is made up to 1 litre using water triply-distilled from acid dichromate and alkaline permanganate solutions in an all-glass system. The chemicals were of analytical grade (ICRU, 1964).

IIIb Chemical Interactions in Ferrous Sulphate Solution

The oxidation of ferrous ions to ferric ions on irradiation with ionising particles was found to be linearly proportional to the absorbed dose (Fricke and Morse, 1929, Miller 1950). It has been known as the Fricke dosimeter. Improvements have been made by Dewhurst (1951) and Weiss et al (1955) who suggested that an amount of chloride ions should be added to the solution in order to neutralise the effect of possible organic impurities in the water. Hardwick (1952) found that the ferric ion so formed by oxidation should be measured at a wavelength of 305mμ which represents the absorption peak of the ferric product.

The mechanism of the reaction in ferrous sulphate is now understood through the work of Weiss (1955) on free radical theory, Allen (1952) on aqueous system and Allen et al (1957). Complications in the chemical reactions arise at very high dose rates (10^8rad/sec). A simplified account of the chemical reactions of ferrous sulphate solution in 0.8N sulphuric acid, receiving a dose less than 10^6 rad/sec, is given in the following paragraph.

The water molecules in the solution decompose into H_2 and H_2O_2

molecules and simultaneously H and OH radicals are also formed, i.e.

$$2H_2O \longrightarrow H_2 + H_2O_2 \quad . \quad . \quad . \quad . \quad . \quad (3.1)$$

$$H_2O \longrightarrow H + OH \quad . \quad . \quad . \quad . \quad . \quad (3.2)$$

The molecules and radicals so formed in turn oxidise Fe^{2+} to Fe^{3+} according to the following equations

$$Fe^{2+} + OH \longrightarrow Fe^{3+} + OH^- \quad . \quad . \quad . \quad . \quad . \quad (3.3)$$

$$H + O_2 \longrightarrow HO_2 \quad . \quad . \quad . \quad . \quad . \quad (3.4)$$

$$Fe^{2+} + HO_2 \longrightarrow Fe^{3+} + HO_2^- \quad . \quad . \quad . \quad . \quad . \quad (3.5)$$

$$HO_2^- + H^+ \longrightarrow H_2O_2 \quad . \quad . \quad . \quad . \quad . \quad (3.6)$$

$$Fe^{2+} + H_2O_2 \longrightarrow Fe^{3+} + OH + OH^- \quad . \quad . \quad . \quad (3.7)$$

IIIc Stability

In the absence of radiation, aerated ferrous sulphate solutions are slowly oxidised by dissolved oxygen. The rate of oxidation is proportional to the square of the concentration of the ferrous ion and to the first power of the oxygen concentration (Haffman and Davidson 1956). For a 10mM ferrous sulphate solution, this oxidation amounts to 2μM/litre per day at 25°C (ICRU 1959). This sets a lower limit to the concentration of the solution with which accurate measurement can be made. It is essential that a control or blank reading be taken on the solution before irradiation. The difference between the final reading and the blank reading indicates the dose received by the specimen.

IIId Temperature effects

The most significant temperature dependent factor is the molar extinction coefficient, which increases with the temperature at which the optical density of the irradiated solution is measured by + 0.69 per cent per degree in the range 20-30°C at 304-305mμ (Scharf and Lee 1961). For high accuracy measurements, a thermally insulated cell holder is desirable.

It has been suggested (ICRU, 1962) that there are advantages in measuring the optical density at 224mμ instead of 304-305mμ. Firstly, the value of the extinction coefficient at 224mμ is 4,565 litre per mol per cm compared with 2,196 at 304-305mμ. Since the optical density

is directly proportional to the extinction coefficient, the sensitivity of the optical density reading will be doubled at the lower wavelength. Secondly, the value of the extinction coefficient is only + 0.13 per cent per degree in the range 20°-30°C.

It has also been suggested that the value of G (yield of ferric ion per 100eV energy absorbed) for Fe^{3+} increases with the temperature at which the solution is irradiated. Hochanadel and Ghormley (1962) found a 0.09 per cent per degree increase between 2 and 65°C; Schwarz (1954) reported (0.04 $\pm$ 0.003) per cent per degree increase between 0° to 70°C; however Shalek et al (1962) could not observe any temperature dependence from 20° to 45°C. The overall results indicate that this temperature effect probably occurs though its magnitude is small, and is not a significant source of error at the 1 per cent precision level.

IIIe Relation between absorbed dose and optical density

The ICRU report (1962) stated that a dose of 5,000 to 50,000 rads of X-rays, Y-rays or fast electron radiation may be given to a 1m M ferrous sulphate solution. The upper limit of dose is fixed so as to avoid depletion of the oxygen content of the solution. If doses greater than 50,000 rads are to be measured, the solution must first be saturated with oxygen and a higher concentration of ferrous sulphate solution (4m M) used.

The relationship between the absorbed dose and the optical density measured is given as

$$D(\text{rads}) = \frac{N.[\Delta(O.D.)].100}{(\Delta\epsilon).10^{3}.G(Fe^{3+}).f.\rho.\ell}$$

where N = 6.023×10^{23} molecules/mole,

$\Delta(OD)$ = difference in O.D. between irradiated solution and unirradiated solution (control),

$\Delta\epsilon$ = difference in molar extinction coefficients ($M^{-1}cm^{-1}$) between ferric and ferrous ions, at the wavelength used for the O.D. measurement,

ρ = density of irradiated solution,

ℓ = optical path length (cm),

f = 6.28×10^{13} eV/rad, a conversion factor, $G(Fe^{3+})$ is the yield in the Fe^{3+} solution = 15.6 (Hochanadel et al 1953, Lazeo et al 1954) for Co^{60} γ-rays.

IV Calculation of Stopping Power Ratio of Ferrous Sulphate in Silica

IVa Monoenergetic Electron Sources

The equation that was used in evaluating the stopping power ratio of a cavity (gas, liquid or solid) in a medium is

$$f_w(T_o) = \frac{(Z/A)_a}{(Z/A)_w}\left\{\left[1 + d\,b_w(T_o)\ln\frac{I_w}{I_a} + d_w(T_o)\right] + (1-d)\left[\frac{\left(\frac{\mu_{en}}{\rho}\right)_a}{\left(\frac{\mu_{en}}{\rho}\right)_w}\frac{(Z/A)_w}{(Z/A)_a} - 1\right]\right\} \quad 3.9$$

Equation 3.9. is similar in form to equation 1.13.

d is the attenuation factor explained in Section VIIb Chapter 1 and it should be noted that d is different from the function $d_w(T_o)$ defined below. I_a and I_w are the average excitation potentials of the cavity material and medium respectively.

bw(To) and dw(To) are functions which have been tabulated for many of the materials employed in this thesis (NBS Handbook 79, 1961). bw(To) accounts for the energy dependence of the mass stopping power ratio. dw(To) accounts for the effects on the mass stopping power ratio of the density differences between the two materials. When both the cavity and walls are in condensed phases, this term is negligible. $\left(\frac{\mu_{en}}{\rho}\right)_a$ and $\left(\frac{\mu_{en}}{\rho}\right)_w$ are the mass energy absorption coefficients of the cavity material and medium respectively. The constants which occur in equation 3.9 will first be discussed in the following sub-sections before equation 3.9 is applied to a particular dosimeter.

IVb Electron Source with a Spectrum of Energies

In any situation where the initial energies of the electrons are distributed over a spectrum, fw(To) must be averaged over the spectrum. The equation for the spectrum of recoil electrons from Compton scattering is

$$f_w(T_\gamma) = \frac{(Z/A)_a}{(Z/A)_w}\left\{\left[1 + d\,a_w(T_\gamma)\ln\frac{I_w}{I_a} + C_w(T_\gamma)\right] + (1-d)\left[\frac{(\mu_{en}/\rho)_a}{(\mu_{en}/\rho)_w}\frac{(Z/A)_w}{(Z/A)_a} - 1\right]\right\} \quad 3.10.$$

$a_w(T_\gamma)$ and $C_w(T_\gamma)$ are tabulated functions analogous to bw(To) and dw(To).

IVc The Average Excitation Potential for Elements and Compounds

The average excitation potential, I is the only constant that is not known to a high degree of accuracy. The data for average excitation potentials can be obtained from NBS handbook 79 (1961) and a report from Fano (1963). Subsequent to this work, a review on the average excitation potential was given by Dalton and Turner (1967). Since the average excitation potentials quoted in the above two sources differ in the worst case by 6 per cent, and since the average excitation potential occurs in a logarithmic term in equation 3.9, there is little difference in the choice. Although Fano's data is the more recent, the values of the average excitation potentials were taken from the NBS handbook 79 as direct comparisons can then be made with extensive earlier calculations based on the same values.

The values for the average excitation potentials for compounds were calculated by Bragg's law. Bragg's law assumed that the atoms in a compound act independently of one another and independently of molecular binding forces, so that the stopping power of the compound is the sum of the stopping powers of its constituents. Bragg's law may be expressed as

$$\ln(I)_{COMPOUND} = \left(\frac{Z}{A}\right)_c^{-1}\sum w_i\frac{Z_i}{A_i}\ln I_i$$

where w_i is the fraction by weight of the i^{th} element.

For low atomic number elements, slight departures from Bragg's law have been demonstrated when these elements are in chemical combination (Thompson, 1952). For these elements, a simple method of correction is to use values of the average excitation potential adjusted for the

chemical state (e.g. saturated, unsaturated, highly chlorinated, etc.) and these values were also taken from NBS Handbook 79. A table of the values of the average excitation potentials used appears in Chapter 4 (Table 4.5).

These values of I were substituted in equation 3.9 and 3.10 to determine the mass stopping power ratio. For the few materials where the tabulation was not available for the function bw(To), it was calculated. It is given fairly accurately by the expression

$$b_w(T_o) \approx \frac{\bar{E}i\left(\ln \sqrt{\frac{e}{2}}\frac{T_o}{I_w}\right)}{\sqrt{\frac{e}{2}}\frac{T_o}{I_w}} \qquad 3.11$$

where E_i is the exponential integral and To is the energy of the incident radiation (NBS Handbook 79). Attix et al (1958) estimated that the greatest error in bw(To) involved in using this expression is a few per cent. Since bw(To) is a small fraction of unity and is added to unity in the bracket of equation 3.9, the overall error in fw(To) is even smaller. The materials for which bw(To) had to be calculated were all of low atomic numbers and $a_w(T_\gamma)$, the value of bw(To) averaged over the starting spectrum of Compton electrons, was taken to be equal to bw(To). For low atomic number materials, this approximation only alters the mass stopping power by at most 0.2 per cent which was considered acceptable.

IVd Mass Attenuation and Mass Energy Absorption Coefficients

The International Commission on Radiological Units and Measurements (Handbook 84, 1962) defines the above coefficients as follows: 'The mass attenuation coefficient $\left(\frac{\mu}{\rho}\right)$ of a material for indirectly ionising particles is the quotient of dN by the product of ρ N and $d\ell$ where N is the number of particles incident normally upon a layer of thickness $d\ell$ and density ρ and dN is the number of particles that experience interactions in this layer

$$\frac{\mu}{\rho} = \frac{1}{\rho N}\frac{dN}{d\ell}$$

For X or gamma radiations

$$\frac{\mu}{\rho} = \frac{\tau}{\rho} + \frac{\sigma}{\rho} + \frac{\sigma_{coh.}}{\rho} + \frac{K}{\rho}$$

where $\frac{\tau}{\rho}$ is the mass photo-electric attenuation coefficient, $\frac{\sigma}{\rho}$ is the total Compton mass attenuation coefficient, $\frac{\sigma_{coh}}{\rho}$ is the mass attenuation coefficient for coherent scattering and $\frac{\kappa}{\rho}$ is the pair-production mass attenuation coefficient.'

'The mass energy absorption coefficient $\frac{\mu_{en}}{\rho}$ of a material for indirectly ionising particles is $\frac{\mu_k}{\rho}(1-G)$ where $\frac{\mu_k}{\rho}$ is the quotient of dE_k by the product of E, ρ and dl where E is the sum of the energies (including rest energies) of the indirectly ionising particles incident normally upon a layer of thickness dl and density ρ and dE_k is the sum of the kinetic energies of all the charged particles liberated in this layer and G is the proportion of the energy of the secondary charged particles that is lost to bremsstrahlung in the material.'

$$\frac{\mu_k}{\rho} = \frac{1}{E\rho}\frac{dE_k}{dl}$$

For X or gamma rays of energy $h\nu$

$$\frac{\mu_k}{\rho} = \frac{\tau_a}{\rho} + \frac{\sigma_a}{\rho} + \frac{\kappa_a}{\rho}$$

where

$$\frac{\tau_a}{\rho} = \frac{\tau}{\rho}\left(1 - \frac{\delta}{h\nu}\right)$$

δ being the average energy emitted as fluorescent radiation per photon absorbed

$$\frac{\sigma_a}{\rho} = \frac{\sigma}{\rho}\frac{\bar{E}_e}{h\nu}$$

Ee being the average energy of the Compton electrons per scattered photon

$$\frac{\kappa_a}{\rho} = \frac{\kappa}{\rho}\left(1 - \frac{2mc^2}{h\nu}\right)$$

Table 4.5 gives the values of the mass energy absorption coefficients (Evans 1968) used in this work.

IV6 The Average Path Length Across a Cavity

As explained in Chapter 1, it is necessary to determine the average path length across a cavity in order to evaluate the weighting, d, and to determine the energy of an electron which will, on average, just cross the

cavity. The expression for finding the average path length, g, across a non reentrant volume is

$$g = \frac{4 \times \text{volume}}{\text{total surface area}}$$

This has been shown by various authors including Weinberg and Wigner (1958).

V Experimental Procedure

The measurements on ferrous sulphate dosimeters were carried out at the Mount Vernon Hospital and then repeated using the Co^{60} source at The Polytechnic. The Co^{60} source at Mount Vernon Hospital approximated to a point source with nearly monoenergetic photons (i.e. the two gamma lines from Co^{60}, 1.17 and 1.33MeV) and very little scattered radiation; but the dose rate was rather low. The Co^{60} source at The Polytechnic was a distributed source with a significant scattered photon component as described in Chapter 2. The measurements at each place are discussed in the following sub-sections.

Va Measurement of Ferrous Sulphate Dosimeter at the Mount Vernon Hospital

The irradiation cells employed were 10cm long tubes of 0.05, 0.2 and 0.6cm internal diameter, and spherical flasks of 3.79cm and 10.3cm internal diameter. To establish electronic equilibrium, a further tube used as a sheath enclosed the tubes and in the case of the flasks, aluminium sheets were used to wrap round the exterior of the flask. Aluminium has nearly the same atomic number, 13, as silicon, 14, so that equilibrium electron spectra of the two materials will not be very different; and in any case, the 1mm thickness of silica which is in contact with the solution will be by far the most important factor in determining the electron spectrum entering the solution (Gray, 1937).

Ferrous sulphate solution was prepared as described in Section IIIa. The solutions were irradiated by a 500 curie Co^{60} source which was 12cm long. This was situated in a brass guide tube of about 0.65cm thick so that the scattered radiation should be minimal. The irradiation cells were placed on a turntable, which rotated during the irradiation to ensure an equal exposure of all the cells. The distance from the centre of the source to the centre of the solution was 33.4cm. Irradiations

of 2, 4, 6, 8 and 10 hours duration were given to the solution. The maximum dose did not exceed 40,000 rads, to avoid an excessive depletion of the oxygen content of the solution.

The increase in optical density due to the oxidation of ferrous ion to ferric ion on irradiation was measured at 304mμ on a 'Uvispek' spectrophotometer. The increase in optical density was measured for each irradiation time for the five cell sizes and was normalised to the result obtained with the 0.6cm diameter tube. Column 2 of Table 3.1 gives the average reading of the measurements normalised in this way, averaged for the five different times. A correction for attenuation of the photons in the ferrous sulphate solution was made to the measurements and is shown in Table 3.1. The normalised optical density corrected for the attenuation effect is given in the same table. The repetition accuracy of the measurement was poor, possibly due to initial lack of experience with the technique, but probably also due to some evaporation loss and temperature difference of the solution before and after irradiation. The average of ten results is quoted in Table 3.1 together with the standard error of the mean. These measurements are also shown in figure 3.1 where they are compared with cavity theory calculated for the Co^{60} γ-lines. The agreement is within the experimental uncertainty.

Vb Measurement of Ferrous Sulphate Dosimeter at The Polytechnic

The irradiation cells and the method of preparation of the ferrous sulphate solution were as described above. The change in optical density was measured at 224mμ (see Section IIId) and 305mμ on a 'Uvispek' spectrophotometer. The following precautions were taken in the course of the measurements.

(i) The initial temperature before and after an experiment was noted, and the maximum difference in temperature was $\pm 4^{\circ}C$. A small corredtion was made to optical density for this temperature difference.
(ii) The experiment for each silica cell size was repeated five times.
(iii) The irradiation cells were placed exactly at the centre of the irradiation chamber.

(iv) Each cell after irradiation was washed thoroughly with distilled water to remove any irradiated solution left, dried with a hair drier and left to cool before filling with ferrous sulphate solution.

A correction for non-uniformity of the photon field in the irradiation chamber was made to the measurements. A graph of the average path length against the percentage change arising from the non-uniformity of the photon field was obtained from the perspex measurement (see Section VI, Chapter 4) and is shown in figure 3.2. The average path length of the silica cells was found using the method described in Section IVe. The corresponding percentage change in the non-uniform photon field was obtained from the graph, figure 3.2.

Table 3.2 gives the measurements at 224mμ before and after being corrected for non-uniformity of the photon field, and the standard error of the mean. One per cent precision was achieved in these measurements. The measurements performed at The Polytechnic are compared with cavity theory calculated for the photon spectrum in the cell shown in figure 3.3 and the agreement is again within the experimental uncertainty, i.e. $\pm$ 1 per cent.

VI Discussion

A dependence of response on dosimeter size has been reported by various authors. Weiss (1952) observed a significant increase in the response in the irradiation cell when the internal diameter fell below 0.8cm. His measurements were repeated by Ghormley (1956) who found the response in cells of 0.4cm internal diameter was 3 per cent greater than in the larger ones, a much smaller effect than that observed by Weiss. The ferrous sulphate solution used by Weiss did not contain any sodium chloride to counteract organic impurities and the large increase in response which he observed may be due to the presence of impurities on the walls. Weiss, Allen and Schwarz (1956) repeated the measurements and found a 6 per cent greater response in cells of 0.4cm internal diameter than in the larger ones. Cavity theory predicts a 2.5 per cent greater response for a 0.4cm internal diameter cell than for the larger ones irradiated by Co^{60} gamma rays. Since the photon

energy spectrum used by these authors was not stated, this seems possibly to be a reasonable agreement. Weiss et al (1956) did not notice this effect in polystyrene cells. This is also in accord with cavity theory, which predicts very little change in the response with size of irradiation cell for closely-matched cavities. Weiss et al (1956) have stated that 'the size and shape of the dosimeter container is not important as long as the internal diameter is greater than 8mm'. Calculations from cavity theory indicate that this statement is only true for a fairly well 'matched' dosimeter and container. For a Fricke dosimeter in an 8mm diameter silica cell irradiated by Co^{60} gamma rays the yield is 1.3 per cent greater than for a very large container according to cavity theory, and the theory indicates that it is not until 6cm diameter that the effect falls to below 0.1 per cent.

Sehested, Brynjolfsson and Holm (1963) found that the response of the Fricke dosimeter depended on the ratio of the surface area to the volume of the irradiation cell. The ratio is related to the average path length across the cavity, which occurs in cavity theory. Sehested et al obtained a change in the absorbed-dose ratio of 6.5 per cent with irradiation cells which had dimensions equivalent to spherical cavities of radius 0.4 to 1.2cm. This result was obtained using glass and polyethylene irradiation cells, where the 'matching' of the container with the solution is closer than with silica. Since silica irradiation cells were used in our experiment, a larger change in the absorbed-dose ratio would be expected. However with the measurements done at Mount Vernon Hospital and at The Polytechnic, no significant change in the absorbed-dose ratio was observed in the range of irradiation cell size from 0.4 to 12.cm. This is in accord with the predictions of cavity theory. Sehested et al have suggested that 'for the glass ampoules, the effect may be due to the lack of gamma-electron equilibrium on the boundaries between glass and dosimetric solution'. However, it is unlikely that their results can be explained entirely on the basis of cavity theory. As their irradiations were performed in a large scattering medium, the photon spectrum in the region of the cavity is uncertain and it is therefore not possible to make a quantitative comparison of cavity

theory with their measurements.

Other workers (Whittaker 1963, Miller and Wilkinson 1952, Puig and Sutton 1959) have reported a size dependence for the Fricke dosimeter but there is not sufficient data in their reports to perform the theoretical calculations and make comparisons with their experimental results. It is particularly interesting to note that Puig and Sutton (1959) using rectangular cavities from 1 to 26mm wide obtained a net increase in response of 6 per cent over this range and almost identical variation of response to that presented in figure 3. They also formulated an empirical equation which has qualitatively the same behaviour as cavity theory.

VII Summary

The measurements performed with Co^{60} gamma rays have shown a size dependence of the Fricke dosimeter contained in silica radiation cells. The magnitude of this size dependence can be accounted for by cavity theory. Thus the calculation of the response of a dosimeter which must be enclosed in a container, will need to include cavity theory.

Table 3.1. Measurements of Optical Density at 304mμ of Ferrous Sulphate Solution in Various Diameters of Silica Cells (Mount Vernon Hospital Co^{60} Gamma Ray Source)

Size (cm)	O.D. normalised at 0.6cm diam. tube	Standard Error	Photon Attenuation Factor	O.D. corrected for attenuation	O.D. corr. for attenuation and nor. at 0.6cm dia. tube
0.05 (tube)	1.065	± .005	0.998	1.067	1.050
0.2 (tube)	1.014	± .006	0.994	1.020	1.004
0.6 (tube)	1.00	± .005	0.984	1.016	1.00
3.79 (flask)	.944	± .004	0.943	1.001	.985
10.3 (flask)	.861	± .004	0.852	1.011	.995

Table 3.2. Measurements of Optical Density at 224mμ of Ferrous Sulphate Solution in Various Diameters of Silica Cells (Polytechnic Co^{60} Gamma Ray Source)

Size (cm)	Optical Density	Standard Error	Photon Attenuation Factor	O.D. corr. for Attenuation	O.D. normalised at 0.6cm diam. tube
0.05 (tube)	.322	± .003	1.064	.303	1.049
0.2 (tube)	.311	± .003	1.064	.292	1.013
0.6 (tube)	.307	± .003	1.064	.289	1.00
3.79 (flask)	.297	± .002	1.038	.286	.991
10.3 (flask)	.286	± .002	1.00	.286	.991

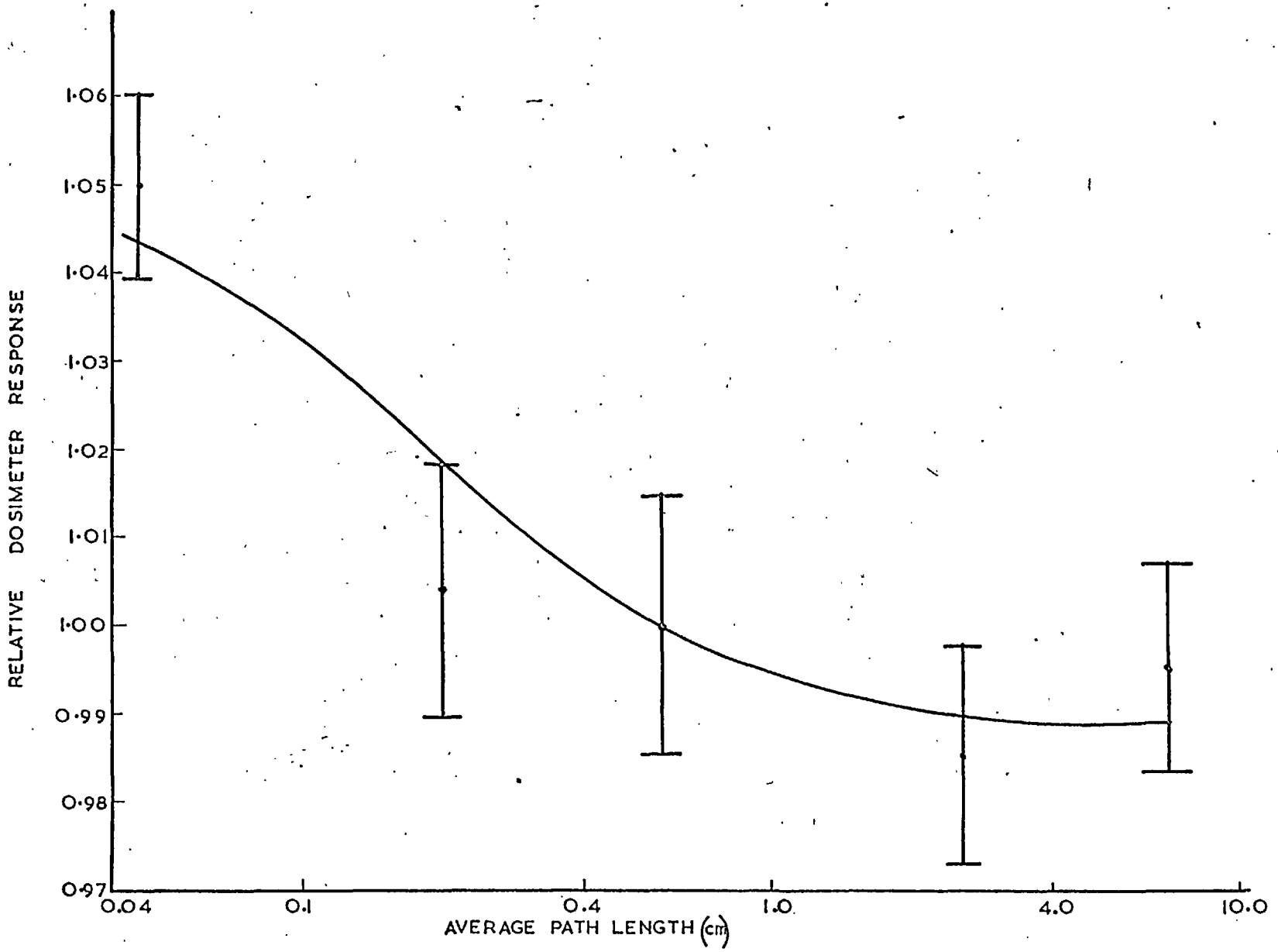

FIG. 3.1. DEPENDENCE OF THE RESPONSE OF THE FRICKE DOSIMETER CONTAINED IN SILICA IRRADIATION CELL UPON THE CELL SIZE, EXPRESSED AS THE AVERAGE PATH LENGTH ACROSS THE CELL. LINE—THEORY, I—— REPRESENTS MEASUREMENTS AT MOUNT VERNON HOSPITAL.

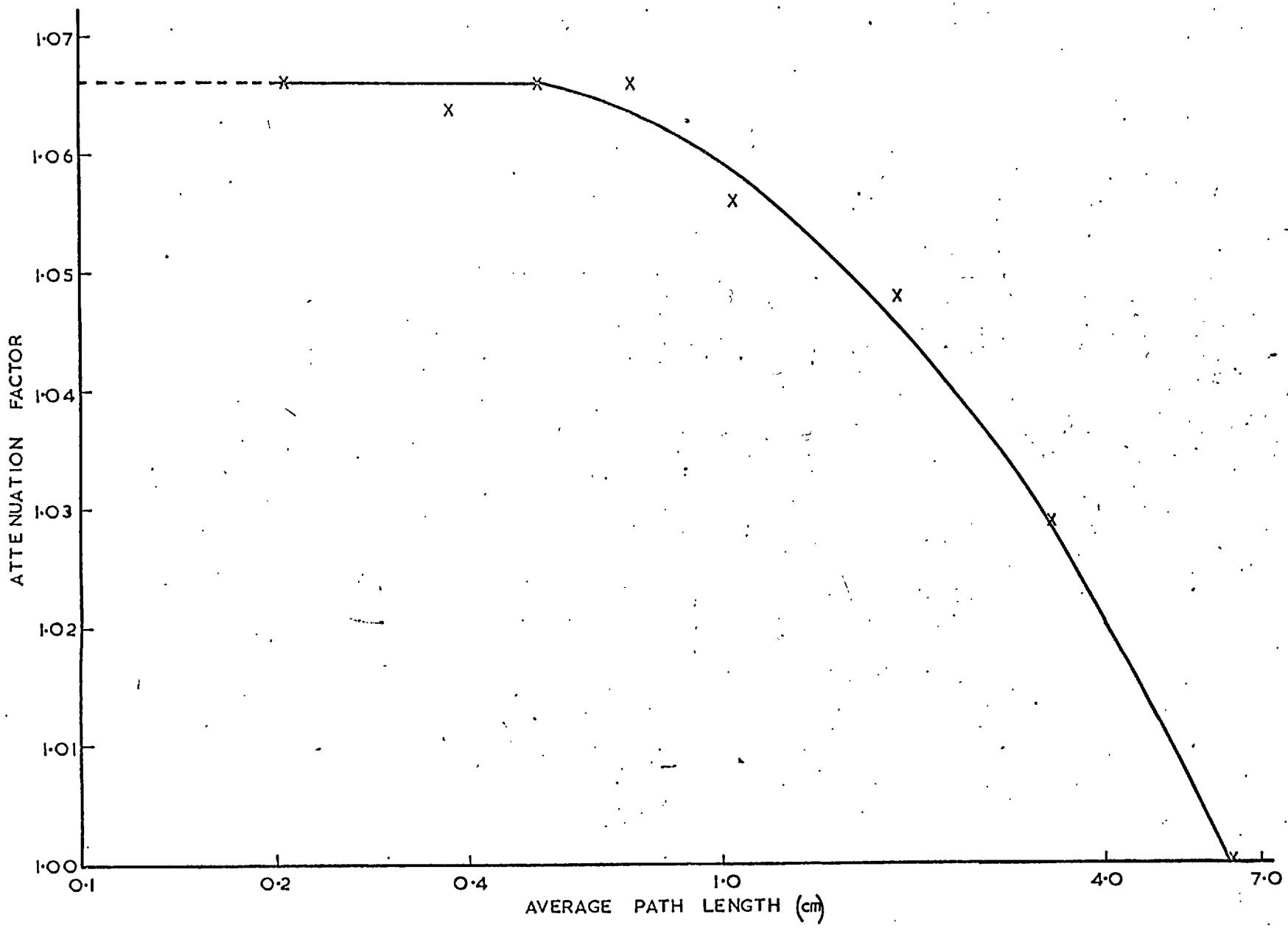

FIG. 3.2. VARIATION OF THE AVERAGE OPTICAL DENSITY OF PERSPEX VOLUMES ARISING FROM GEOMETRICAL AND ABSORPTION ATTENUATION VERSUS THE VOLUME OF THE PERSPEX EXPRESSED AS THE AVERAGE PATH LENGTH ACROSS THE VOLUME.

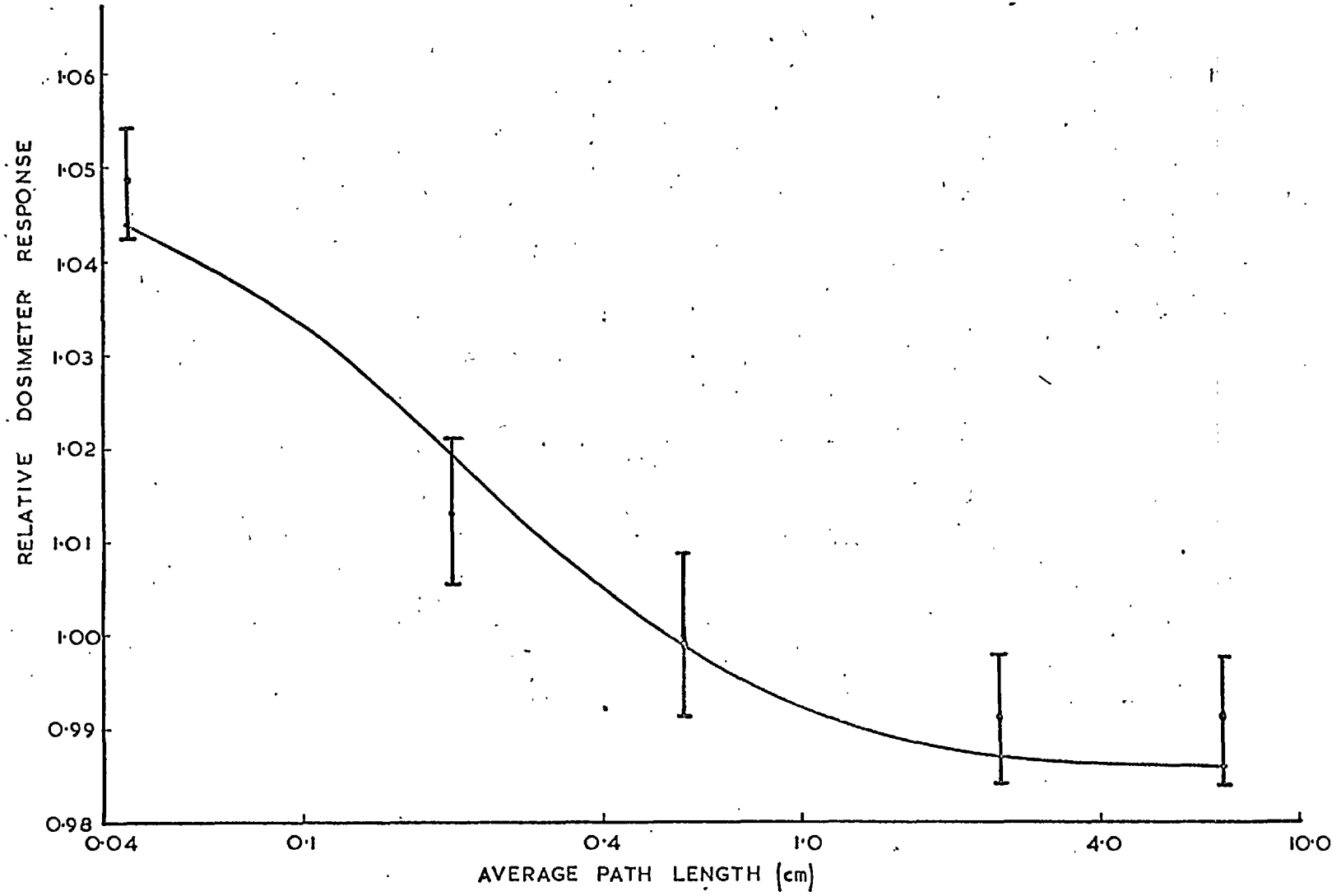

FIG. 3.3. DEPENDENCE OF THE RESPONSE OF THE FRICKE DOSIMETER CONTAINED IN SILICA IRRADIATION CELL UPON THE CELL SIZE, EXPRESSED AS THE AVERAGE PATH LENGTH ACROSS THE CELL. LINE—THEORY, ⊢— REPRESENTS MEASURMENTS AT THE POLYTECHNIC

CHAPTER 4

THE EXPERIMENTAL EXAMINATION OF GENERAL CAVITY THEORY APPLIED TO A SOLID STATE DOSIMETER

I Introduction

The primary concern of this chapter is a detailed experimental examination of Burlin's theory of cavity ionisation. Since generality is claimed for this theory it should be valid for all cavity dimensions and any combination of the atomic numbers of the cavity material and surrounding medium. Previous to the work reported in this thesis, the only experimental tests conducted were on gas-filled cavities whose dimensions were much smaller than the range of the electrons. The work on the Fricke dosimeter reported in Chapter 3 covered a large range of cavity size extending up to cavity dimensions very much greater than the range of the electrons, but the atomic number of the cavity and the wall were not greatly different so that the test of cavity theory was not the most severe. The high degree of cleanliness and chemical inertness demanded by the Fricke system prevented higher atomic number walls being used. This chapter describes experiments performed with a solid state dosimeter of low atomic number surrounded by walls varying from low to high atomic number and also covering a large range of cavity size extending up to cavity dimensions very much greater than the range of the electrons. It is the most stringent test of cavity theory possible.

A secondary concern of this chapter and Chapter 5 is to demonstrate the application of cavity theory to solid state dosimeters. Rapid progress has been made in solid state dosimeters in recent years due mainly to the work of Schulman (1959), Attix (1962), Boag (1963) and Fowler (1963a, b). The advantages of these dosimeters are as follows.
(a) High density (1000 - 4000 times more atoms per cm^3 than air) leads to small dosimeter size; further, the average energy required to produce an ion pair (i.e. W) in solids is less than that in air.
(b) Frequently, the charges induced by irradiation remain for a long

period which enables measurements to be made at a later time.

(c) Colour changes during irradiation are useful for determining spatial dose distribution.

(d) Higher dose-rates can be measured with solid state dosimeters than ionisation chambers.

II Requirements for the Solid State Dosimeter

The choice of a particular solid state dosimeter depends on the following factors.

(a) Since experiments are to be performed with various sizes of detecting material surrounded by different wall materials, a low cost solid state detector would be preferred.

(b) A reproducibility of 1 per cent is an essential requirement in this work, since some of the variations in response with dosimeter size which are being investigated, are expected to be a few per cent.

(c) The response should be proportional to the absorbed dose, irrespective of the nature of the incident radiation.

(d) Normal fluctuations in room temperature should not produce significant changes in the measurement.

(e) The induced changes in the measurable parameter should not vary greatly with time after irradiation.

Clear perspex is chosen as the dosimeter for the present work since it satisfies most of the above requirements. Perspex was first suggested as a radiation dosimeter by Day and Stein (1951); and was described fully by Boag et al (1958) and to a lesser extent by Davidson and Sutton (1964), Orton (1966) and Whittaker and Lowe (1966). The perspex used in these experiments was obtained from a batch specially made for dosimetry purposes. It is known commercially as 'perspex acrylic HX' but will be simply referred to as perspex throughout this chapter.

III General Principles of the Perspex Dosimeter

IIIA Relationship between Optical Density and Absorbed Dose.

The calibration between optical density at 292 mμ for 0.3cm thick perspex and absorbed dose was carried out by Boag et al (1955)

using calorimetric dosimetry and the relationship obtained for a particular batch is given by

$$R(\text{megarads}) = k_1 + \frac{k_2 D}{t},$$

t is the thickness in millimetres of the perspex,
D is the difference in optical density between the irradiated and unirradiated sample,
k_1 and k_2 are determined experimentally and may vary with the particular batch of perspex and thickness of perspex used, (Orton 1959, 1965).

The linearity between R and D applies between doses of 0.06 to 3 megarads in 0.1cm thick samples, and 0.06 to 1.5 megarads in 0.3cm thick samples.

IIIb Preparation and Handling

The thicknesses of the special perspex obtained commercially are specified as 0.1cm and 0.3cm. However, for the 0.1cm perspex, there is a variation from .070 to .116cm from piece to piece. For the 0.3cm material, the variation is between 0.260 to 0.320cm. The exact thickness of each piece was therefore measured with a micrometer.

The following procedure for cleaning the perspex is recommended by the United Kingdom panel in Gamma and Electron Irradiation.

The samples are soaked and stirred (by finger) for 30 minutes in a detergent solution such as Teepol. They are dipped in dilute acetic acid, washed several times in distilled water and then washed with alcohol. Finally they are dried between filter papers. The optical density of the perspex pieces used in the experiment was measured both before and after irradiation on a Hilger and Watt 'Uvispek'. Investigation of the variation of optical density with wavelength for this batch of perspex receiving a dose of 1.17 megarads, using the present spectrophotometer, showed a peak around 292 mμ as is given in figures 4.1 and 4.2 for the 0.1cm and 0.3cm perspex pieces respectively. This was in agreement with the measurements of Boag et al (1958) who also observed a peak around 292 mμ using a Unicam spectrophotometer. This presence of a peak was later shown to be due to the particular type of spectrophotometer

used. When the measurements were commenced in 1967, there were some doubts as to whether a maximum in the induced optical density occurred at around 292 mμ. In discussion, Berry and Marshall of the United Kingdom Panel on Gamma and Electron Radiation suggested that two wavelengths 292 mμ and 305 mμ should be used. Measurements were made at both these wavelengths throughout the work reported here.

Before irradiation, the thickness of each piece was measured. This was found to be necessary because preliminary checks were made on fifty pieces of 0.1cm and 0.3cm perspex, each taken at random. The initial optical density corrected for thickness varied by up to ± 6 per cent. If uncorrected, this would have exceeded the other experimental errors. Table 4.1 shows the measurements on some of the pieces and illustrates the importance of measuring the optical density prior to irradiation for accurate work.

It was observed that scratches on the perspex hardly changed the optical density reading but any traces of grease from the fingers in handling reduced the reading by as much as 4 per cent. Therefore tweezers were used for handling the clean perspex.

IIIc Fading

Fading occurs in the ultra violet absorption induced in perspex by radiation (Boag et al 1958). The fading characteristic of the 0.1cm and 0.3cm pieces were studied over a period of one year.

The 0.1cm pieces in groups of seven were given doses of 1.41, 2.47, 3.53 and 5.65 megarads. The optical density after irradiation was measured at 292 mμ and 305 mμ at convenient intervals for the first 48 hours and then daily, later weekly and eventually monthly.

Table 4.2 gives the results of seven pieces of 0.1cm perspex receiving a dose of 1.41 megarads. Column 2 represents the average optical density measured at 292 mμ of the seven pieces, and this average value is normalised to the average maximum value of these pieces which occurred between 10 and 60 hours after irradiation. Column 3 gives the standard error of the mean of the seven pieces. The measurements at 305 mμ are given in Columns 5 and 6.

The fading of the induced optical density with time at the four dose levels for 0.1cm perspex is shown in Figures 4.3 to 4.6. The induced optical density for all these doses reached a maximum within forty-eight hours after irradiation and then decreased by approximately four per cent per week. After six months it remained constant.

The 0.3cm pieces (10 altogether) were given a dose of 1.41 megarads and measurements were repeated at intervals as above. The induced optical density reached a maximum between 10 and 80 days after irradiation, depending on the individual piece, and then decreased by approximately 3 per cent a month (Figure 4.7).

A possible explanation which could account for the fading suggested by Orton (1965) is as follows. Radiation which causes an increase in optical density produces free radicals in the perspex. After irradiation, free radicals produced in the perspex either react with one another forming some type of 'conjugated double bond system' which increases the optical density and is very stable, or they decay. If the perspex is stored in air, oxygen diffuses into the perspex from the edges and reacts with any free radicals and 'bleaches out' the optical density associated with them. The UV absorption in the perspex decreases during this process of 'bleaching' by oxygen. When the bleached zones meet, the fading stops. The fact that there is an effect remaining when fading stops is due to the stability of the 'conjugated double bond systems' which give rise to the permanent change in optical density observed after complete oxygen diffusion.

Orton (1965) developed in detail a diffusion theory equation based on the above processes, and this fitted quite accurately with his experimental points. A comparison with Orton's results indicates that the general trend of the decay curves shows little difference, and the remaining effect of optical density is about 25 per cent of the maximum value in each case. The time after irradiation (3000 hrs) in which fading stops is also the same in both cases.

Table 4.3 shows the 'residual' optical density of 0.1cm perspex pieces at various doses measured 420 days after irradiation and was expressed as a fraction of the maximum optical density.

IV Experimental Procedure

Eight different sizes of rectangular box were made from each of the following materials:- perspex, carbon, aluminium, copper, tin and lead. The total impurity content in each of the materials is specified by the manufacturers as being less than 0.1 per cent. The first five box sizes formed parallel plate cavities having a cross section of 1cm × 4cm and thicknesses of 0.1, 0.2, 0.3, 0.5 and 1cm. The dimensions in cm of the other three larger boxes are $2 \times 2 \times 4$, $4 \times 4 \times 4$ and $8 \times 8 \times 8 cm^3$. The thicknesses of each material for all the eight box sizes are sufficient to establish electronic equilibrium within the material as shown in Table 2.1.

The following procedures apply to all the experiments using perspex pieces described in this chapter.

(a) The irradiation time for each box size was four hours, which corresponds to a dose of 1.41 megarads.

(b) The boxes containing perspex pieces were supported by various 'paper cylinders' (paper was used to minimise absorption and scattering) of different heights so that the centre of the perspex inside each box coincided with the centre of the Co^{60} irradiation chamber unit.

(c) Before irradiation, the perspex pieces were cleaned as described in section IIIb, their thickness measured and the optical density measured at 292 mμ and 305 mμ on the same spectrophotometer used throughout the experiment.

(d) After irradiation, the perspex pieces were kept in a dark dry place at room temperature and then measured 24 hours later at 292 mμ and 305 mμ. The reading which will henceforth be called the experimental result is obtained by taking the difference between the irradiated measurement and the unirradiated measurement, and then dividing the difference by the thickness of the perspex piece so as to express the experimental result as optical density per mm .

(e) The optical density per mm thus obtained is related to the absorbed dose averaged over thicknesses of 1mm and 3mm. The absorbed dose in the perspex cavity varies with distance from the walls. To determine the absorbed dose averaged throughout the cavity the mean

value of the optical density was found from all the perspex pieces within the boxes up to a size of 4 × 4 × 4cm. For the 8 × 8 × 8cm box, 108 pieces spaced evenly throughout the volume of the cavity were measured and the mean optical density and mean absorbed dose were found.

(f) The experimental results were normalised to the theoretical value of the largest box, as a convenient way to compare experimental and theoretical results.

(g) Measurements were corrected for decay of Co^{60} source.

(h) The 0.1cm thick perspex pieces were used for the 0.1, 0.2, 0.3, 0.5 and 1cm thick boxes as described earlier. For the 0.1, 0.2 and 0.3 thick boxes, the experiment was repeated five times for each case. For the 0.5 and 1cm thick boxes, it was repeated twice. The 0.3cm thick perspex was used for the three largest box sizes and because of the large number of pieces to be measured, the experiment was performed once.

V Cross Calibration between the 0.1cm and 0.3cm thick Perspex

Both the 0.1cm and 0.3cm perspex pieces were used for each complete range of box sizes made of perspex. Since the fading characteristic of the 0.1cm (Fig. 4.3 - 4.6) and 0.3cm pieces (Fig. 4.7) were not the same, in particular since the maximum optical density difference from controls does not occur at the same time after irradiation, a cross calibration was carried out between the 0.1cm and 0.3cm perspex.

The 1 × 1 × 4cm perspex box was filled with a mixture of 0.1cm and 0.3cm perspex pieces which were arranged as shown in Fig. 4.8a. The positions of the 0.1cm and 0.3cm perspex were interchanged as shown in Fig. 4.8b to eliminate the effect of slight nonuniformity in the radiation field. From these two arrangements, the average reading (OD) per mm of the eight 0.1cm perspex and the average reading of the four 0.3cm perspex were determined. The ratio of the optical density per mm of the 0.1cm to the 0.3cm perspex was found to be 0.966 at 292 mμ and 0.956 at 305 mμ. Since the 0.3cm perspex pieces were used to fill the three largest boxes, 2 × 2 × 4, 4 × 4 × 4 and 8 × 8 × 8cm,

the average readings in each of these boxes were multiplied by 0.966 and 0.956 for 292 mμ and 305 mμ respectively, thus calibrating the 0.3cm perspex against the 0.1cm perspex.

VI Correction for Attenuation of the Photon Field

The general theory of cavity ionisation assumes an unattenuated radiation field. In contrast, the radiation field in the experiments was subjected to both geometric attenuation arising from the source geometry (see Section VI Chapter 2) and attenuation due to absorption in the dosimeter (Section IV Chapter 2). To correct for attenuation effects, use was made of the fact that the stopping power ratio of a perfectly matched dosimeter (i.e. identical wall and cavity material) is unity, irrespective of dosimeter size. Therefore any variation in the response of a matched dosimeter with size must be due to attenuation effects.

Eight boxes of the same dimensions as before were made of perspex (i.e. a perspex wall) and were filled with perspex pieces. The correction which was employed is illustrated with the following example. In column 2 of Table 4.4 the readings for perspex pieces in perspex walls were normalised on the reading for the largest box. The normalised values obtained with the lead walls is given in column 3 of the same table. These 'lead values' for each box size were corrected for attenuation effects by dividing them by the 'perspex value' of the same box size, shown in column 4.

The same procedure was applied to the other wall materials.

VII Calculations by Cavity Theory

The equation used for calculating the mass stopping power ratio of perspex in various wall materials is

$$f_w(T_\gamma) = \frac{(\bar{Z}/A)_p}{(\bar{Z}/A)_w}\left\{\left[1 + d\,a_w(T_\gamma)\ln\frac{I_w}{I_p}\right] + (1-d)\left[\frac{(\mu_{en}/\rho)_p(\bar{Z}/A)_w}{(\mu_{en}/\rho)_w(\bar{Z}/A)_p} - 1\right]\right\} \qquad 4.1$$

The suffixes 'p' and 'w' refer to the perspex and wall material in this context. The average excitation potential, Ip, of perspex was calculated using Bragg's law described in Section IVc of Chapter 3. The values of Ip, Iw, $\left(\frac{\mu_{en}}{\rho}\right)_p$ and $\left(\frac{\mu_{en}}{\rho}\right)_w$ are given in Table 4.5. $f_w(T_\gamma)$ was averaged over the slowing down spectrum of photo-electric and Compton electrons. Table 4.6 presents the mass stopping power ratio at various incident photon energies for perspex of various sizes enclosed in perspex, carbon, aluminium, copper, tin and lead materials.

It was stated in Section IIIb of Chapter 2 that Costrell's (1962) results (Table 2.3 of Chapter 2) for the photon spectrum from teletherapy units was used for the photon spectrum in the irradiation chamber. Table 4.7 gives the mass stopping power ratio weighted according to Costrell's spectrum.

VIII Variation of Optical Density with Cavity Size (Calculations and Experiments)

Figures 4.9-4.13 show the measurements of the mean optical density per mm with size variations for the five materials. The experimental values are shown as crosses and the lines represent the theory. As explained earlier, the calculations and measurements are normalised to the value of the largest size box. The experimental results have been corrected for (a) cross calibration between 0.1 and 0.3cm thick perspex (described in Section V) and (b) correction for attenuation of the photon field (Co^{60} γ-rays). Table 4.8 gives these measurements.

The measurements in the carbon boxes (Figure 4.9) show that when the cavity medium (perspex) and wall (carbon) are nearly matched, there is little change in the response for variation of size, which is in accord with cavity theory.

The measurements in the lead boxes (Figure 4.13) show the greatest variation in optical density with size, where a large difference in atomic number between the wall and cavity occurs. Even under such severe experimental conditions, the agreement between results and calculations is good.

The measurements with aluminium, copper and tin (Figures 4.10-4.12) all show good agreement with the calculations.

IX Variation of Optical Density with Atomic Number (Calculations and Experiments)

The mean optical density per mm was determined as described earlier and is recorded in Table 4.9. These values had to be corrected for the effects of absorption and scattering of photons in the chamber wall. This has been discussed in Section IV of Chapter 2 and the values of the mean optical density per mm were multiplied by the correction factors contained in Table 2.6. The correction factor of perspex was assumed to be the same as carbon. The resulting values are shown in Table 4.12 normalised to the values for perspex for each box size.

Cavity theory predicts that the variation in the response (i.e. mean optical density) with the wall material will be

$$\therefore \text{Response} = \text{Constant} \left[\frac{\left(\frac{\mu_{en}}{\rho}\right)_w}{\left(\frac{\mu_{en}}{\rho}\right)_p}\right] . f_w(T_\gamma) \qquad 4.2$$

The mass energy absorption coefficients were taken from Table 4.5 and the mass stopping power ratios from Table 4.6. Table 4.11 shows the values obtained by equation 4.2 weighted according to Costrell's spectrum and the values are normalised on the values for perspex.

Figure 4.12 compares these experimental results shown as points with the predictions of cavity theory shown as continuous lines for various box sizes. Experimental values agree closely with theory in that both show a marked dependence on atomic number for small cavity sizes but little dependence on atomic number for large cavity sizes. In view of the uncertainty in the mass energy absorption coefficients arising from uncertainty in the photon spectrum, this result is considered an excellent confirmation of the theoretical treatment. It is therefore concluded that Burlin's general theory of cavity ionisation is correct since it predicts accurately the response of a perspex dosimeter with size and atomic number of the surrounding medium when

irradiated by Co^{60} γ-rays. This cavity theory should therefore be capable of predicting the response of any other solid state dosimeter.

Table 4.1

Optical density of unirradiated 1mm and 3mm perspex measured at 292 mμ with respect to air as blank

1mm pieces			3mm pieces		
Optical Density	Thickness (mm.)	OD/mm	Optical Density	Thickness (mm)	OD/mm
.231	.814	.2842	.684	.2812	.2381
.244	.853	.2865	.679	.2871	.2365
.255	.891	.2858	.674	.2819	.2342
.274	.942	.2904	.675	.2898	.233
.274	.950	.2884	.693	.2901	.2390
.282	.979	.288	.700	.2917	.2401
.288	.981	.2940	.670	.2928	.2288
.287	.990	.2901	.695	.2942	.2362
.295	.991	.2974	.675	.2943	.2295
.286	.992	.2885	.696	.2945	.2362
.286	.994	.2881	.698	.2946	.2371
.2952	1.013	.2915	.677	.2958	.2289
.293	1.013	.2924	.704	.2978	.2365
.291	1.027	.2833	.719	.2985	.2409
.301	1.036	.2905	.711	.2996	.2374
.3135	1.044	.3003	.740	.3004	.2465
.3145	1.048	.3001	.731	.3008	.2431
.321	1.051	.3054	.698	.3012	.2317
.323	1.062	.3041	.711	.3034	.2343
.3175	1.070	.2967	.715	.3038	.2355
.3175	1.075	.2953	.752	.3042	.2471
.3190	1.078	.2959	.753	.3060	.2462

Table 4.2

Measurement of Optical Density at 292 mμ and 305 mμ of 0.1cm perspex receiving 1.41 megarads over a period of 1 year

Time	$(OD)_{292}$ NOR.	Standard error	Time	$(OD)_{305}$ NOR.	Standard error
HOURS			HOURS		
1	.9661	.0048	1	.9840	.0048
4	.9840	.0048	4	.9944	.0048
20	.9988	.0069	20	.9988	.0069
27	.9685	.0048	27	.9802	.0046
47	.9784	.0048	47	.9797	.0069
92	.9597	.0084	92	.9458	.0069
121	.9317	.0066	121	.9174	.0048
149	.9172	.0052	149	.9034	.0062
169	.9010	.0048	169	.8944	.0074
193	.8925	.0042	193	.8771	.0036
265	.8558	.0062	265	.8312	.0068
290	.8467	.0050	290	.8214	.0033
DAYS			DAYS		
25	.7187	.0063	25	.6601	.0042
33	.6190	.0048	33	.5715	.0036
39	.5507	.0064	39	.5057	.0047
48	.4891	.0036	48	.4392	.0037
60	.4214	.0038	60	.3164	.0021
73	.3768	.0026	73	.2531	.0015
85	.3365	.0015	85	.2382	.0015
110	.2681	.0034	110	.2198	.0020
133	.2360	.0021	133	.2043	.0012
151	.2255	.0012	151	.1997	.0026
182	.2220	.0015	182	.2008	.0024
208	.2290	.0015	208	.2015	.0018
218	.2301	.0018	218	.2021	.0017
239	.2194	.0021	239	.2017	.0013
259	.2211	.0014	259	.2014	.0016
278	.2262	.0012	278	.2002	.0010
300	.2240	.0010	300	.2002	.0014
332	.2210	.0012	332	.2012	.0016
361	.2217	.0014	361	.2017	.0010
388	.2210	.0012	388	.2009	.0018
421	.2208	.0013	421	.2012	.0020

Table 4.3. Residual Optical Density 420 days after Irradiation for 0.1cm Perspex pieces at Various Doses Expressed as a Fraction of the Maximum Optical Density

Dose (Megarads)	$\frac{(OD)\ 420\ days\ at\ 292\ m\mu}{(OD)\ max\ at\ 292\ m\mu}$	$\frac{(OD)\ 420\ days\ at\ 305\ m\mu}{(OD)\ max\ at\ 305\ m\mu}$
1.41	.221	.202
2.47	.253	.214
3.53	.272	.218
5.65	.278	.221

Table 4.4. Correction of the Readings Obtained in the Lead Box for Attenuation of the Photon Field by Reference to the Readings Obtained in the Perspex Box

Size (cm)	$(OD)_{292}$ NORM perspex in perspex	$(OD)_{292}$ NORM perspex in lead	$(OD)_{292}$ NORM perspex in lead corrected
0.1x1x4	1.064	1.511	1.420
0.2x1x4	1.062	1.340	1.262
0.3x1x4	1.065	1.2780	1.200
0.5x1x4	1.065	1.192	1.119
1x1x4	1.056	1.124	1.064
2x2x4	1.048	1.089	1.039
4x4x4	1.029	1.059	1.029
8x8x8	1.00	1.00	1.00

Table 4.5. Values of the Average Excitation Potential I and the Mass Energy Absorption Coefficients of Photons in Various Materials

Material	I (eV)	$\frac{\mu_{en}}{\rho}$ (cm²/gm) at Various Energies (MeV) .15	.3	.5	.7	.9	1.25
$FeSO_4$ solution (a)	69.8	.0277	.0319	.0330	.0325	.0315	.0296
Silica (a)	129.2	.0280	.0291	.0297	.0293	.0277	.0265
Perspex (a)	68.1	.0266	.0310	.0322	.0315	.0306	.0286
Carbon (a)	78.4	.0245	.0287	.0297	.0292	.0284	.0268
Aluminium (a)	164	.0285	.0282	.0286	.0282	.0273	.0258
Copper (a)	306	.106	.0370	.0298	.0279	.0265	.0247
Tin (a)	517	.442	.0843	.0416	.0324	.0279	.0248
Lead (a)	812	1.154	.2590	.0951	.0596	.0429	.0328

Sources where $\frac{\mu_{en}}{\rho}$ were taken

(a) Evans, R. D., (1968)
(b) Jayachandran, C., (1968) Obtained from Davisson, C. M. (1965)
(c) Interpolation from Evans, R. D., (1968)
(d) ICRU Handbook 78 (1959)

Table 4.5.(continued). Values of the Average Excitation Potential I and the Mass Energy Absorption Coefficients of Various Materials

Materials	I (eV)	$\frac{\mu_{en}}{\rho}$ (cm²/gm) at Various Energies (MeV) .01	.02	.03	.04	.06	.08
Ferrous Sulphate[a]	69.8	4.7900	.5120	.1490	.0677	.0320	.0262
Silica[a]	129.2	18.4310	2.1805	.6207	.2596	.0844	.0460
Air[a]	85.0	4.61	11.5110	.1480	.0668	.0305	.0243
Teflon[b]	101.1	6.40	.6760	.1997	.0878	.0370	.0264
Lithium Fluoride[b]	84.3	5.687	.5860	.1610	.0685	.0303	.0229
Lithium Borate[b]	85.4	3.830	.459	.117	.0562	.0270	.0227
Calcium Fluoride[c]	149	50.81	6.662	1.966	.8216	.2484	.1134
Calcium Sulphate[c]	141.3	41.14	5.32	1.553	.6460	.1971	.0917
Muscle[d]	72.1	4.96	1.544	.154	.0677	.0312	.0255
Bone[d]	79.7	19.0	2.51	.743	.305	.0979	.0520

Table 4.5.(continued). Values of the Average Excitation Potential I and the Mass Energy Absorption Coefficients of Various Materials

Materials	$\frac{\mu_{en}}{\rho}$ (cm²/gm) at Various Energies (MeV)						
	.10	.20	.40	.60	.80	1.0	1.50
Ferrous Sulphate[a]	.0256	.0297	.0328	.0329	.0321	.0309	.0282
Silica[a]	.0341	.0279	.0296	.0296	.0289	.0277	.0253
Air[a]	.0234	.0268	.0295	.0295	.0289	.0278	.0254
Teflon[b]	.0214	.0266	.0292	.0293	.0285	.0275	.0251
Lithium Fluoride[b]	.0215	.0249	.0273	.0273	.0266	.0258	.0236
Lithium Borate[b]	.0224	.0266	.0293	.0293	.0286	.0277	.0253
Calcium Fluoride[c]	.0683	.0319	.0300	.0295	.0286	.0276	.0243
Calcium Sulphate[c]	.0571	.0308	.0301	.0297	.0298	.0278	.0253
Muscle[d]	.0252	.0297	.0325	.0326	.0318	.0308	.0281
Bone[d]	.0386	.0302	.0316	.0315	.0306	.0297	.0270

Table 4.6. Mass Stopping Power Ratio of Perspex to Various Materials of the Boxes used in the Experiments at Different Incident Photon Energies

Material	Energy (MeV)	Size of Perspex Boxes (cm) 0.1x1x4	0.2x1x4	0.3x1x4	0.5x1x4	1x1x4	2x2x4	4x4x4	8x8x8
Perspex	1.25	1.00	1.00	1.00	1.00	1.00	1.00	1.00	1.00
	0.90	1.00	1.00	1.00	1.00	1.00	1.00	1.00	1.00
	0.70	1.00	1.00	1.00	1.00	1.00	1.00	1.00	1.00
	0.50	1.00	1.00	1.00	1.00	1.00	1.00	1.00	1.00
	0.30	1.00	1.00	1.00	1.00	1.00	1.00	1.00	1.00
	0.15	1.00	1.00	1.00	1.00	1.00	1.00	1.00	1.00
Carbon	1.25	1.0738	1.0710	1.0700	1.0692	1.0685	1.0679	1.0676	1.0673
	0.90	1.0799	1.0788	1.0784	1.0781	1.0779	1.0777	1.0776	1.0775
	0.70	1.0804	1.0797	1.0794	1.0791	1.0789	1.0788	1.0788	1.0788
	0.50	1.0848	1.0845	1.0844	1.0843	1.0842	1.0842	1.0841	1.0841
	0.30	1.0807	1.0804	1.0803	1.0803	1.0802	1.0802	1.0801	1.0801
	0.15	1.0859	1.0858	1.0857	1.0857	1.0857	1.0857	1.0857	1.0857
Aluminium	1.25	1.1508	1.1331	1.1266	1.1713	1.1174	1.1134	1.1113	1.1100
	0.90	1.1478	1.1359	1.1319	1.1287	1.1263	1.1238	1.1226	1.1217
	0.70	1.1377	1.1285	1.1254	1.1230	1.1211	1.1193	1.1183	1.1177
	0.50	1.1257	1.1230	1.1200	1.1165	1.1106	1.1101	1.1098	1.1097
	0.30	1.1072	1.1037	1.1025	1.1015	1.1008	1.1001	1.0998	1.0995
	0.15	.9392	.9366	.9357	.9350	.9348	.9339	.9337	.9335

Table 4.6 (continued). Mass Stopping Power Ratio of Perspex to Various Materials of the Boxes used in the Experiments at Different Incident Photon Energies

Material	Energy (MeV)	Size of Perspex Boxes (cm) 0.1x1x4	0.2x1x4	0.3x1x4	0.5x1x4	1x1x4	2x2x4	4x4x4	8x8x8
Copper	1.25	1.2479	1.2102	1.1964	1.1852	1.1678	1.1684	1.1639	1.1610
	0.90	1.2184	1.1903	1.1808	1.1732	1.1675	1.1618	1.1588	1.1568
	0.70	1.1802	1.1575	1.1499	1.1438	1.1392	1.1347	1.1323	1.1307
	0.50	1.1187	1.1017	1.0961	1.0915	1.0881	1.0847	1.0829	1.0818
	0.30	.8678	.8545	.8500	.8465	.8438	.8411	.8397	.8388
	0.15	.2722	.2627	.2596	.2570	.2552	.2533	.2523	.2516
Tin	1.25	1.3279	1.2548	1.2280	1.2063	1.1899	1.1736	1.1650	1.1593
	0.90	1.2321	1.1725	1.1523	1.1361	1.1240	1.1119	1.1055	1.1013
	0.70	1.0912	1.0384	1.0207	1.0066	.9960	.9854	.9798	.9761
	0.50	.8705	.8726	.8133	.8019	.7933	.7847	.7802	.7772
	0.30	.4349	.4050	.3950	.3871	.3811	.3751	.3720	.3699
	0.15	.0944	.0792	.0741	.0700	.0670	.0639	.0623	.0613
Lead	1.25	1.2110	1.0691	1.0171	.9749	.9643	.9432	.9115	.8947
	0.90	.9795	.8624	.8226	.7908	.7669	.7431	.7305	.7222
	0.70	.7496	.6514	.6187	.5924	.5727	.5531	.5427	.5358
	0.50	.4981	.4272	.4035	.3846	.3799	.3204	.3562	.3438
	0.30	.2092	.1694	.1562	.1456	.1376	.1296	.1256	.1227
	0.15	.0263	.0449	.0390	.0344	.0309	.0274	.0256	.0244

Table 4.7. Mass Stopping Power Ratio of Perspex to Various Materials for the boxes used in the experiment Weighted according to Costrell's Spectrum

Size of Perspex (cm)	Wall Materials					
	Perspex	Carbon	Aluminium	Copper	Tin	Lead
0.1x1x4	1.00	1.0738	1.1508	1.2184	1.3279	1.2117
0.2x1x4	1.00	1.0710	1.1331	1.1903	1.2548	1.0691
0.3x1x4	1.00	1.0700	1.1266	1.1808	1.2280	1.0171
0.5x1x4	1.00	1.0692	1.1213	1.1732	1.2063	.9749
1x1x4	1.00	1.0685	1.1174	1.1675	1.1899	.9432
2x2x4	1.00	1.0679	1.1134	1.1618	1.1736	.9110
4x4x4	1.00	1.0676	1.1113	1.1588	1.1650	.8947
8x8x8	1.00	1.0673	1.1100	1.1568	1.1593	.8838

Table 4.8. Measurements of mean Optical Density of Perspex in Various Materials Normalised to Largest Box. The Data have been Corrected for Cross-Calibration and Attenuation of the Photon Field

Size of Perspex (cm)	Wall Materials					
	Perspex	Carbon	Aluminium	Copper	Tin	Lead
0.1x1x4	1.00	1.016	1.042	1.103	1.194	1.420
0.2x1x4	1.00	1.007	1.023	1.077	1.107	1.262
0.3x1x4	1.00	1.008	1.015	1.054	1.090	1.200
0.5x1x4	1.00	1.002	1.010	1.034	1.063	1.120
1x1x4	1.00	1.001	1.008	1.023	1.026	1.066
2x2x4	1.00	1.003	1.006	1.009	1.026	1.037
4x4x4	1.00	1.003	1.002	1.005	1.012	1.026
8x8x8	1.00	1.00	1.00	1.00	1.00	1.00

Table 4.9. Measurements of Mean Optical Density of Perspex in Different Materials Normalised to the Mean Optical Density in the Perspex Box

Size of Perspex (cm)	Wall Materials					
	Perspex	Carbon	Aluminium	Copper	Tin	Lead
0.1x1x4	1.00	1.002	1.0302	1.067	1.142	1.292
0.2x1x4	1.00	.991	1.011	1.044	1.062	1.141
0.3x1x4	1.00	.986	1.003	1.027	1.031	1.091
0.5x1x4	1.00	.976	.992	1.016	1.019	1.034
1x1x4	1.00	.985	.999	1.019	1.010	.997
2x2x4	1.00	.992	1.008	1.001	.998	.976
4x4x4	1.00	.985	1.004	.998	.992	.953
8x8x8	1.00	.980	1.007	1.008	.983	.946

Table 4.10. Measurement of Mean Optical Density of Perspex in Different Materials Normalised to the Mean Optical Density in the Perspex Box and corrected for Absorption and Scattering of the Photons

Size of Perspex (cm)	Wall Materials					
	Perspex	Carbon	Aluminium	Copper	Tin	Lead
0.1x1x4	1.00	1.002	1.030	1.066	1.176	1.394
0.2x1x4	1.00	.991	1.010	1.043	1.094	1.231
0.3x1x4	1.00	.986	1.002	1.026	1.062	1.177
0.5x1x4	1.00	.976	.991	1.015	1.050	1.115
1x1x4	1.00	.985	.998	1.018	1.040	1.076
2x2x4	1.00	.992	1.007	1.00	1.028	1.053
4x4x4	1.00	.985	1.003	.977	1.022	1.028
8x8x8	1.00	.980	1.006	1.007	1.012	1.020

Table 4.11. Variation of Mean Optical Density with Box Wall Material Relative to Perspex Box Calculated by Cavity Theory

Size of Perspex (cm)	Wall Materials					
	Perspex	Carbon	Aluminium	Copper	Tin	Lead
0.1x1x4	1.00	1.006	1.035	1.073	1.152	1.412
0.2x1x4	1.00	1.004	1.021	1.043	1.088	1.238
0.3x1x4	1.00	1.003	1.015	1.032	1.065	1.175
0.5x1x4	1.00	1.002	1.011	1.023	1.046	1.124
1x1x4	1.00	1.002	1.008	1.016	1.032	1.086
2x2x4	1.00	1.001	1.004	1.009	1.006	1.048
4x4x4	1.00	1.001	1.003	1.005	1.018	1.028
8x8x8	1.00	1.001	1.002	1.003	1.011	1.015

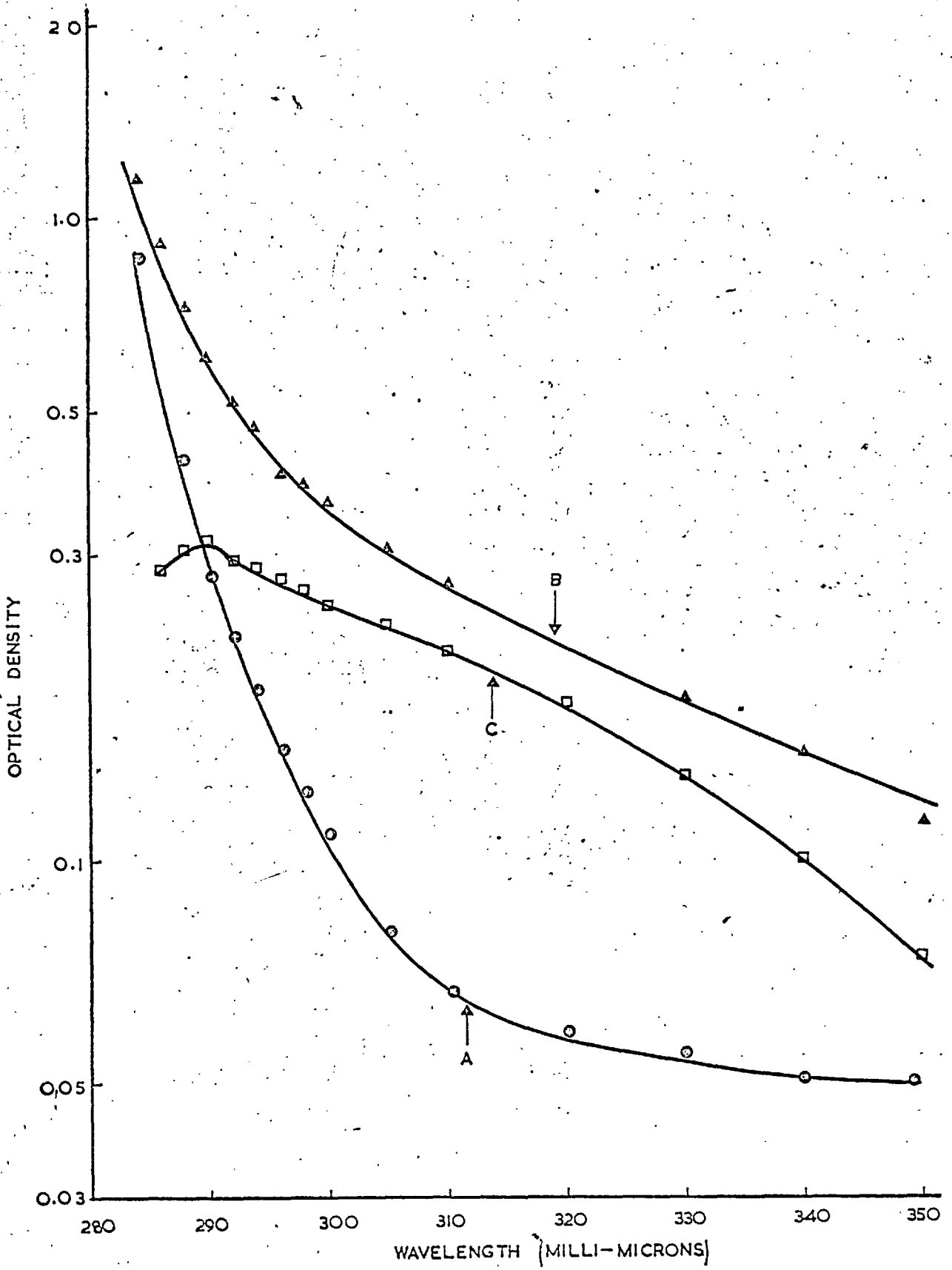

FIG. 4.1. ULTRAVIOLET ABSORPTION OF 0.1x1x4 cm PERSPEX RECEIVING A DOSE OF 1.17 Mega-rads. NORMAL PERSPEX (A), IRRADIATED PERSPEX (B), CURVE (C) IS THE DIFFERENCE BETWEEN (A) AND (B).

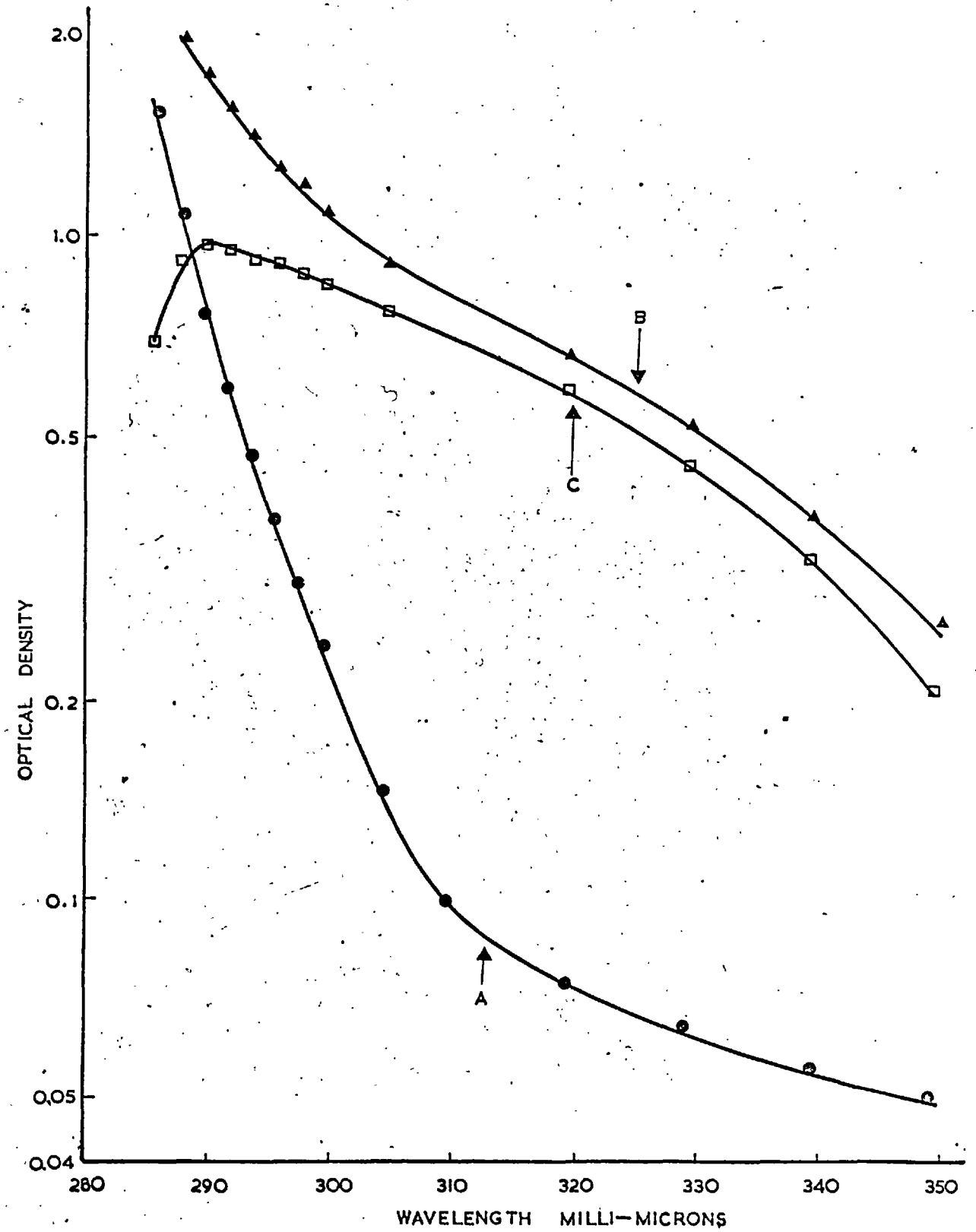

FIG.4.2. ULTRAVIOLET ABSORPTION OF 0·3x1x4cm PERSPEX RECEIVING A DOSE OF 1.17 Mega-rads. NORMAL PERSPEX (A), IRRADIATED PERSPEX (B), CURVE (C) IS THE DIFFERENCE BETWEEN (A) AND (B).

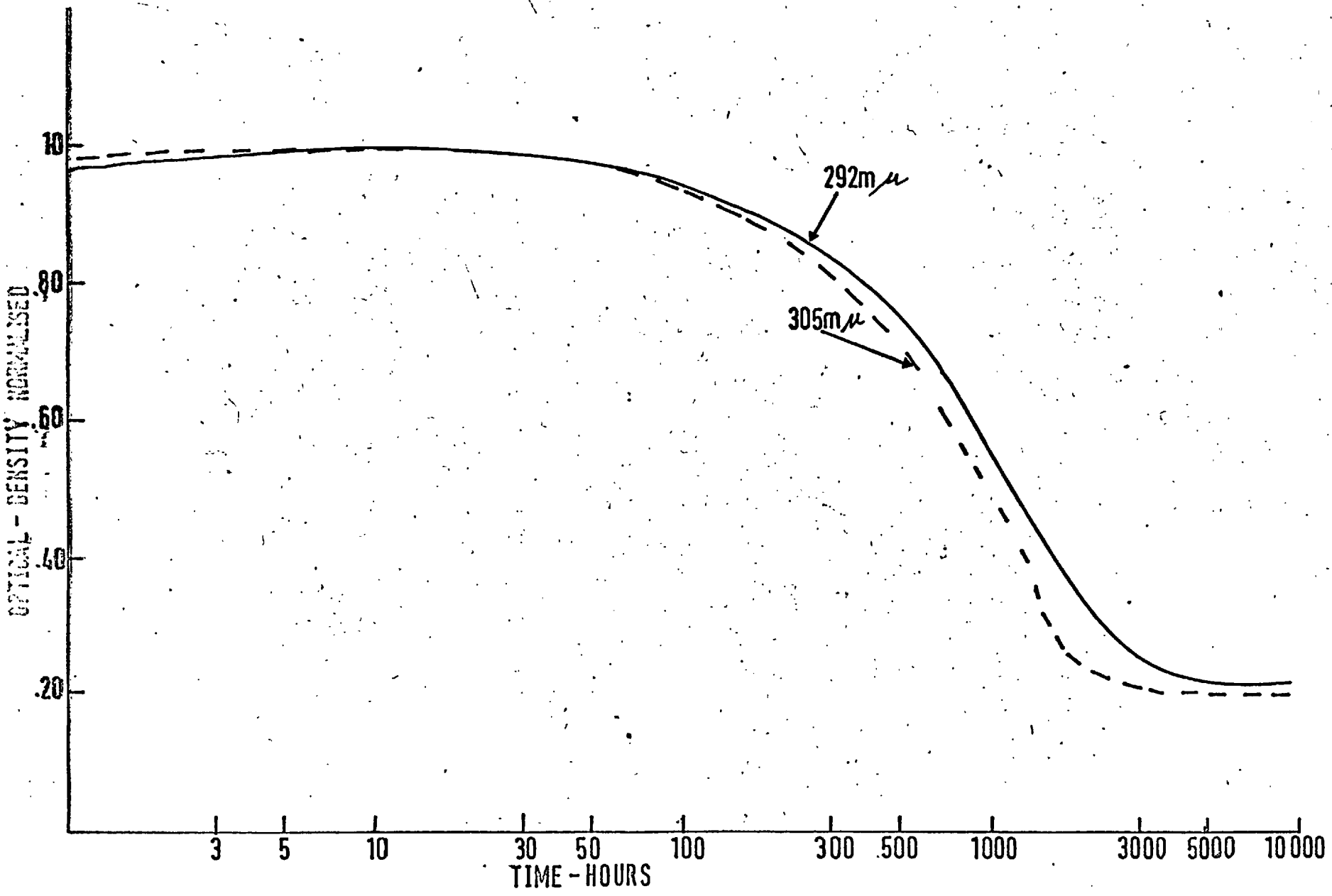

FIG. 4.3. FADING CURVES FOR 0.1 cm PERSPEX RECEIVING A DOSE OF 1.41 MEGARADS.

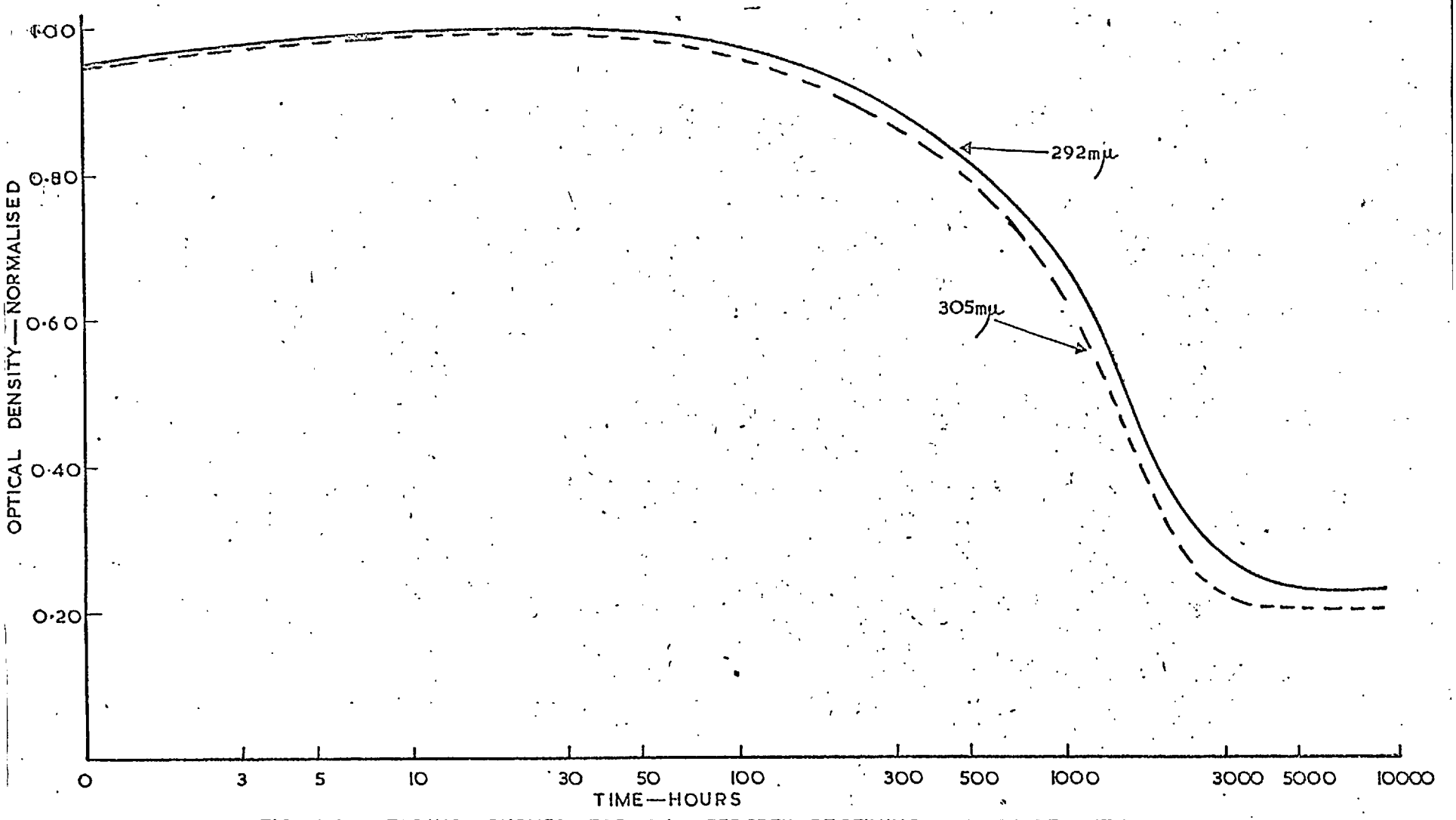

FIG. 4.4. FADING CURVES FOR 0·1cm PERSPEX RECEIVING A DOSE OF 2·47 MEGARADS.

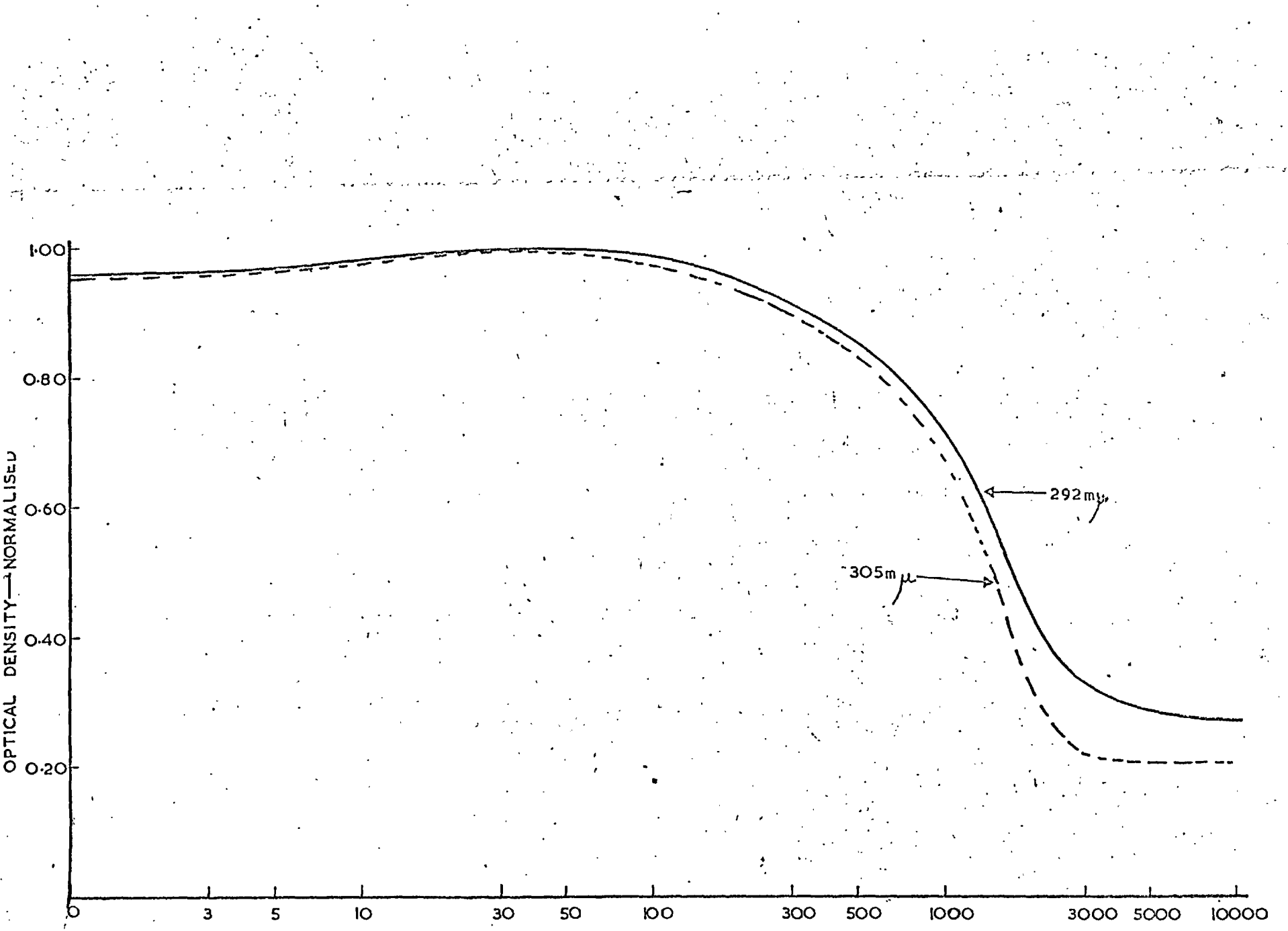

FIG. 4.5. FADING CURVES FOR 0.1cm PERSPEX RECEIVING A DOSE OF 3·53 MEGARADS.

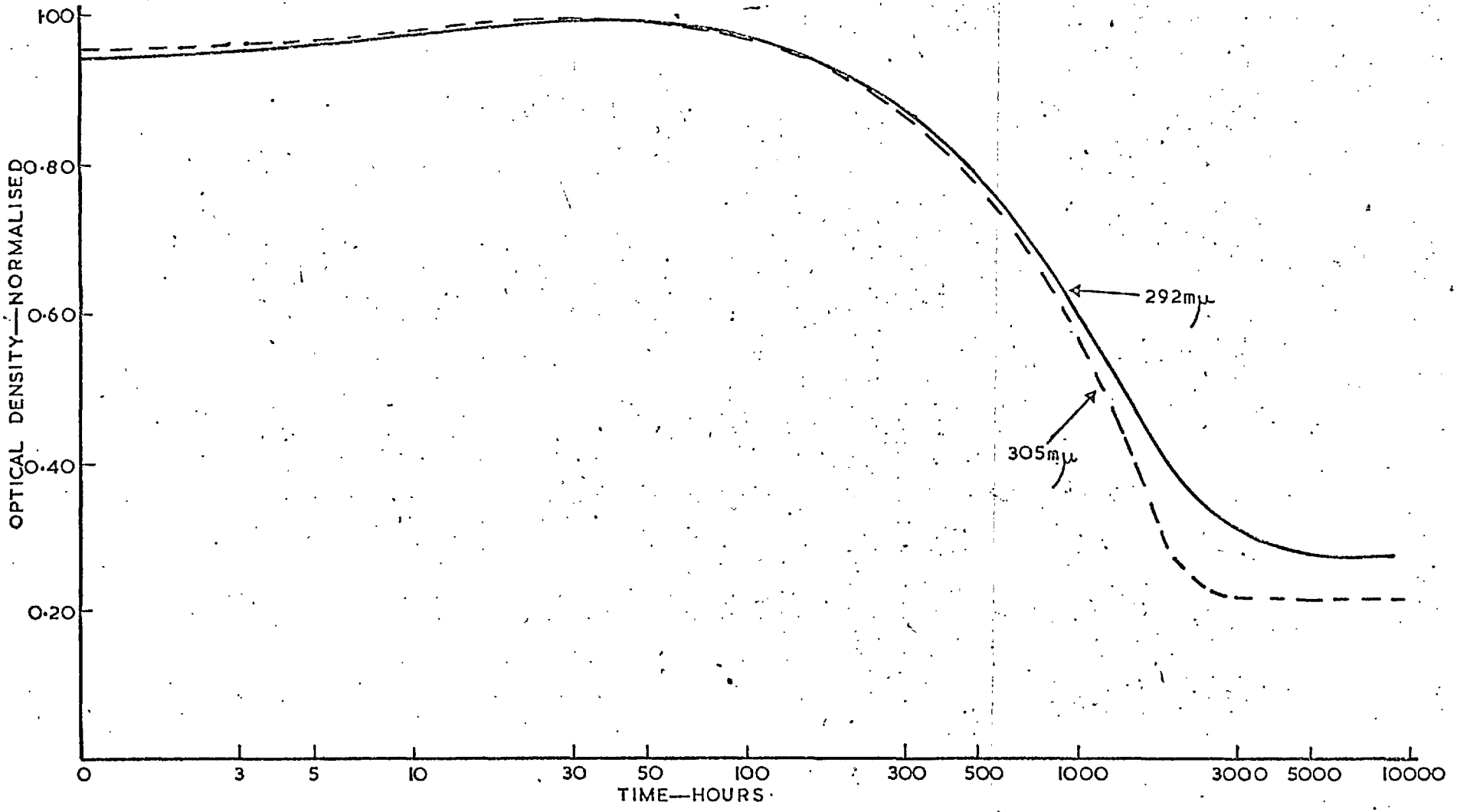

FIG. 4.6. FADING CURVES FOR 0·1cm PERSPEX RECEIVING A DOSE OF 5·65 MEGARADS.

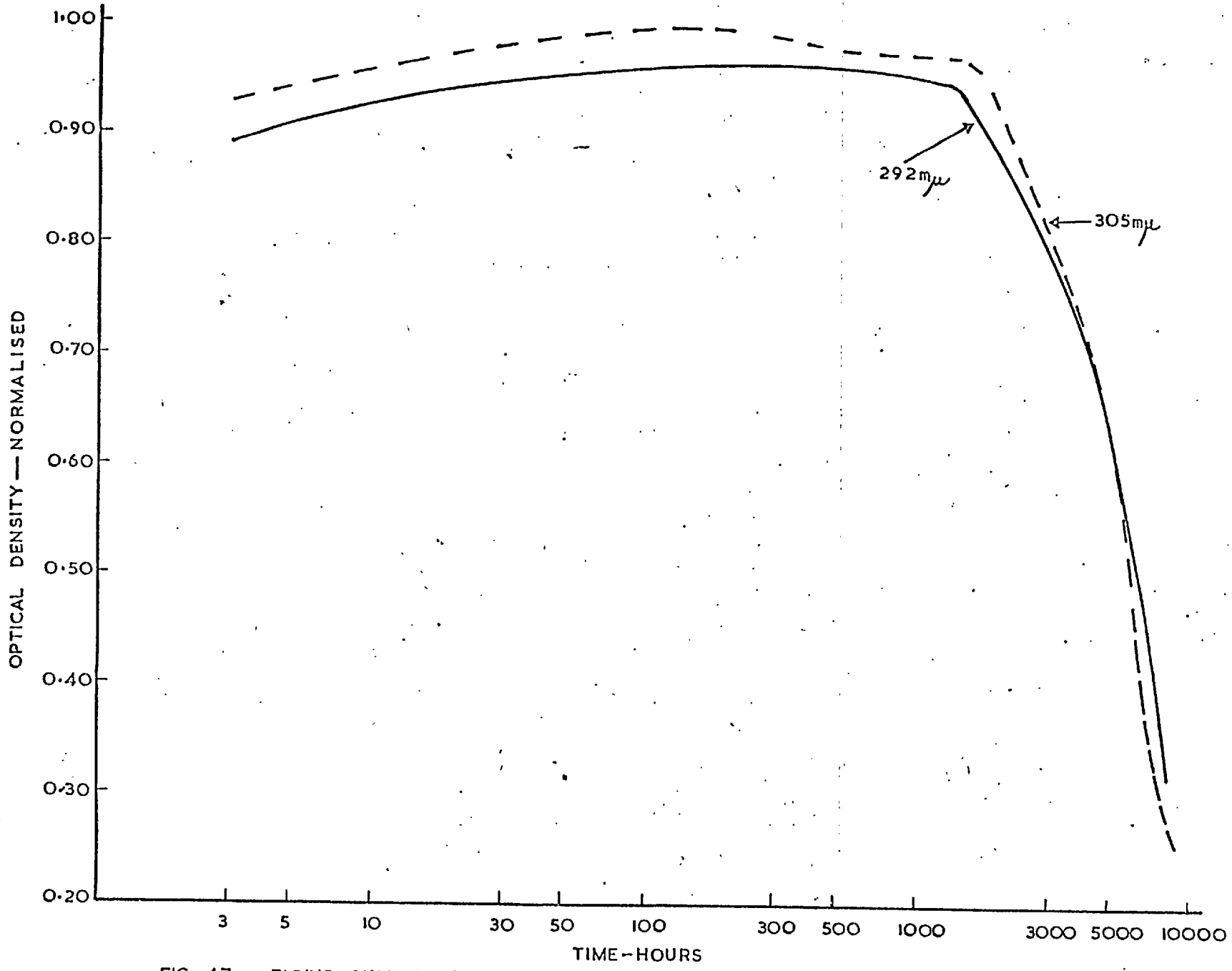

FIG. 4.7. FADING CURVES FOR 0·3cm PERSPEX RECEIVING A DOSE OF 1·41 MEGARADS.

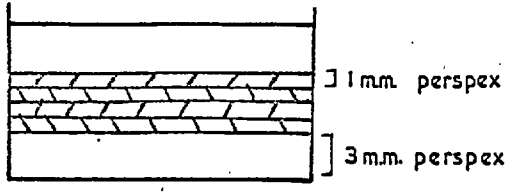

FIG 4.8(a)

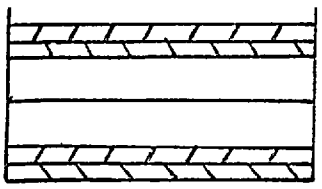

FIG 4.8(b)

ARRANGEMENTS FOR 0.1cm AND 0.3cm PERSPEX FOR CROSS-CALIBRATION.

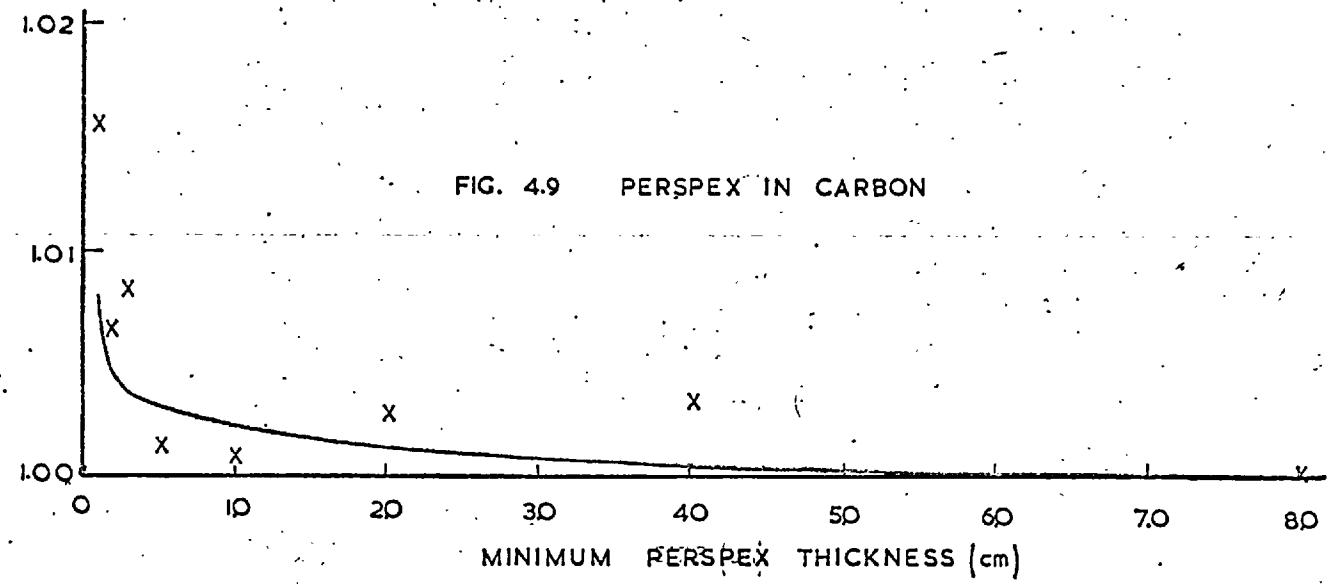

FIG. 4.9 PERSPEX IN CARBON

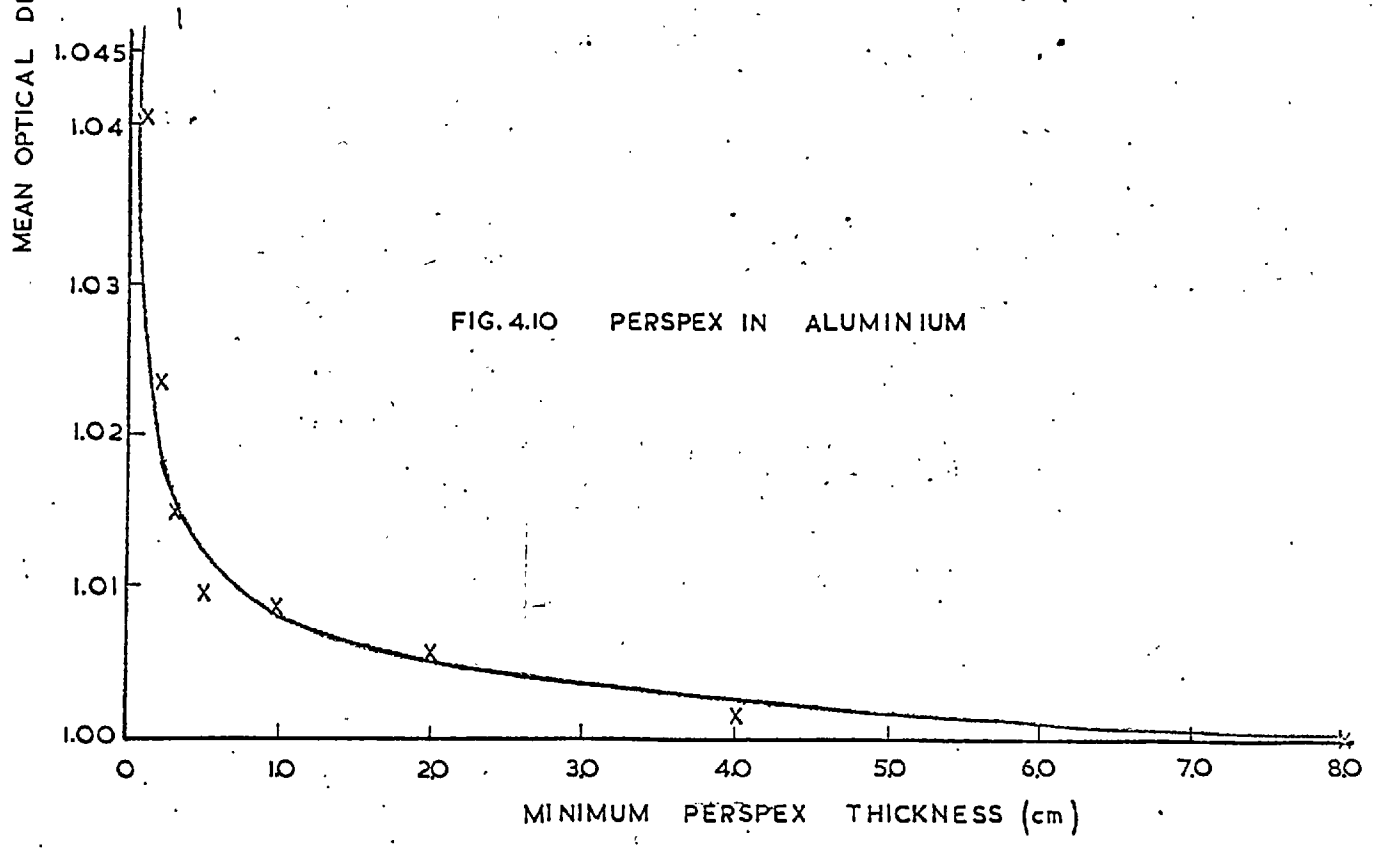

FIG. 4.10 PERSPEX IN ALUMINIUM

FIG. 4.9 & 4.10. VARIATION OF MEAN OPTICAL DENSITY OF PERSPEX AGAINST MINIMUM LINEAR DIMENSION OF THE CAVITY. (THEORY——, EXP. X)

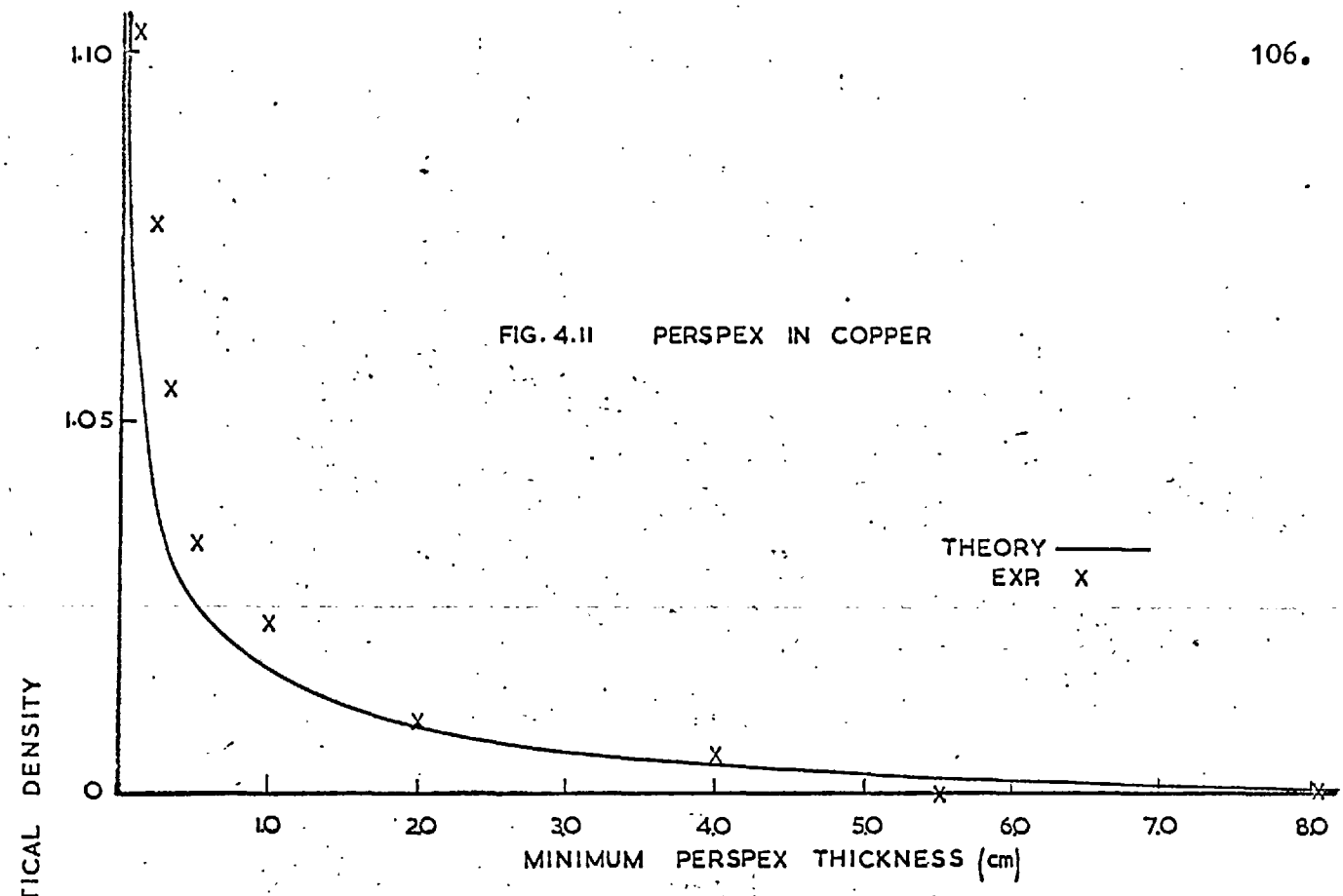

FIG. 4.11 PERSPEX IN COPPER

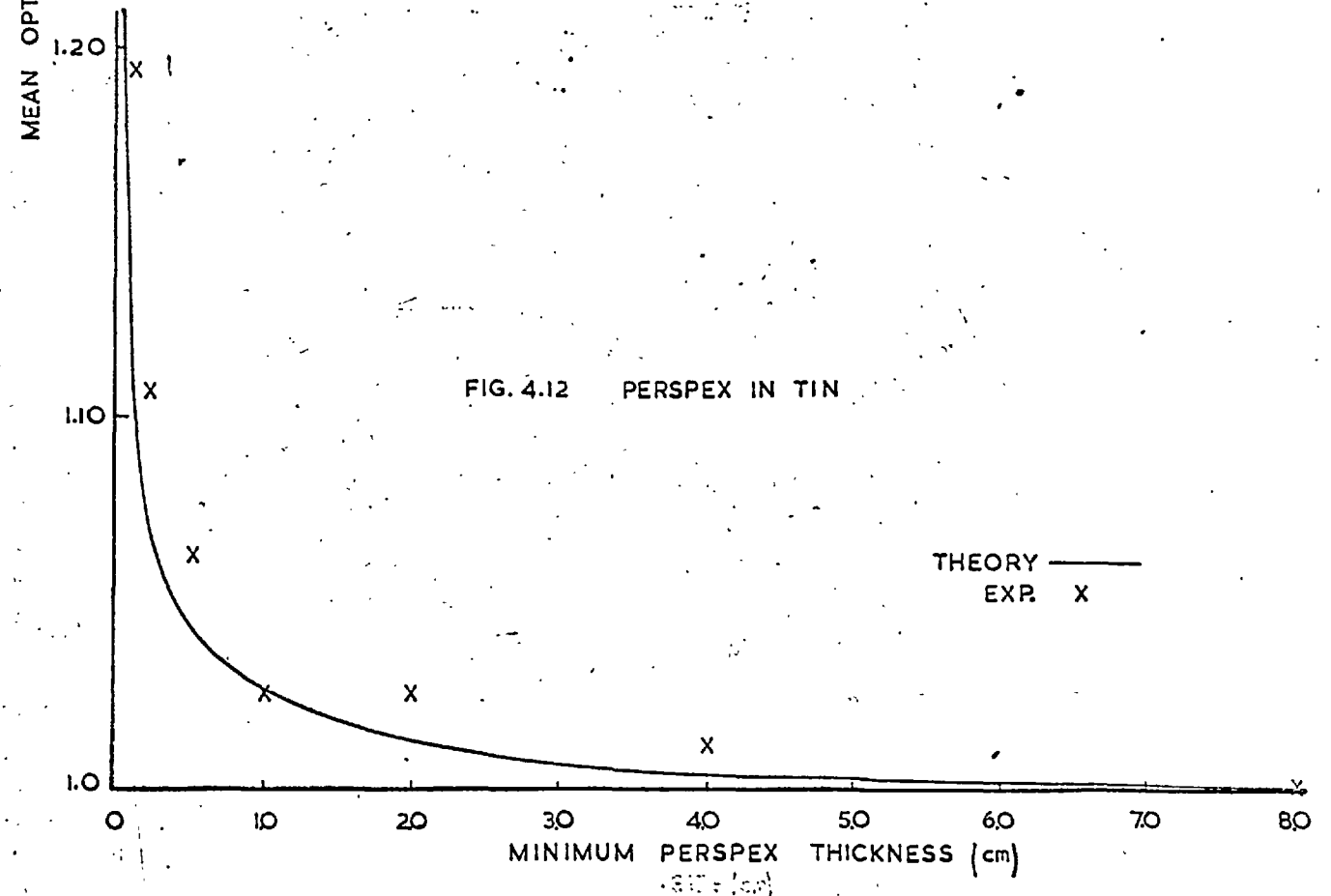

FIG. 4.12 PERSPEX IN TIN

FIG. 4.11. & 4.12. VARIATION OF MEAN OPTICAL DENSITY OF PERSPEX AGAINST MINIMUM LINEAR DIMENSION OF THE CAVITY.

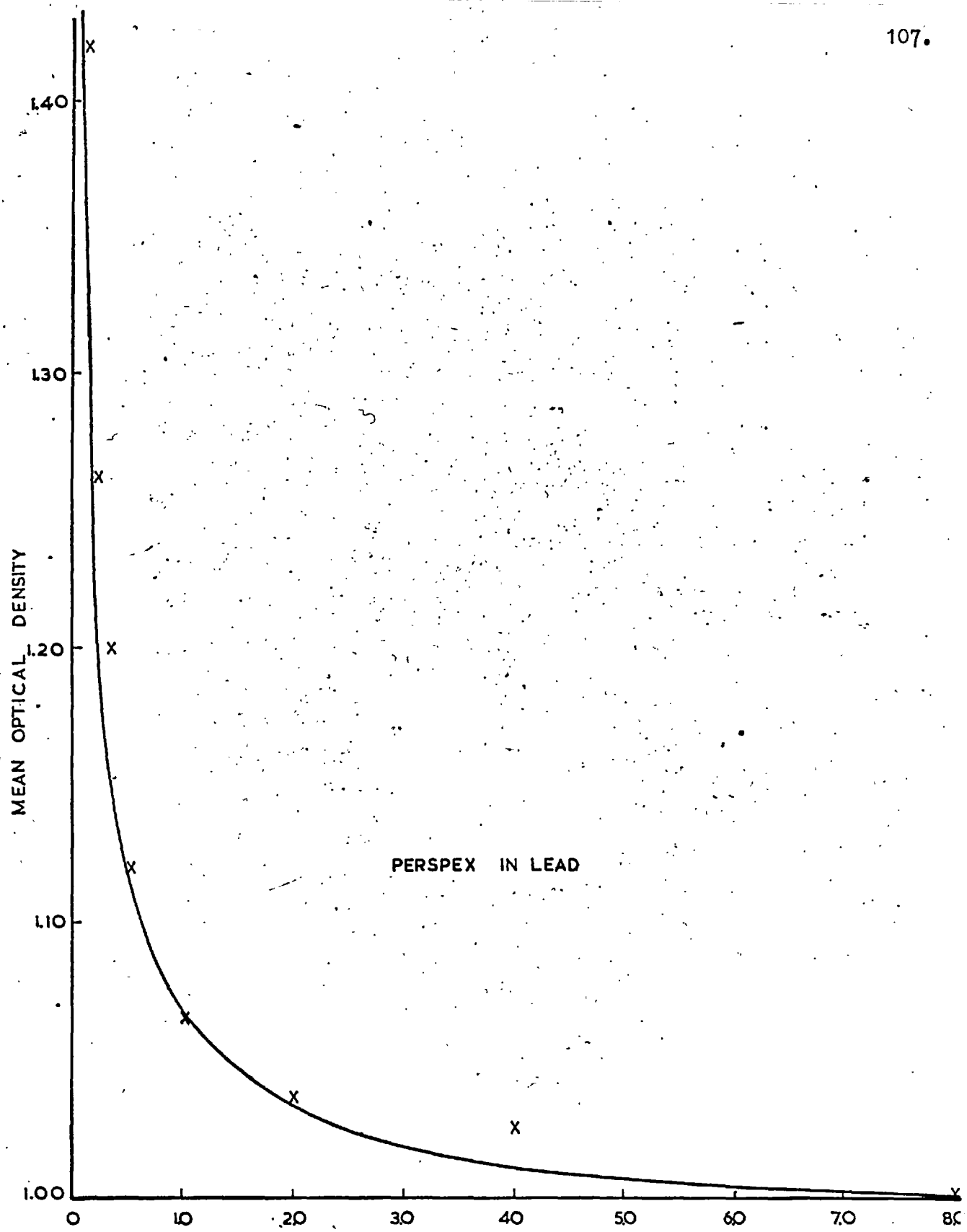

FIG. 4.13 VARIATION OF MEAN OPTICAL DENSITY OF PERSPEX AGAINST MINIMUM LINEAR DIMENSION OF THE CAVITY.

THEORY ——— EXPERIMENT X

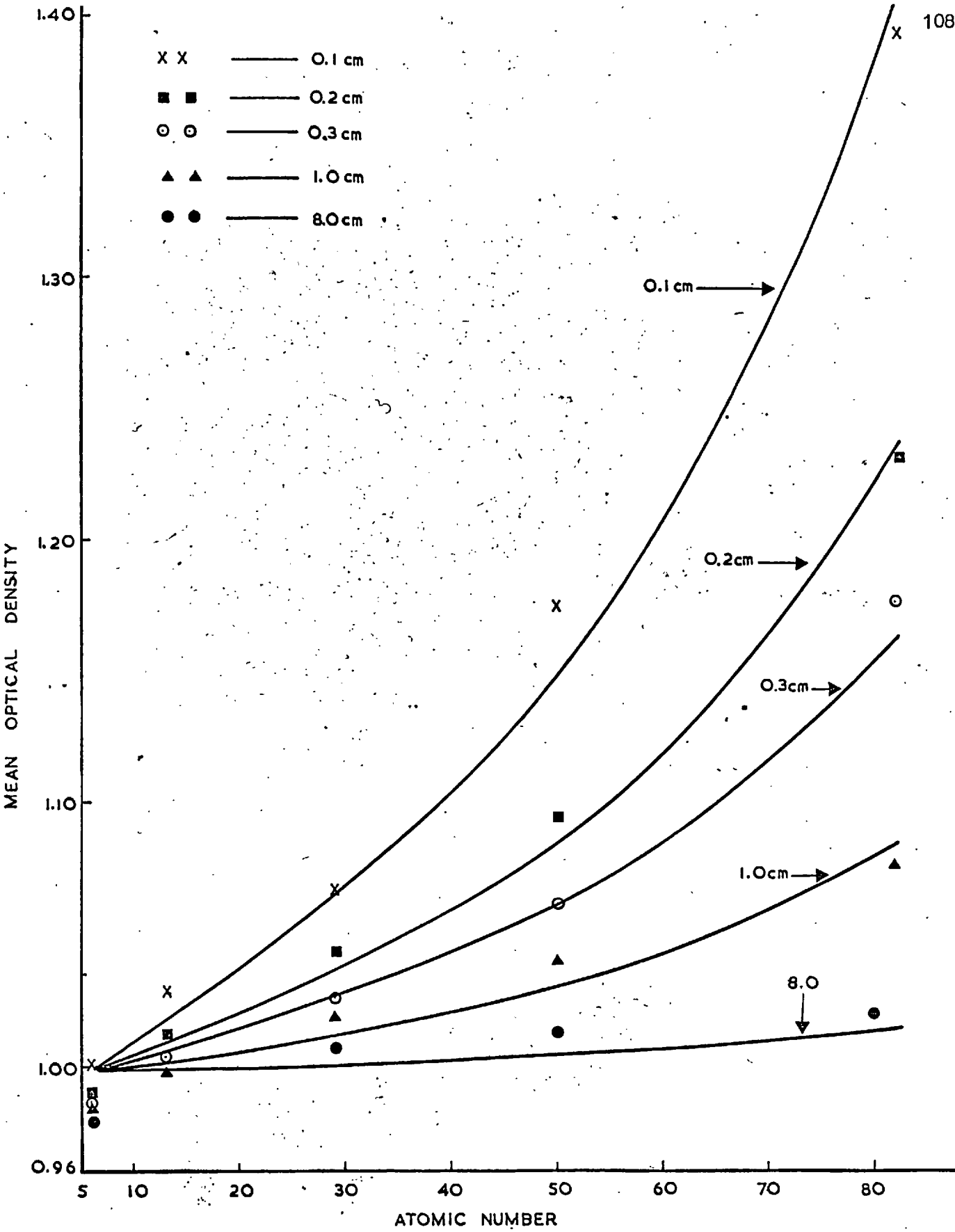

FIG. 4.14. VARIATION OF MEAN OPTICAL DENSITY OF PERSPEX WITH ATOMIC NUMBER OF THE WALL MATERIAL.

THEORY —— EXPERIMENT X ■ ⊙ ▲ ●

CHAPTER 5

APPLICATION OF CAVITY IONISATION THEORY AT LOW PHOTON ENERGIES TO RADIATION DETECTORS

I Introduction

A general theory of cavity ionisation (Burlin 1966) which took into account the modification of the electron spectrum by the cavity has been discussed in Chapter 1. The weighting factor, d, in equation 17 was evaluated by the use of the mass energy absorption coefficient for electrons, β, and β was calculated from Loevinger's (1956) formula. In this chapter, an example of the use, with high energy photons, of general cavity ionisation theory with Loevinger's formula is given first.

However, the application of cavity theory to photons of energy less than 200keV presents difficulties because the electrons have energies below the range for which the Loevinger formula was intended. Therefore, later in this chapter, another method of evaluating the mass energy absorption coefficient for electrons and hence the weighting factor, d, is developed.

II Application of Cavity Theory to a Solid State Dosimeter at High Photon Energies

The experiments of Bjarngard and Jones (1966) can be used to illustrate the application of cavity ionisation theory to a solid state dosimeter at high photon energies. Bjarngard and Jones, using Co^{60} (1.25MeV) γ-rays, irradiated discs of different thicknesses of thermoluminescent materials. They used up to 30 per cent by weight of either LiF or CaF_2:Mn incorporated in teflon. The materials were sandwiched between carbon and lead. The disc of the dosimeter was cut with a microtome to various thicknesses between 15 - 380 microns.

The calculations were performed using Loevinger's expression for the mass energy absorption coefficient of the electrons with due

weighting for the photo-electric and Compton electrons. To cover the extremes used in the experiment, 30 per cent LiF, 30 per cent CaF_2:Mn in teflon and 100 per cent teflon were considered. These are shown in Figure 5.1 as the ratio of the response of the dosimeter sandwiched between lead to that of carbon versus dosimeter thickness. The agreement between the calculations and Bjarngard and Jones' measurements is within experimental error. Thus for high energy photons, the general theory of cavity ionisation (incorporating Loevinger's expression) which was found successful for ionisation chambers is also correct in predicting the response of a solid state dosimeter.

III Evaluation of the Mass Energy Absorption Coefficient, β, of Electrons at Low Energies

Few direct measurements of the mass absorption coefficient of electrons, β, at low energies have been reported. The most plentiful data on directly ionising particles, especially electrons, are on their range, although these are by no means satisfactory. A method of relating the mass absorption coefficient of electrons to their range was therefore sought. Since the attenuation of electrons is approximately an exponential function (Schmidt, 1906, Hahn and Meitner, 1908), the simplest method is to define the range as a fixed attenuation (i.e. $e^{-\beta R}$ = constant) and to solve the equation to obtain β.

The range, R, of an electron is a rather imprecise quantity due to the effects of straggling and change of direction. The two ranges referred to most frequently are as follows.

(a) The extrapolated range, Ro, which is usually determined by extrapolating the slope of the percentage of particle transmission against the thickness of absorber. The extrapolated range corresponds to a residual electron transmission of 2-5 per cent (Bichsel 1968), which in turn corresponds to a residual energy transmission of 0.66 to 1.66 per cent (Cole, 1967). $R_o \approx R$ 3 per cent particle transmission $\approx R$ 1 per cent energy transmission.

(b) The maximum range, Rmax, as [illegible] is usually determined by the absorber thickness necessary to attenuate the incident electrons to an 'undetectable level'. This undetectable level will in fact depend on the measuring system. The maximum range corresponds to the thickness in an absorber where the energy transmission has dropped to about 0.1 per cent of its initial value, which in turn corresponds to a residual electron transmission of 0.3 per cent (Berger and Seltzer, 1964).

$R_{max} \approx R_{0.3\%\text{particle transmission}} \approx R_{0.1\%\text{energy transmission}}$.

This choice probably gives undue weight to the few electrons that happen to have long ranges. Also, the maximum range is less well defined than the extrapolated range because it depends on instrument sensitivity. While it is true that the maximum energy in a spectrum of electrons is the dominant parameter in determining the range, it was felt that some allowance should be made for the fact that, in cavity ionisation theory, the relevant spectrum of electrons is not monoenergetic and has many electrons with less than the maximum energy. Thus a range equal to 1 per cent of particle transmission was considered the best choice in calculating β at low energies, viz:- $e^{-\beta R} = 0.01$.

IV Investigation of the Criticality of the Input Parameters

To show that the choice of the percentage of the particle transmission was not too critical, calculations by cavity theory for 0.3, 1 and 3 per cent particle transmission were performed for lithium fluoride in air, ferrous sulphate in silica and tissue in bone, using ranges from Berger and Seltzer's (1964) tables (to be discussed later). The computer calculations covered all practical sizes for each system. Results from these calculations are presented in figures 5.2, 5.3 and 5.4 which give the change in response of these systems with photon energies. The sizes in each system were chosen to show the greatest variation for the 0.3, 1, 3 per cent particle transmission. In figures 5.2 and 5.3, for LiF in air and ferrous sulphate in silica respectively, there is little difference in the calculations for the 0.3, 1 and 3 per cent particle transmission. In figure 5.4 for tissue in bone, the differences

are greater and this is due to greater differences that occur in the atomic numbers between tissue and bone.

Two methods of defining R were considered in the equation $e^{-\beta R} = 0.01$. The first was Katz and Penfold's (1952) range-energy equation

$$R_o(gm/cm^2) = 0.412\,\bar{E}^n \qquad 5.1$$

where $n = 1.265 - 0.0954 \ln \bar{E}$

for $0.01 \leq \bar{E} \leq 2.5$ MeV

The second was the range calculated using the continuous slowing down approximation (CSDA) and tabulated by Berger and Seltzer (1964). [illegible]. These CSDA ranges are multiplied by a 'foreshortening factor' F, where $F = R_{max}/R_{CSDA}$ where Rmax is the experimental range from Gubernator and Flammerfeld (1959). F is not a sensitively varying parameter with energy. Thus the range obtained by the second method is $R = F \times R_{CSDA}$.

The two methods of evaluating R were found not to affect significantly the final calculations by cavity theory. This is illustrated in Figure 5.5 for lithium fluoride in air, Figure 5.6 for ferrous sulphate in silica and Figure 5.7 for tissue in bone. The figures relate to a photon energy of 500keV where the variation, using Katz and Penfold, Berger and Seltzer ranges, was found from a whole series of computer calculations to be maximal. Since the range data of Berger and Seltzer were much more recent, and cover an extensive range of atomic numbers these were selected whenever they were available. Otherwise, Katz and Penfold's expression (equation 5.1) was used for cavity theory calculations at low photon energies.

V Application of Cavity Theory to Thermoluminescent Dosimeters Irradiated by Low Energy Photons

Four materials, lithium fluoride, calcium fluoride, calcium sulphate and lithium borate have been used as thermoluminescent dosimeters. These dosimeters are frequently irradiated as powders either with air between the particles or embedded in a teflon matrix. The

energy deposited in the particles and hence their light emission will be influenced by their surroundings. Cavity theory has been used to calculate the variation of thermoluminescent response with photon energy and particle size in the extreme case (i.e. when the particles are separated by distances of the same order as the electron range) using equation 4.2. The ranges used in these calculations were found using Katz and Penfold's expression (equation 5.1) since Berger and Seltzer's data did not include the ranges in calcium fluoride, calcium sulphate and lithium borate. The average excitation potentials of these materials were found using Bragg's law (Section IVc, Chapter 4) and are given in Table 4.5. The mass energy absorption coefficients used are also shown in Table 4.5.

Va Application of Cavity Theory to Lithium Fluoride Dosimeter in Air and Teflon Irradiated by Low Energy Photons

Lithium fluoride (LiF) is a widely used solid state radiation dosimeter and has been shown experimentally to exhibit a response at low energies which is dependent on the grain size of the powder (Zanelli, 1968). Cavity theory adapted as described above was therefore applied to calculate the response of LiF for various particle sizes when irradiated in air. Figure 5.8 shows the variation of response of LiF with photon energy when irradiated for various diameter grains. Zanelli's experimental points are shown in Figure 5.9 and compared with the prediction of cavity theory for his particular particle sizes. The trend of the experimental results is the same as the theory, though the magnitude of the variation is greater.

Figure 5.10 shows the variation of response with energy for a 180 microns diameter LiF particle when irradiated in air. Measurements by Jayachandran (1968) using 180 $\pm$ 30 microns diameter LiF particles and irradiating 40-45mg of LiF on a 0.001 inch melinex tray at four different energies are also shown in Figure 5.10. Both the calculated results and Jayachandran's measurements are normalised at 48keV photon energy and agree to within the limits of experimental error.

It should be noted that in most experimental work, including that of Zanelli and Jayachandran, the lithium fluoride particles are in contact and in consequence the variation predicted from cavity theory will be reduced. This is not necessarily the case when lithium fluoride particles are imbedded in a teflon matrix, and the results of similar calculations for this case are shown in Figure 5.11.

Vb Application of Cavity Theory to Calcium Fluoride, Calcium Sulphate and Lithium Borate in Air and Teflon Irradiated by Low Energy Photons

Figures 5.12 to 5.17 show the response of various diameter grains of calcium fluoride, calcium sulphate and lithium borate in air and teflon, with energy. A maximum or minimum response occurs for these thermoluminescent dosimeters between 0.03 and 0.09MeV photon energy, depending on whether the stopping power of the surroundings are greater or less than the dosimeters. The explanation of the shape of the curves in Figures 5.8, 5.9 and 5.11 and Figures 5.12 to 5.17 is basically the same as that presented in discussing the Fricke dosimeter below.

VI Application of Cavity Theory to the Fricke Dosimeter Irradiated by Photons of Energy 0.02 - 3.0MeV

Experiments and calculations using cavity theory with Loevinger's expression for β have been discussed in Chapter 3 for the Fricke dosimeter irradiated by Co^{60} γ-rays. The calculations are now extended using the method described above, using Bergers and Seltezer's ranges, to evaluate the Fricke dosimeter response to photons of energy 0.02 - 3.0MeV.

Figure 5.18 shows the variation of dosimeter response with photon energyes for spherical irradiation cells of various radii. At 0.02MeV, photo-electric absorption is the dominant process but the photo-electrons barely penetrate into the ferrous sulphate solution even in the smallest cell. As the incident energy increases, the energy of the photo-electrons and their range increases and they penetrate through a

considerable depth into the solution in the smallest cell. In consequence the response of the dosimeter rises to a maximum at about ·05MeV. Further increase in the incident energy, say at 0.2MeV, reduces the proportion of photo-electrons to approximately 10 per cent but the proportion of Compton electrons increases to approximately 90 per cent. At 0.2MeV incident energy, the mean energy of a Compton electron is ·01MeV. Thus again, the electrons generated in the silica contribute little to the energy deposited in the ferrous sulphate solution. This accounts for the 'dip' in the curve at 0.2MeV. As the incident energy is further increased, the mean energy of the Compton electrons increases, depositing more of their energy in the dosimeter resulting in an increase in the response. The 'hump' in the curve for the 0.1cm radius spherical cavity just below 1MeV is associated with the values chosen for the mass energy absorption coefficients, and its magnitude is not greater than the uncertainty in these values.

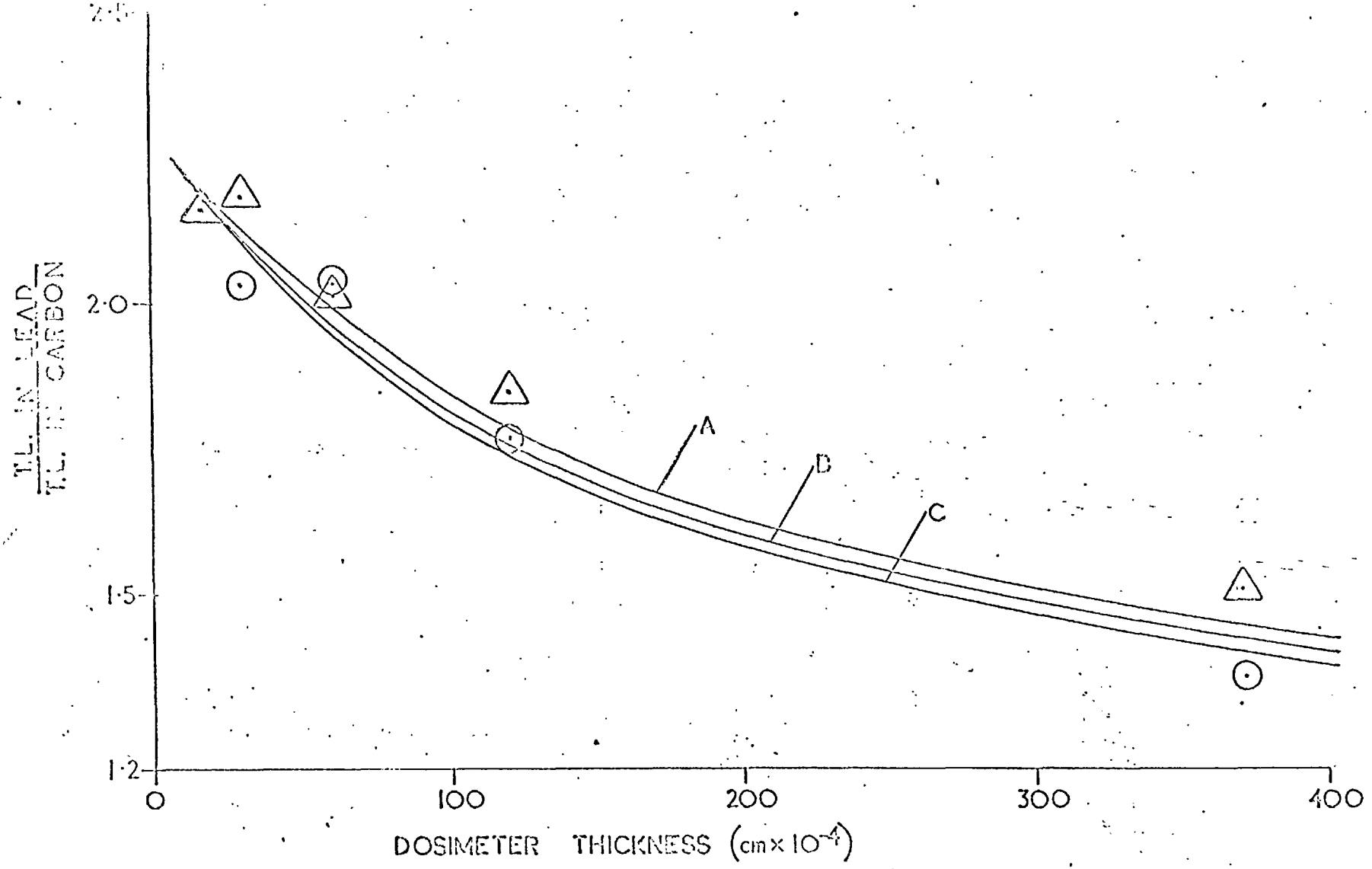

FIG. 5.1. THE RATIO OF THE DOSE IN PHOSPHOR–TEFLON DOSIMETERS IMBEDDED IN LEAD TO THE DOSE WHEN IMBEDDED IN GRAPHITE IRRADIATED WITH Co^{60} GAMMA RAYS VERSUS DOSIMETER THICKNESS.

EXPERIMENTAL RESULTS (FROM BJARNGARD & JONES, 1966): LiF—Teflon DISCS — ⊙. CaF_2:Mn—Teflon DISCS — △.

THE LINES REPRESENT: A — Teflon.
B — 30% LiF + 70% Teflon.
C — 30% CaF_2:Mn + 70% Teflon.

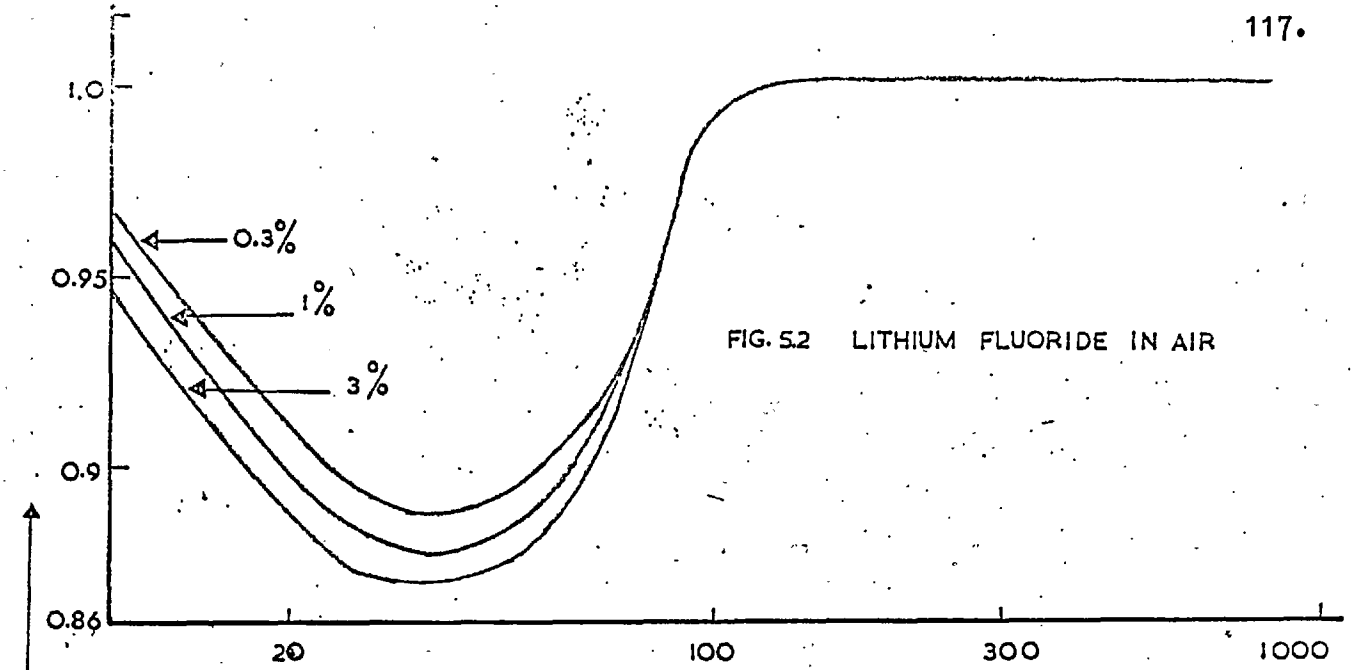

FIG. 5.2 LITHIUM FLUORIDE IN AIR

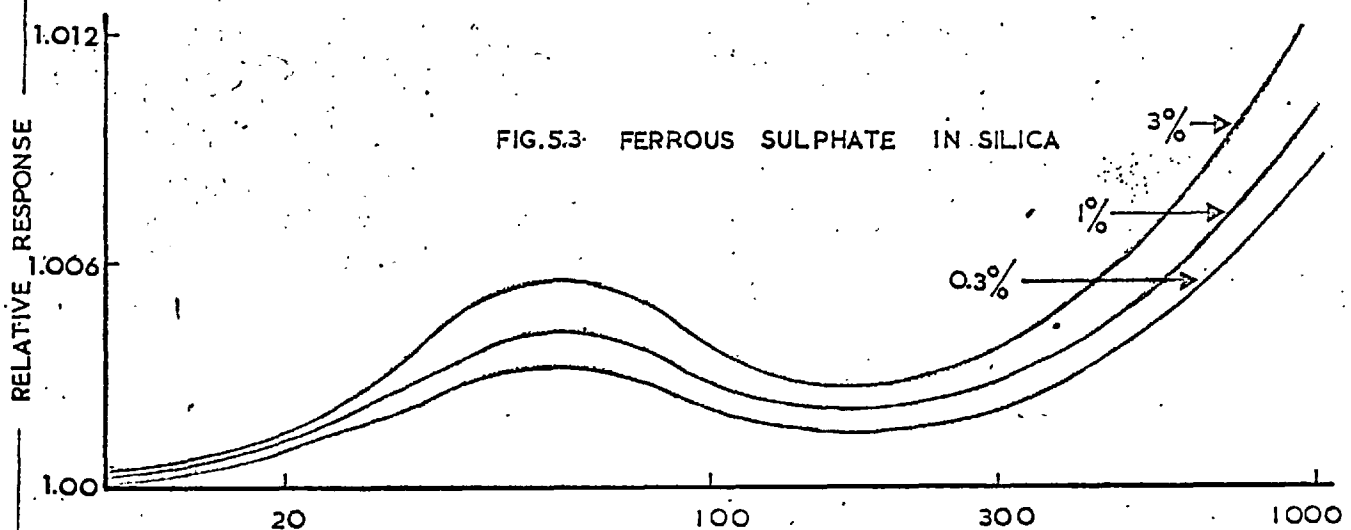

FIG. 5.3 FERROUS SULPHATE IN SILICA

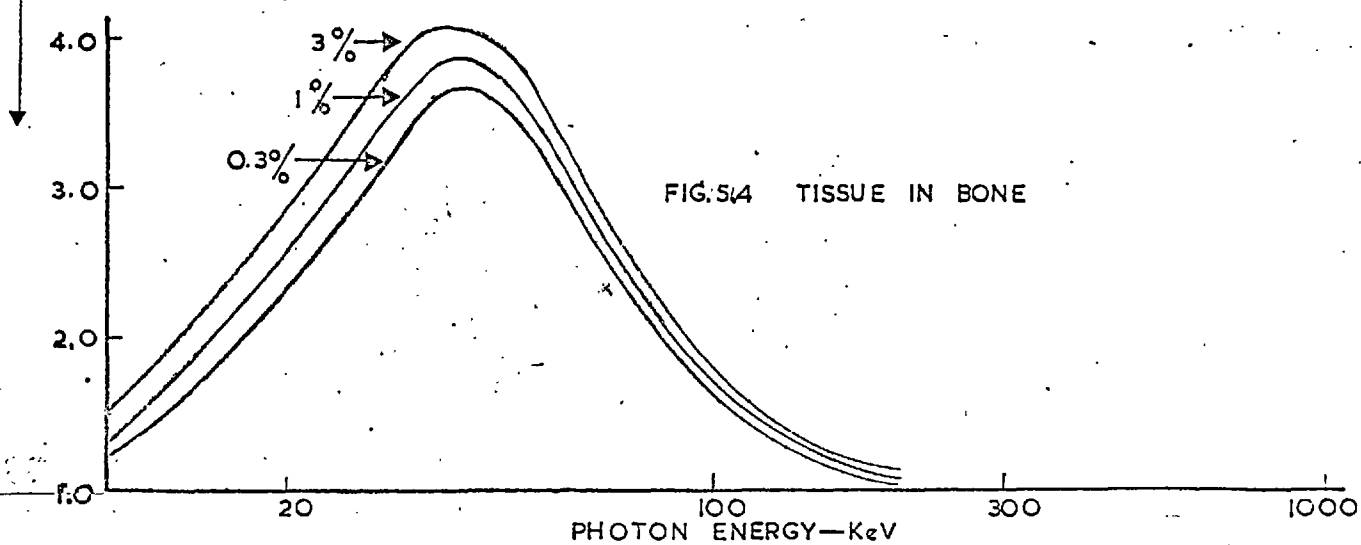

FIG. 5.4 TISSUE IN BONE

RELATIVE RESPONSE

PHOTON ENERGY—KeV

FIGS. 5.2—5.4. THE EFFECT OF TERMINATING THE RANGE AT DIFFERENT PERCENTAGE OF PARTICLE TRANSMISSION ON CAVITY THEORY CALCULATION.

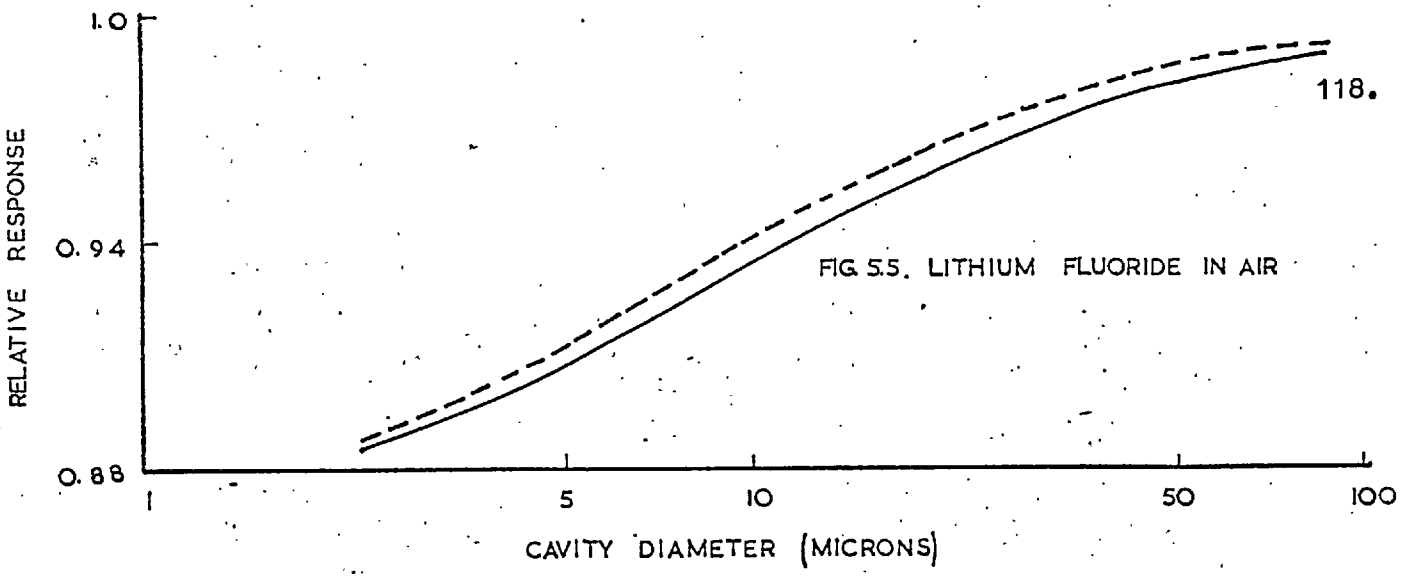

FIG. 5.5. LITHIUM FLUORIDE IN AIR

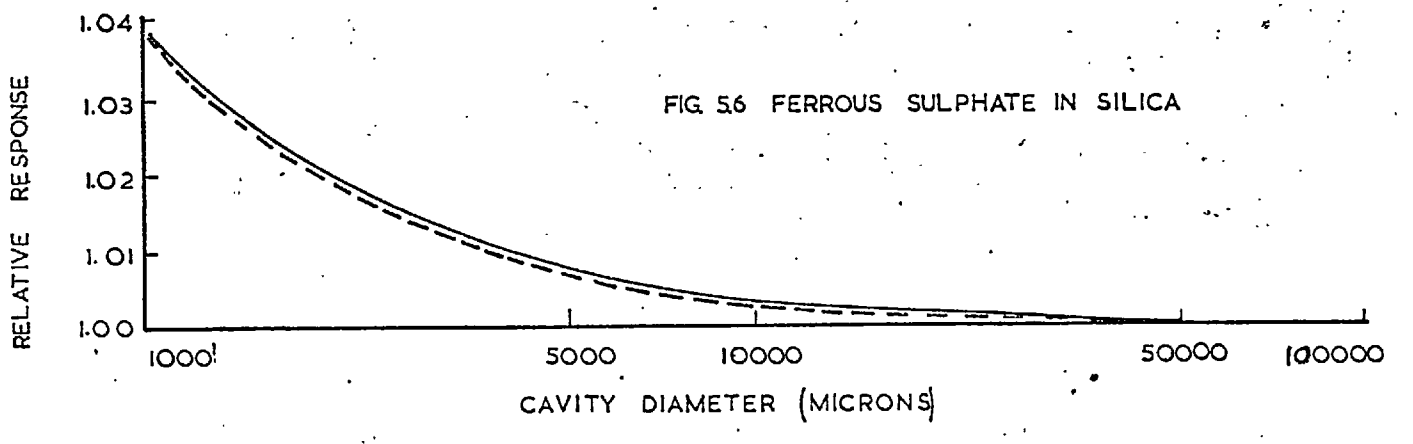

FIG. 5.6 FERROUS SULPHATE IN SILICA

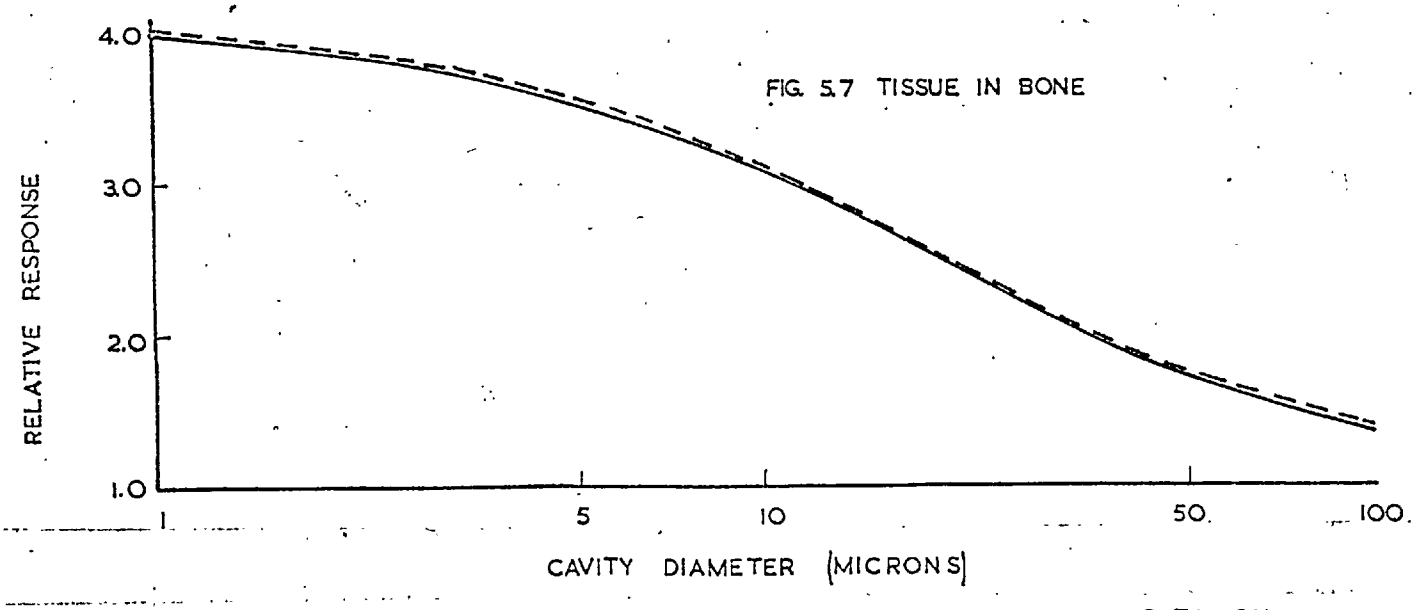

FIG. 5.7 TISSUE IN BONE

FIG. 5.5—5.7 THE EFFECT OF DIFFERENT ELECTRON RANGE DATA ON CAVITY THEORY CALCULATION. SOLID LINE— BERGER & SELTZER, BROKEN LINE— KATZ & PENFOLD.

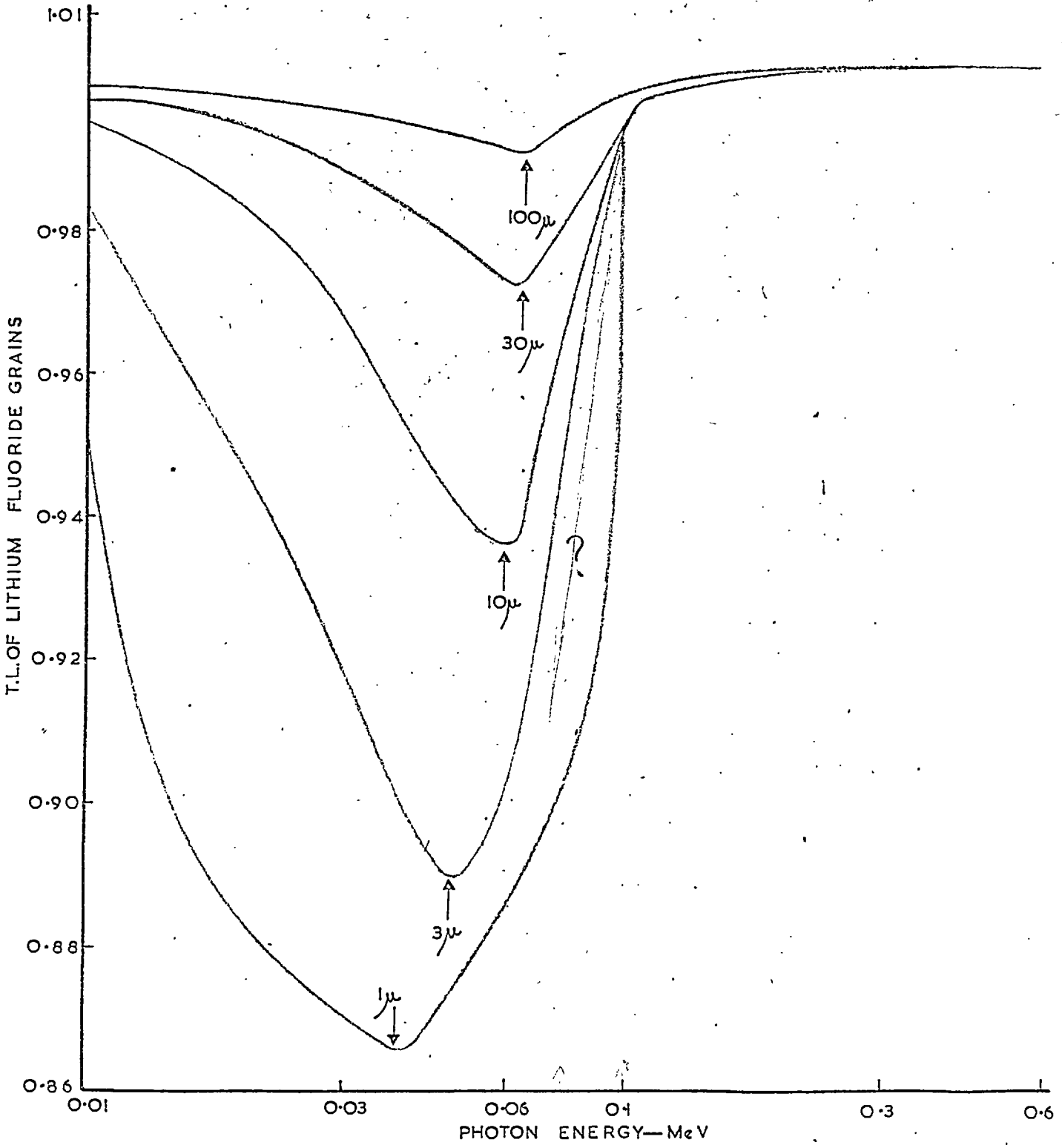

FIG. 5.8. VARIATION OF RESPONSES OF LITHIUM FLUORIDE GRAINS IRRADIATED IN AIR WITH PHOTON ENERGY. THE DIAMETERS OF THE GRAINS ARE INDICATED ON THE GRAPH.

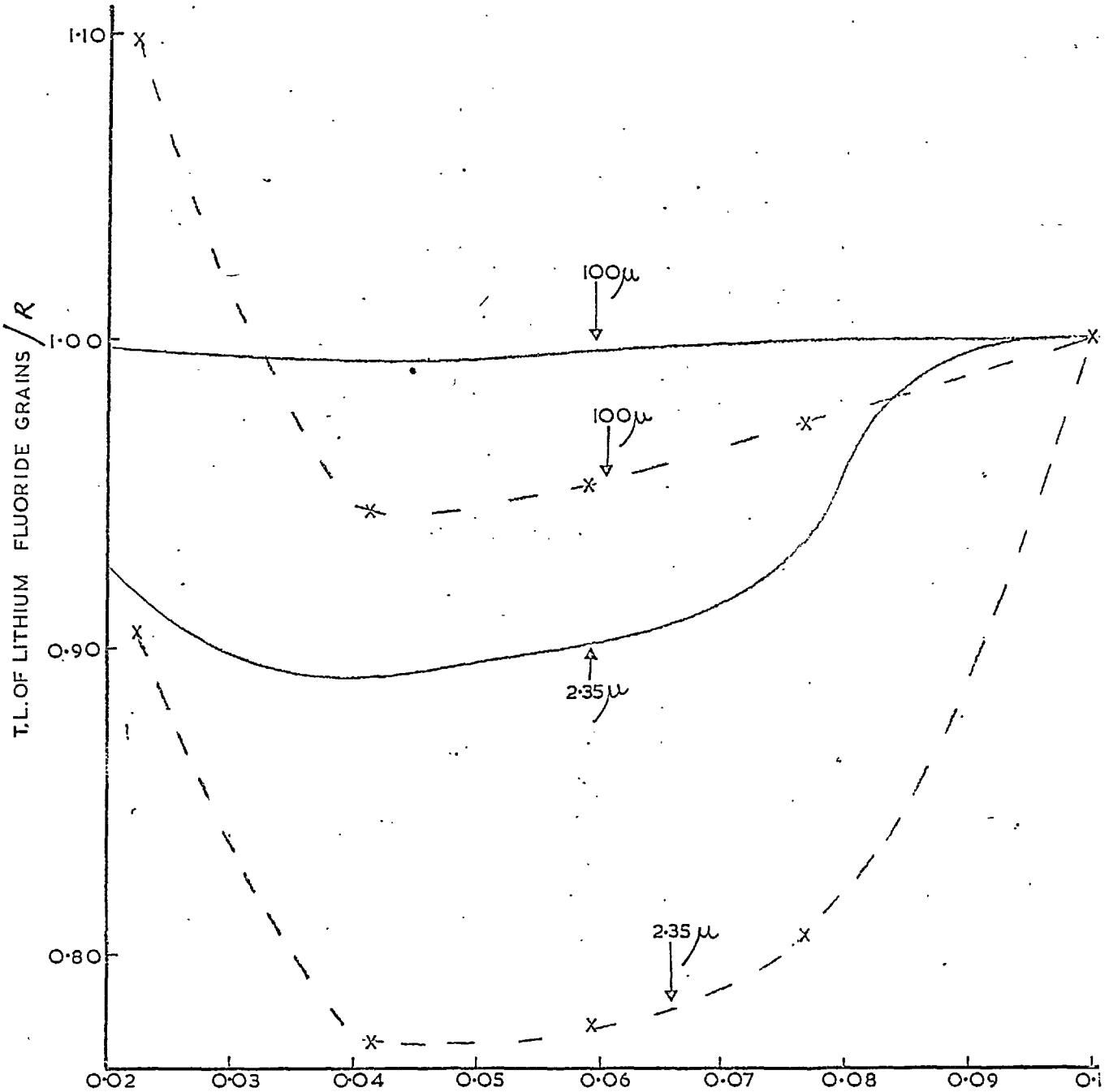

FIG.5.9. VARIATION OF RESPONSES OF LITHIUM FLUORIDE IRRADIATED IN AIR WITH PHOTON ENERGY. THE DIAMETERS OF THE GRAINS ARE INDICATED ON THE GRAPH. SOLID LINE—CAVITY THEORY; BROKEN LINE—EXPERIMENTAL MEASUREMENTS (ZANELLI, 1968).

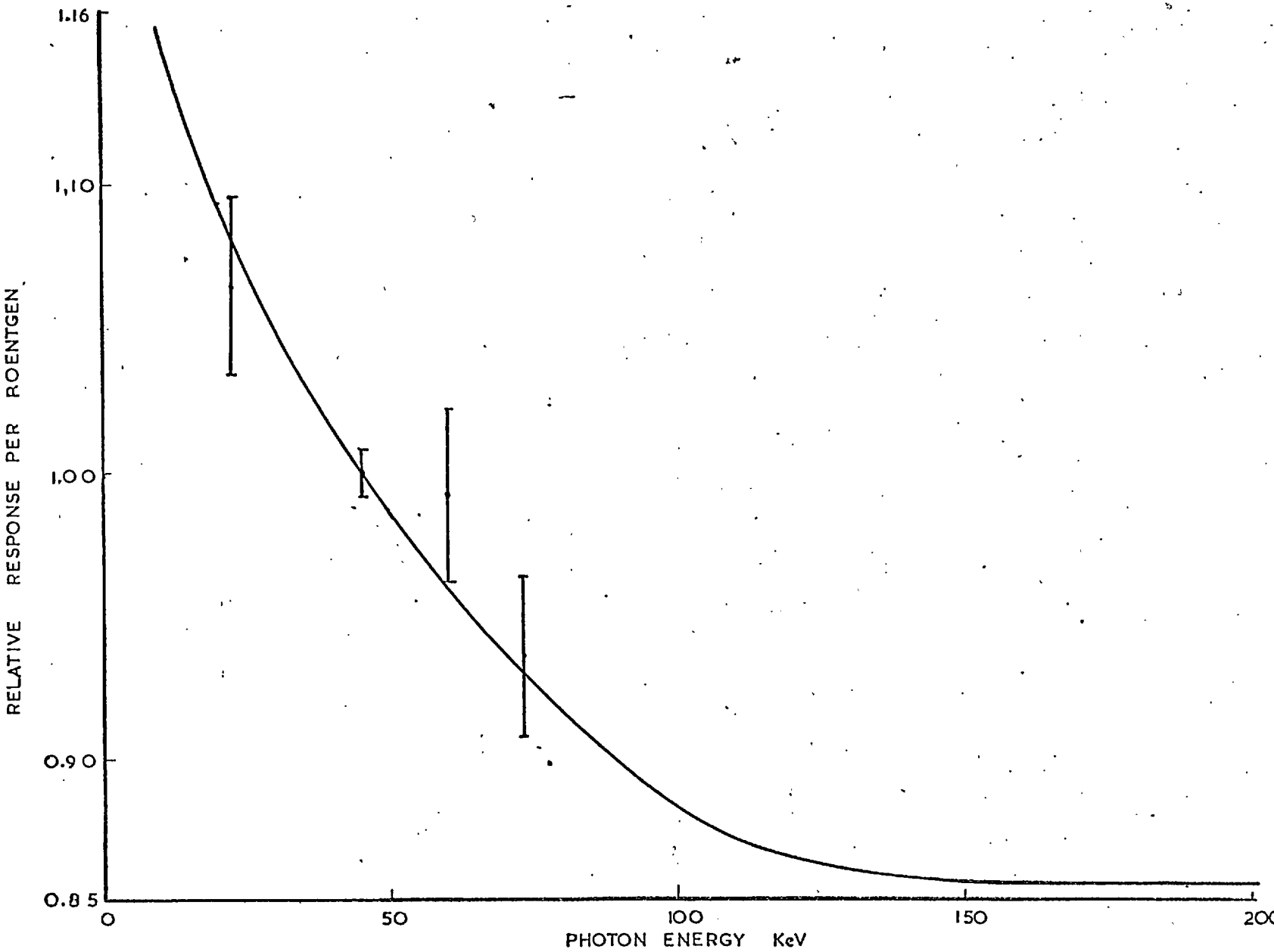

FIG. 5.10. RELATIVE RESPONSE OF A 180 MICRONS DIAMETER LiF GRAIN IN AIR VERSUS PHOTON ENERGY. SOLID LINE — CAVITY THEORY. POINTS — JAYACHANDRANS MEASUREMENT (1968).

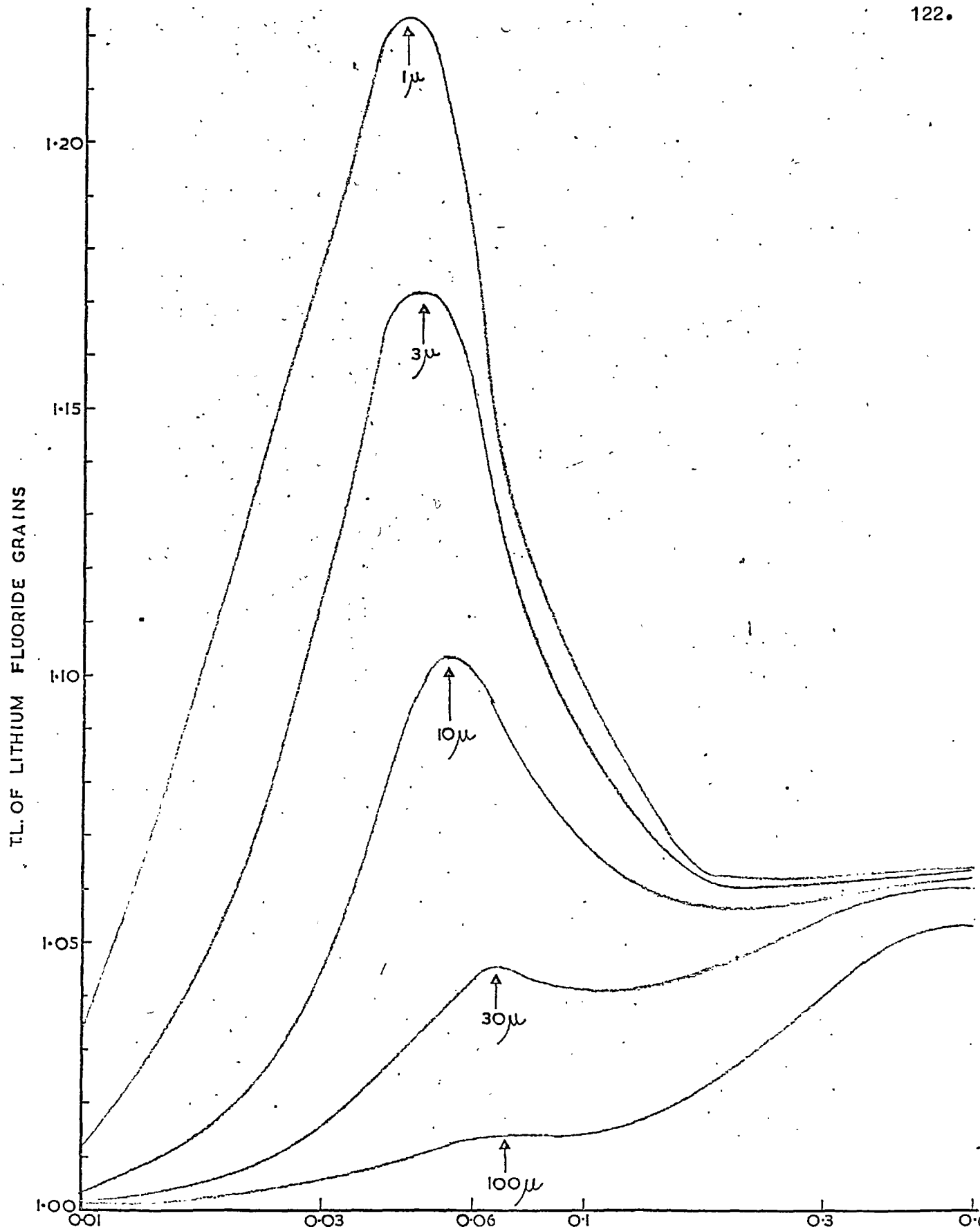

FIG. 5.11. VARIATION OF RESPONSES OF LITHIUM FLUORIDE GRAINS IRRADIATED IN TEFLON WITH PHOTON ENERGY. THE DIAMETERS OF THE GRAINS ARE INDICATED ON THE GRAPH.

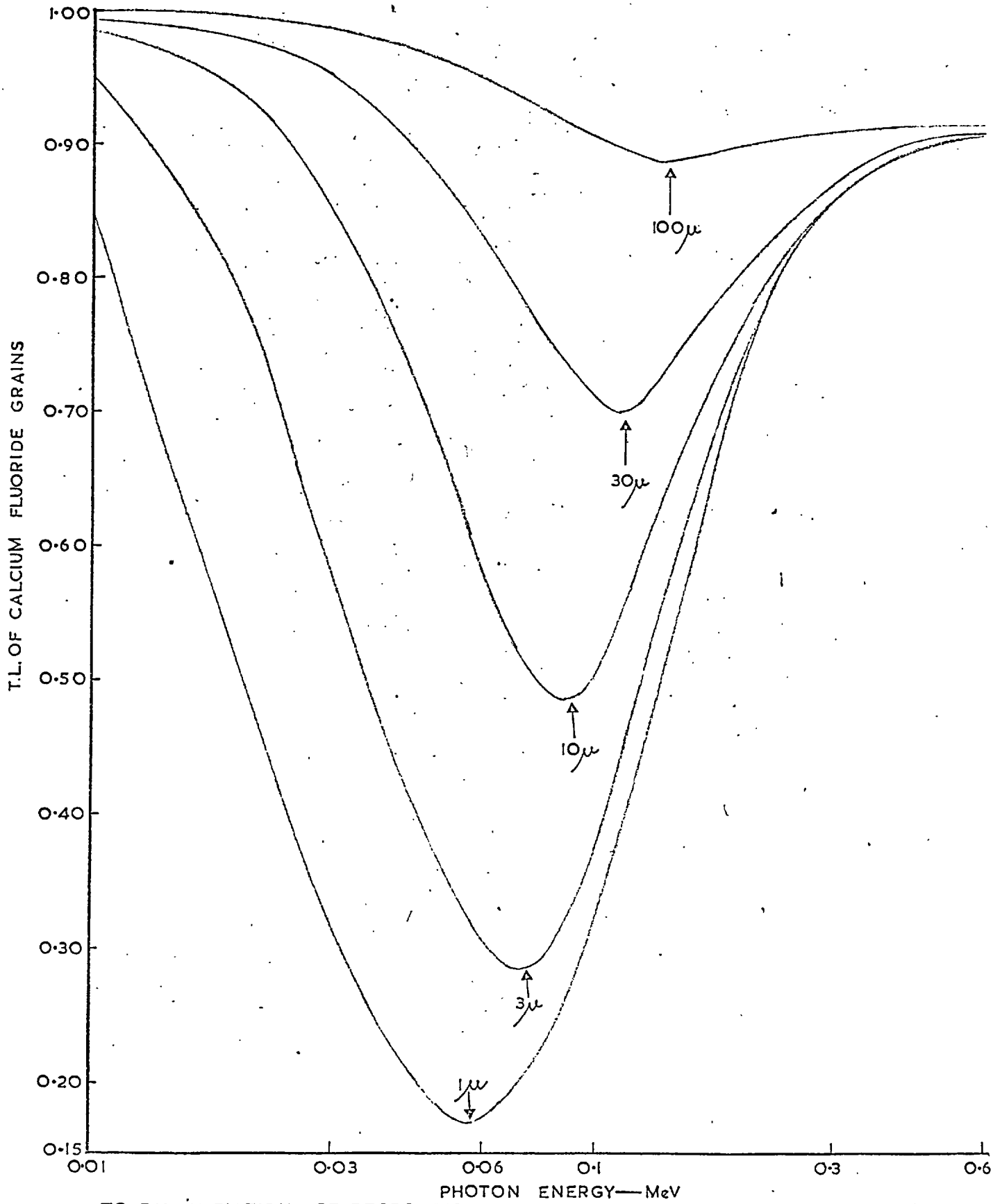

FIG. 5.12. VARIATION OF RESPONSES OF CALCIUM FLUORIDE GRAINS IRRADIATED IN AIR WITH PHOTON ENERGY. THE DIAMETERS OF THE GRAINS ARE INDICATED ON THE GRAPH.

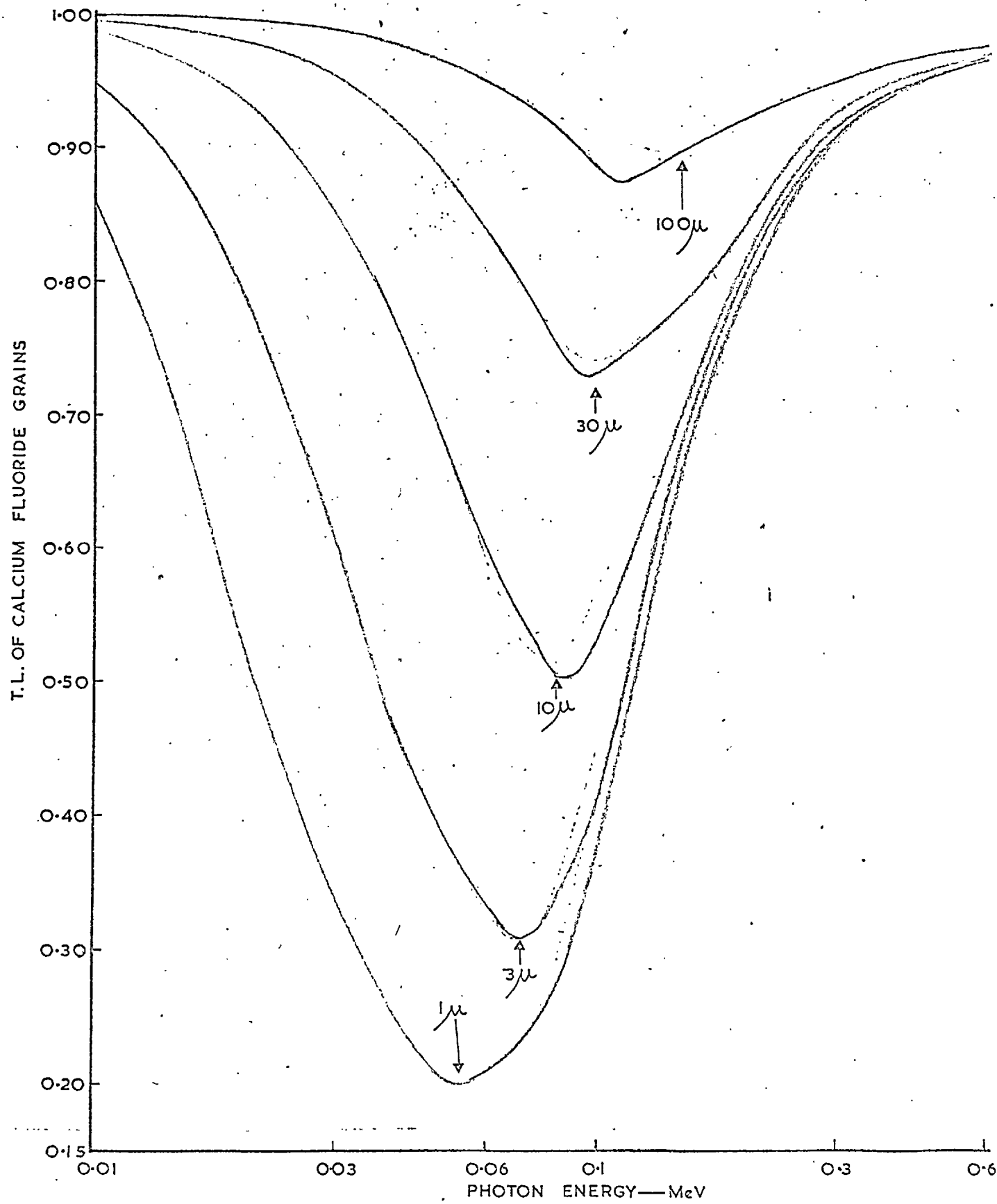

FIG. 5.13. VARIATION OF RESPONSES OF CALCIUM FLUORIDE GRAINS IRRADIATED IN TEFLON WITH PHOTON ENERGY. THE DIAMETERS OF THE GRAINS ARE INDICATED ON THE GRAPH.

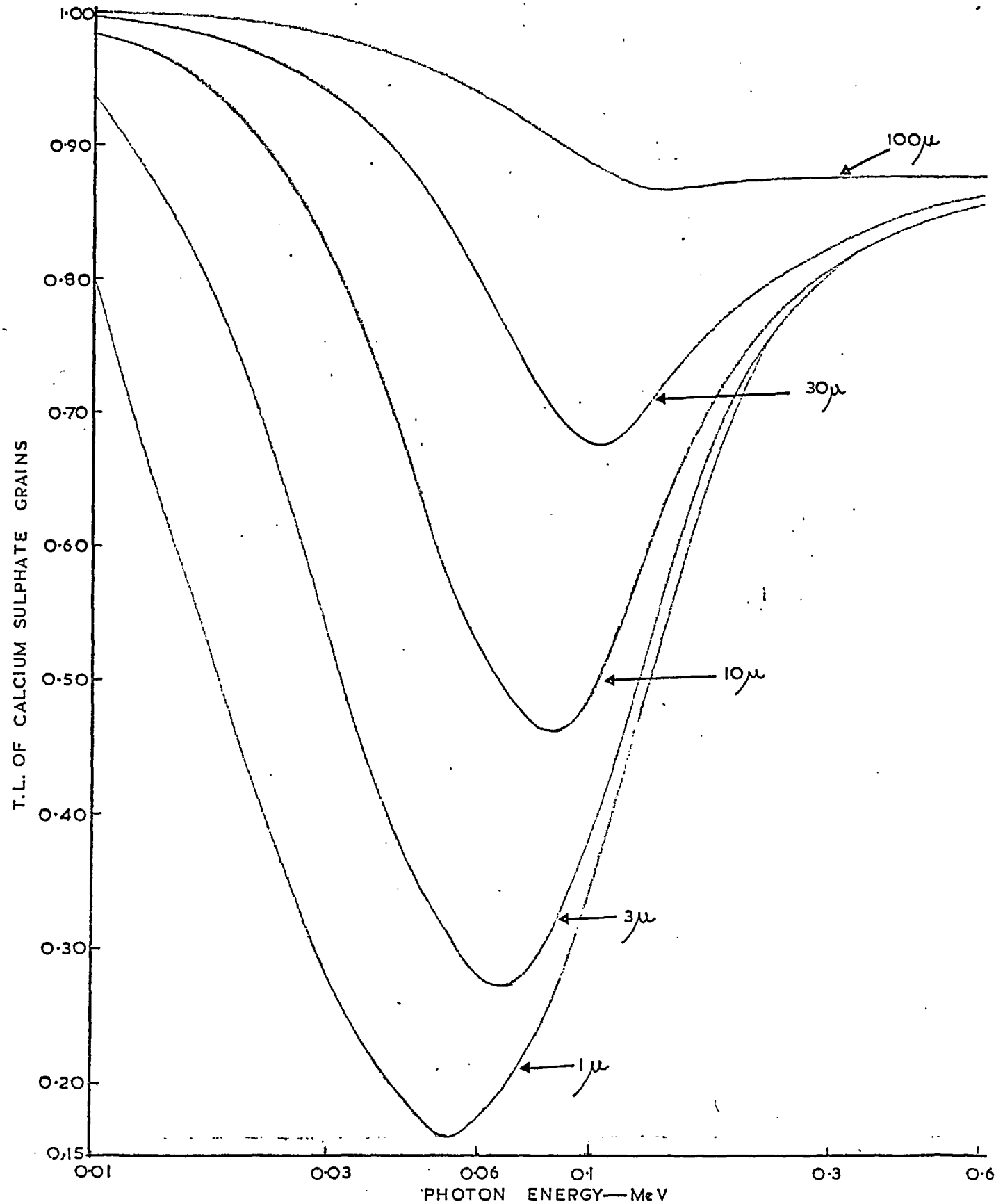

FIG. 5.14. VARIATION OF RESPONSES OF CALCIUM SULPHATE GRAINS IRRADIATED IN AIR WITH PHOTON ENERGY. THE DIAMETERS OF THE GRAINS ARE INDICATED ON THE GRAPH.

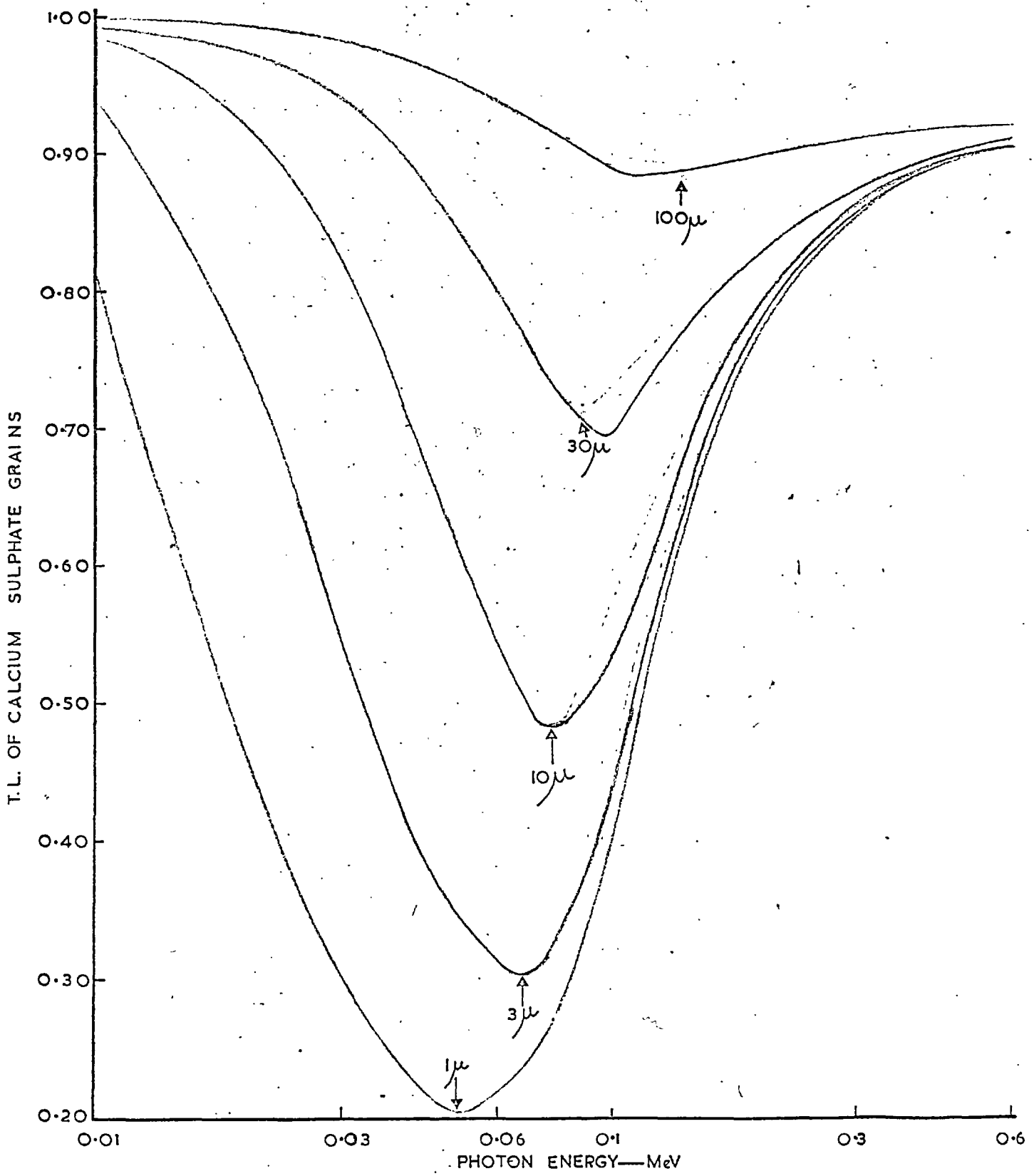

FIG. 5.15. VARIATION OF RESPONSES OF CALCIUM SULPHATE GRAINS IRRADIATED IN TEFLON WITH PHOTON ENERGY. THE DIAMETERS OF THE GRAINS ARE INDICATED ON THE GRAPH.

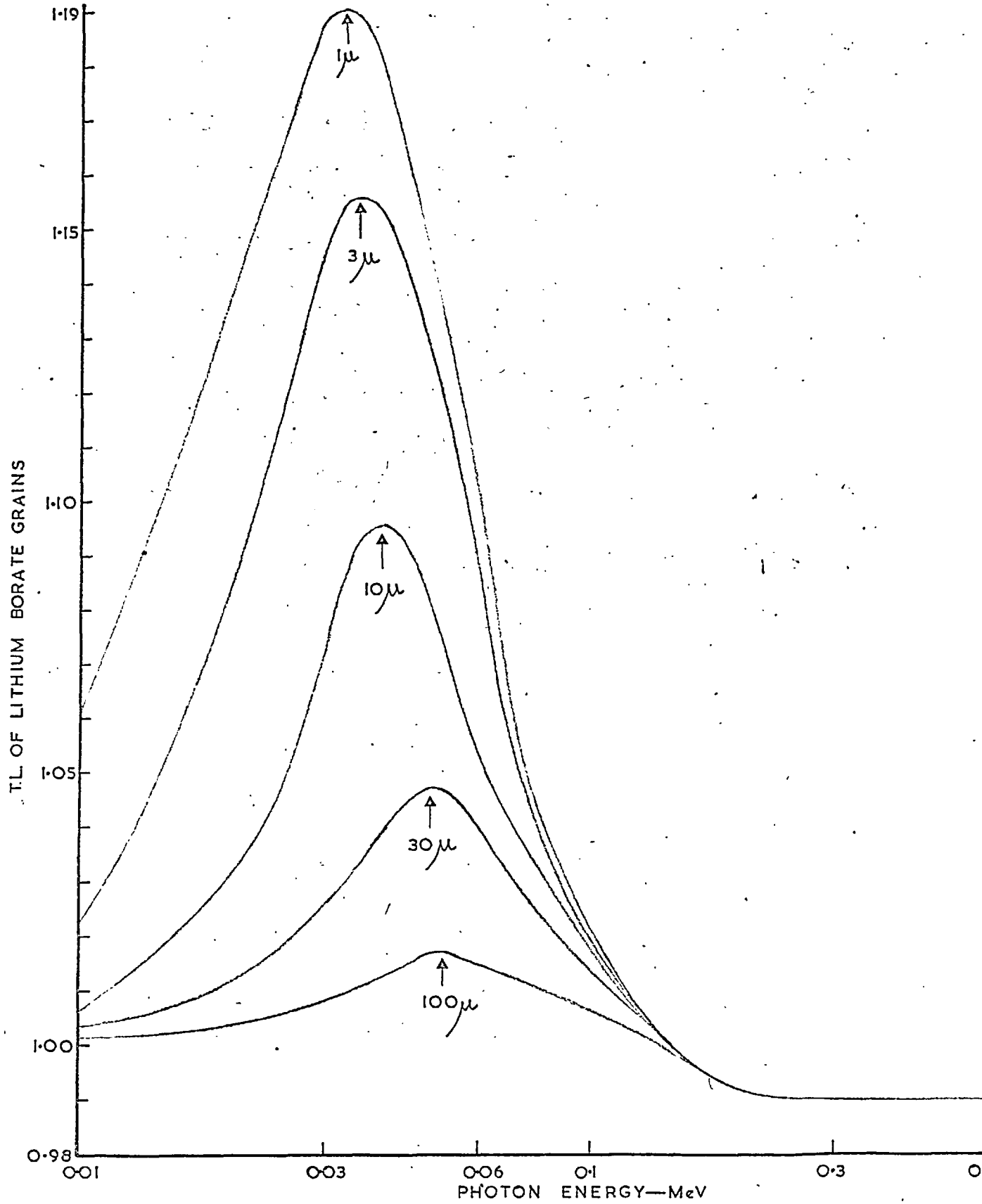

FIG. 5.16. VARIATION OF RESPONSES OF LITHIUM BORATE GRAINS IRRADIATED IN AIR WITH PHOTON ENERGY. THE DIAMETERS OF THE GRAINS ARE INDICATED ON THE GRAPH.

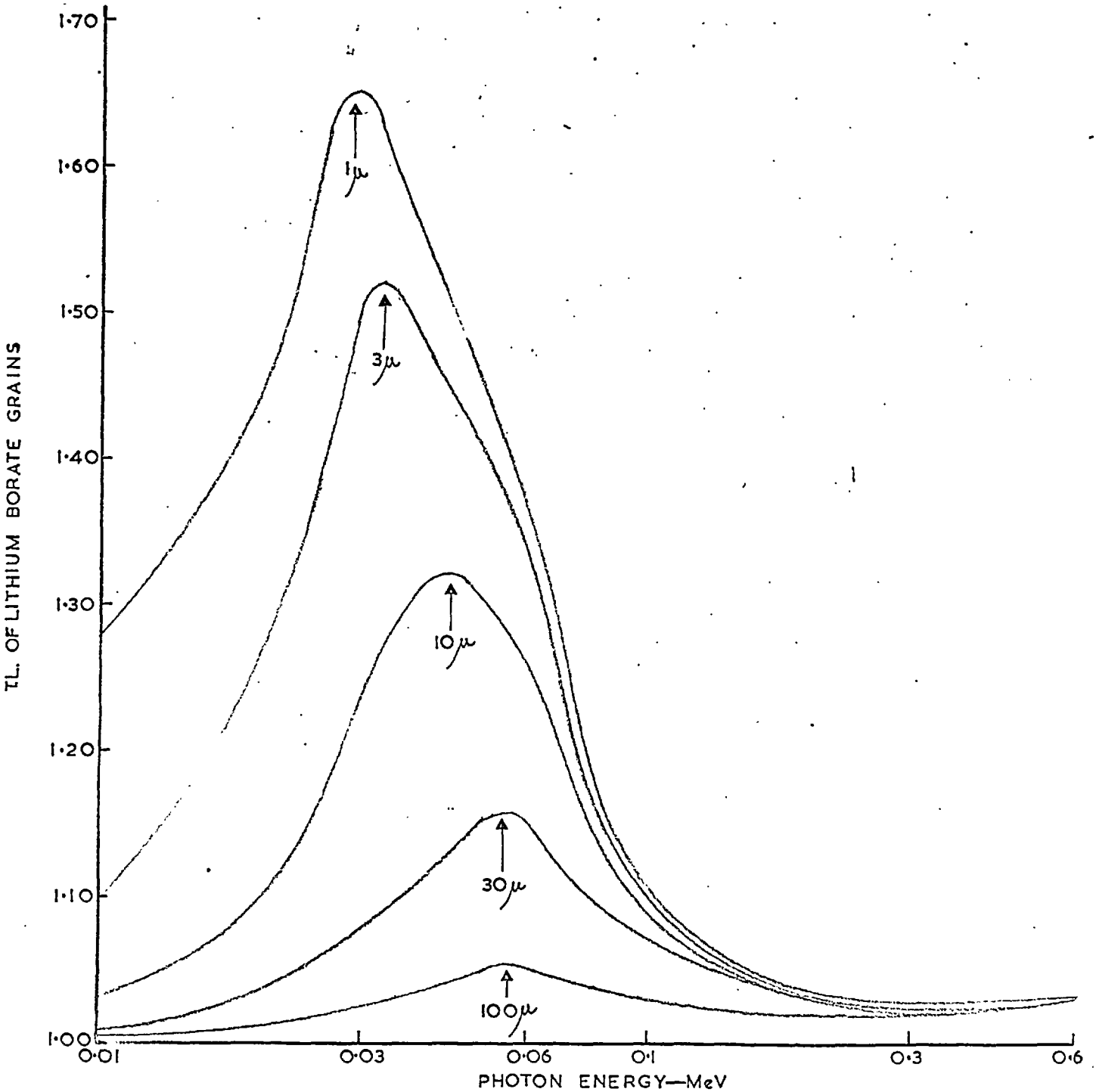

FIG. 5.17. VARIATION OF RESPONSES OF LITHIUM BORATE GRAINS IRRADIATED IN TEFLON WITH PHOTON ENERGY. THE DIAMETERS OF THE GRAINS ARE INDICATED ON THE GRAPH.

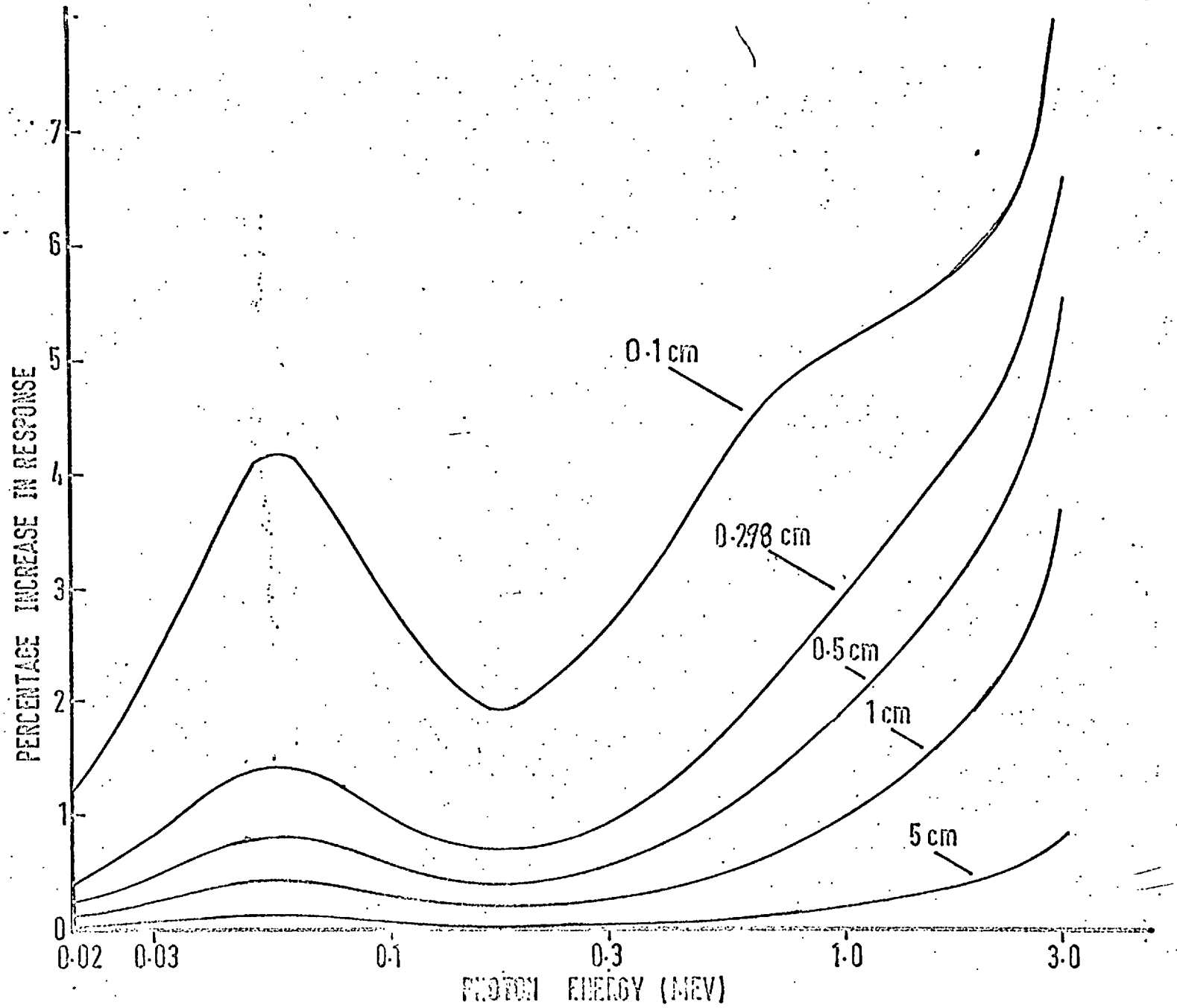

FIG. 5.18 PERCENTAGE INCREASE IN THE RESPONSE OF A FERROUS SULPHATE DOSIMETER IN VARIOUS SPHERCAL SILICA IRRADIATION CELLS OF SILICA VERSUS PHOTON ENERGY. THE RADII OF OF THE CELLS ARE INDICATED ON THE GRAPH.

CHAPTER 6

CALCULATION OF THE ABSORBED DOSE IN SOFT TISSUE INCLUSIONS IN BONE BY CAVITY IONISATION THEORY

I Introduction

In many diagnostic and therapeutic processes involving the use of radiation in patients, the bone is subjected to radiation. Since bone has a higher atomic number than soft tissue, the absorbed dose in bone will be different from that in soft tissue. When the body is irradiated with low energy X-rays (less than 0.2MeV), electrons are ejected from the bone, through photo-electric and Compton interactions, which have a sufficient range to give rise to an additional dose to the layers of soft tissue adjacent to the bone. It is necessary to know the dose given to these adjacent tissues in order to avoid a level of dosage which would result in their malfunction. For example, bone formation might no longer be maintained by the osteocytes.

There are three cases which are of interest in the dosimetry of bone and tissue (Spiers, 1967): (a) the osteocytes and tissues within the Haversian canals, (b) endosteal layers, one or two cells deep in cortical and trabecular bone and (c) active bone marrow in trabecular cavities.

This chapter reviews some of the earlier theoretical and experimental work in bone dosimetry for external and internal radiation sources. Cavity theory is then applied to calculate the dose in irradiated trabecular bone. The calculations, which are limited to external photon sources, are compared with the results of other workers.

II Basic Assumptions of Earlier Theoretical Calculations in Bone Dosimetry

The assumptions occuring in early theoretical approaches were as follows.

1. The electrons are liberated isotropically
2. They travel in straight lines
3. The range (R) of these electrons is equivalent to 70 per cent of

the range L which is calculated from the continuous slowing down approximation, i.e. $R = 0.70 \times \int -dE/(dE/dx) = 0.70 \times L$

4. The energy dissipated along the track is uniform, i.e. the linear energy transfer is uniform.

Other assumptions will be discussed later.

III Tissue Cavities Surrounded by a Thickness of Bone Adequate to Establish Electronic Equilibrium

Most workers have assumed that the thickness of the bone surrounding a soft tissue cavity is sufficient to establish electronic equilibrium. The following aspects of this problem have been treated:

(a) the distribution of dose with distance from the bone/tissue interface,

(b) the mean dose in a cavity of a particular size,

(c) the mean dose in a group of cavities.

These are reviewed below.

IIIa The Distribution of Dose with Distance from the Interface

Spiers (1949) calculated the variation in ionisation density perpendicular to a plane bone and soft-tissue interface, irradiated by monoenergetic photons (20 - 200 kVp X-rays). He added the contributions from two plane bone surfaces, separated by a thin soft-tissue element, and obtained curves showing the ionisation density in small parallel plane cavities from 1 micron to 100 microns in width. Woodard and Spiers (1953) extended Spiers (1949) calculation to take account of the complete photon spectrum of X-rays generated at 185 - 1000kVp. They obtained a summation for the energy absorption in the tissue over all secondary electron energies produced in bone by the photon spectrum. Due to the difficulties involved, these calculations were limited to plane parallel slabs, although the tissue elements within bone are very unlike this geometry. Fowler (1957), using 40 - 200kVp X-rays, measured the dose to polythene adjacent to plane glass (representing bone) by means of conducting charges induced in the polythene. His results showed general agreement with Woodard and Spiers (1953) calculation.

The next advance was due to Kononenko (1957) who determined the mean doses in cylinders and the dose at any point in a spherical cavity irradiated by α-particles (4.46MeV) arising in bone medium. His expression was a fundtion of the monoenergetic particle ranges and could be applied to any type of charged particle provided that the energy distribution was known. Using a cylindrical ionisation chamber, whose walls were impregnated with isotopes emitting α-particles, he varied the pressure of the ionisation chamber and his measurements agreed with his calculations to within 10 per cent.

Charlton and Cormack (1962a, b), using numerical integration, derived the dose near a plane interface and within cylindrical cavities both for external irradiation by X-rays (20 - 200kVp) and internal irradiation by α-particles (1 - 10MeV). Assumptions 1 to 3 were made in their calculations. Instead of using a linear energy transfer model (i.e. assumption 4), Charlton and Cormack used an expression for the variation of energy deposition along the particle track of the ionising particles by a range-energy relation, $R = AE^m$, where A and m are constants determined from experimental data. They used a value of 1.75 for m for X-rays of 200kVp and 1.5 for m for α-particles.

Howarth (1965) using α-particles, extended the basic formula of Charlton and Cormack. Assumptions 1 to 3 and the range-energy relation above (i.e. m = 1.5) were used in his calculations. He computed detailed tables giving the geometric function D/Do for planar, cylindrical and spherical geometries, where D is the dose at a point and Do the dose to a very small volume of soft tissue surrounded by bone.

Burlin and Hancock (1967), using a vacuum chamber irradiated by Cs^{137} γ-rays, measured the dose in tissue-like material (carbon) next to higher atomic number materials. They measured the current due to low energy electrons emerging from the surface and thus estimated the absorbed dose in a very thin layer (~ 100Å) near an interface.

IIIb Mean Dose in a Cavity of a Particular Size

Most of the authors mentioned in sub-section IIIa also calculated

the mean dose in a cavity of a particular size. Their work, and that of others, is summarised in Table 6.1.

Wingate et al (1962) performed a detailed measurement using an extrapolating chamber with both bone and tissue equivalent walls, and obtained the dose in parallel plane cavities for various X-ray energies (20 - 210kVp). Their results agree to within 5 per cent with Spiers (1949, 1951) calculations.

Aspin and Johns (1963) computed the values of the dose inside cylindrical cavities by taking into account the spectrum of the electrons generated by the known incident photon energies (70 - 250kVp X-rays and 1.25MeV γ-rays). They used the inactivation of a bacteriophage, which is tissue equivalent, as a detector to measure the dose in microscopic capillaries (2 - 22μ in radius). Their experimental and calculated results are in reasonable agreement at the photon energies used.

IIIc Mean Dose in a Group of Cavities

The mean dose in a group of cavities surrounded by bone has received little attention. This is because little, if any, information has been available on the distribution of cavity size to form a basis for calculation, while measurement has been hindered by the physical difficulties of introducing a dosimeter into cavities a few microns in diameter. The calculations used by the various people mentioned in sub-section IIIa could be applied to find the mean dose in a group of cavities provided the distribution of the cavity size is known.

Ellis (1966) employed five radiation qualities, 20 - 100keV effective X-rays and 1.25MeV γ-rays, and used ferrous sulphate as the dosimeter within a sintered glass disc having a range of pore sizes. His results agreed with Woodard and Spiers (1953) calculations for cavities greater than 40 microns diameter and for effective photon energies greater than 30keV.

Recently, Zanelli (1967) filled the spaces in a trabecular bone with finely ground LiF particles (2.3 microns diameter). Using various X-ray energies (22 - 100 keV) and Co^{60} γ-rays, he measured the mean tissue dose. His results agree reasonably with the calculation

of Spiers (1967) based on a knowledge of the distribution of the bone cavity sizes.

IV Tissue Cavities Surrounded by a Thickness of Bone Inadequate to Establish Electronic Equilibrium

Engstrom (1957) et al using a 'sandwiched' bone model have calculated the dose distribution in plane layers of marrow between plane slabs of bone with a uniform deposition of Sr^{90} + Y^{90} emitting β-particles. The thickness of bone was fixed at 70 microns and the layers of marrow varied between 50 microns to 900 microns. The mean dose given to marrow of a particular thickness was also evaluated. Their calculations were not comparable to other people's results because the thicknesses of the 'bone' and 'marrow' were different.

Spiers and Chesters (1962) used 125 microns thick layers of a dense liquid (50 per cent solution of $CaBr_2$ and density 1.5 gm per c.c) containing Sr^{90} + Y^{90}, as bone equivalent, and 500 microns thick layers of polyethylene as marrow equivalent, thus forming a sandwiched model of trabecular bone. They measured the β-particle dose rate in the polyethylene layer by using a plastic scintillator. Their results, obtained by increasing the layers of 'bone' and 'marrow' until equilibrium was reached, were 10 per cent less than the calculated results of Spiers (1949).

V Calculation of Absorbed Dose in Soft Tissue Inclusions in Bone by Cavity Theory

Equation 6.1 relates the inclusion dose to soft tissue dose, i.e.

$$f_w(\bar{T}_0) = \frac{\left(\frac{Z}{A}\right)_M}{\left(\frac{Z}{A}\right)_B}\left\{\left[1 + d\,b_w(\bar{T}_0)\ln\frac{I_B}{I_M} + (1-d)\left(\frac{\left(\frac{\mu_{en}}{\rho}\right)_M}{\left(\frac{\mu_{en}}{\rho}\right)_B}\frac{\left(\frac{Z}{A}\right)_B}{\left(\frac{Z}{A}\right)_M} - 1\right)\right]\right\} \quad 6.1$$

where the suffixes 'B' and 'M' refer to the bone and muscle in this context. The stopping power ratio for muscle to bone was first calculated using the Bragg-Gray equation, i.e. $\frac{(Z/A)_M}{(Z/A)_B}\left\{1 + b_w(\bar{T}_0)\ln\frac{I_B}{I_M}\right\}$,

with the aid of Table 8.3 of ICRU (1959). The stopping power ratio is then modified by considering the other terms in equation 6.1. The manner in which d is being evaluated for low energy electrons has been discussed in Chapter 5. The values of the mass energy absorption coefficient are taken from Table 4.5 (ICRU (1959).

The mean thickness of the lamellae in spongy bone is 100 microns (Engstrom et al (1958), Robertson and Godwin (1954)) and this would be penetrated by an electron of about 130keV. The calculations using equation 6.1 were confined to a photon energy below 200keV. For a 200keV photon traversing bone, Compton interactions are dominant (92 per cent) and the mean energy of the Compton electron is about 45keV. Thus these calculations were performed for the case where the tissue cavities are surrounded by a thickness of bone adequate to establish electronic equilibrium.

The calculated results are presented in figure 6.1 and figure 6.2 for a range of cavity sizes. A maximum value of the mean excess dose (i.e. the mean dose in tissue surrounded by bone minus the mean dose in tissue surrounded by tissue) occurs between 40 - 60keV for sizes ranging from 2 microns to 900 microns diameter.

The variation of the energy absorbed with photon energy in a 5 micron diameter cylindrical soft tissue cavity in bone, calculated by several workers, is presented in figure 6.3. This is compared with the calculation by cavity theory for a spherical cavity of 5 microns diameter. Figure 6.4 represents similar comparisons for a 10.6 microns diameter cavity.

Figures 6.5 and 6.6 give the ratio of the inclusion dose to the soft tissue dose as a function of cavity sizes. The present results are compared with the calculated results of Woodard and Spiers (1953) and the experimental results of Ellis (1966) at effective photon energies of 34keV and 71keV.

The differences in the results between cavity theory and other calculations are attributed to the different assumptions involved. Differences, between the calculations for monoenergetic photons irradiating

a single pore size and experiments involving a spectrum of photon energies and a spectrum of pore sizes (e.g. Ellis 1966), are to be expected. Subject to these qualifications, the results thus obtained from cavity theory calculations agree reasonably well with other approaches to the problem of bone dosimetry and certainly are within the spread of values given by other methods.

Table 6.1

Calculations and Measurements of the Mean Doses for Tissue-Filled Cylindrical Cavities Surrounded by Bone

Author	Photon Energy keV	Diameter of cavities in microns
Spiers (1949)	20 - 200	1 - 40
Woodard and Spiers (1953)	185 - 1250	1 - 50
Kononenko (1957)	20 - 200	1 - 50
Charlton and Cormack (1962a, b)	20 - 200	1 - 50
Aspin and Johns (1963)	70 - 1250	2 - 50
Wingate et al	20 - 210	2 - 25

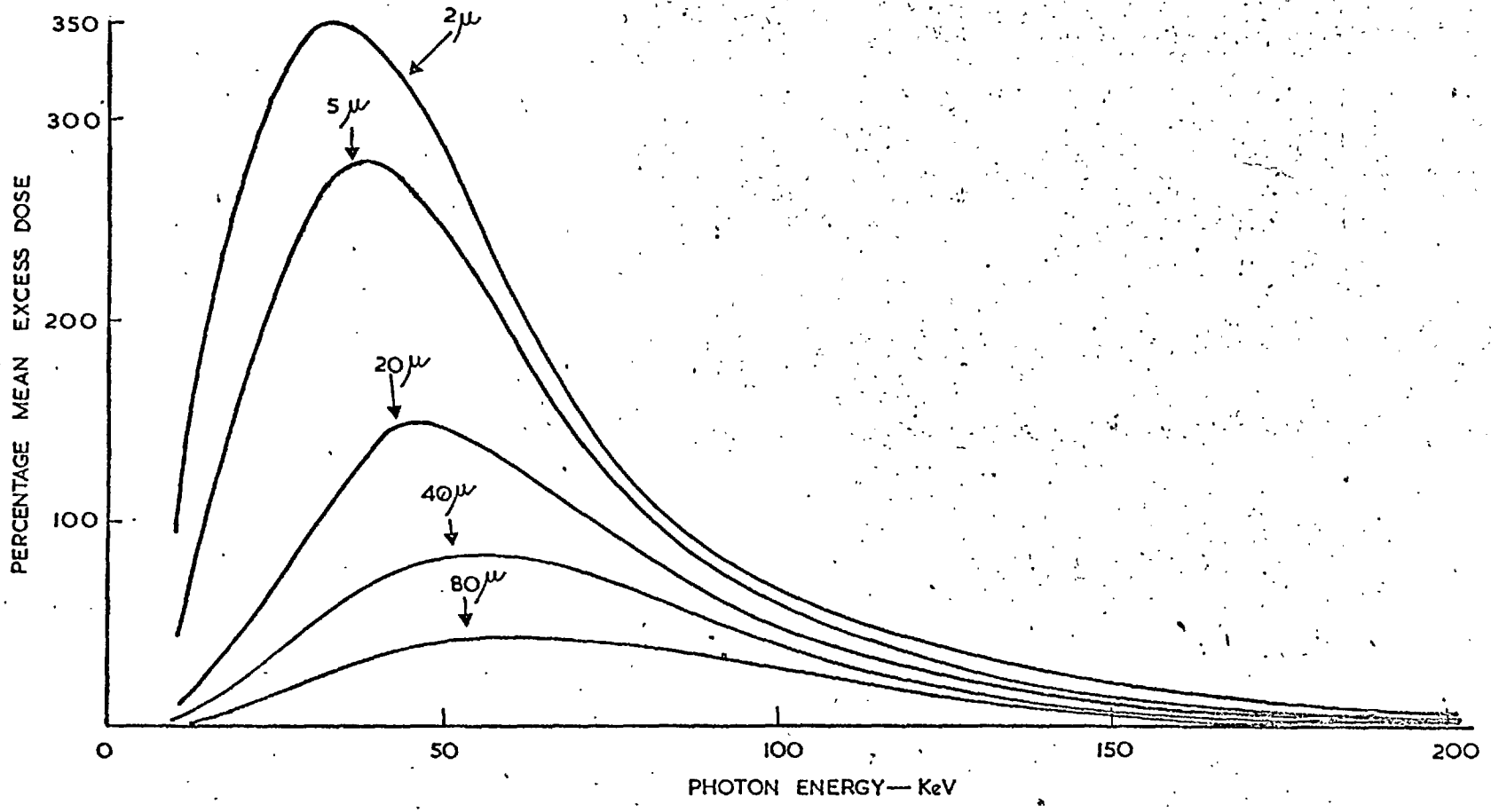

FIG. 6.1. MEAN EXCESS DOSE TO SOFT TISSUE INCLUSIONS IN BONE VERSUS PHOTON ENERGY FOR VARIOUS PORE SIZES CALCULATED BY CAVITY THEORY. THE DIAMETERS OF THE PORE (ASSUMED TO BE SPHERICAL) ARE SHOWN ON THE GRAPH.

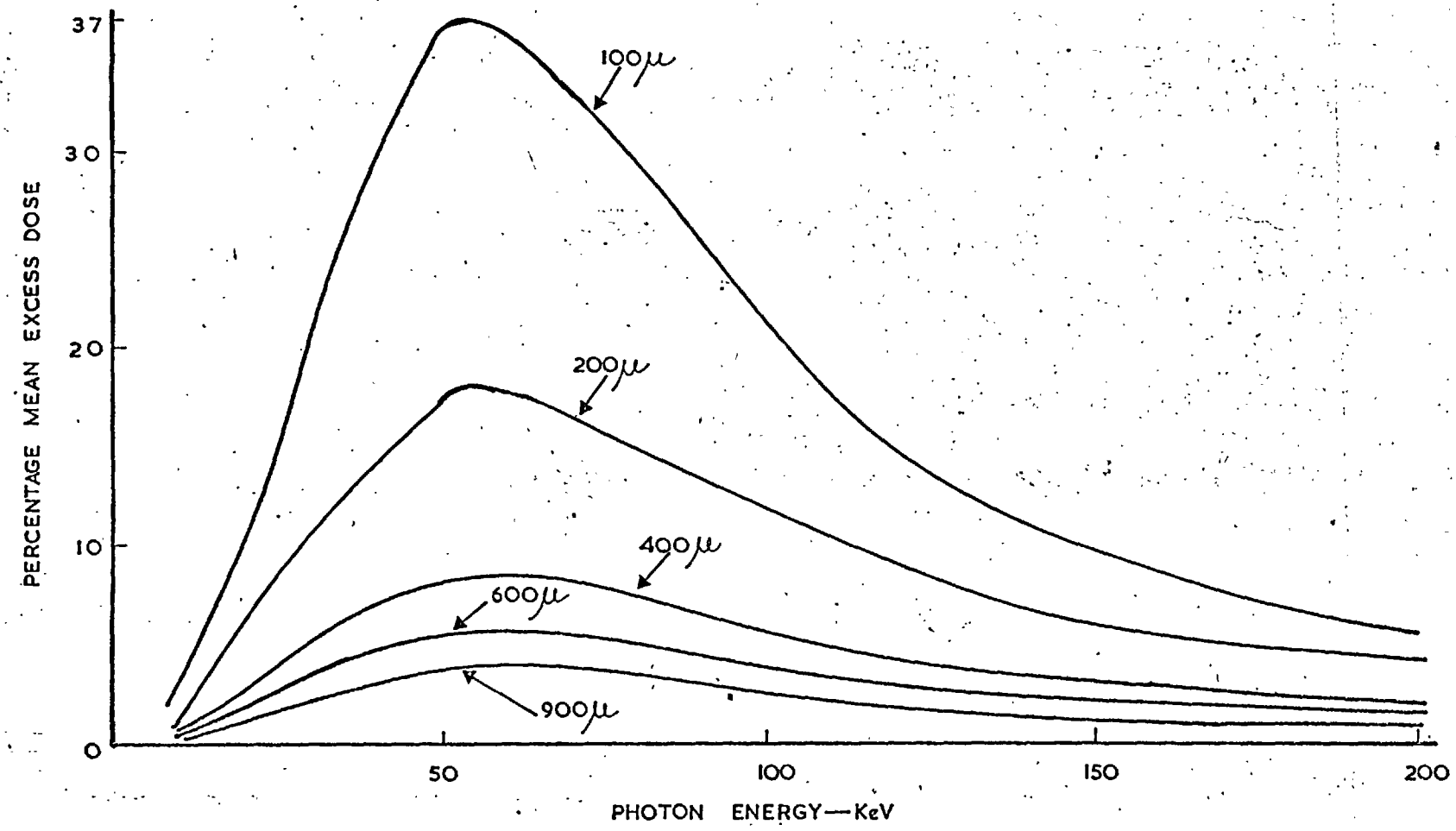

FIG. 6.2. MEAN EXCESS DOSE TO SOFT TISSUE INCLUSIONS IN BONE VERSUS PHOTON ENERGY FOR VARIOUS PORE SIZES CALCULATED BY CAVITY THEORY. THE DIAMETERS OF THE PORE (ASSUMED TO BE SPHERICAL) ARE SHOWN ON THE GRAPH.

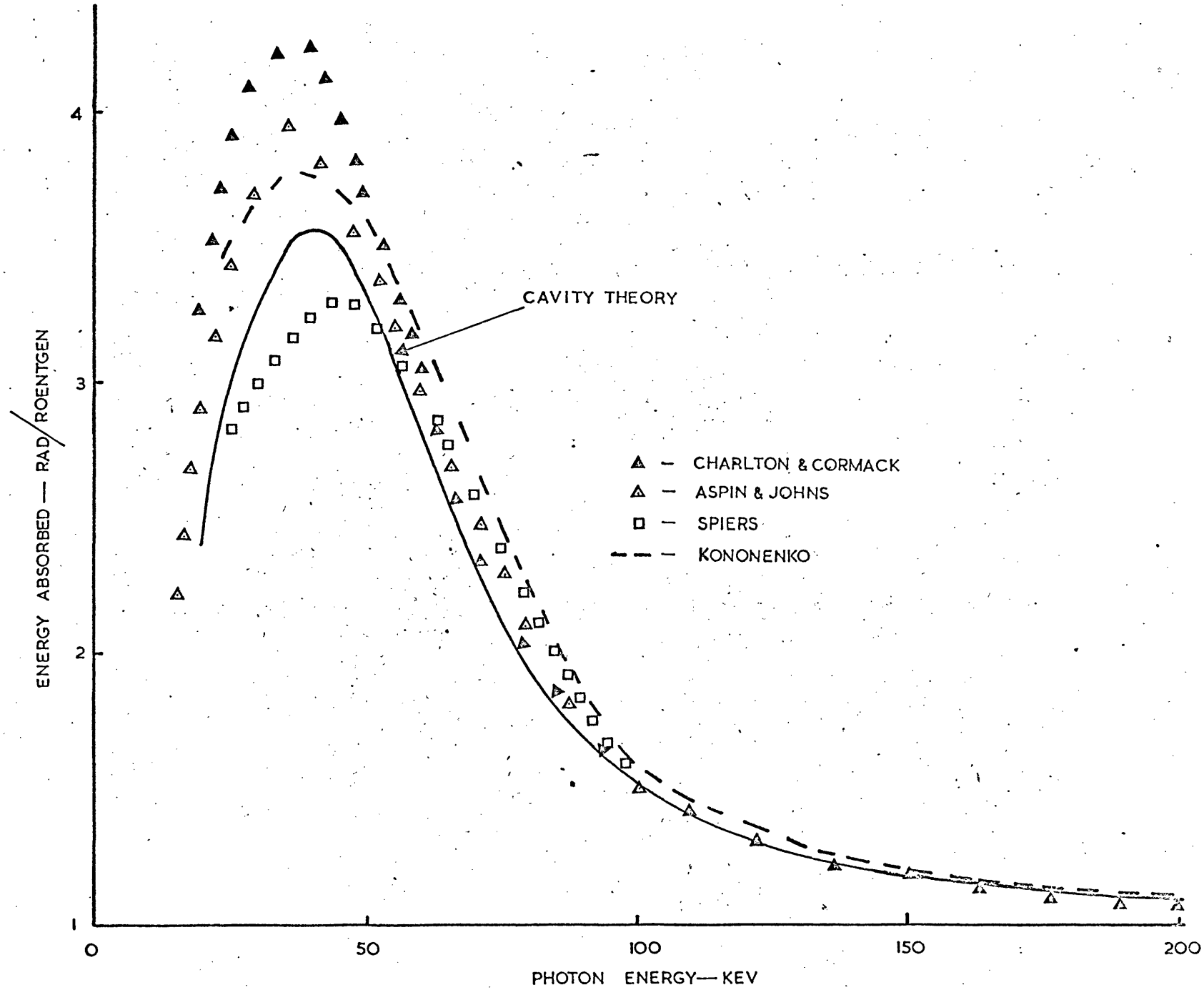

FIG 6.3 THE MEAN DOSE TO A 5 MICRON DIAMETER TISSUE CAVITY IN BONE PER ROENTGEN VERSUS PHOTON ENERGY.

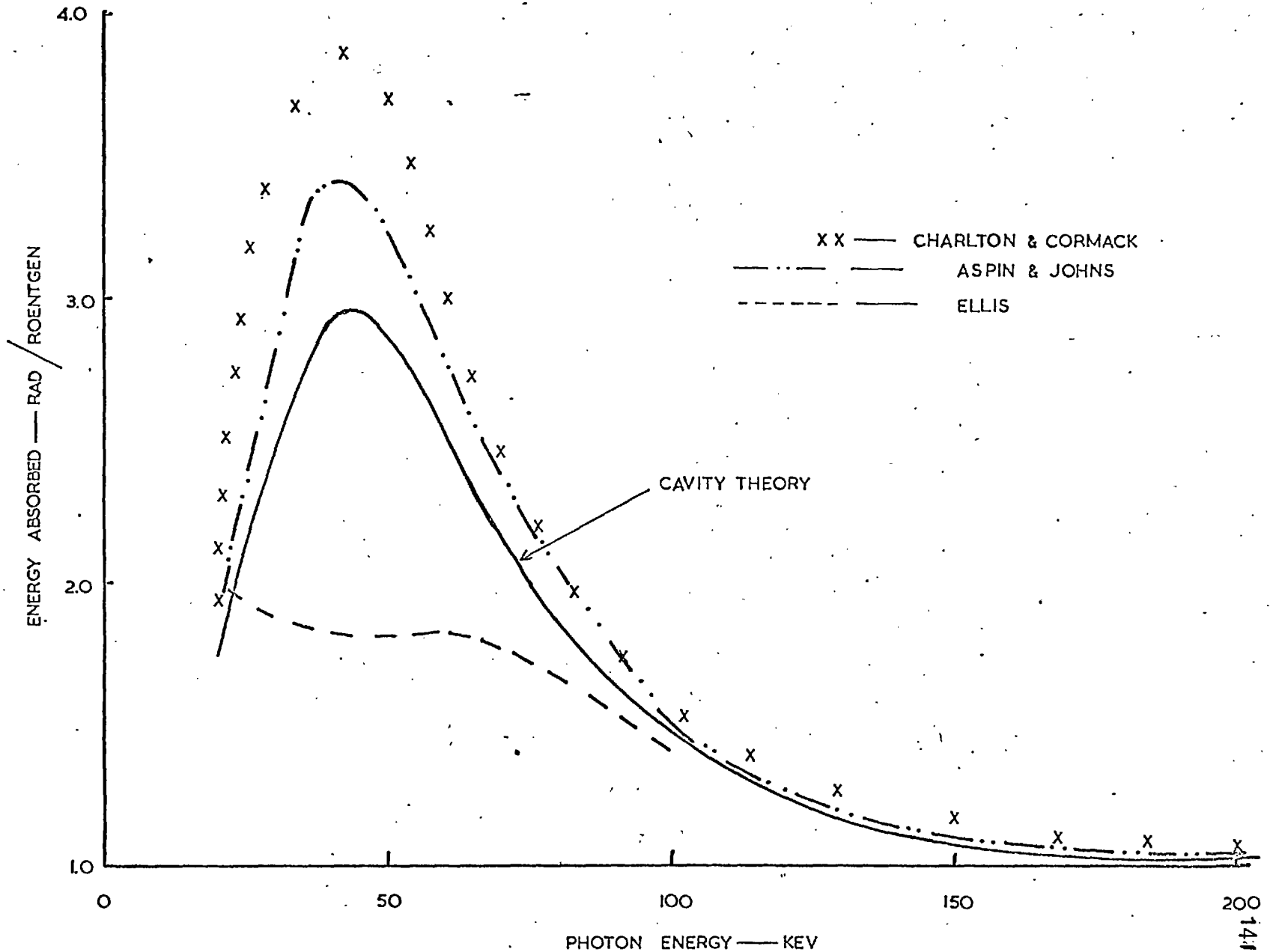

FIG. 6.4. THE MEAN DOSE TO A 10·6-MICRON DIAMETER TISSUE CAVITY IN BONE.

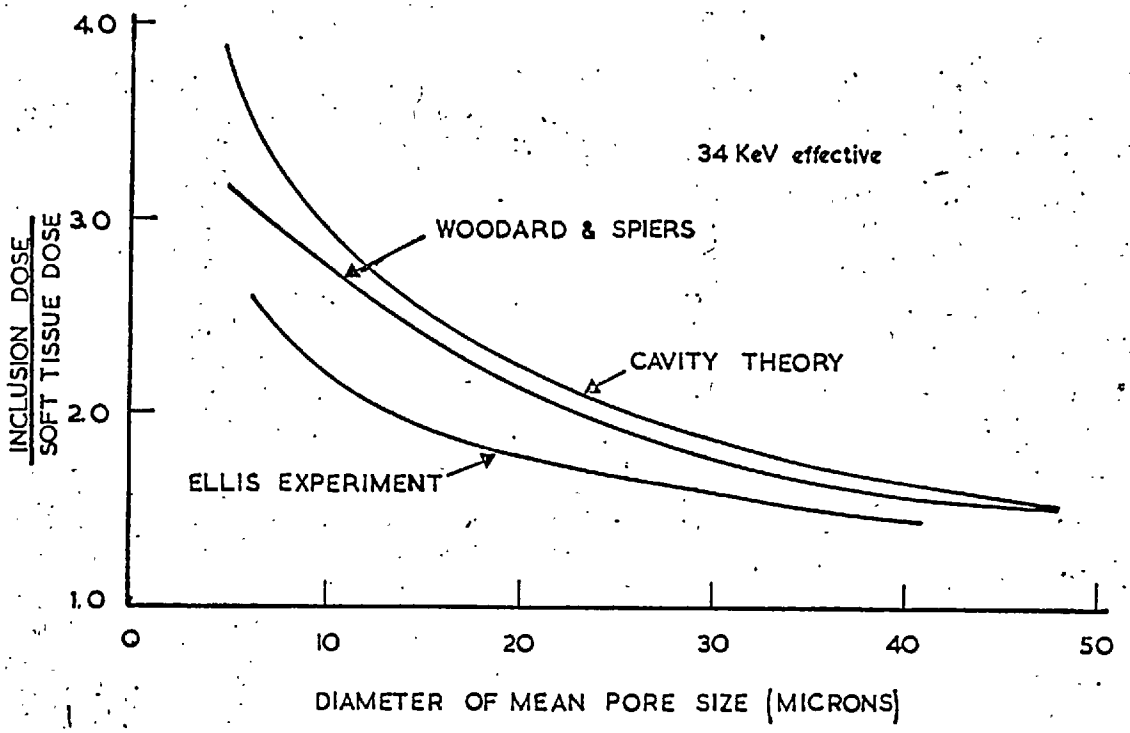

FIG. 6.5. COMPARISONS OF CAVITY THEORY OF THE INCLUSION DOSE VERSUS PORE SIZE FOR 34 KeV EFFECTIVE X-RAYS WITH THE RESULTS OF OTHER WORKERS.

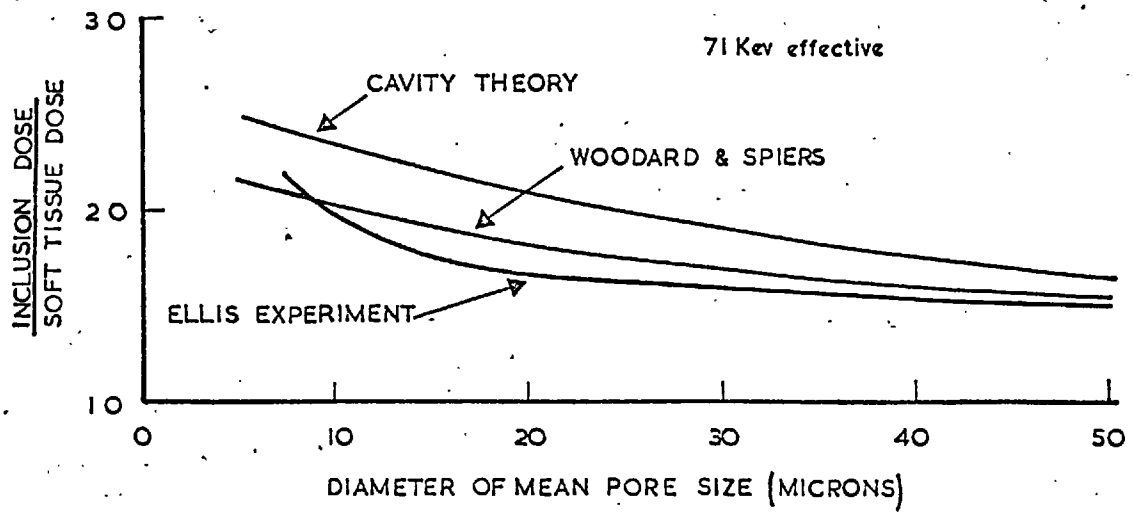

FIG. 6.6. COMPARISONS OF CAVITY THEORY OF THE INCLUSION DOSE VERSUS PORE SIZE FOR 71 KeV EFFECTIVE X-RAYS WITH THE RESULTS OF OTHER WORKERS.

CHAPTER 7

DISCUSSION

I The Validity of General Cavity Ionisation Theory

The earlier theories of cavity ionisation applied to cavities whose dimensions are small compared with the ranges of the directly ionising particles. In practice, their validity was limited to gas filled cavities irradiated by high energy photons or electrons. For example, the Spencer-Attix theory is satisfactory for ionisation chambers filled with gas at atmospheric pressure and irradiated by 1MeV photons up to a size of cavity with a mean linear dimension of 1cm (Burlin, 1962). Burlin (1966) introduced a theory of cavity ionisation that removed the size restriction and potentially was quite general in its application. Before this theory could be widely used, its validity needed to be established over a wide range of atomic number and size (i.e. from cavity sizes very much smaller than the electron range to those very much greater than the electron range). Burlin demonstrated the reliability of the theory using ionisation chambers of widely different atomic number. However, the ionisation chambers were small compared with the electron ranges and therefore only covered a small fraction of the range of cavity size required. Using monoenergetic isotope sources, it is not practicable to increase the dimensions of ionisation chambers to values where all the electrons within the chamber are generated therein by photons. However it is possible to achieve such a condition when condensed state dosimeters are used, and this has been undertaken in this thesis.

Due to its greater density, it was possible to increase the size of the Fricke dosimeter until virtually all the electrons within the dosimeter were generated by photon interactions within the dosimeter and the number entering from the wall ~~were~~ was negligible. A sphere of about 10cm diameter realised this condition for Co^{60} gamma rays. The general theory and the measurements on the Fricke dosimeter agreed to within the limits of experimental error. The experiments with the Fricke

dosimeter extended the dimensions of the dosimeter to the largest sizes it is desired to examine, but only for a combination where the atomic numbers of the dosimeter and the surrounding medium do not differ greatly. It was not feasible to surround chemical systems with media of high atomic number due to difficulties associated with chemical impurities. In order to cover the same size range with materials having greatly differing atomic numbers, solid state dosimeters were employed.

It was possible with solid state dosimeters to make measurements extending from dosimeter dimensions small relative to the electron ranges up to the dosimeters which are very much larger than the electron ranges and to do this for media having widely differing atomic numbers. Bjarngard and Jones' experiments, with very thin slices of teflon incorporating thermoluminescent materials in the matrix sandwiched between layers of lead, have been compared with cavity theory. The smallest thickness they used was comparable with the size of the ionisation chambers (in gm/cm^2) and their results thus cover the small cavity sizes. The response of the dosimeter versus dosimeter thickness was in reasonable agreement with theory.

The intermediate and large cavity sizes have been covered by the extensive measurements made with the perspex dosimeter. The experiments using clear perspex as a low atomic number dosimeter embedded in perspex, carbon, aluminium, copper, tin and lead gave a wide variation of the atomic number between the dosimeter and the wall materials. The dosimeter size was increased until virtually all the electrons in the dosimeter were generated therein. The agreement between experiment and the predictions of the general cavity theory for the variation of dosimeter response with (a) atomic number of the walls and (b) with size, were in good agreement.

It is therefore concluded that the general theory of cavity ionisation is valid for dosimeters of all phases for all possible combinations of atomic number and cavity size, at least for photon energies of 1.25MeV at which these experiments were conducted.

II Some Applications of General Cavity Ionisation Theory to Condensed Media

The applications of cavity ionisation theory to condensed state media may be grouped under three headings: (a) where it is desired to measure the dose in the material of a dosimeter but the surrounding medium or its container interferes with its response, (b) where it is desired to derive the dose in the medium from a dosimeter embedded in it, (c) special situations.

IIa Correction for Interface Effects

All liquid dosimeters must be contained within an irradiation cell, which will probably not be matched ideally to the dosimeter. A correction to the dosimeter will then be necessary due to the effects of the walls. This may be done by cavity ionisation theory and has been illustrated by the calculation on the Fricke dosimeter, which has been confirmed experimentally (Chapter 3). Similarly, where a powder is incorporated in a teflon matrix, its response with photon energy will be influenced by the teflon and the particle size. Calculations have been undertaken to illustrate this effect in the case of thermoluminescent powders incorporated in teflon (Chapter 5). Similar effects will occur whenever small dosimeters, such as powders, are irradiated even when they are situated in air or vacuum. Representative calculations have also been undertaken for thermoluminescent powders (Chapter 5).

IIb Dose in a Medium

The derivation of the dose to a medium from the dose in a dosimeter embedded in it is of course the basic function of cavity theory. This application will occur with the use of most dosimeters but, by way of illustration, the relation between the dose to lithium fluoride embedded in tissue to the tissue dose is presented in figure 7.1.

IIc Special Situations

Various specialised applications of cavity ionisation theory may

occur and the most obvious of these, bone dosimetry, has been considered (Chapter 6). These calculations and others have necessitated an alternative method to Burlin's of evaluating the electronic energy absorption coefficient, β. Using this method, cavity theory is extended to low energy photons ($<$ 200keV) and the absorbed dose in tissue surrounded by bone was calculated (Chapter 6). The calculations agree well with those of other workers.

III Conclusion

The general theory of cavity ionisation has been verified experimentally for cavity sizes extending from dimensions very much smaller than, up to dimensions very much larger than, the range of the electrons over a wide range of atomic numbers. It may therefore be applied with confidence to the condensed state. In particular it may be used to correct for the interface effects, to calculate the absorbed dose in a medium from the measured dose in a detector and is used in special situations such as bone. Examples of each of these applications have been presented.

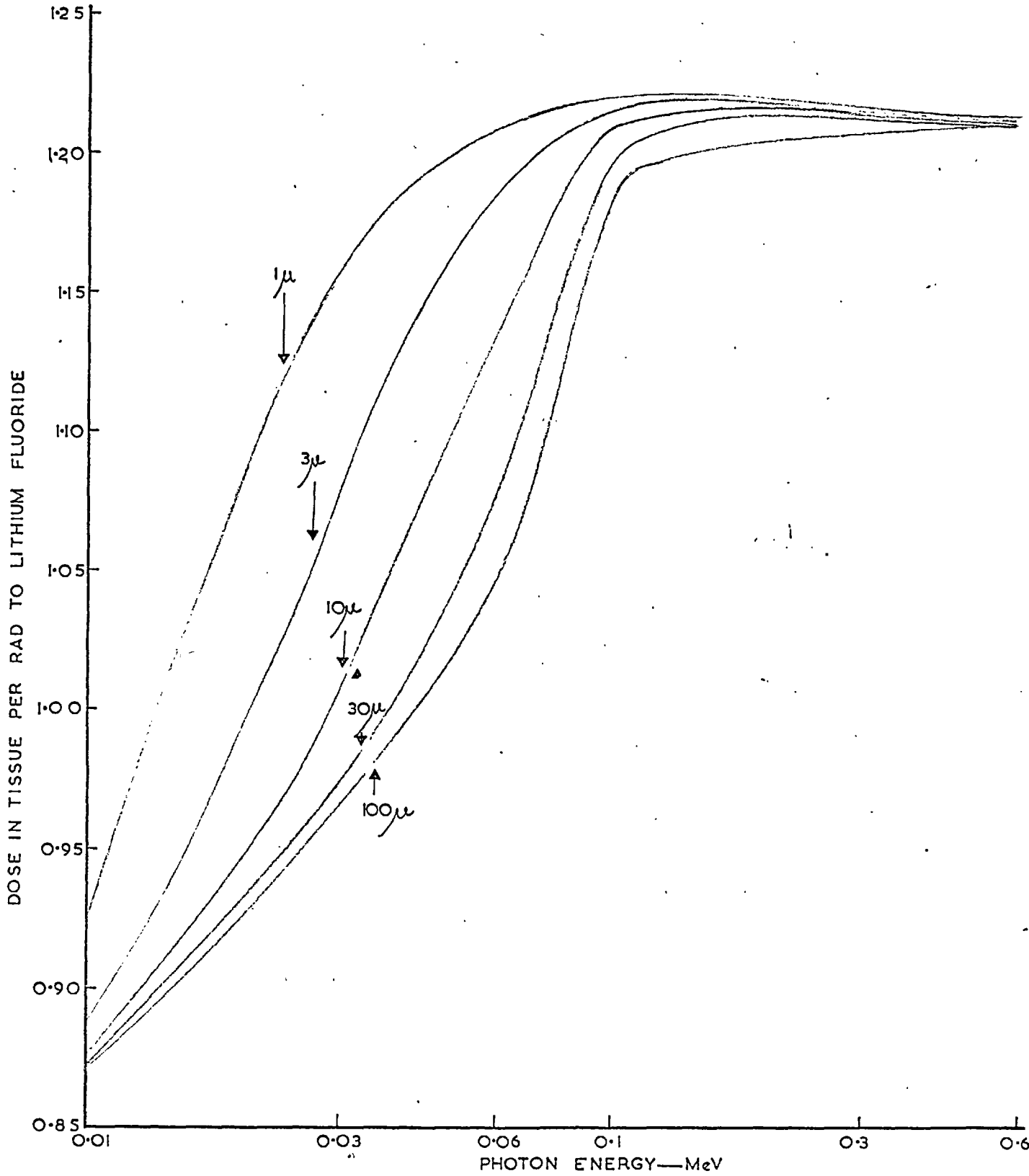

FIG. 7.1. VARIATION OF RESPONSES OF LITHIUM FLUORIDE GRAINS IRRADIATED IN SOFT TISSUE WITH PHOTON ENERGY. THE DIAMETER OF THE GRAINS ARE INDICATED ON THE GRAPH.

```
      PROGRAM FOR DOSE DISTRIBUTION IN COBALT-60 UNIT

      DIMENSION Q(20),B(8)
      READ 2,A,R,T,B1
      READ 40,(B(I),I=1,8)
  500 READ 3,(Q(I),I=1,20)
      IF(Q(1))60,50,60
   60 PRINT 90
      DO=0
      DO 80 I=1,20
      D1=(T*Q(I))/(A*R)
      D2=ATANF(B1/R)+ATANF((A-B1)/R)
      D3=D1*D2
   80 DO=DO+D3
      DO 30 K=1,8
      EN=0
      DO 10 J=1,7
      EN=EN+10.
      DR=0
      DO 20 I=1,20
      S=I
      H=SQRTF((R*R)+(EN*EN)+2.*R*EN*COSF(.3142*S))
      DR1=(T*Q(I))/(A*H)
      DR2=ATAN(B(K)/H)+ATANF((A-B(K))/H)
      DR3=DR1*DR2
   20 DR=DR+DR3
      DRDO=DR/DO
      N=EN
      NB=B(K)
   10 PRINT 70,NB,N,DR,DRDO
      PRINT 250
  250 FORMAT(//)
   30 CONTINUE
      PRINT 250
      PRINT 250
      GO TO 500
    2 FORMAT(F4.0,F4.0,E9.1,F4.0)
    3 FORMAT(20F4.0)
   40 FORMAT(8F4.0)
   70 FORMAT(5X,I3,5X,I3,3X,E11.4,3X,F7.4)
   90 FORMAT(7X,1HB,7X,1HN,9X,2HDR,8X,5HDR/DO/)
   50 CALL EXIT
      END
```

PROGRAM FOR STOPPING POWER RATIO OF FERROUS SULPHATE IN SILICA USING CAVITY THEORY AT VARIOUS PHOTON ENERGIES.

```
      DIMENSION D(17),G1(17),EN1(17),FZT1(17),FZT2(17),FZT3(17)
      READ 450,(G1(I),I=1,17)
  450 FORMAT(13F6.0)
      READ 6,ZAM,ZAB
      PRINT 140,ZAM,ZAB
      DO 50 K=1,6
      READ 51,E,EMUM,QBM,EMUB,R
      EMU=4.6052/R
      IF(E)150,100,150
  150 PRINT 52,E,EMUM,QBM,EMUB
      PRINT 503,R
      PRINT 170
      Y=.667E-04
C     TO WORK OUT D
      DO 1 I=1,17
      EMUSG=EMU*G1(I)*Y
      IF(EMUSG-441.)111,2,2
    2 D(I)=1./EMUSG
      GO TO 1
  111 D(I)=(1.-EXPF(-EMUSG))/EMUSG
    1 CONTINUE
C   ! TO WORK OUT MAIN EQUATION
      A3=EMUB/EMUM
      DO 11 I=1,17
      FZT1(I)=(ZAM/ZAB)*(1.+D(I)*QBM+(1.-D(I))*((EMUM/EMUB)*
     1(ZAB/ZAM)-1.))
      FZT2(I)=.869*FZT1(I)
   11 FZT3(I)=A3*FZT1(I)
      DO 33 I=1,17
   33 PRINT 5,G1(I),FZT1(I),FZT2(I),FZT3(I)
    5 FORMAT(8X,F11.3,4(4X,F9.4))
   50 CONTINUE
    6 FORMAT(2F7.4)
   51 FORMAT(5F7.4)
   52 FORMAT(5X,3HE= ,F7.4,4X,9HMEUA(M) =,F8.4,4X,5HQAL =,
     1F7.4,4X,7HMU(B) =,F8.4/)
  140 FORMAT(/5X,5HZAM =,F8.4,5X,5HZAB =,F8.4)
  170 FORMAT(14X,1HG,12X30HFZT1          FZT2          FZT3)
  503 FORMAT(5X,3HR =,F10.2)
  100 CALL EXIT
      END
```

PROGRAM FOR STANDARD DEVIATION OF PERSPEX
EXPERIMENTAL VALUES FOR DECAY CURVES.

```
*FANDK0408
    8 PRINT 235
  235 FORMAT(///)
      READ 17
      PRINT 17
   17 FORMAT(20H                          /)
      DIMENSION  M(4),D(21),             N(4)
    6 READ 100,(M(I),I=1,4),(D(I),I=1,16)
  100 FORMAT (A3,A4,A4,A4,16F3.2)
      IF(M(1)-4555400)7,8,7
    7 XN=0.
      S=0.
      SS=0.
      DO 1 I=1,20
      IF(D(I)-9.)2,9,2
    2 XN=XN+1.
      D(I)=D(I)/10.
      S=S+D(I)
    1 SS=SS+D(I)**2
    9 AV=S/XN
      SE=SQRT(ABSF((SS-S*S/XN)/((XN-1.)*XN)))
      PRINT 101,(M(I),I=1,4),AV,SE,XN
  101 FORMAT(A3,3A4,F7.4,F7.4,I4)
      GO TO 6
  555 CALL EXIT
      END
```

PROGRAM FOR STOPPING POWER RATIO OF PERSPEX IN VARIOUS MATERIALS USING CAVITY THEORY AT VARIOUS PHOTON ENERGIES.

```
      DIMENSION FZTT(13),FZTP(13),FZTC(13),D(13),G(13),FUZ(13)
      READ 200,(G(I),I=1,13)
  100 READ 300,A,B,T1,ZZ,AZ,EMUG,EMUZ,FIA,FIZ,EMU,E
      IF(G(1))360,350,360
  360 PRINT 400
      PRINT 600,T1,ZZ,AZ
      PRINT 70,A,B,FIZ
      PRINT 80,FIA,EMUG,EMUZ
      PRINT 90,EMU,E
      DO 1 I=1,13
      EX1=EMU*G(I)
      EX2=EXPF(-EX1)
      EX3=1.-EX2
    1 D(I)=EX3/EX1
      T2=ZZ/AZ
      T3=T1/T2
      AB=FIZ/FIA
      AL=A*LOG(AB)
      BL= B*LOG(AB)
      T5=EMUG/EMUZ
      T6=T2/T1
      DO 2 J=1,13
      T4=1.+D(J)*AL
      T7=T4+((1.-D(J))*(T5*T6-1.))
      FZTC(J)=T3*T7
      T9 = 1.+ D(J)*BL
      T8 = T9+((1.-D(J))*(T5*T6-1.))
      FZTP(J)=T3*T8
      FZTT(J)=.65*FZTC(J)+.35*FZTP(J)
    2 FUZ(J)=(EMUZ/EMUG)*FZTT(J)
      DO 3 K=1,13
      EN=FZTT(K)/FZTT(13)
    3 PRINT 500,G(K),FZTC(K),EN,FUZ(K)
   70 FORMAT(5X,4HA = ,F8.4,4X,4HB = ,F8.4,4X,5HIZ = ,F6.0/)
   80 FORMAT(5X,5HIA = ,F6.1,4X,5HUG = ,F9.5,4X,5HUZ = ,F9.5/)
   90 FORMAT(5X,4HU = ,F9.4,5X,4HE = ,F9.4//)
  200 FORMAT(11F7.4)
  300 FORMAT(2F7.4,F6.4,F4.0,F6.1,2F8.5,F5.1,F5.0,F8.4,F8.4)
  400 FORMAT(5X,16H LEAD INPUT DATA//)
  500 FORMAT(4X,6(F7.4,4X))
  600 FORMAT(5X,8HZG/AG = ,F7.4,4X,5HZZ = ,F5.0,4X,5HAZ = ,
     1F7.1/)
      GO TO 100
  350 CALL EXIT
      END
```

PROGRAM FOR STOPPING POWER RATIO OF LITHIUM FLUORIDE, LITHIUM BORATE, CALCIUM SULPHATE AND CALCIUM FLUORIDE IN AIR AND IN TEFLON USING CAVITY THEORY AT VARIOUS PHOTON ENERGIES.

```
      DIMENSION D(17),G1(17),EN1(17),FZT1(17),FZT2(17),
     1FZT3(17),FZT4(17)
      READ 450,(G1(I),I=1,16)
      READ 222
      PRINT 222
      READ 6,ZAM,ZAB
      PRINT 140,ZAM,ZAB
      DO 50 K=1,13
      READ 51,E,EMUM,QBM,EMUB
      IF(E)150,100,150
  150 PRINT 52,E,EMUM,QBM,EMUB
      EN = 1.265 - 0.0954 * LOGF(E)
      R = .412 * E**EN
      PRINT 170
      EMU=4.6052/R
      Y=0.92E-04
C     TO WORK OUT D
      DO 1 I=1,16
      EMUSG=EMU*G1(I)*Y
      IF(EMUSG-441.)111,2,2
    2 D(I)=1./EMUSG
      GO TO 1
  111 D(I)=(1.-EXPF(-EMUSG))/EMUSG
    1 CONTINUE
C     TO WORK OUT MAIN EQUATION
      A3=EMUB/EMUM
      DO 11 I=1,16
      FZT1(I)=(ZAM/ZAB)*(1.+D(I)*QBM+(1.-D(I))*((EMUM/EMUB)*
     1(ZAB/ZAM)-1.))
      FZT2(I)=.869*FZT1(I)
      FZT3(I)=A3*FZT1(I)
   11 FZT4(I)=FZT1(I)*(1./A3)
      DO 33 I=1,16
   33 PRINT 5,G1(I),FZT1(I),FZT2(I),FZT3(I),FZT4(I)
   50 CONTINUE
    5 FORMAT(8X,F11.3,4(4X,F9.4))
    6 FORMAT(2F7.4)
   51 FORMAT(4F7.4)
   52 FORMAT(5X,3HE= ,F7.4,4X,9HMEUA(M) =,F8.4,4X,5HQAL =,
     1F7.4,4X,7HMU(B) =,F8.4/)
  140 FORMAT(/5X,5HZAM =,F8.4,5X,5HZAB =,F8.4)
  170 FORMAT(14X,1HG,12X30HFZT1          FZT2          FZT3,9X,
     14HFZT4)
  222 FORMAT(50H
  450 FORMAT(13F6.0)
  100 CALL EXIT
      END
```

PROGRAM FOR ABSORBED DOSE IN SOFT TISSUE INCLUSION IN BONE
USING CAVITY THEORY FOR PHOTON ENERGY LESS THAN 200KEV.

```
      DIMENSION D(17),G1(17),EN1(17),FZT1(17),FZT2(17),FZT3(17)
      READ 450,(G1(I),I=1,17)
  450 FORMAT(13F6.0)
      READ 6,ZAM,ZAB
      PRINT 140,ZAM,ZAB
      DO 50 K=1,6
      READ 51,E,EMUM,QBM,EMUB,R
      EMU=4.6052/R
      IF(E)150,100,150
  150 PRINT 52,E,EMUM,QBM,EMUB
      PRINT 503,R
      PRINT 170
      Y=.7186E-04
C     TO WORK OUT D
      DO 1 I=1,17
      EMUSG=EMU*G1(I)*Y
      IF(EMUSG-441.)111,2,2
    2 D(I)=1./EMUSG
      GO TO 1
  111 D(I)=(1.-EXPF(-EMUSG))/EMUSG
    1 CONTINUE
C     TO WORK OUT MAIN EQUATION
      A3=EMUB/EMUM
      DO 11 I=1,17
      FZT1(I)=(ZAM/ZAB)*(1.+D(I)*QBM+(1.-D(I))*((EMUM/EMUB)*
     1(ZAB/ZAM)-1.))
      FZT2(I)=.869*FZT1(I)
   11 FZT3(I)=A3*FZT1(I)
      DO 33 I=1,17
   33 PRINT 5,G1(I),FZT1(I),FZT2(I),FZT3(I)
    5 FORMAT(8X,F11.3,4(4X,F9.4))
   50 CONTINUE
    6 FORMAT(2F7.4)
   51 FORMAT(5F7.4)
   52 FORMAT(5X,3HE= ,F7.4,4X,9HMEUA(M) =,F8.4,4X,5HQAL =,
     1F7.4,4X,7HMU(B) =,F8.4/)
  140 FORMAT(/5X,5HZAM =,F8.4,5X,5HZAB =,F8.4)
  170 FORMAT(14X,1HG,12X30HFZT1          FZT2          FZT3)
  503 FORMAT(5X,3HR =,F10.2)
  100 CALL EXIT
      END
```

Acknowledgements

I wish to express my sincere gratitude for the invaluable advice and unfailing support of Dr. T. E. Burlin and Professor J. F. Fowler, who supervised this work. Thanks are due to Mr. J. Yarwood for his guidance. I would also like to thank Mrs. O. Routledge and my wife for their help in preparing the computer programmes. The technical assistance of Messrs. M. Brown, A. Fidler and A. Redhead are also appreciated.

Finally I wish to thank the Science Research Council for financial support of the apparatus for this work.

References

Allen, A. O., 1952, Discussions Faraday Soc., 12, 79.

Allen, A. O., Hogan, V. V., and Rothschild, W. G., 1957, Rad. Res., 7, 603.

Attix, F. H., and Ritz, V. H., 1957, J. Res. Nat. Bur. Stand., 59, 293.

Attix, F. H., De La Vergne, L., and Ritz, V. H., 1958, J. Res. Nat. Bur. Stand., 60, 235.

Attix, F. H., 1962, U.S. Naval Res. Lab. Report 5777.

Barnard, G. P., Axton, E. J., and Marsh, A. R. S., 1959, Phys. Med. Biol., 3, 366.

Berger, M. J., and Seltzer, S. M., 1964, Nat. Aero. Space Admin. Report SP-3008.

Berger, M. J., and Seltzer, S. M., 1964, Nat. Aero. Space Admin. Report SP-3012.

Bichsel, H., 1968, Radiation Dosimetry, Vol. 1, Academic Press, London.

Bjarngard, B. E., and Jones, D., 1966, Symposium on Solid State and Chemical Radiation Dosimetry in Medicine and Biology (IAEA., Vienna).

Boag, J. W., Dolphin, G. W., and Rotblat, J., 1958, Radiat. Res., 9, 589.

Boag, J. W., 1963a, 'Actions chimiques et biologiques des radiations', (M. Haissinsky ed.), 6th series, Chapter 1, Masson, Paris.

Boag, J. W., 1963b, Brit. J. Radiol., 36, 779 (abstract).

Bragg, W. H., 1910, Phil. Mag., 20, 385.

Bragg, W. H., 1912, Studies in Radioactivity (Macmillan, New York).

Burch, P. R. J., 1955, Radiat. Res., 3, 361.

Burlin, T. E., 1961, Phys. Med. Biol., 6, 33.

Burlin, T. E., 1961, Ph.D. thesis, London University.

Burlin, T. E., 1962, Brit. J. Radiol., 35, 343.

Burlin, T. E., 1966a, Phys. Med. Biol., 11, 255.

Burlin, T. E., 1966b, Brit. J. Radiol., 39, 727-734.

Burlin, T. E., 1968, Rad. Dosimetry, Vol. 1, Ch. 8, Academic Press, London.

Charlton, D. E., and Cormack, D. V., 1962a, Radiat. Res., 17, 34.

Charlton, D. E., and Cormack, D. V., 1962b, Brit. J. Radiol., 35, 473.

Charlton, D. E., and Cormack, D. V., 1967, Microdosimetry Symposium, Ispra, Italy.

+ Aspin, N., and Johns, H.E., 1963, Brit. J. Radiol., 36, 350.

o Burlin, T. E., and B.W. Hancock, 1967, Microdosimetry Symposium, Ispra, Italy.

Clarkson, J. R., 1941, Phil. Mag., 31, 437.
Cole, A., 1967, Nat. Bur. Stand., Technical Note 187.
Cormack, D. V., and Johns, H. E., 1954, Rad. Res., 1, 133.
Cormack, D. V., 1967, Private Communication with T. E. Burlin.
Costrell, L., 1962, Health Phys., 8, 261.
Curie, M., Debierne, A., Eve, A. S., Geiger, H., Hahn, O., Lind, S. C., Meyer, S., Rutherford, E., and Schweidler, E., 1931, Rev. Mod. Phys., 3, 427.
Dalton, P., and Turner, J. E., 1968, Health Physics, 15, 257.
Davidson, G., and Sutton, H. C., 1964, Int. J. App. Rad. Isotopes, 15, 741.
Davisson, C. M., 1965, 'α, β, γ ray Spectroscopy' Vol. 1, 829, ed. K. Siegbahn.
Day, M. J., and Stein, G., 1951, Nature, 168, 644.
Dewhurst, H. A., 1951, J. Chem. Phys., 19, 1329.
Ellis, R. E., 1966, Brit. J. Radiol., 39, 211.
Engelke, B. A., and Oetzmann, W., 1967, Symposium in Microdosimetry, Ispra, Italy.
Engstrom, A., Bjornstedt, R., Clemedson, C. J., and Nelson, A., 1957, Bone and Radiostrontium (John Wiley, New York).
Epp, E. R., Woodard, H. Q., and Weiss, H., 1959, Radiat. Res., 11, 184.
Estulin, I. V., 1953, J. Exp. Theor. Phys., USSR., 24, 221.
Evans, R. D., and Evans, R. O., 1948, Rev. Mod. Phys., 20, 305.
Evans, R. D., 1955, The Atomic Nucleus, McGraw Hill, New York.
Evans, R. D., 1968, Rad. Dosimetry, Vol. 1, Chapter 3, Academic Press, London.
Fowler, J. F., 1957, Brit. J. Radiol., 30, 361.
Fowler, J. F., 1963a, Phys. Med. Biol., 8, 1.
Fowler, J. F., 1963b, Nucleonics, 21, 60.
Fricke, H., and Morse, S., 1927, Am. J. Roentgenol Radium Therapy, 18, 430.
Fricke, H., and Morse, S., 1929, Phil. Mag., 7, 129.
Ghormley, J. A., 1956, quoted by Weiss et al.
Gleason, G. T., Taylor, J. D., and Tabern, D. L., 1951, Nucleonics, 8, 12.
Gray, L. H., 1929, Proc. Roy. Soc. A., 122, 647.
Gray, L. H., 1936, Proc. Roy. Soc. A., 156, 578.
Gray, L. H., 1937, Radiation Dosimetry Brit. J. Radiol., 10, 721.
Gray, L. H., 1940, Brit. J. Radiol., 13, 25.

Greening, J.R., 1954, Brit. J. Radiol., 27, 163.
Greening, J. R., 1957, Brit. J. Radiol., 30, 254.
Greening, J. R., 1964, Phys. Med. Biol., 9, 143.
Hahn, O., and Meitner, L., 1908, Z. Phys., 9, 321, 697.
Harwick, T. J., 1952, Can. J. Chem., 30, 23.
Hindmarsh, M., Owen, M., Vaughan, J., Ramerton, L. F., and Spiers, F. E., 1958, Brit. J. Radiol., 31, 518.
Hochanadel, C. J., and Ghormley, J. A., 1953, J. Chem. Phys., 21, 880.
Hochanadel, C. J., and Ghormley, J. A., 1962, Radiat. Res., 16, 653.
Howarth, J., 1965, Brit. J. Radiol., 38, 51.
Huffman, R. E., and Davidson, N., 1956, J. Am. Chem. Soc., 78, 4836.
International Commission on Radiological Units and Measurements, 1956, Nat. Bur. Stand., Handbook 78.
International Commission on Radiological Units and Measurements, 1959, Nat. Bur. Stand. Handbook 78.
International Commission on Radiological Units and Measurement, 1961, Nat. Bur. Stand., Handbook 79.
International Commission on Radiological Units and Measurements, 1964, Nat. Bur. Stand., Handbook 85.
Jacobs, N., and Spiers, F. W., 1962, Second Int. Congress Rad. Res., Abstracts of Papers, 213.
Jayachandran, C. A., 1968, Ph.D. thesis, University of London.
Katz, G. W. C., and Penfold, A. S., 1952, Rev. Mod. Phys., 24, 28.
Kononenko, A. M., 1957, Biofizika Academy USSR, 2, 98.
Laurence, G. C., 1937, Canad. J. Res. A., 15, 67.
Lazo, R. M., Dewhurst, H. A., and Burton, M., 1954, J. Chem. Phys., 22, 1370.
Loevinger, R., 1956, Radiology, 66, 55.
Loevinger, R., Japha, E. M., and Brownell, G. L., 1956, Rad. Dosimetry, Academic Press, New York.
Mayneord, W. V., and Roberts, J. F., 1937, Brit. J. Radiol., 10, 365.
Mie, G., 1904, Ann. Phys., Lpz., 13, 857.
Miller, N., 1950, J. Chem. Phys., 18, 79.
Miller, N., and Wilkinson, J., 1952, Disc. Faraday Soc., 12, 50.
Mooney, R. W., and Szasz, G. J., May, 1962, 'Discussion on Radiation Chemistry', ONRL-48-32, Office of Naval Research, London.

Odeblad, E., 1955, Acta. Radiol., Stockholm, 43, 310.
Orton, C. G., 1959, M.Sc. thesis, University of London.
Orton, C. G., 1965, Ph.D. thesis, University of London.
Orton, C. G., 1966, Phys. Med. Biol., 11, 377.
Puig, J. A., and Sutton, J., 1959, J. Chem. Phys., 56, 699.
Robertson, J. S., and Godwin, J. T., 1954, Brit. J. Radiol., 27, 241.
Scharf, K., and Lee, R. M., 1961, Rad. Res. Abstract no.135, 14, p.498.
Schested, K., Brynjolfsson, A., and Holm, N. W., 1963, Danish Atomic Energy Commission Res. Estab., Riso, Riso Rep. No.62.
Schmidt, H. W., 1906, Z. Phys., 7, 764.
Schulman, J. H., 1959, Aogr. Nucl. Energy., Ser XII, 1-3, 150.
Schwarz, H. A., 1954, J. Am. Chem. Soc., 76, 1587.
Snieder, W. S., 1967, Private communication.with T. E. Burlin.
Spencer, L. V., and Fano, U., 1954, Phys. Rev., 93, 1172.
Spencer, L. V., 1955, Phys. Rev., 98, 1597.
Spencer, L. V., and Attix, F. H., 1955, Radiat. Res., 3, 239.
Spiers, F. W., 1949, Brit. J. Radiol., 22, 521.
Spiers, F. W., 1951, Brit. J. Radiol., 24, 356.
Spiers, F. W., 1959, Report of the International Commission on Radiological Units and Measurements, Nat. Bur. Stand. Handbook No.78.
Spiers, F. W., 1967, Microdosimetry Symposium, Ispra, Italy.
Spiers, F. W., 1967, Brit. J. Radiol., 39, 216.
Thompson, T. J., 1962, University of California Radiation Laboratory Report, 1910, Berkeley.
Weinberg and Wigner, 1958, Physical Theory of Neutron Chain Reactions, pp.715-6.
Weiss, J., 1952, Nucleonics, 10, p.28.
Weiss, J., 1953, Nature, 748, 1944.
Weiss, J., Allen, A. O., and Schwarz, H. A., 1955, Proc. Intern. Conf. Peaceful uses At. Energy, Geneva, Vol.14, p.179.
Whittaker, B., 1963, UKAEA Rep., AERE-R-3073.
Whittaker, B., and Lowe, C. A., 1967, Int. J. App. Rad. Isotopes, 18, 89.
Wingate, C. L., Gross, W., and Failla, G., 1962, Radiology, 79, 984.
Woodard, H. Q., and Spiers, F. W., 1953, Brit. J. Radiol., 26, 38.

Worthing, A. G., and Geffner, J., 1943, Treatment of Experimental Data (John Wiley and Sons Inc., New York).

Whyte, G. N., 1954, Nucleonics, 12, 18-21.

Zanelli, G. D., 1967, Microdosimetry Symposium, Ispra, Italy.

Zanelli, G. D., 1968, Phys. Med. Biol., 13, 393.

PUBLICATIONS

Reprint from

"SOLID STATE AND
CHEMICAL RADIATION DOSIMETRY
IN MEDICINE AND BIOLOGY"

INTERNATIONAL ATOMIC ENERGY AGENCY
VIENNA, 1967

SOME APPLICATIONS OF CAVITY THEORY TO CONDENSED-STATE RADIATION DOSIMETRY

T.E. BURLIN AND F.K. CHAN
DEPARTMENT OF MATHEMATICS AND PHYSICS,
THE POLYTECHNIC, LONDON,
ENGLAND, UNITED KINGDOM

Abstract

SOME APPLICATIONS OF CAVITY THEORY TO CONDENSED-STATE RADIATION DOSIMETRY. Measurement of the absorbed dose in a medium exposed to ionizing radiation necessitates the introduction of a radiation-sensitive device into the medium. Normally this device differs from the medium in both atomic number and density and therefore constitutes a discontinuity, which is referred to as a "cavity". Through association with the ionization chamber the term "cavity" often denotes a gas-filled space in a solid. There is no fundamental reason for this limitation and generally the cavity may be in the solid, liquid or gaseous phase.

Both the Bragg-Gray and the Spencer-Attix theories are applicable to sizes which do not modify the electron energy spectrum established in the surrounding medium. This limits the application of these theories to solid and liquid radiation dosimeters having dimensions of about 10^{-3} cm and they are therefore seldom of practical use.

Cavity theory can be modified to account for the change in the shape of the energy spectrum due to the presence of the cavity and also for the change in the total energy in the spectrum. This modification removes the limitation of the size of cavity, to which cavity theory is applicable, thus permitting its use with solid and liquid state dosimeters.

The ferrous sulphate dosimeter is considered as a specific example. The response as a function of the size of the irradiation cell is calculated. The results are compared with experiment and many in part explain the area/volume dependence of this dosimeter reported by other workers.

1. INTRODUCTION

Measurement of the absorbed dose in a medium exposed to ionizing radiation necessitates the introduction of a radiation-sensitive device into the medium. Normally this device will differ from the medium in both its density and the atomic numbers of its constituents. It therefore constitutes a discontinuity, which will be referred to as a 'cavity'. Through association with the ionization chamber the term 'cavity' often denotes a gas-filled space in a solid medium. There is no fundamental reason for this limitation and generally the cavity may be in the solid, liquid or gaseous phase and may be more or less dense than the surrounding medium.

Consider a cavity in this general sense, situated in an infinite medium. As a specific example, assume there is in the medium a uniformly-distributed source of β rays and that the production of bremsstrahlung X rays by the electrons is negligible. The absorbed dose, D_m, imparted in a time interval, t, is equal to the energy released from the radioactive nuclide per unit mass of material, i.e.

$$D_m = C_m E_m t \qquad (1)$$

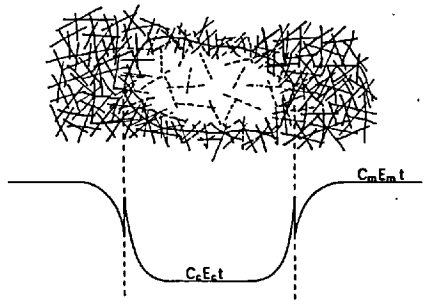

FIG. 1. Cavity within an infinite medium. The broken and full lines represent β rays from the cavity material and the medium, respectively

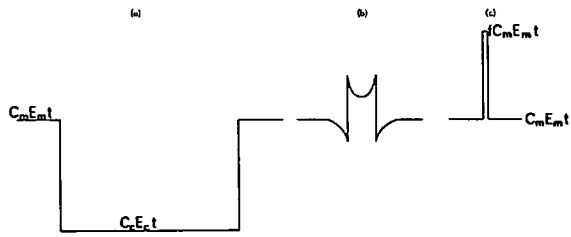

FIG. 2. Dose distribution in the region of cavities of different sizes relative to the β-ray ranges
(a) Very large
(b) Intermediate
(c) Very small

where C_m is the mean activity per unit mass of the medium during time interval t, E_m is the mean β-ray energy per disintegration.

Into this medium is introduced a cavity of a second material containing a uniformly-distributed β-emitter of mean activity per unit mass, C_c, during a time interval t and of mean β-ray energy E_c per disintegration. If $C_m E_m t > C_c E_c t$ the modification of the absorbed-dose distribution produced by the presence of the cavity will be as represented in Fig. 1. At sufficiently large distances from the cavity boundary, the absorbed dose in each material reaches a constant value which is equal to the absorbed dose in an infinite medium composed of these materials and is given by Eq. (1). Near the cavity boundary the absorbed-dose distribution will also depend on the scattering properties of the two materials, as has been shown by Dutreix and Bernard [1, 2]. At the boundary there is a discontinuity in the absorbed dose due to the difference in the electron stopping power of the two materials.

Now consider the dose distribution for three sizes of cavity. Fig. 2a represents the distribution for a cavity, whose linear dimensions are very much greater than the ranges of the β-rays. The scale prevents the detail in the region of the interface being shown. The energy deposited in the cavity in the interface region is a negligible fraction of the total energy deposited in the cavity. The mean absorbed dose in the cavity is determined by the source within the cavity, namely ($C_c E_c t$). Figure 2c represents the other extreme, where the linear dimensions

of the cavity are very much smaller than the ranges of the β rays. In this case the fluence of electrons within the cavity is virtually that which exists in the medium in the absence of the cavity. The mean absorbed dose in the cavity is determined by the source outside the cavity, namely $C_m E_m t$, times the ratio of the mass stopping powers for electrons of the two materials, rather than the source within the cavity. Figure 2b represents the intermediate case, where the linear dimensions of the cavity are comparable with the ranges of the β rays and the mean absorbed dose in the cavity is between the extremes already considered. It can be considered as a modification of the situation for a very small cavity; the cavity size now being adequate to perturb the fluence of electrons crossing it from the medium.

This simple picture is essentially the same as will occur when a radiation detector is placed in a medium. If the medium is irradiated by X or γ rays the directly-ionizing particles generated in the medium and the cavity are secondary electrons rather than β rays. If the medium is irradiated by neutrons the directly-ionizing particles generated are protons and recoil nuclei. Solid state and chemical radiation dosimeters usually do not have linear dimensions which are small compared with the ranges of the directly-ionizing particles, though some work has been done under these conditions, Ritz and Attix [3]. Sometimes the linear dimensions of condensed-state dosimeters are very much greater than the ranges of the directly-ionizing particles, in which case the relation between the dose in the cavity and the dose in the medium is simple. In the case of X and γ rays, for example, provided bremsstrahlung production is negligible, the absorbed doses are in the ratio of the mass-energy-transfer coefficients of the cavity and the medium. Often the linear dimensions of condensed-state dosimeters fall into the intermediate class, where the relation of the absorbed dose in the detector and its response to the absorbed dose in the medium is much more complex. Evaluation of the absorbed dose in the radiation-sensitive device from the measured parameter will vary with each dosimeter. The correction arising due to any container necessary for a particular dosimeter or the deduction of the absorbed dose to the medium from the absorbed dose in the device must be calculated from a theory of cavity ionization. This paper outlines a theory of cavity ionization which treats the entire range of cavity sizes discussed above and applies it to the Fricke dosimeter as a specific example.

2. DEVELOPMENT OF CAVITY THEORY

The first formal statement of cavity ionization theory was due to Gray [4, 5], but because of Bragg's [6, 7] qualitative anticipation of Gray's work, his result has become known as the Bragg-Gray equation, viz:

$$D_m = \frac{1}{f} D_c$$

$$\left(= \frac{1}{f} W J_m \text{ for an ionization chamber}\right)$$

where D_m is the absorbed dose in the medium
D_c is the absorbed dose in the cavity
f is the mass stopping power ratio for the directly-ionizing particles of the gas to the medium for a particular cavity.
W is the average energy expended by the directly-ionizing particles per ion pair produced.
J_m is the ion pair formed per unit mass of gas.

Early theories evaluated the stopping power ratio on the assumption that the directly-ionizing particles lose energy continuously, initially treating the stopping-power ratio as independent of energy [5], but later averaging over the slowing-down spectrum of directly-ionizing particles, Lawrence [8]. Later theories, Spencer and Attix [9], Burch [10], took account of the discrete-energy losses by directly-ionizing particles in evaluating the stopping-power ratio. All these theoretical treatments of cavity ionization rest on the assumptions:
(1) The spectrum of directly-ionizing particles set up in the medium is not modified by the presence of the cavity;
(2) The number of interactions of indirectly-ionizing particles which generate directly-ionizing particles within the cavity is negligible.

To satisfy these requirements the linear dimensions of the cavity must be kept very small compared with the ranges of the indirectly-ionizing particles (i. e. these theories are limited to the situation represented by Fig. 2c). For a condensed-phase dosimeter in a medium irradiated by 1MeV photons the linear dimensions of the cavity would have to be kept below about 10^{-3} cm if this condition is to be fulfilled. For low-energy photons and neutrons this size requirement would be even more restrictive. It is for this reason that the above cavity theories have seldom been of practical use in solid state and chemical dosimetry.

3. MODIFICATION OF CAVITY THEORY

Experiments, Greening [11], Attix, De La Vergne and Ritz [12], Burlin [13, 14], particularly those where the gas pressure in an ionization chamber has been varied, have shown the superiority of the Spencer-Attix theory, and where deviations have been observed they have been attributed at least in part to the perturbation of the electron spectrum established in the wall by the cavity. Therefore the Spencer-Attix theory only will be considered here, and will be modified to account for perturbation effects of the cavity. The description given here will be brief and non-mathematical but a fuller account will appear elsewhere, Burlin [15]. While cavity theory can be applied to neutrons, protons, β rays etc., in order to avoid vagueness or repetition this discussion will be limited to a cavity situated in a medium irradiated by photons.

The Spencer-Attix theory, Spencer and Attix [9], Spencer [16], expresses the stopping-power ratio for electrons of the gas to the medium by the equation:

$$f_Z\left(T_0, \Delta\right) = \frac{\left(\frac{Z}{A}\right)_c}{\left(\frac{Z}{A}\right)_m}\left\{1 + \frac{1}{T_0}\left[\int_{\Delta}^{T_0} R_m(T_0, T)\left(\frac{B_c(T)}{B_m(T)} - 1\right) dT + \Delta\, R_m(T_0, \Delta)\left(\frac{B_c(\Delta)}{B_m(\Delta)} - 1\right)\right]\right\}$$

where T_0 is the initial energy of the electrons
Z is the atomic number
A is the atomic weight
$R(T_0, T)$ is the ratio of the total electron flux to the primary electron flux at an energy T when the initial energy of the electrons is T_0.
B(T) is the stopping number of electrons of energy T
Δ is the energy of an electron which will, on average, just cross the cavity.

The term in the outer brackets is the electronic stopping-power ratio. When the cavity material has the same density, atomic composition and molecular binding as the medium (i.e. the cavity is perfectly 'matched'), this term is unity, the second term in the outer bracket being zero. When the cavity is not perfectly 'matched' to the medium in which it is stituated, the stopping number of the cavity material and the medium are not equal so that the second term in the outer bracket is not zero and its magnitude will depend on the electron spectrum established in the medium through the factor, $R_z(T_0, T)$.

Now consider a cavity of intermediate size (see Fig. 2b). The basic assumptions of cavity theory listed above now no longer hold. The first condition is violated in that the electron spectrum set up in the medium is now significantly attenuated as it crosses the cavity. Let us be guided by experimental results in deciding how this affects the shape of the electron spectrum and hence the Spencer-Attix equation. The energy distribution of an electron spectrum changes little during absorption, Fournier and Guillot [17], Dudley [18], Brownell [19], Parker [20], so the electron-energy spectrum and hence $R_z(T_0, T)$ will be assumed to be constant during the absorption of the electron spectrum of the wall as it crosses the cavity. Then, if the electron spectrum emerging from the wall is reduced on average by a factor, d, in traversing the cavity, the contribution of the second term in the outer bracket of the Spencer-Attix equation will be reduced by a factor, d. The factor d is evaluated by noting that the absorption of electrons is nearly exponential, Schmidt [21], Hahn and Meitner [22], Odeblad [23]. The effective mass absorption coefficient, β, is determined uniquely by the maximum energy, at least for β-ray spectra (Curie, Debierne, Eve, Geiger, Hahn, Lind, Meyer, Rutherford, and Schweidler [24], Gleason, Taylor, and Tabern [25], Katz and Penfold [26] and in this case was calculated from the expression of Loevinger [27]. If g is the average path length of electrons crossing the cavity, then on average the electron spectrum emerging from the wall will be attenuated by a factor

$$\frac{\int_0^g e^{-\beta x}\, dx}{\int_0^g dx} = \frac{1 - e^{-\beta g}}{\beta_g} = d$$

The second basic assumption of cavity theory is violated in that the photons do generate electrons in significant numbers within the cavity. Since the resulting electron spectrum will have the same maximum energy as that generated in the medium, it can be shown to be a corollary of the above treatment that the electron spectrum generated in the gas on average builds up to (1-d) of its equilibrium value. If this spectrum

has its equilibrium-energy distribution, and total energy, then its electronic stopping-power ratio would be that of a perfectly 'matched' cavity, namely unity. Therefore, as far as the spectral shape is concerned, the contribution of these electrons to the second term in the outer bracket of the Spencer-Attix equation is zero. However, the total energy in the equilibrium electron spectrum per unit photon fluence per electron in the two materials is not equal but is proportional to the electronic energy-absorption coefficients of the photons in the medium and in the cavity material ($_m\mu'_{en} : {}_c\mu'_{en}$). Thus, while for a 'matched' cavity the contribution to the electronic stopping-power ratio of the equilibrium spectrum of electrons generated in the gas would be unity, for an unmatched cavity the contribution will be $1 \times {}_c\mu'_{en} / {}_m\mu'_{en}$. In the case we are considering the electron spectrum generated in the cavity only reaches a fraction, (1-d), of its equilibrium value. Thus the contribution to the electronic stopping-power ratio should be $(1-d) \times 1 \times {}_c\mu'_{en} / {}_m\mu'_{en}$ and not $(1-d) \times 1$, which is inherent in the treatment so far. This necessitates the electronic stopping-power ratio being corrected by the addition of a term

$$(1-d) \times 1 \times \left(\frac{{}_c\mu'_{en}}{{}_m\mu'_{en}} - 1 \right) = (1-d) \left(\frac{\left(\frac{\mu_{en}}{\rho}\right)_c}{\left(\frac{\mu_{en}}{\rho}\right)_m} \frac{\left(\frac{Z}{A}\right)_m}{\left(\frac{Z}{A}\right)_c} - 1 \right)$$

where $\left(\frac{\mu_{en}}{\rho}\right)_c$ and $\left(\frac{\mu_{en}}{\rho}\right)_m$ are the mass energy-absorption coefficients of the cavity material and the medium, respectively.

Introducing these corrections into the Spencer-Attix equation we obtain

$$f_Z(T_0, \Delta) = \frac{\left(\frac{Z}{A}\right)_c}{\left(\frac{Z}{A}\right)_m} \left\{ 1 + \frac{d}{T_0} \left[\int_\Delta^{T_0} R_m(T_0, T) \left(\frac{\beta_c(T)}{\beta_m(T)} - 1 \right) + \Delta R_m(T_0, \Delta) \left(\frac{\beta_c(\Delta)}{\beta_m(\Delta)} - 1 \right) \right] + (1-d) \left(\frac{\left(\frac{\mu_{en}}{\rho}\right)_c}{\left(\frac{\mu_{en}}{\rho}\right)_m} \frac{\left(\frac{Z}{A}\right)_m}{\left(\frac{Z}{A}\right)_c} - 1 \right) \right\}$$

This expression does not impose on the cavity dimensions the limitations resulting from the basic assumptions of earlier theories. It is therefore applicable to any radiation dosimeter, regardless of its dimensions. For condensed-phase radiation dosimeters situated in a condensed-phase medium differences in the correction for the polarization of the medium by the charged particles, the 'density effect' between two materials, Sternheimer [28, 29], can often be neglected and

the equation has the simpler form

$$f_Z(T_0,\Delta)=\frac{\left(\frac{Z}{A}\right)_c}{\left(\frac{Z}{A}\right)_m}\left\{1+\frac{d}{T_0}\ln\frac{I_m^2}{I_c^2}\left[\int_\Delta^{T_0}\frac{R_m(T_0,T)}{\beta_m(T)}dT+\frac{\Delta R_m(T_0,\Delta)}{\beta_m(\Delta)}\right]+(1-d)\left(\frac{\left(\frac{\mu_{en}}{\rho}\right)_c}{\left(\frac{\mu_{en}}{\rho}\right)_m}\frac{\left(\frac{Z}{A}\right)_m}{\left(\frac{Z}{A}\right)_c}-1\right)\right\}$$

where I_m and I_c are the mean excitation potentials of the medium and the cavity material, respectively.

If the cavity is very large, d approaches zero and the expression reduces to the ratio of the mass energy-absorption coefficient of the cavity material to the medium (see Fig. 2c). If the cavity is very small, d approaches unity and the expression reduces to the Spencer-Attix theory (see Fig. 2a). When data from the Spencer-Attix theory are not available. a similar modification may be applied to obtain the mass stopping-power ratio from the Bragg-Gray theory.

4. FRICKE DOSIMETER

It was decided to initiate an experimental examination of the application of cavity theory to condensed-phase radiation dosimetry using the Fricke dosimeter (ferrous sulphate dosimeter). The Fricke dosimeter was chosen because it is a well-established dosimeter, for which the reproducibility and ease of measurement are good and which is capable of 1% precision, ICRU[30]. As pyrex or silica irradiation cells are preferred [30], silica irradiation vessels were adopted. ^{60}Co gamma rays were selected for the first irradiations, and later 250-kV X rays were used. This choice was in part motivated by the report of a size-dependence of the response of the Fricke dosimeter in some experiments using a ^{60}Co gamma-ray source, Sehested, Brynjolfsson and Holm [31]. It was of interest to see if similar observation could be repeated inde-

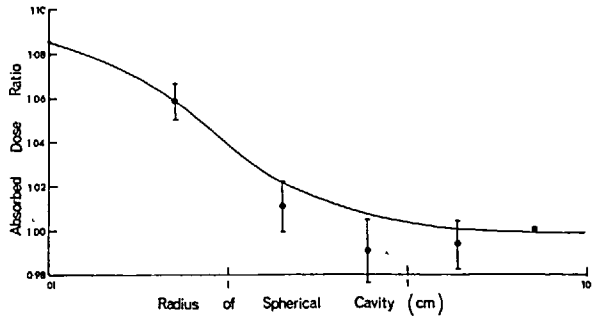

FIG. 3. Absorbed dose in ferrous-sulphate-solution cavity in silica relative to the absorbed dose in an infinite cavity irradiated by ^{60}Co γ rays

pendently with a different experimental set-up, and to determine to what extent they could be explained by cavity theory.

The calculations were performed using data on the mean excitation potential of the elements from a US National Committee on Radiation Protection Report [32] and from Fano [33] and data on the mass energy-absorption coefficients obtained from Grodstein [34] and White [35]. The results are represented by the line in Fig. 3 for ^{60}Co gamma rays. The ratio of the absorbed dose received by a ferrous-sulphate solution in a cavity of finite size surrounded by silica to the absorbed dose received by a ferrous sulphate solution in an infinite cavity is plotted against the radius of a spherical cavity.

5. EXPERIMENT

The irradiation cells employed were 10-cm-long tubes of 0.05, 0.2 and 0.6 cm internal diameter and spherical flasks of 3.79 and 10.3 cm internal diameter. To ensure that electronic equilibrium was established within the silica, the wall was built up to 2 mm of silica equivalent. This was achieved in the case of the tubes by using a further tube as a sheath round the irradiation vessel, and in the case of the flask by wrapping aluminium sheet round the exterior. Aluminium has nearly the same atomic number, 13, as silicon, 14, so that equilibrium electron spectra of the two materials will not be very different, and in any case the 1-mm thickness of silica, which is in contact with the solution, will be by far the most important factor in determining the electron spectrum entering the solution, Gray [36]. The solution was 1 m$\underline{M}$ in ferrous sulphate, 1 m$\underline{M}$ in sodium chloride (to counteract the effect of possible organic impurities) and 0.8 $\underline{N}$ in sulphuric acid [30]. The water was triply-distilled from acid dichromatate and alkaline permanganate solutions in an all-glass system, and the chemicals were of analytical grade [30]. The maximum dose did not exceed 40 000 rad to avoid an excessive depletion of the oxygen content of the solution.

The solutions were irradiated by a 500-Ci ^{60}Co source which was 120 mm long. This was situated in a brass guide tube of about 6.5 mm thickness so that the scattered radiation should be minimal. The irradiation cells were placed on a turntable, which rotated during the irradiation to ensure an equal exposure of all the cells. The distance from the centre of the source to the centre of the solution was 33.4 cm.

The ferric ion was measured with a Hilger Type H700.307 spectrophotometer at 304 nm. The thermal oxidation was taken into account by measuring the difference in the ferric-ion concentration between the irradiated solution and the unirradiated solution which had been stored for the same length of time. The measurements were not made in a constant temperature cell holder. This, together with possible evaporation losses and lack of experience by the authors with this particular dosimeter, may explain why the 1% repetition accuracy indicated by the ICRU [30] was not achieved. These results are regarded as provisional and it is hoped that further work will enable us to achieve the same order of accuracy as other workers.

6. RESULTS

The results of ten measurements, which had a mean absorbed-dose ratio and a standard error of the mean as shown are presented for the ^{60}Co irradiation in Fig. 3. The mean path length across the cavity must be known in order to compare experiment and theory. The mean path length across a sphere of radius, R, is 4/3 R and this has been used in presenting the theoretical results for spherical cavities. The mean path length across the tubes has been taken as 8/3 R so that the tubes would correspond to spherical cavities of radius 2R. The experimental results, corrected for photon attenuation in the solution, have been normalized on the theoretical value for a spherical cavity of radius 0.05 cm and are recorded as the points on Fig. 3. The results show reasonable agreement with the predictions of the modified cavity theory.

7. DISCUSSION

Sehested, Brynjolfsson and Holm [31] found that the response of the Fricke dosimeter depended on the ratio of the surface area to the volume of the irradiation cell. This ratio is related to the mean path length across the cavity, which occurs in the above theory. Sehested et al. obtained a change in the absorbed-dose ratio of 6.5%, with irradiation cells which had dimensions equivalent to spherical cavities of radius 0.4 to 1.2 cm. This result was obtained using glass and polyethylene irradiation cells, where the 'matching' of the container with the solution is closer than with silica. A larger change in the absorbed-dose ratio would be expected in our experiments, using silica irradiation cells. With the experimental set-up described in this paper, we were not able to repeat the results of Sehested, Brynjolfsson and Holm and, in point of fact, in the range of irradiation cell size from 0.4 to 1.2 cm, no significant change in the absorbed-dose ratio was observed. This is in accord with the predictions of cavity theory. Sehested et al. have suggested that "for the glass ampoules, the effect may be due to the lack of γ-electron equilibrium on the boundaries between glass and dosimetric solution". (This is of course essentially the problem dealt with by the modified-cavity theory presented here). However, while this effect may explain in part their results, it is unlikely that they can be explained entirely on the basis of cavity theory. As their irradiations were performed in a large scattering medium, the photon spectrum in the region of the cavity is uncertain and it is therefore not possible to make a quantitative comparison of this theory with their measurements.

Weiss, Allen and Schwarz [37] found a 6% greater yield in glass cells of 0.4 cm diam. than in larger ones, while Ghormley [38] obtained a 3% greater yield for the same cell size, but neither indicate the energy of the radiation source employed. Cavity theory indicates that a 0.4-cm-diam. silica irradiation cell irradiated with ^{60}Co γ rays would give a 2.2% greater yield than larger cells. In the absence of any knowledge of the photon energies used by these authors, this seems reasonable agreement. Weiss et al. did not notice this effect in polystyrene cells. This is also in accord with cavity theory, which predicts very little change in the yield with size of irradiation cell for closely-matched

cavities. Weiss, Allen and Schwarz [37] have stated that "the size and shape of the dosimeter container is not important as long as the internal diameter is greater than 8 mm". Calculations from cavity theory indicate that this statement is only true for a fairly well-'matched' dosimeter and container. For a Fricke dosimeter in an 8-mm diam. silica cell irradiated by ^{60}Co γ rays the yield is 1.3% greater than for very large containers, according to cavity theory, and the theory indicates that it is not until 6 cm diam. that the effect falls to below 0.1%.

Other workers [39-41], have reported a size dependence for the Fricke dosimeter, but there is not sufficient data in their report to perform the theoretical calculations and make comparisons with their experimental results. It is particularly interesting to note that Puig and Sutton [41] obtained similar experimental results to those reported here, and also that they formulated an empirical equation, which has qualitatively the same behaviour as the above theory.

The experiments reported here with high-energy photons, 1.25 MeV, have demonstrated a size dependence of the Fricke dosimeter contained in silica radiation cells. The magnitude of this size dependence can be accounted for by cavity theory. Similar situations will arise in many solid state and chemical dosimeters which are used in practice. Thus the calculation of the response of a dosimeter which must be enclosed in a container, will need to include cavity theory. The deduction of the absorbed dose in a medium from the absorbed dose to a solid or liquid dosimeter embedded in it is, of course, the essential function of cavity theory.

ACKNOWLEDGEMENTS

The authors' thanks are due to Dr. G. E. Adams and Mr. B. D. Michael for their advice, to Sir Oliver Scott for the use of radiation facilities at the British Empire Cancer Campaign Research Unit in Radiobiology, and to Professor J. F. Fowler and Mr. J. Yarwood for their encouragement. This work was supported by the Science Research Council.

REFERENCES

[1] DUTREIX, J., BERNARD, M., Etude de flux des électrons secondaires et de leur rétrodiffusion. Application à la détermination de l'ionisation à l'interface entre deux milieux différents exposés à des RX de haute énergie , Biophysik 2 (1965) 179.

[2] DUTREIX, J., BERNARD, M., Dosimétrie au voisinage des interfaces dans l'expérimentation radiobiologique avec des rayonnements X et γ de haute énergie, Int.J.Radiat.Biol.10 2 (1966) 177.

[3] RITZ, V.H., ATTIX, F.H., "A solid state Bragg-Gray cavity chamber", Selected Topics in Radiation Dosimetry, IAEA, Vienna (1961) 481.

[4] GRAY, L.H., The absorption of penetrating radiation , Proc.R.Soc. 122 (1929) 647.

[5] GRAY, L.H., An ionisation method for the absolute measurement of gamma-ray energy , Proc.R. Soc.A 156 (1936) 578.

[6] BRAGG, W.H., The consequences of the corpuscular hypothesis of the gamma and X-rays , Phil. Mag. 20 (1910) 385.

[7] BRAGG, W.H., Studies in Radioactivity, Macmillan, New York, (1912).

[8] LAWRENCE, G.C., The measurement of extra hard X rays and gamma rays in roentgens , Canad. J.Res.Soc.A.5 (1937) 67.

[9] SPENCER, L.V., Attix, F.H., A theory of cavity ionisation , Rad.Res.3 (1955) 239.

[10] Burch, P.R.J., Cavity ion chamber theory , Rad.Res. 3 (1955) 361.
[11] GREENING, J.R., An experimental examination of theories of cavity ionisation , Br.J.Radiol. 30 (1957) 254.
[12] ATTIX, F.H., DE LA VERGNE, V.H. et al. Cavity ionisation as a function of wall material , Bur. Stand.J.Res.60 (1958) 3.
[13] BURLIN, T.E., An examination of theories relating the absorption of gamma ray energy in the medium to the ionisation produced in a cavity, Physics Med.Biol.6 1 (1961) 33.
[14] BURLIN, T.E., Further examination of theories relating the absorption of gamma ray energy in a medium to the ionisation produced in a cavity , Physics Med.Biol. 4 2 (1966) 255.
[15] BURLIN, T.E., General theory of cavity ionisation , Br.J.Radiol. (1966) (in press).
[16] SPENCER, L.V., Note on the theory of cavity ionisation chambers , Rad.Res.25 (1965) 352.
[17] FOURNIER, G., GUILLOT, M., L'absorption exponentielle des rayons β du radium E , Actual. scient. ind.5 (1930) 57.
[18] DUDLEY, R.A., Thesis, Mass.Inst.Tech. (1951).
[19] BROWNELL, G.L., Interaction of phosphorus-32 beta rays with matter , Nucleonics 10 6 (1952) 30.
[20] PARKER, R., (1965) Private communication.
[21] SCHMIDT, H.H., Z. Phys. 7 (1906) 764.
[22] HAHN, O., MEITNER, L., Die β-Strahlspektren von Radioactinium und seinerZerfallsprodukten , Z.Phys. 34 (1925) 795.
[23] ODEBLAD, E., Approximate formulae describing transmission and absorption of beta rays , Acta. radiol. (Stockholm) 43 (1955) 310.
[24] CURIE, M., DEBIERNE, A., EVE, A.S., GEIGER, H., HAHN, O., LIND, S.C., MEYER, S., RUTHERFORD, E., SCHWEIDLER, E., The radioactive constants as of 1930, Rep.Int.Radium Standards Comm.Rev.mod.Phys. 3 (1931) 427.
[25] GLEASON, G.I., TAYLOR, J.D., TABERN, D.L., Absolute beta counting at Defined Geometrics , Nucleonics 8 5 (1951) 12.
[26] KATZ, G.W.C., PENFOLD, A.S., Range energy relations for electrons and the determination of beta-rays and point energies by absorption , Rev.mod.Phys.(1952) 28.
[27] LOEVINGER, R., The dosimetry of β-sources in tissues. The point source function , Radiobiology. 66 (1956) 55.
[28] STERNHEIMER, R.M., The density effect for the ionisation loss in various materials , Phys.Rev.88 (1952) 851.
[29] STERNHEIMER, R.M., The density effect for the ionisation loss in various materials , Phys.Rev. 103 (1956) 511.
[30] International Commission on Radiological Units and Measurements, National Bureau of Standards, Handbook 85 (1964).
[31] SEHESTED, K., BRYNJOLFSSON, A., HOLM, N.W., Danish Atomic Energy Commission Res.Estab., Riso, Riso Rep.No.62 (1963).
[32] U.S. National Committee on Radiation Protection Report, National Bureau of Standards, Handbook 79 (1961).
[33] FANO, U., Penetrations of protons, alpha particles and meson, A.Rev.nucl.Sci. 13 (1963) 1.
[34] GRODSTEIN, G.H., X-ray attenuation coefficients from 10 kV to 100 MeV, Nat.Bur.Stand. Circ. 583 (1957).
[35] WHITE, G.R., Nat.Bur.Stand.Rep. 100 (1952).
[36] GRAY, L.H., Radiation dosimetry , Br.J.Radiol. 10 (1937) 721.
[37] WEISS, J., ALLEN, A.D., SCHWARZ, H.A., "Use of the Fricke ferrous sulphate dosimeter for gamma-ray doses in the range 4 to 40 kr," Proc. 1st UN Int.Conf. PUAE 14 (1956) 179.
[38] GHORMLEY, J.A., Quoted by Weiss et al. (1956)
[39] WHITTAKER, B., The G-value and the reproducibility of the ferrous-ferric dosimeter, UKAEA Rep. AERE-R-3073 (1963).
[40] MILLER, N., WILKINSON, J., Disc.Faraday Soc.12 (1952) 50.
[41] PUIG, J.A., SUTTON, J., J.chem.Phys. 56 (1959) 699.

DISCUSSION

J.W. BOAG: Dr. Burlin's very interesting paper will demonstrate to those working in solid state and chemical dosimetry that they can use in their studies the mathematical and analytical methods which have

proved so valuable in ionization dosimetry. The problem, as Dr. Burlin says, is the same, and yet sometimes one feels that the proper mathematical and analytical treatment has not been applied sufficiently to the newer systems. It will be interesting to see whether the kind of agreement which Dr. Burlin has in fact shown to exist in the case he has taken as his illustration is also found in other systems when they are analysed in the same careful way.

T. E. BURLIN: Since there are conflicting reports as to the extent to which cell size affects the response of Fricke dosimeters in plastic irradiation cells, and I am at a loss to explain many of the reports on the basis of cavity theory, may I myself ask the experts on chemical dosimetry a question? It has been said that if you clean or pre-irradiate plastic cells, repeatable results are obtained and there is therefore no chemical effect at the walls. This does not seem conclusive to me. It is a necessary, but not a sufficient, condition for the elimination of chemical action at the surface. Is it possible that radiation-induced chemical reactions which are proportional to absorbed dose can occur at the walls of plastic irradiation cells? This would still yield repeatable results for a particular cell size but would give rise to a size dependence which may differ from one plastic to another.

W. MINDER: Chemical changes must surely occur in the container material, and this may be of some importance under conditions of irradiation with heavy particles, especially neutrons. I do not think that effects of this kind would influence the results of measurements with photons.

J. BOOZ: You say that a liquid or a solid state detector irradiated with ^{60}Co-gamma rays can be regarded as infinitely small, in the meaning of the Bragg-Gray principle, if it is smaller than 10 μm. However, the results obtained by Dr. Berstein with an LiF dosimeter of 15 μm thickness and presented in paper SM-78/24 indicate that the dosimeter thickness can perhaps be greater than 10 μm without deviating from the Bragg-Gray principle too much. Would you comment on this, please?

T. E. BURLIN: The size I quoted is based on results obtained with ionization chambers. With ^{60}Co γ rays (1.2 MeV) the Spencer-Attix theory is in reasonable agreement with experiment for a chamber of about 1 cm diam. no matter how different the atomic numbers of the wall material and the filling gas. This would be true for air ($Z = \sim 7$) in a lead ($Z = 82$) chamber, for instance. However, if the walls are more closely matched to the gas, it is not until the cavity size is larger that the departure from the Spencer-Attix theory is significant. In the limit (i.e. a perfectly-matched cavity) there is no departure from theory whatever the size of the cavity, as has been established rigorously by Fano's theorem. If we look carefully at Fig. 5 of paper SM-78/24, we note that the agreement is good for carbon ($Z = 6$) and aluminium ($Z = 13$) which are not too grossly mismatched with the plastic, but there is considerable disagreement for lead ($Z = 82$). The cavity theory described above would give a lower value for lead than the Spencer-Attix theory and you will note that this was found to be the case experimentally.

In Fig. 4 of the same paper the theoretical point is for a 1-μm thickness and the available data for the Spencer-Attix theory only cover

thicknesses of a few microns in solid, with the result that comparison is difficult. However, the Bragg-Gray theory would predict a line parallel to the abscissa, while the same theory as modified above would certainly give a qualitative dependence such as was in fact found, and possibly reasonable quantitative agreement also.

Printed by the IAEA in Austria

Correspondence

(The Editors do not hold themselves responsible for opinions expressed by correspondents)

THE EDITOR–SIR,

CAVITY IONISATION THEORY APPLIED TO SOLID STATE RADIATION DETECTORS

Cavity ionisation theory has traditionally been associated with the determination of absorbed dose using gas-filled ionisation chambers by means of the equation:

$$D_m = \frac{1}{f} D_c$$

$$= \frac{1}{f} W \mathcal{J}_c \text{ for an ionisation chamber}$$

where D_m is the absorbed dose in the medium (the wall material in the case of an ionisation chamber),
D_c is the absorbed dose in the cavity,
f is the mass stopping power ratio for the directly ionising particles of the cavity material to the medium for a particular cavity,
W is the average energy expended by the directly ionising particles per ion pair formed, and
$\mathcal{J}_c$ is the number of ion pairs formed per unit mass of gas.

As the average energy expended by the directly ionising particles per ion pair formed can be regarded as constant in nearly all practical situations, the mass stopping power ratio is the critical parameter to evaluate. This has been done with increasing refinement (Gray, 1936, Laurence, 1937, Spencer and Attix, 1955, Burch, 1955).

Experiments with 1·25 MeV photons (Greening, 1957, Attix, De la Vergne and Ritz, 1958, Burlin, 1961) indicate that even with gross differences in the atomic numbers of the wall and the gas (*e.g.* an air-filled lead chamber), the Spencer-Attix theory is satisfactory for ionisation chambers filled with gas at atmospheric pressure up to a size of cavity with mean linear dimensions of 1 cm. (The parameter entering the theory is the mean path length across the cavity and this depends on both its linear dimensions and shape.) This would correspond to a condensed state device with mean linear dimensions up to about 10 μ. The photon energy considered is favourable to large cavity dimensions. For low-energy photons and neutrons the maximum cavity dimensions to which theory can be applied are very much smaller. It is for this reason that the above cavity theories have seldom been of practical use in solid-state and chemical dosimetry.

A recent theory of cavity ionisation (Burlin, 1966), which took acount of the pertubation of the directly ionising particle fluence by the cavity material, has been successfully applied to ionisation chambers with linear dimensions larger than 1 cm and it has been pointed out that this theory is also applicable to solid-state dosimeters.

One recent set of experiments, which can be used to provide a fairly stringent test of the use of this theory with solid state radiation dosimeters, is that of Bjarngard and Jones (1966). They were concerned to demonstrate the uses of thermoluminescent dosimeters of LiF and CaF_2:Mn incorporated in teflon. This material can be cut into thin discs (15 μ) with a microtome and used for surface dosimetry studies. In one set of experiments discs of different thicknesses were sandwiched between different materials and irradiated with ^{60}Co γ rays.

Bjarngard and Jones (1966) used up to 30 per cent by weight of either LiF or CaF_2:Mn in the teflon so three calculations were performed (viz. 30 per cent LiF, 30 per cent CaF_2:Mn, and 100 per cent teflon) to cover all possibilities. The three cases are shown in the figure as the ratio of the response of the dosimeter sandwiched between lead to that between carbon versus dosimeter thickness. The differences which occurred between the three calculations were small. The experimental results of Bjarngard and Jones (1966) are also shown in the figure.

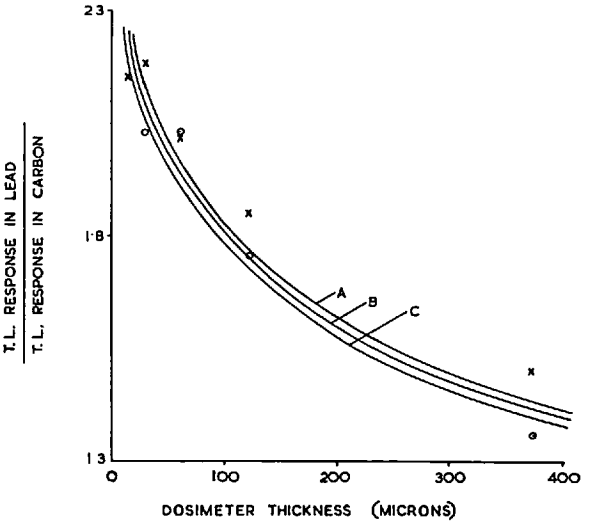

The ratio of the dose in phosphor-teflon dosimeters imbedded in lead to the dose when imbedded in graphite irradiated with ^{60}Co γ rays, as a function of dosimeter thickness.

Experimental results (from Bjarngard and Jones, 1966):
LiF–Teflon discs – ⊙
CaF_2:Mn–Teflon discs – ×
The lines represent the calculations from the modified cavity theory (Burlin, 1966).
A—Teflon
B—30 per cent LiF + 70 per cent Teflon
C—30 per cent CaF_2:Mn + 70 per cent Teflon

The reasonable agreement obtained in this situation where the cavity material (mainly teflon) and the medium (lead) have very different atomic numbers suggests that cavity ionisation theory can be usefully applied to solid state radiation detectors. It also lends support to the treatment of cavity ionisation employed by Burlin (1966), although the details of that treatment are obviously capable of refinement.

Yours, etc.,

T. E. BURLIN,
F. K. CHAN.
Department of Mathematics and Physics,
The Polytechnic, Regent Street,
London, W.1.

REFERENCES

ATTIX, F. H., DE LA VERGNE, L., and RITZ, V. H., 1958, *J. Res. natn. Bur. Stand.*, *60*, 235.
BJARNGARD, B. E., and JONES, D., 1966, *Symposium on solid state and chemical radiation dosimetry in medicine and biology* (I.A.E.A., Vienna).
BURCH, P. R. J., 1955, *Radiat. Res.*, *3*, 361.
BURLIN, T. E., 1961, *Phys. Med. Biol.*, *6*, 33; 1966, *Br. J. Radiol.*, *39*, 727.
GRAY, L. H., 1936, *Proc. R. Soc. A.*, *122*, 647.
GREENING, J. R., 1957, *Br. J. Radiol.*, *30*, 254.
LAURENCE, G. C., 1937, *Can. J. Res. A.*, *15*, 67.
SPENCER, L. V., and ATTIX, F. H., 1955, *Radiat. Res.*, *3*, 239.

Reprint from the Proceedings of the Conference 'Microdosimetry',
Ispra, Italy, November 13-15, 1967.

THE INFLUENCE OF INTERFACES ON DOSIMETER RESPONSE

T.E. BURLIN and F.K. CHAN

Department of Mathematics and Physics, The Polytechnic,
309 Regent Street London, W.1. GREAT BRITAIN

ABSTRACT

A dosimeter is rarely identical with the medium in which the absorbed dose is to be measured. When an unmatched dosimeter is placed in a medium its response will be modified due to interface effects. The magnitude of the interface effects on the dosimeter response will be a function of the size of the dosimeter relative to the range of the directly ionising particles. A theory, which accounts for interface effects, has been examined experimentally on several different dosimeters and results covering a large range of dosimeter size and atomic number are presented.

1. Introduction

A radiation sensitive device placed in a medium irradiated by X or Y rays to measure the absorbed dose is not always matched' to the medium. Indeed, perfect matching demands that both the mass energy absorption coefficients of the photons and the mass stopping power of the electrons are identical for the medium and the radiation detector. This is seldom true in a rigorous sense. The 'unmatched' radiation detector is bounded by interfaces, which will influence its response. The magnitude of the interface effects on the dosimeter will depend on the extent of the difference in the mass energy absorption coefficients of the photons and in the mass stopping power of the electrons between the medium and the dosimeter. Gray (1) derived the relation between the absorbed dose in a medium and the absorbed dose in a dosimeter within the medium. His theory was limited to dosimeters small compared to the range of the directly ionising particles. Such dosimeters, usually ionisation chambers, are conventionally called Bragg-Gray cavities. This paper considers the response of a dosimeter in a medium when its size is increased to dimensions very much greater than the conventional Bragg-Gray cavity. A later paper in this symposium considers the dosimeter's response when its size is reduced to dimensions very much smaller than a conventional Bragg-Gray cavity.

The situation in the region of the interface is represented diagrammatically in Figure 1. The solid lines represent the electrons generated by the photons in the medium, M, while the broken lines represent the electrons generated in the dosimeter, D. In the region of the interface the electron spectrum within the dosimeter is comprised of a contribution from the electron spectrum entering from the surrounding medium and a contribution from the electron spectrum generated within the material of the dosimeter. The relative magnitude of these two contributions varies with distance from the interface, as is illustrated in Figure 2. Suppose the medium is of higher atomic number than the dosimeter and that it is irradiated by low energy photons. The number of electrons generated in the wall per gm will be greater than in the dosimeter. These electrons, M, will enter the dosimeter from the medium and be attenuated with the distance from the wall until they are reduced to zero at their maximum range. The photons also generate in the dosimeter electrons, D, which build up to an equilibrium value. The number of electrons, N, at any point in the dosimeter will result from the summation of these two components.

This distribution will be modified when the size of the dosimeter is such that the regions of influence of the opposite interfaces overlap as illustrated in Figure 3a. The number of electrons falls to a minimum at the centre of the dosimeter though not down to the equilibrium value of electrons generated in the dosimeter. This represents the intermediate case between two extremes.

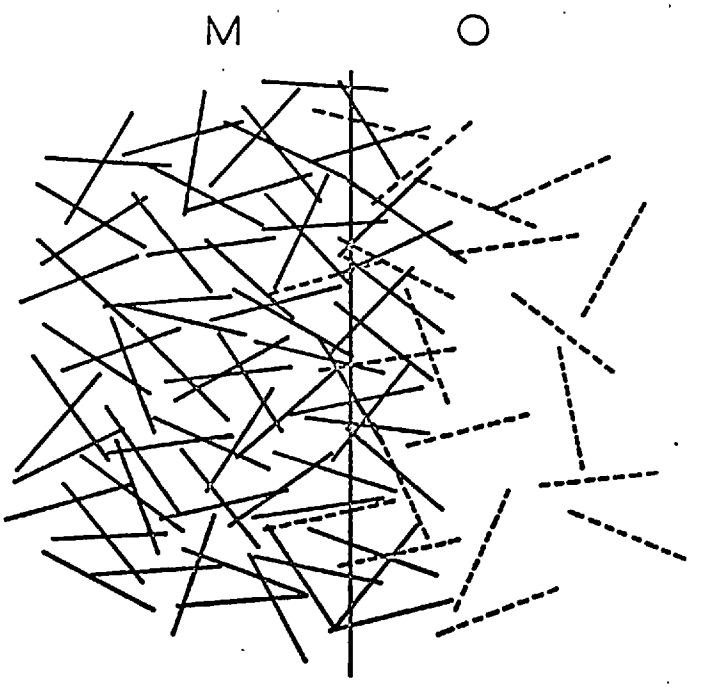

Figure 1 Electrons in the region of an interface

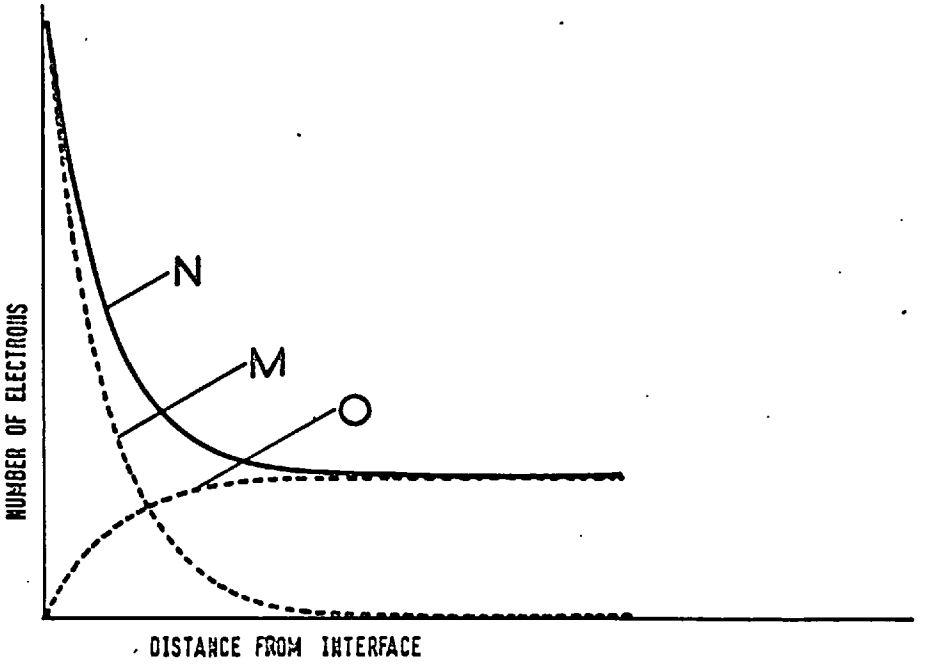

Figure 2 Number of electrons versus distance from the interface

M - electrons entering the dosimeter from the medium

O - electrons generated in the dosimeter by photon interactions

N - total number of electrons

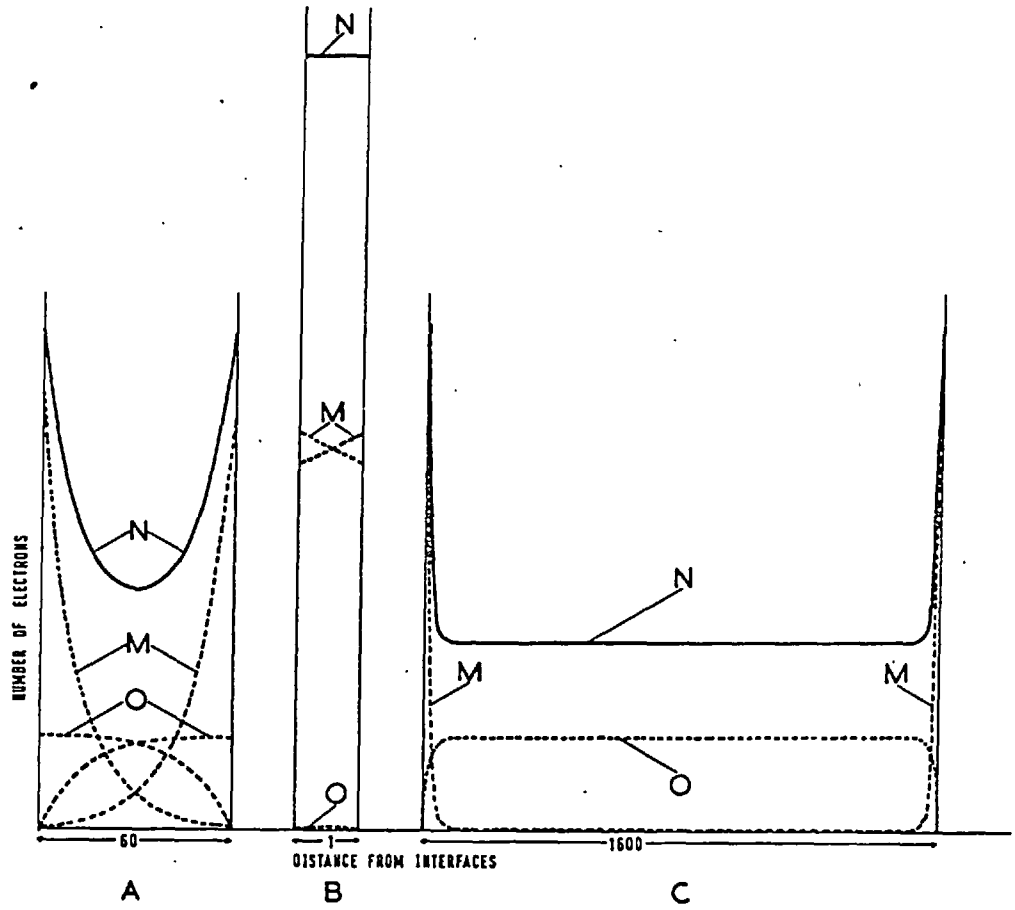

Figure 3 Electron distribution in dosimeters of different size

M - electrons entering the dosimeter from the medium

O - electrons generated in the dosimeter by photon interactions

N - total number of electrons

3A Dosimeter with dimensions comparable with the electron range

3B Dosimeter with dimensions small compared with the electron range

3C Dosimeter with dimensions large compared with the electron range

When the linear dimensions of the dosimeter are very much smaller than the range of the electrons, as illustrated in Figure 3b, the electrons in the dosimeter are virtually only those generated in the medium and crossing the dosimeter. When the linear dimensions of the dosimeter are very much greater than the range of the electrons, as illustrated in Figure 3c, the electrons in the dosimeter are virtually only those generated within the dosimeter. The energy deposited within the dosimeter, and hence its response, will be a function of the net electron spectrum within the dosimeter and of the stopping power of the dosimeter material. This must then be related to the energy deposited in the medium in order to determine the absorbed dose in the medium from the dosimeter response.

2. Cavity Ionisation Theory

The first formal treatment of this problem was due to Gray (1), although Bragg (2) discussed it in qualitative terms. The resulting relation between the absorbed dose in the medium, D_m, and the absorbed dose in the cavity, D_c, is known as the Bragg-Gray equation viz.:

$$D_m = \frac{1}{f} D_c$$

where f is the mass stopping power ratio for the electrons of the dosimeter material to the medium. The application of this equation has primarily been to ionisation chambers in which case

$$D_m = \frac{1}{f} WJ$$

where J is the ion pairs produced per unit mass of gas and W is the average energy expended in the gas per ion pair formed and can be regarded constant for nearly all practical situations.

Gray evaluated the mass stopping power ratio for the situation represented by Figure 3b. His theory had to be limited to dosimeters, which were small compared with the electron range, in that it was assumed that:

1. The electron spectrum set up in the medium was not modified in crossing the dosimeter.
2. The number of electrons generated within the dosimeter itself was negligible.

Since Gray's work, the mass stopping power ratio has been evaluated with increasing refinement, some theories including the effects of discontinuous energy losses by the electrons (3, 4, 5), but all resting on the above two assumptions and therefore limited to very small dosimeters.

Recently a theory which does not make these assumptions (6) has been presented. The Spencer-Attix expression for the mass stopping power ratio is

$$f_z(T_o,\Delta)=\frac{\left(\frac{Z}{A}\right)_G}{\left(\frac{Z}{A}\right)_z}\left\{1+\frac{1}{T_o}\left[\int_\Delta^{T_o}R_z(T_o,T)\left(\frac{B_G(T)}{B_z(T)}-1\right)dT+\Delta.R_z(T_o,\Delta)\left(\frac{B_G(\Delta)}{B_z(\Delta)}-1\right)\right]\right\}$$

This expression has been taken and modified by the introduction of two terms which account for the interface effects viz.

1. An attenuation term, d, which accounts for the attenuation of the electrons entering the dosimeter from the medium, thus eliminating the first assumption.
2. A build-up term, $\left(1-d\right)\left[\frac{\left(\frac{\mu_{en}}{\rho}\right)_G}{\left(\frac{\mu_{en}}{\rho}\right)_z}.\frac{\left(\frac{Z}{A}\right)_z}{\left(\frac{Z}{A}\right)_G}-1\right]$ which accounts for the build-up of the electrons within the dosimeter, thus eliminating the second assumption.

Thus the two components of the electron spectra, which occur in the region of an interface are both dealt with in evaluating the mass stopping power ratio from the resulting equation viz.

$$f_z(T_o,\Delta)=\frac{\left(\frac{Z}{A}\right)_G}{\left(\frac{Z}{A}\right)_z}\left\{1+\frac{d}{T_o}\left[\int_\Delta^{T_o}R_z(T_o,T)\left(\frac{B_G(T)}{B_z(T)}-1\right)dT+\Delta.R_z(T_o,\Delta)\left(\frac{B_G(\Delta)}{B_z(\Delta)}-1\right)\right]+\left(1-d\right)\left[\frac{\left(\frac{\mu_{en}}{\rho}\right)_G}{\left(\frac{\mu_{en}}{\rho}\right)_z}.\frac{\left(\frac{Z}{A}\right)_z}{\left(\frac{Z}{A}\right)_G}-1\right]\right\}$$

Since d is a function of the dimensions of the dosimeter this formula is applicable to any size of dosimeter be it large or small compared to the range of the electrons. It has therefore been called a general theory of cavity ionisation.

The most critical test that can be applied to these theories is the variation of response with dosimeter size (or the gas pressure in the case of ionisation chambers) for two reasons.

1. Early theories predict the response per unit mass of the dosimeter is independent of its size while later theories predict a size dependent response.
2. No additional data (such as mass energy absorption coefficients when the wall material is varied or values of the average energy expended per ion pair formed when the gas is varied,) is required.

There is therefore less uncertainty associated with the comparison with theory.

These theories have been tested over the entire range of dimensions represented in Figure 3 with several different dosimeters. Some of the results of these experiments on gaseous, liquid and solid state dosimeters are presented below.

3. Gaseous Dosimeter - Ionisation Chambers

When ionisation chambers with linear dimensions less than 1cm are irradiated by photons of about 1MeV, the electron spectrum emerging from the wall is virtually unattenuated in crossing the cavity and the number of electrons generated in the cavity is insignificant (see Figure 3b). In such a situation the Spencer-Attix theory is found to be in excellent agreement with the experimental results, as illustrated in Figures 4 and 5. Figure 4 shows the ionisation per gm in a lead chamber filled with air and irradiated by 0.66MeV photons (^{137}Cs γ rays) is plotted against the pressure (7). The variation in the response of the ionisation chamber with the pressure is in close agreement with the predictions of the Spencer-Attix theory but did not support the constancy predicted by the Bragg-Gray theory. Figure 5 shows the variation of the ionisation per gm with the atomic number of the wall for an air filled chamber irradiated by 1.25MeV photons (^{60}Co γ rays). (8) The experimental results agree with the Spencer-Attix theory rather than the Bragg-Gray theory again demonstrating the importance of discontinuous energy losses. If the dimensions of the ionisation chamber are increased by an order of magnitude the Spencer-Attix theory no longer agrees with experiment as is illustrated in Figure 6. The ionisation per gm of air in a lead chamber of the guarded field type of 10cm diameter and height is plotted against the pressure, a ^{198}Au source being used (6). Considerable deviation from both the Bragg-Gray and the Spencer-Attix theories occurs but the general theory is in close agreement with the experiment.

While the experiments performed with ionisation chambers at these energies show excellent agreement with the general theory of cavity ionisation, they only cover a small fraction of the range of sizes discussed earlier and represented in Figure 3. Using these monoenergetic isotope sources it is not practical to increase the dimensions of ionisation chambers to values where virtually all the electrons within the chamber are generated therein by the photons. However it is possible to achieve such a condition when condensed state dosimeters are used. These are now considered.

4. Liquid Dosimeter - Fricke

The most frequently used liquid dosimeter - the Fricke dosimeter - has frequently been the subject of discussion as to interface (wall) effects on its response (9, 10, 11). As pointed out above, the general cavity theory should describe such effects quantitatively. Due to its greater density it is possible to increase the size of the Fricke dosimeter until virtually all

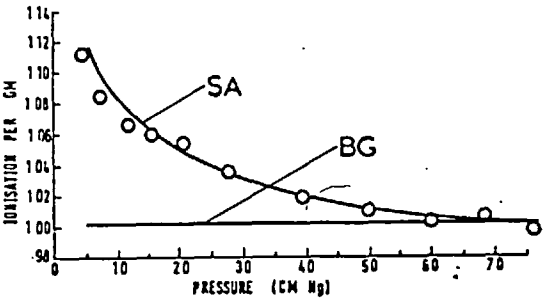

Figure 4 Ionisation per gm of air in a lead chamber irradiated by ^{137}Cs Y-rays

BG - Bragg-Gray theory

SA - Spencer-Attix theory

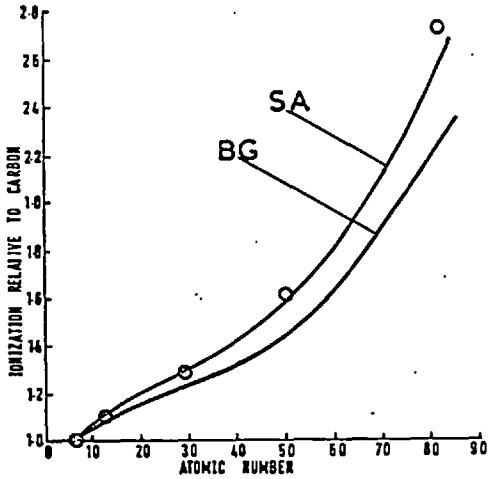

Figure 5 Ionisation per gm of air versus atomic number of the wall material ^{60}Co Y-rays.

BG - Bragg-Gray theory

SA - Spencer-Attix theory

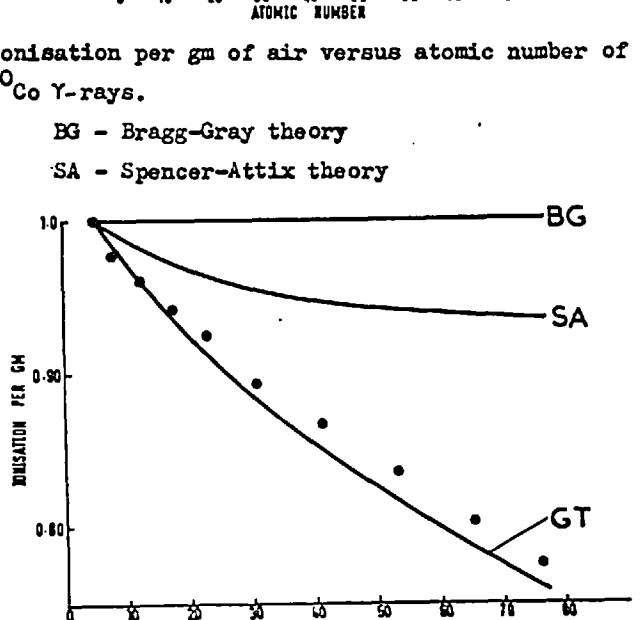

Figure 6 Ionisation per gm of air in a lead chamber irradiated by ^{198}Au Y-rays

BG - Bragg-Gray theory

SA - Spencer-Attix theory

GT - General theory

the electrons within the dosimeter are generated by photon interactions within the dosimeter and the number entering from the wall are negligible. A sphere of about 10cm diameter realises this condition for ^{60}Co Y rays.

Measurements have been made using silica irradiation vessels having a wall thickness adequate to establish electronic equilibrium for the ^{60}Co Y rays used in the irradiation (12). The response of the Fricke dosimeter has been plotted relative to the response of a perfectly matched dosimeter in Figure 7. It will be noted that for vessels in excess of 6cm diameter the response is constant. This is because interface (wall) effects are negligible, the number of electrons entering the ferrous sulphate solution being negligible compared to the number of electrons generated within it. (See Figure 3c). The general theory and the measurements agree to within the limits of experimental error.

The experiment with the Fricke dosimeter extended the dimensions of the dosimeter to the largest sizes it is desired to examine (Figure 3b), but only for a combination where the atomic numbers of the dosimeter and the surrounding medium do not differ greatly. It did not seem feasible to surround chemical systems with media of high atomic number due to difficulties associated with chemical impurities. In order to cover the same size range with materials having greatly differing atomic numbers, solid state dosimeters were employed.

5. Solid Dosimeters - Thermoluminescence, Perspex

It is possible with solid state dosimeters to make measurements extending from dosimeter dimensions small relative to the electron ranges (covered by ionisation chambers) up to the dosimeters which are very much larger than the electron ranges, and to do this for media having widely differing atomic numbers. For example, Bjarngard and Jones (13) have reported experiments where very thin slices of teflon, incorporating thermoluminescent materials in the matrix, were sandwiched between layers of lead and irradiated by ^{60}Co Y rays. The smallest thickness they used are comparable with the size of the ionisation chambers in gm/cm^2 and their results all fall within the intermediate range of dosimeter size depicted by Figure 3a. Figure 8 presents Bjarngard and Jones experimental points together with the prediction of general cavity theory (14). Bjarngard and Jones used up to 30 per cent by weight of either LiF or CaF_2:Mn in the teflon so three calculations were performed (viz. 30 per cent LiF, 30 per cent CaF_2:Mn, and 100 per cent teflon) to cover all possibilities. The response of the dosimeter sandwiched between lead to that between carbon is shown versus dosimeter thickness and reasonable agreement is obtained with theory.

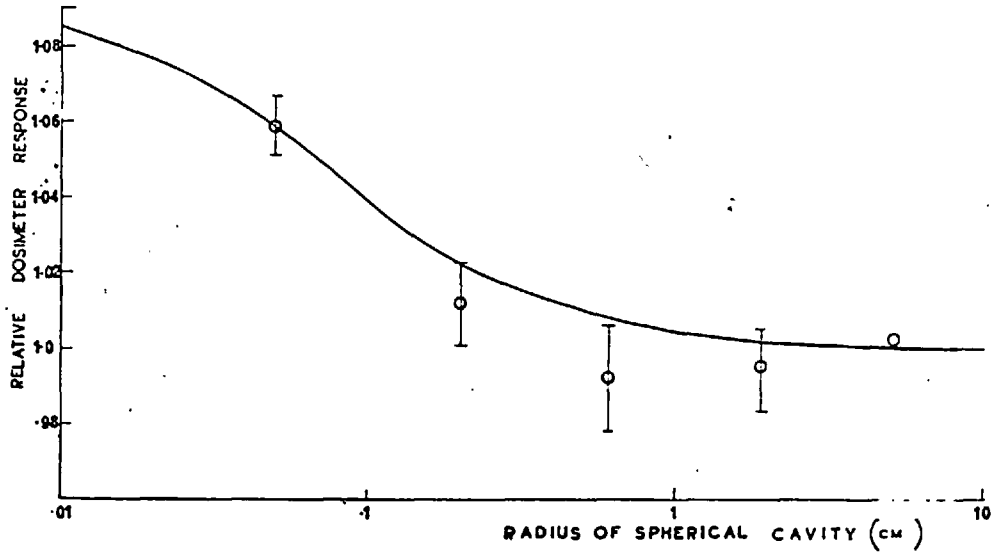

Figure 7 Response of the Fricke dosimeter versus size of silica container. The line has been calculated from the general theory.

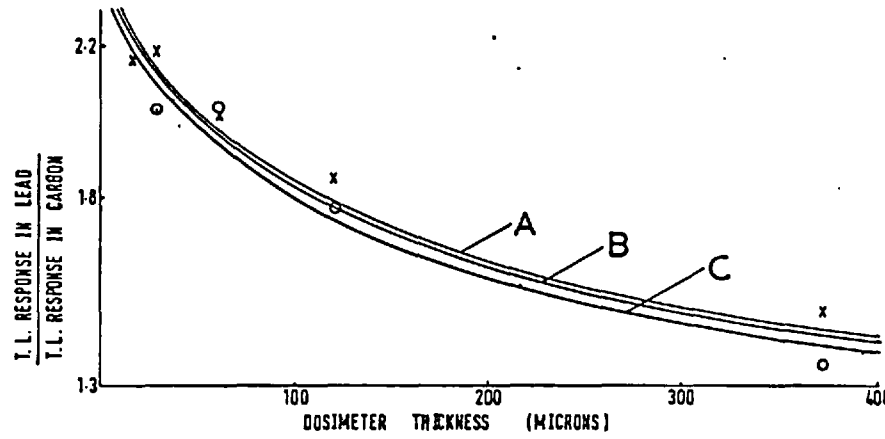

Figure 8 The ratio of the dose in phospher-teflon dosimeters imbedded in lead to the dose when imbedded in graphite irradiated with ^{60}Co γ rays, as a function of dosimeter thickness.

Experimental results (from Bjarngard and Jones, 1966):

LiF-Teflon discs - ○

CaF_2:Mn-Teflon discs - ×

The lines represent the calculations from the modified cavity theory (Burlin, 1966).

A - Teflon

B - 30 per cent LiF + 70 per cent Teflon

C - 30 per cent CaF_2:Mn + 70 per cent Teflon

Clear perspex was chosen as a suitable low atomic number dosimeter to imbed in a high atomic number material, lead in this instance, and increase the size until virtually all the electrons in the dosimeter are generated therein. A batch of perspex specially prepared for dosimetry purposes was used in these measurements. The increase in optical density at 292 millimicrons due to radiation was measured. The results for ^{60}Co Y irradiation are presented in Figure 9 where the dosimeter response has been plotted relative to the response of a perfectly matched dosimeter. Even under such severe experimental conditions as these the general theory of cavity ionisation correctly predicts the size dependance of the response of the dosimeter.

6. Conclusion

A theory of cavity ionisation, which is free from the assumption of earlier theories and hence unlimited in the size of dosimeter to which it is applicable, has been formulated. This general theory has been tested using several dosimeters situated in media whose atomic number differs greatly from the media and have extended from a size where the dosimeter response is determined solely by electrons entering from its surroundings up to a size where its response is determined solely by the electrons generated by photon interactions within it. No significant deviation of experiment from theory was noted over the entire range. It is therefore concluded that the general theory of cavity ionisation successfully accounts for the influence of interface effects on dosimeter response.

One qualification must be associated with this general conclusion. It has been shown that ionisation chambers of small dimensions and/or at low gas pressure cavity theory cannot be applied with confidence because low energy electrons (0 - 25eV) transferred between the electrodes contribute to the current (15). This is discussed in detail in the later paper in this symposium.

Acknowledgements

We wish to thank Professor J. F. Fowler and Mr. J. Yarwood for their advice, Mr. D. L. A. Jones and Sir Oliver Scott for allowing us to use the radiation facilities at Mount Vernon Hospital, and Mr. A. Redhead for technical assistance. This work was supported by the Science Research Council.

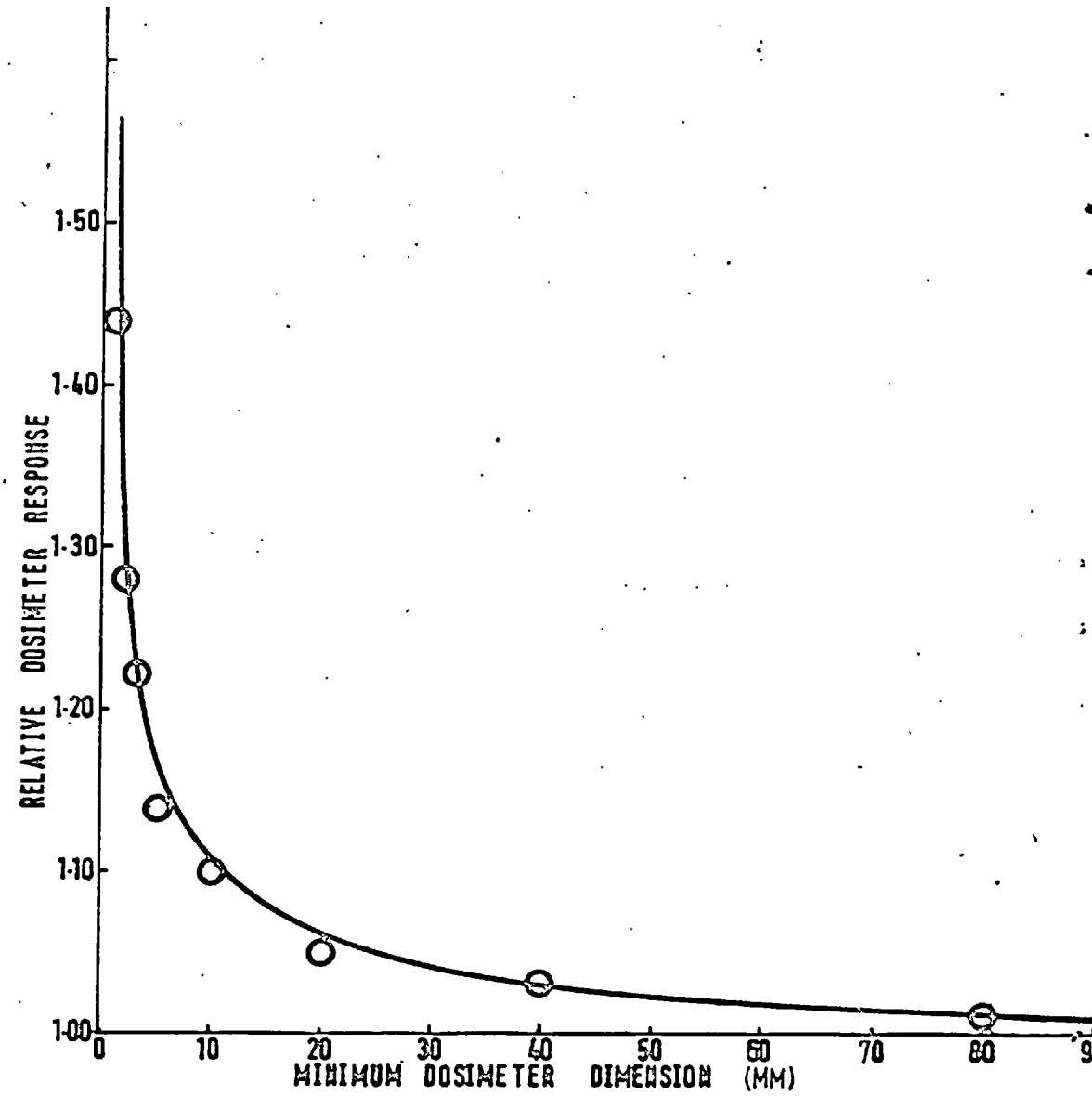

Figure 9 Response of clear perspex versus size of lead container. The line has been claculated from the general theory.

References

(1) Gray, L. H., 'An Ionisation Method for the absolute measurement of gamma-ray energy'. Proc. Roy. Soc., A156, 578, (1936)

(2) Bragg, W. H., 'Studies in Radioactivity'. Macmillan, New York, 1912.

(3) Laurence, G. C., 'The measurement of extra hard X-rays and gamma-rays in roentgens'. Can. J. Res., A15, 67, (1937)

(4) Spencer, L. V., and Attix, F. H., 'A theory of cavity ionisation'. Radiat. Res., 3, 239, (1955)

(5) Burch, P. J. R., 'Cavity ion chamber theory'. Radiat. Res., 4, 361, (1955)

6) Burlin, T. E., 'A general theory of cavity ionisation'. Brit. J. Radiol., 39, 727, (1966)

(7) Burlin, T. E., 'Further examination of theories relating the absorption of gamma-ray energy in a medium to the ionisation produced in a cavity'. Phys. Med. Biol., 11, 255, (1966)

(8) Burlin, T. E., 'An experimental examination of theories relating the absorption of gamma-ray energy in a medium to the ionisation produced in a cavity'. Phys. Med. Biol., 6, 33, (1961)

(9) Miller, N., and Wilkinson, V., 'Actinometry and radiolysis of pure liquids'. Disc. Faraday Soc., 12, 50, (1952)

(10) Puig, J. A., and Sutton, J., 'Effet des parois en verre dans la dosimetrie au sulfate ferreux'. J. Chim. Phys., 56, 699, (1959)

(11) Sehested, K., Brynjolfsson, A., and Holm, N. W., 'Determination of the absorption curve in water of ^{60}Co gamma rays and determination of the strength of a 6 curie ^{60}Co source by means of ferrous-sulphate dosimetry'. Danish A.E.C. Res. Estab. Riso., Riso. Rep. No 62 (1963)

(12) Burlin, T. E., and Chan, F. K., 'Some applications of cavity theory to condensed-state radiation dosimetry' in Solid State and Chemical Radiation Dosimetry in Medicine and Biology, IAEA, Vienna, 1967.

(13) Bjarngard, B. E., and Jones, D., 'Thermoluminescent dosimeters of LiF and CaF_2:Mn incorporated in teflon' in 'Solid State and Chemical Radiation Dosimetry in Medicine and Biology', IAEA, Vienna, 1967.

(14) Burlin, T. E., and Chan, F. K., 'Cavity ionisation theory applied to solid state radiation detectors'. Brit. J. Radiol., 40, 556, (1967)

(15) Burlin, T. E., 'The limits of validity of cavity ionisation theory'. Brit. J. Radiol., 35, 343, (1962)